

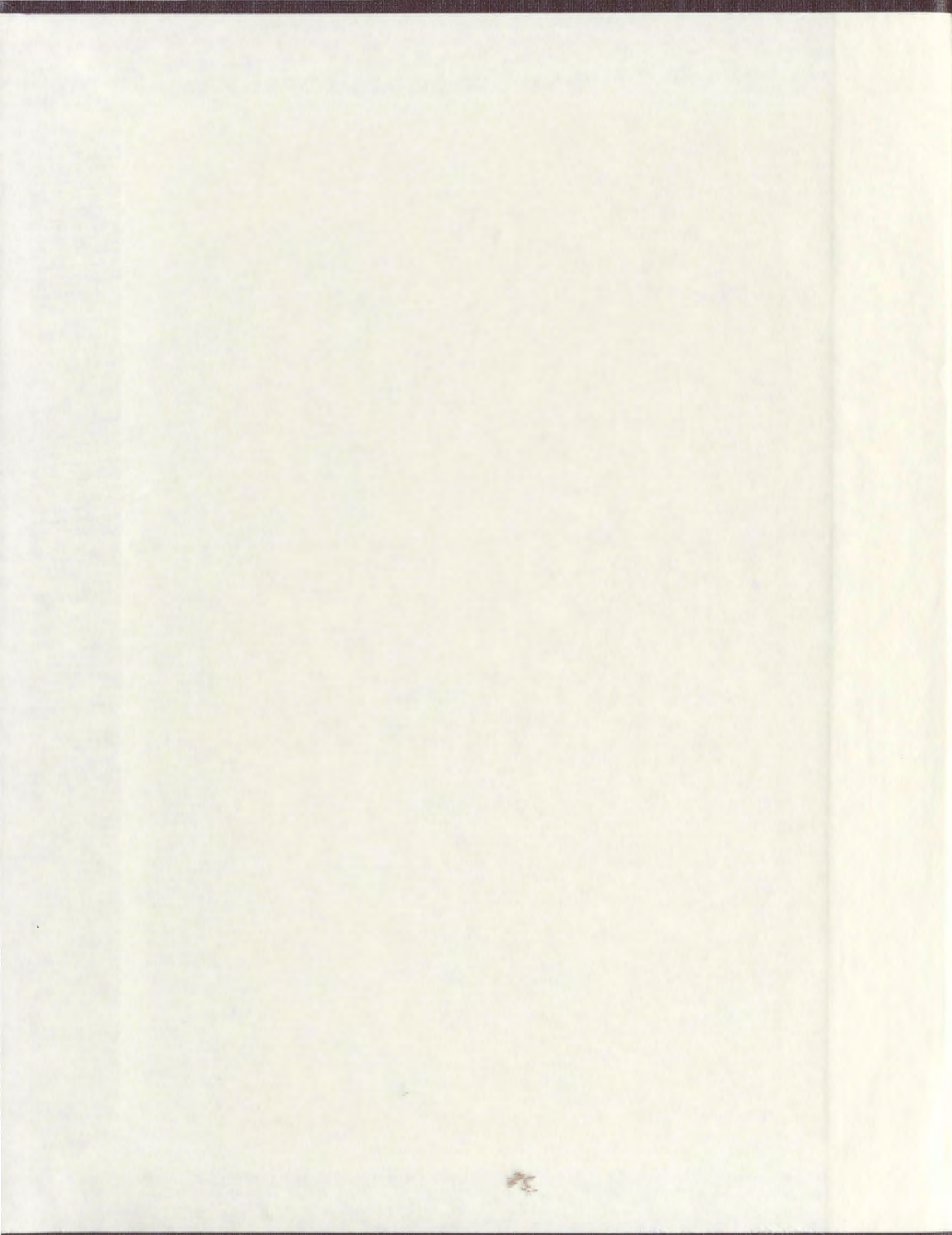
THE DEVELOPMENT OF THE HI-DAPT II HIGH
RESOLUTION SUB-BOTTOM PROFILING SYSTEM

CENTRE FOR NEWFOUNDLAND STUDIES

**TOTAL OF 10 PAGES ONLY
MAY BE XEROXED**

(Without Author's Permission)

PETER HARVEY HUNT



INFORMATION TO USERS

This manuscript has been reproduced from the microfilm master. UMI films the text directly from the original or copy submitted. Thus, some thesis and dissertation copies are in typewriter face, while others may be from any type of computer printer.

The quality of this reproduction is dependent upon the quality of the copy submitted. Broken or indistinct print, colored or poor quality illustrations and photographs, print bleedthrough, substandard margins, and improper alignment can adversely affect reproduction.

In the unlikely event that the author did not send UMI a complete manuscript and there are missing pages, these will be noted. Also, if unauthorized copyright material had to be removed, a note will indicate the deletion.

Oversize materials (e.g., maps, drawings, charts) are reproduced by sectioning the original, beginning at the upper left-hand corner and continuing from left to right in equal sections with small overlaps. Each original is also photographed in one exposure and is included in reduced form at the back of the book.

Photographs included in the original manuscript have been reproduced xerographically in this copy. Higher quality 6" x 9" black and white photographic prints are available for any photographs or illustrations appearing in this copy for an additional charge. Contact UMI directly to order.

UMI

A Bell & Howell Information Company
300 North Zeeb Road, Ann Arbor, MI 48106-1346 USA
313/761-4700 800/521-0600

**The Development of the HI-DAPT II High
Resolution Sub-bottom
Profiling System**

BY

© Peter Harvey Hunt

**A thesis submitted to the School of Graduate
Studies in partial fulfilment of the
requirements for the degree of
Master of Science**

**Department of Earth Sciences
Memorial University of Newfoundland
June 1995**

St. John's

Newfoundland



National Library
of Canada

Acquisitions and
Bibliographic Services

395 Wellington Street
Ottawa ON K1A 0N4
Canada

Bibliothèque nationale
du Canada

Acquisitions et
services bibliographiques

395, rue Wellington
Ottawa ON K1A 0N4
Canada

Your file Votre référence

Our file Notre référence

The author has granted a non-exclusive licence allowing the National Library of Canada to reproduce, loan, distribute or sell copies of this thesis in microform, paper or electronic formats.

The author retains ownership of the copyright in this thesis. Neither the thesis nor substantial extracts from it may be printed or otherwise reproduced without the author's permission.

L'auteur a accordé une licence non exclusive permettant à la Bibliothèque nationale du Canada de reproduire, prêter, distribuer ou vendre des copies de cette thèse sous la forme de microfiche/film, de reproduction sur papier ou sur format électronique.

L'auteur conserve la propriété du droit d'auteur qui protège cette thèse. Ni la thèse ni des extraits substantiels de celle-ci ne doivent être imprimés ou autrement reproduits sans son autorisation.

0-612-25850-5

Canada

ABSTRACT

A new sub-bottom profiling system, the HI-DAPT II, was designed, assembled and field tested. The system is adaptable to a variety of marine acoustic sources thus suited to any aqueous environment. The system uses a digital signal processing (DSP) board with 2 channels of 16 bit analog-to-digital conversion, embedded in a PC chassis, to acquire and process sub-bottom data. Conventional post-stack processing algorithms such as frequency filtering, automatic gain control, swell filter, predictive deconvolution and spiking deconvolution have been coded to run on the DSP to enable processing of the data between successive shots. A two-channel hydrophone streamer consisting of a single hydrophone and a line array is used to collect sub-bottom data. Raw data are stored together with a time stamp and processing parameters on a magneto-optical disk. Processed data are displayed on a CRT and output to a thermal plotter. The HI-DAPT II system was field tested over a portion of the West Florida Sand Sheet, 37 km south of Panama City Florida, as part of the Coastal Benthic Boundary Layer Special Research Project. The objective of the HI-DAPT-II survey was to delineate the vertical extent of the sand sheet in the area. Three, 5 km-long, seismic lines were acquired over the long axis of a grid as well as two tie lines. A series of tests was performed to determine the optimum processing parameters. Processed data, displayed in wiggle trace/variable area format, revealed two main reflecting horizons. The shallowest reflector is interpreted to represent an erosional cycle during the deposition of the sand sheet which occurred 10,000-7,500 ybp. The deepest, high-amplitude reflector exhibits

erosional features. This reflector is interpreted to be the top of the Mio-Pliocene Intracoastal Formation. Field tests have demonstrated how this system has overcome some of the limitations of conventional sub-bottom profiling systems.

ACKNOWLEDGMENTS

I would like to express my deep appreciation to my committee chair, Dr. Jim Wright, for his encouragement and insightful guidance. Dr. Wright has been a source of inspiration since I first began studying geophysics. I would also like to thank Dr. William Scott, a friend and former colleague, for sitting on my committee.

Funding for this research was provided through a grant from the Atlantic Canada Opportunities Agency to the Centre for Cold Ocean Resources Engineering (C-CORE). Thank you to the President of C-CORE, Mr. Jack Clark, for allowing me to conduct my thesis research on this project and for his approval for the thesis to be written on this topic. My sincerest appreciation to Mr. Steve Inkpen for his help, suggestions and assistance throughout the development phase. I would also like to thank Dr. Aubrey Anderson (Texas A&M) and Dr. Mike Richardson (Naval Research Labs) for their assistance in making the Panama City field trials possible. I would like to express my gratitude to Dr. Norman Guinasso (Texas A&M) for his persistence in seeing me bring this thesis to its completion.

My greatest thanks goes to my family; without Nancy's continual support and the inspiration I receive from our three children, my venture into Academia would have never been possible.

Table of Contents

	page
ABSTRACT	ii
ACKNOWLEDGMENTS	iv
LIST OF TABLES	vii
LIST OF FIGURES	viii
1.0 Introduction	1
1.1 Review of sub-bottom profiling technology	1
1.2 Reflection Seismology	4
1.3 Limitations of conventional sub-bottom profilers	5
1.4 Outline of thesis	6
2.0 System Design and Design Criteria	7
2.1 General system description	7
2.2 Acoustic source characteristics	11
2.3 Hydrophone array design	17
2.3.1 Line array	20
2.4 Digital data acquisition	26
2.4.1 Analog signal conditioning	26
2.4.2 Analog-to-digital conversion	27
2.5 Data processing, display and storage	30
2.6 HI-DAPT overview	31
3.0 Data Processing Software Development	32
3.1 Software development environment	33
3.2 HI-DAPT II data processors	34
3.2.1 Convolutional model for a seismic trace	34
3.2.2 Bandpass filters	37
3.2.3 Deconvolution	38
3.2.3.1 Spiking deconvolution	40
3.2.3.2 Predictive deconvolution	44
3.3 Bottom tracking and swell compensation	46
3.3.1 First break picking	48
3.3.2 Automatic bottom tracking	49

3.3.3 Swell compensation	49
3.4 Trace scaling	50
3.4.1 Spherical divergence corrections	52
3.4.2 Automatic gain control	52
3.5 Horizontal stacking	53
3.6 Miscellaneous utilities	54
3.6.1 Noise spike removal	54
3.6.2 Trace mixing	55
3.6.3 Instantaneous amplitude	56
3.70 Video and hardcopy display	56
3.7.1 CRT display	58
3.7.2 Thermal plotter display	58
4.0 Panama City Sea Trials	60
4.1 Geologic setting	62
4.2 Methodology	64
4.2.1 Trial one, August 10, 1993	64
4.2.2 Trial two, August 11, 1993	67
4.2.3 Trial three, August 12, 1993	68
4.3 Data processing	68
4.3.1 Preliminary data examination	69
4.3.2 Bandpass filter tests	69
4.3.2 Predictive deconvolution tests	70
4.3.4 Automatic gain tests	74
4.3.5 Processed Seismic Sections	74
4.4 Seismic/geologic interpretation	75
4.4.1 Seismic characterization	76
4.4.2 Interpretation	77
5.0 Conclusions	80
Glossary	83
References	86
Appendix A DSP96002 Specifications	89
Appendix B Seismic Sections	90

TABLES

Table	page
2.1 Commercial components of HI-DAPT II	8
2.2 Characteristics of common marine sources	12
2.3 Programmable sample rates	28

FIGURES

Figure	page
2.1 HI-DAPT II Sub-bottom Profiling System.	9
2.2 Graphical comparison of marine seismic sources.	13
2.3 Schematic of C-CORE multi-tip sparker source.	14
2.4 Amplitude spectra of 121 tip sparker source at 480, 750 and 1080 Joule power.	16
2.5 Amplitude spectrum of modified sparker	18
2.6 Hydrophone receiving array and filter	19
2.7 Array response for line array	22
2.8 Comparison of line array vs single phone at shallow water site	24
2.9 Comparison of line array vs single phone at deep water site	25
3.1 Flow chart for data processors	35
3.2 General operation of bandpass filter	39
3.3 General procedure for spiking deconvolution	43
3.4 Common sources of multiple reflections	45
3.5 General procedure for predictive deconvolution	47
3.6 Application of swell filter	51
3.7 Instantaneous amplitude of 3.5 kHz profiler	57
4.1 Site plan for Panama City sea trials	61
4.2 Geologic setting for northeastern Gulf of Mexico	63
4.3 HI-DAPT II deep tow configuration	65
4.4 Seismic Profile 13-14.	Appendix B
4.5 Seismic Profile 4-3	Appendix B
4.6 Seismic Profile 16-15	Appendix B
4.7 Seismic tie lines	Appendix B
4.8 Bandpass panels	Appendix B
4.9 Source ghosts	71
4.10 Autocorrelation of a single trace	72
4.11 Prediction deconvolution gap tests	Appendix B
4.12 Prediction operator length tests	Appendix B
4.13 Automatic gain window tests	Appendix B
4.14 Processed seismic Profile 13-14	Appendix B
4.15 Processed seismic Profile 4-3	Appendix B
4.16 Processed seismic Profile 16-15	Appendix B
4.17 Processed seismic Profile 17-18	Appendix B
4.18 Processed seismic Profile 19-20	Appendix B

1.0 INTRODUCTION

High resolution geophysical methods are employed in the offshore environment to obtain a comprehensive picture of the sea-floor morphology, and underlying shallow stratigraphy (Trabant, 1984). Traditionally, sub-bottom profiling systems have existed exclusively in an analog domain. Whereas the advantages of digital data acquisition and processing techniques are well known in exploration seismology, these same techniques have only begun to appear in the high resolution seismic industry. Rapid advances in digital technology have allowed these techniques to be applied to high resolution sub-bottom profilers. This thesis describes the development and field test of a new sub-bottom profiling system which incorporates digital data acquisition and real time processing.

1.1 Review of Sub-bottom Profiling Technology

High resolution geophysical surveys have been performed in the offshore since the early 1960s. High resolution seismic reflection systems operating at acoustic frequencies between 1 and 14 kHz are grouped within the general category of sub-bottom profilers (Trabant, 1984). Within this category, systems can be subdivided into broadband and band limited systems based upon the spectral characteristics of the pressure signature generated by the source (Simpkin and Davis, 1994). Band limited sub-bottom profiling systems were first

developed in the early 1960s at Magnolia Petroleum Company's research laboratory and were based upon a magneto-strictive transducer operating at a frequency of 3.8 kHz. Since that time, a host of band limited systems has appeared. Typically, these systems use broadly resonant piezo-electric or magneto-strictive transducers in a sonar configuration (Simpkin and Davis, 1994). The same transducer is usually used to transmit and receive. An amplified waveform is transmitted to the transducer to provide a burst of acoustic energy. The tuned nature of these systems provides an efficient means to generate sufficient energy for the penetration of soft sediments with a relatively low driving voltage. Data are usually displayed on an electrostatic strip chart recorder and recorded in analog format on magnetic tape.

In most cases, broad band systems are identified primarily by the nature of the pressure impulse that is developed by a sudden release of stored electrical energy into a transducer (Simpkin and Davis, 1994). The most common sources in this category are boomers and sparkers. Although the mechanism by which each generates a pressure wave is different, both are driven from a capacitor bank, usually housed on the ship. A boomer is an electro-dynamic source whereas the sparker generates a pressure wave by vaporizing water as electrical energy is discharged between two electrodes in water. Sub-bottom profilers which use these sources require a hydrophone streamer to record reflected and scattered acoustic signals. Traditionally, data have been displayed on an electrostatic chart recorder and recorded in analog format on magnetic tape.

Another type of broad-band system which has appeared over the last decade is the chirp sonar. This system is similar to the band-limited type as described above in that it uses a piezoelectric transducer to produce a pressure wave. The systems differs in that the chirp source drives the transducer with a computer generated frequency modulated(FM) pulse that sweeps over the frequency range of 200 Hz to 30 kHz (Schock and LeBlanc, 1990). The recorded data are passed through a matched filter to provide the output trace.

Acoustic source technology has remained relatively constant over the last several decades while the handling of sub-bottom profiler data has seen a steady progression into the digital domain. Digital front-end recording systems with high dynamic range analog-to-digital conversion and limited digital processing capabilities have been manufactured by companies such as Elics and GeoAcoustics Limited. The Sonar Enhancement System™ by GeoAcoustics was one of the first digital front-ends to be commercialized. This system offered digital acquisition with a programmable sample rate. Data were stored in digital format on an optical disk. Processing capabilities included bottom tracking, time variant gain and bandpass filtering. The DELPH II™ by Elics offered storage of raw digital data and limited processing such as automatic gain control, high and low pass filters and a swell filter. Post-processing capabilities such as deconvolution are also available.

1.2 Reflection Seismology

The seismic method is by far the most important geophysical technique in terms of expenditures and the number of geophysicists involved (Telford *et al.*, 1976). Much of seismic theory was developed before instruments with sufficient sensitivity to measure seismic events were available. The reflection seismic process uses an acoustic source to impart acoustic energy into the earth. In the case of marine operations, the source is towed in the water column and produces a pressure wave which travels towards the sea floor and into seabed sediments. Acoustic impedance is the product of a material's compressional wave velocity and density. As the acoustic energy encounters a boundary that exhibits an acoustic impedance contrast the energy is partitioned. A very small portion of the incident energy is reflected from the interface. It is this reflected energy that makes reflection seismology possible. Impedance contrasts result from a difference in the physical properties of a material and not necessarily a difference in sediment type. For example, a consolidated mud overlain by a similar material of less density will provide a reflection. Reflection strengths vary not only with the degree of acoustic impedance contrast but also with the geometry of an interface. In cases where a reflecting horizon is smooth the amplitude will be large in comparison to the reflection from an irregular interface with a similar acoustic impedance contrast. A solid knowledge of marine geology and the physical processes that exist in nature is required to interpret a reflection seismic profile.

1.3 Limitations of Conventional Sub-bottom Profilers

Conventional sub-bottom profilers operate in the analog domain. Traditionally the only output from these systems has been a dry paper recorder. A poor choice of filter parameters or time variant gain on the recorder meant that information was permanently lost if analog recording was not available. A second limitation was the inability to enhance the data by removing unwanted artifacts such as surface ghosts, bubble pulses and multiple reflections. These unwanted components often masked reflectors of interest making an interpretation difficult or in some cases impossible. Band-limited sources produce monochromatic data which is not suited for digital processing techniques designed to increase the temporal resolution of the data. Conversely, the broad-band systems had desirable source characteristics but did not have the capability to utilize this bandwidth with advanced processing techniques.

While the digital front-ends described in the Section 1.1 offered a tremendous improvement over traditional analog systems, they still lacked the necessary processing capabilities required to implement the majority of signal processing requirements for high-resolution, sub-bottom data.

1.4 Outline of Thesis

This study details the development of a sub-bottom profiling system, the HI-DAPT II, designed to overcome the limitations of existing sub-bottom profiling systems. The design of the system and hardware necessary to implement such a design are described in Chapter 2. Constraints imposed by real-time operation and physical constraints imposed by the nature of high-resolution sources and survey procedures are also documented in Chapter 2. Chapter 3 describes the signal processing development and explains the rationale behind each of the included processors. A description of the software development environment is also provided. The first major field test of the system, conducted in Panama City, Florida, is described in Chapter 4. This chapter also provides a brief geological description of the test site, an examination of the effectiveness of the processing and the seismic interpretation of the processed data. An attempt to interpret the geologic significance is made using survey data from the Northwest Gulf of Mexico and some well data from the onshore. Conclusions, recommendations and a direction for further research are discussed in Chapter 5.

2.0 SYSTEM DESIGN AND DESIGN CRITERIA

The main objective in designing the HI-DAPT II sub-bottom profiler was to develop a computer based system which was capable of acquiring high-quality, sub-bottom data and processing these data in the time interval between successive shots. It was important that the system be adaptable to a large number of sources and be able to operate in various marine and freshwater environments. The system would store digital data and provide a high quality graphical output on both a CRT and paper record. Conventional post-stack processing algorithms, written to run on a digital signal processing (DSP) board, would be used to provide a high quality processed section during data collection. The processing parameters were to be menu selectable such that they could be adjusted during a survey to ensure high quality data. Where possible, off-the-shelf system components were used to reduce the development time (see Table 2.1). The followings sections describe the design criteria and hardware configuration used in the development.

2.1 General System Description

The HI-DAPT II Sub-bottom Profiling System shown in Figure 2.1 is best described in terms of the following three subsystems: (1) source, (2) receiver, and (3) data processing and display. In brief, the source sub-system consists of a modified multi-element sparker source mounted in a custom built tow body, a seismic energy system and a custom built

Table 2.1 Commercial products used in developing HI-DAPT II Sub-bottom Profiler.

Component Name	Function
Huntec Seismic Energy Units Model M3 PCU Model 2000 ESU	generate and store energy required for sparker to generate acoustic pressure wave
Ariel DSP 96002 digital signal processing board	digital signal processing board with Motorola DSP96002 parallel processor and analog-to-digital convertors
Frequency Devices Model 902 filter and amplifier	2 channel programmable high pass filter and amplifier for signal conditioning prior to analog-to-digital conversion
Alphatronix INSPIRE II optical disk drive	1 Gbyte erasable magneto-optical disk drive for data storage
Oyo GS 612 thermal plotter	provide high quality hard copy of processed data
Sona 486 PC	486, 33 MHZ PC with SVGA CRT for display and host to DSP board
Telydne Geotech Research Array	2 channel hydrophone streamer for recording sub-bottom data

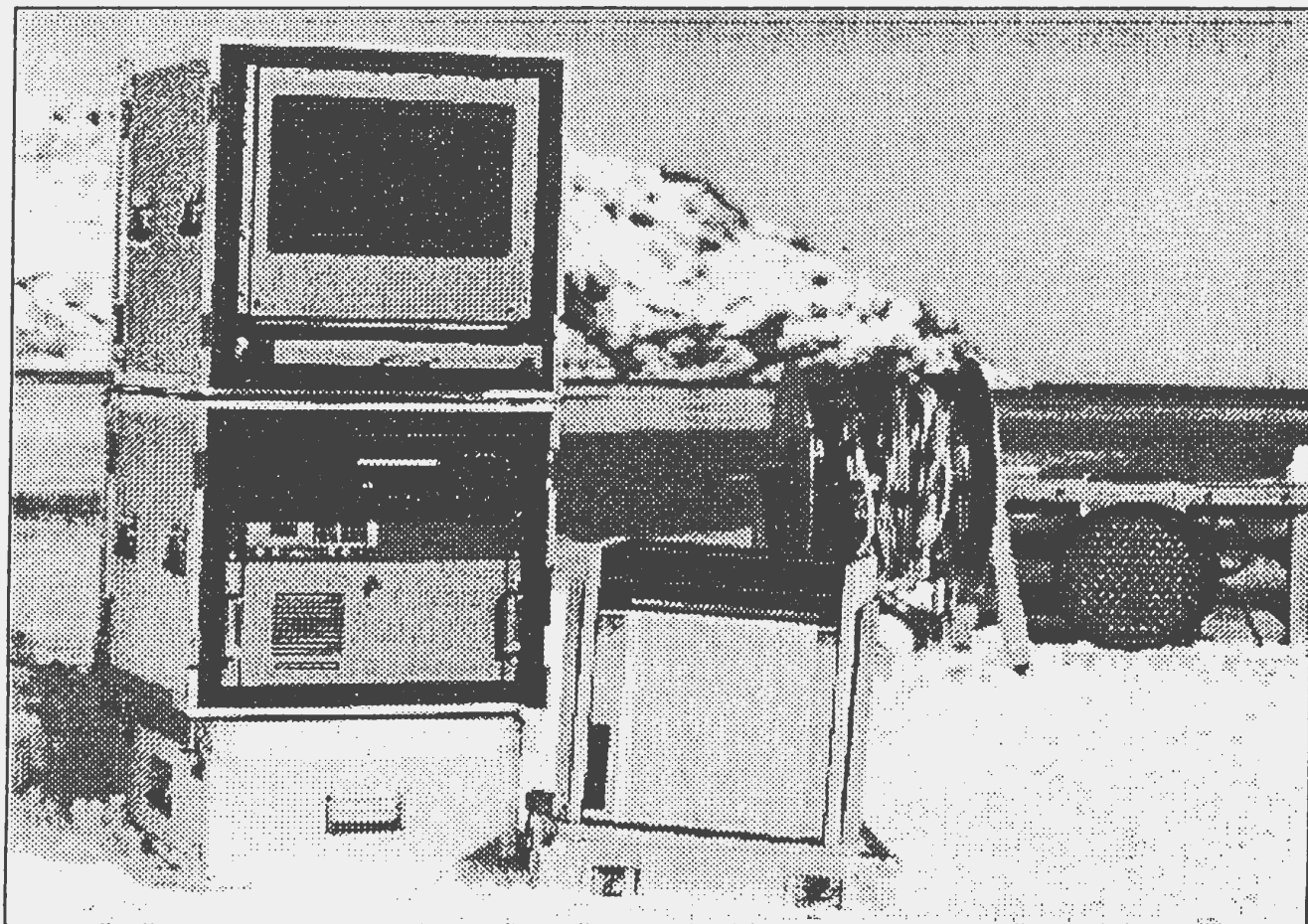


Figure 2.1 The HI-DAPT II Sub-bottom Profiling System.(L-R) Rack mount digital front end, thermal plotter, hydrophone streamer and reel, sparker source in towfish.

100 m power cable complete with underwater mate-able connections. The receiver subsystem includes a two-channel hydrophone streamer with a 100 m lead-in cable and a two-channel programmable filtering amplifier. The data processing, display and storage subsystem includes the following rackmounted components: (1) a 486 PC which contains a two-channel DSP processing board, (2) custom acquisition/processing/display software, (3) a CRT display, (4) an erasable optical disk drive, (5) a thermal plotter, and (6) an uninterrupted power supply.

The general operation of the system is described as follows. The processing software initiates the generation of a trigger pulse simultaneously with the onset of analog-to-digital (A/D) conversion. The trigger pulse causes the seismic energy unit to discharge electrical energy through the sparker source generating a pressure wave in the water column. This pressure wave is transmitted through the water and reflected from the seabed and from other acoustic boundaries located below the seabed. The hydrophone array receives these pressure waves together with environmental noise and transmits electrical signals to the analog amplifier. The returns from both channels are passed through analog high pass filters to remove the effects of the ocean swell/waves and amplified (if required) to match the full scale sensitivity of the analog-to-digital convertors. The analog signals are digitized by the A/Ds contained in the PC. Raw digital data are stored together with navigation information on an optical disk. Raw data then undergoes signal processing and is displayed on a CRT with a hard copy generated on the thermal plotter. The following subsections describe the hardware

and system configuration in greater detail.

2.2 Acoustic Source Characteristics

An ideal seismic source should produce an instantaneous positive shock wave, characterized by a very quick rise in pressure, followed by a rapid decay (Trabant, 1984). Table 2.2 lists a number of marine seismic sources available for use today which strive to attain this goal. The type of source used varies with the depth of penetration and the degree of temporal resolution required. As can be seen from Figure 2.2, a trade-off exists between a source's frequency content (which in turn governs temporal resolution) and the depth of penetration. This trade-off exists because of the preferential attenuation of high frequency seismic signals as they pass through the subsurface.

The source used in the HI-DAPT II profiling system is an adaptation of a multi-element sparker array. This source, developed at the Centre for Cold Oceans Resources Engineering for use on a stationary seismic device, is described in detail by English *et al.* 1991. The source shown in Figure 2.3 is constructed of a cylindrical high density polyethylene container [1] measuring 152 mm in height and 457 mm in diameter. Contained within this housing is a 13 mm polyethylene disk [2] secured by polyethylene welding. Attached to the underside of this disk is a 3 mm thick stainless steel plate [3] which is connected to the high voltage line of the seismic energy power supply. The source can be equipped with a

Table 2.2 Characteristics of common marine sources used in the acquisition of marine seismic data(after Trabant, 1984).

Source	Energy	Firing Rate	Pulse	Penetration
EG&G Boomer	electro-dynamic plate	0.17 sec	400-14,000 Hz 107 m bar m	40 m
EG&G 1 kj sparker	electrical capacitive discharge	0.75 sec	200-5,000 Hz	150 m
EG&G 4.6 kj sparker	electrical capacitive discharge	2 sec.	100-3,000 Hz	450 m
EG&G 8 kj sparker	electrical capacitive discharge	2 sec.	70-1,500 Hz	1,200 m
EG&G 15.4 kj sparker	electrical capacitive discharge	2 sec.	40-500 Hz	3,500 m
Flexichoc	implosion of hydraulic separated plates	2 sec.	30- 1,000 Hz 3.0 bar m	1,500 m
Minisleeve exploder	explosion within elastic sleeve	0.33 sec. sequentially or 2 sec. otherwise	50-1,000 Hz 5.0 bar m	1,500 m
245 litre watergun	implosion of water slug	0.5 sec.	50-1,000 Hz 3.8 bar m	1000 m
655 litre airgun	implosion of air bubble	0.25 sec.	10-150 Hz @ -20 dB 1.25 bar m	600 m

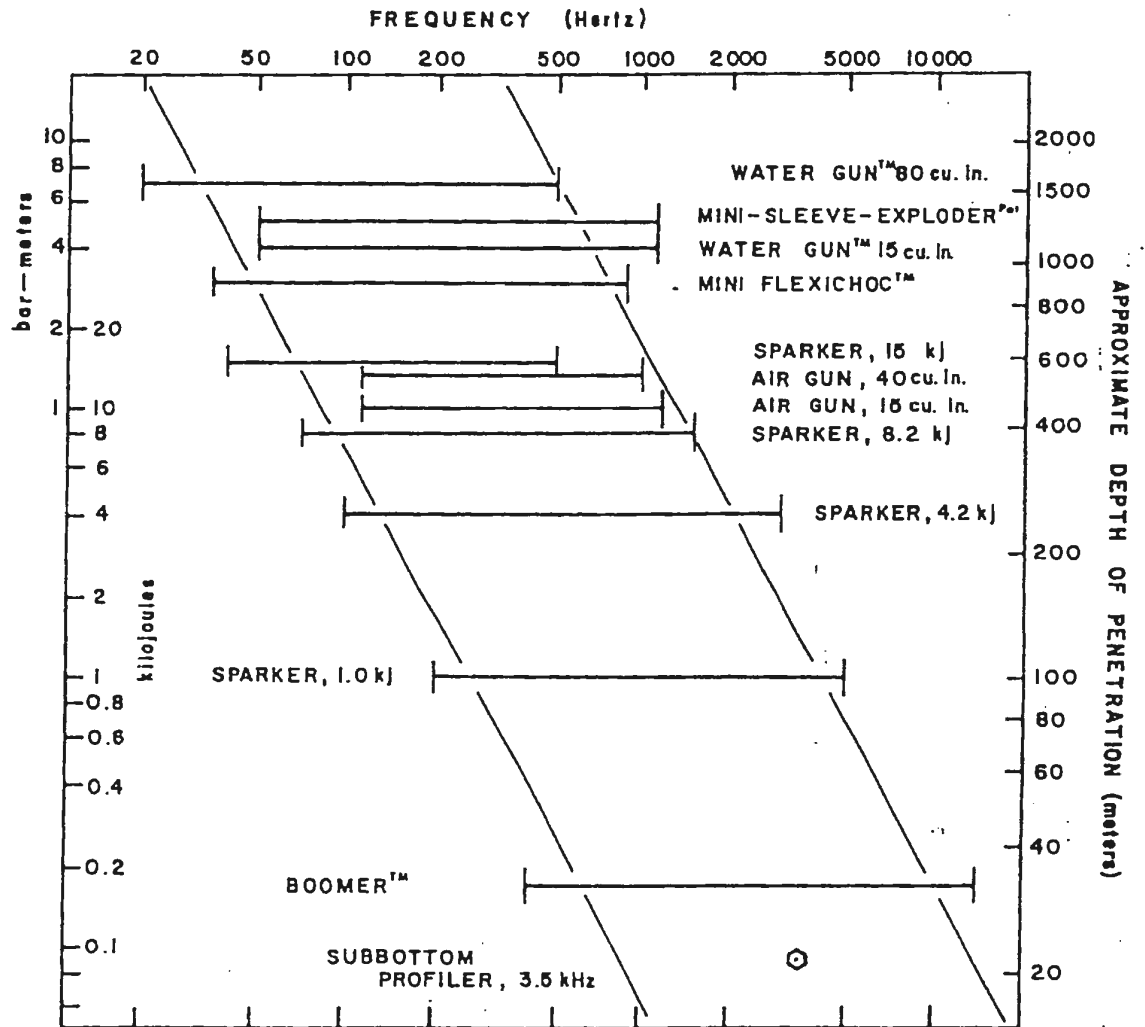
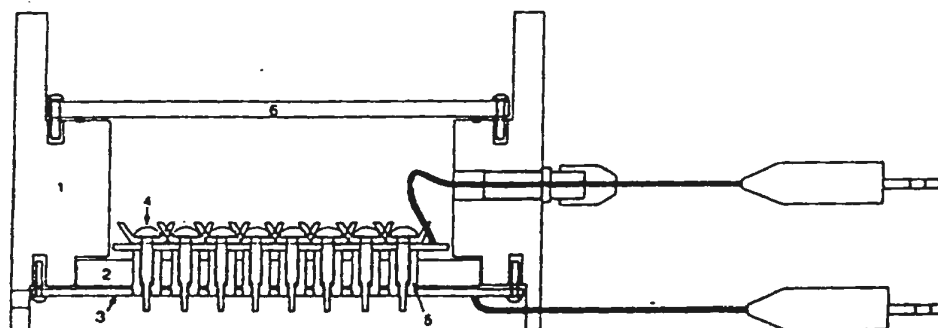
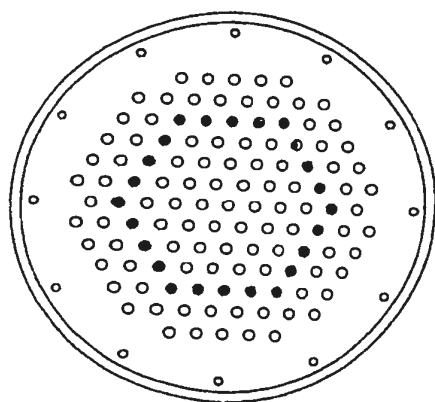


Figure 2.2 Graphical comparison of a number of high resolution seismic source parameters, frequency, power, and penetration (after Trabant, 1984).

Cross-sectional view of sparker



- [1] outer jacket constructed from high density polyethylene cylinder
- [2] 13 mm polyethylene disk secured with polyethylene welding
- [3] 3 mm stainless steel plate connected to the high voltage positive (+)
- [4] stainless steel electrodes connected to the high voltage negative (-)
- [5] electrically insulating nylon inserts
- [6] top cover

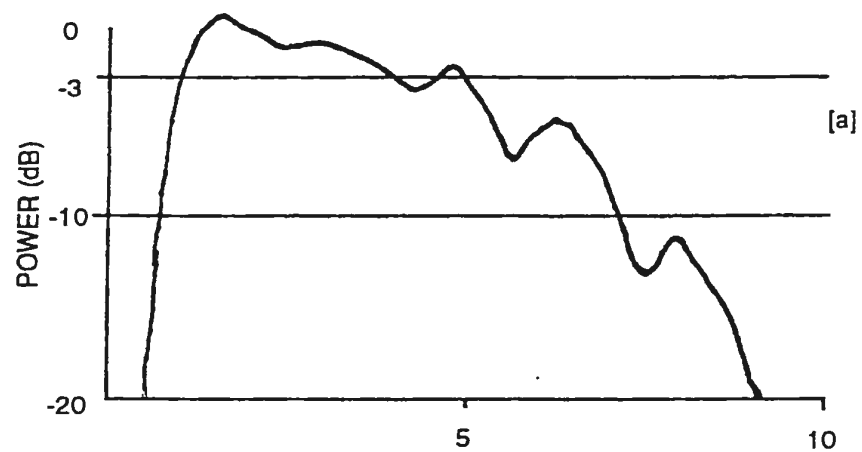


**Bottom view of
sparker source**

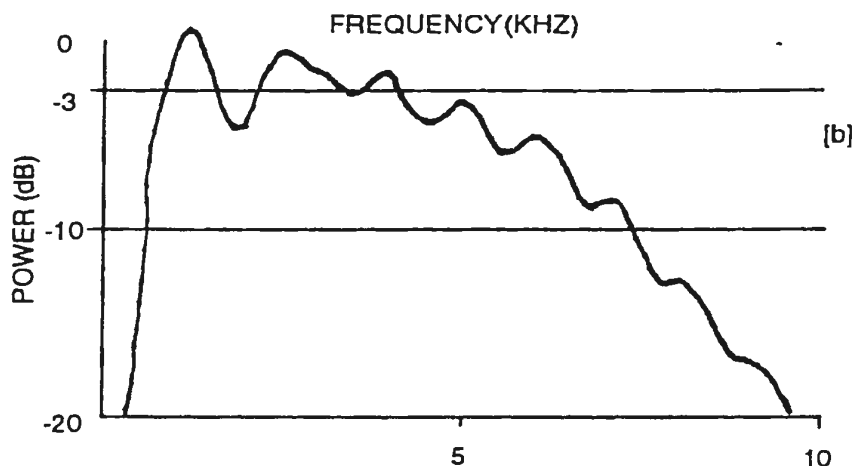
Figure 2.3 Cross-sectional view of C-CORE multi-tip sparker source (TOP) and plan view showing electrode configuration (BOTTOM) (Black electrodes represent those active for Panama City sea trials (see Chapter 4)).

maximum of 121 stainless steel electrodes [4], all machined to .05 mm tolerance. These tips are threaded into nylon inserts [5] which in turn are threaded into the polyethylene and stainless steel disks. The stainless steel electrodes are connected to the high voltage ground of the seismic power energy power supply. The nylon inserts insulate electrically all but the tips of the electrodes from the stainless steel plate. All electrodes are connected electrically within the housing and the entire housing filled with a petroleum wax to prevent corrosion of the electrodes and eliminate the air cavity which could cause acoustic reflections. A top cover [6] constructed of high density polyethylene is attached with ten screws. Figure 2.4 shows the amplitude spectra for the 480 J, 750 J and 1080 J power settings using the 121 tip configuration. The figure demonstrates that as the power increases from 480 J (A) to 1080 J the spectrum decreases in both bandwidth and center frequency (mid-point of the amplitude spectrum at - 3 dB) decrease.

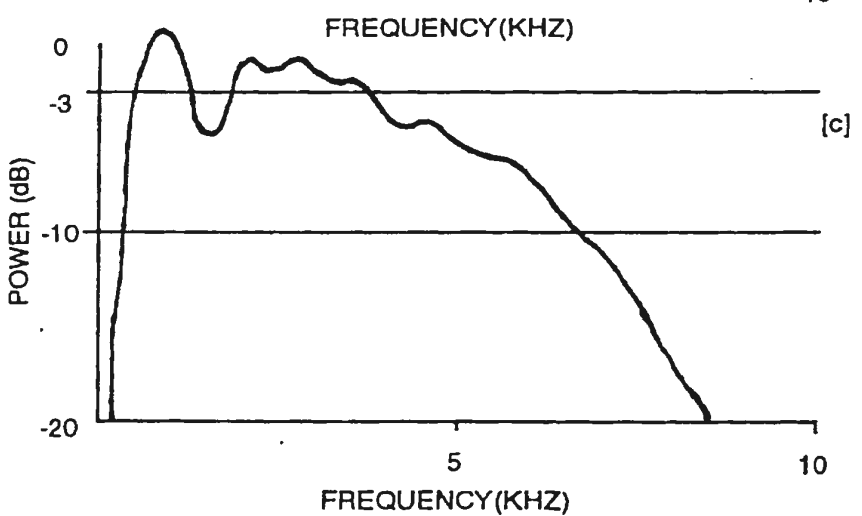
The sparker was modified to provide a larger amplitude signal for use in a surface towed mode. Originally the electrical connections between all but twenty-five electrodes were disconnected such that the energy-per-tip, and hence the amplitude of the signal, would be increased. This configuration, tested in Conception Bay in June 1993, provided an adequate signal for approximately an hour of use before the amplitude of the signal began to decrease. A close examination of the source revealed that tips which were electrically disconnected from the seismic energy power source were firing. This resulted from the leakage of seawater into the housing reconnecting the isolated tips thereby decreasing the



480 J
bandwidth = 4200 Hz
centre freq. = 3000 Hz



750 J
bandwidth = 3800 Hz
centre freq. = 2300 Hz



1080 J
bandwidth = 3500 Hz
centre freq. = 2150

Figure 2.4 Amplitude spectra for a 121 tip sparker at power level settings of [a] 480 J, [b] 750 J, [c] 1080 J.

energy-per-tip and the amplitude of the seismic signal. Leakage in the nylon inserts also provided an alternate path to ground for the electrical energy. This problem was overcome by removing the isolated tips and plugging the holes with 13 mm nylon screws. The remaining tips were removed from their nylon inserts and re-sealed with a silicon sealant before being rethreaded into the sparker body. Figure 2.5 shows a record and the resulting spectral analysis from the modified sparker recorded in the Gulf of Mexico. A comparison of this figure with Figure 2.4[c] shows the effect of varying the number of Joules per tip. The frequency spectrum of the modified sparker signature is narrower in bandwidth and lower in center frequency than that displayed in Figure 2.4[c]. Although not evident from Figures 2.4 and 2.5, the modified sparker produces a larger amplitude signal than its 120 tip counterpart. The tradeoff for the larger amplitude signature is the magnitude of the bubble pulse (Figure 2.5 at 6 ms.). The bubble pulse, with a period of 4 ms, manifests itself in the frequency spectrum as the 250 Hz comb. The bubble effect can be reduced by digital signal processing and is not as serious an impediment as it would be for a conventional analog system.

2.3 HYDROPHONE ARRAY DESIGN

The HI-DAPT II system is equipped with a custom built streamer. The streamer consists of twenty individual hydrophones configured as two separate channels (Figure 2.6). The first channel, a point receiver, consists of the innermost hydrophone located 4293 +/- 5 cm. from the head of the streamer. The second channel contains the remaining nineteen

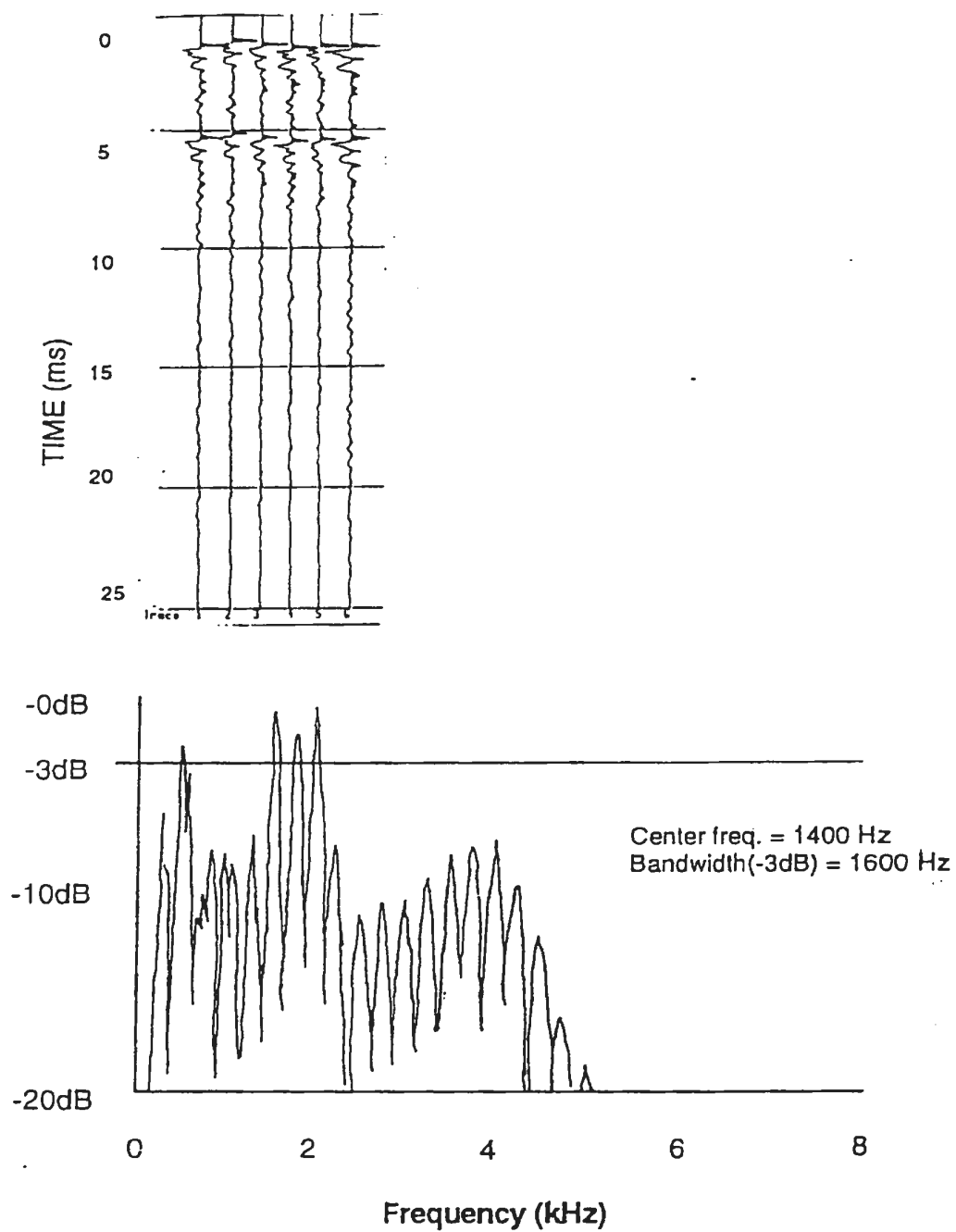


Figure 2.5 Seabed reflection and spectral characteristics for modified C-CORE sparker(24 tips) at 1080 J power level recorded by line array in Gulf of Mexico.

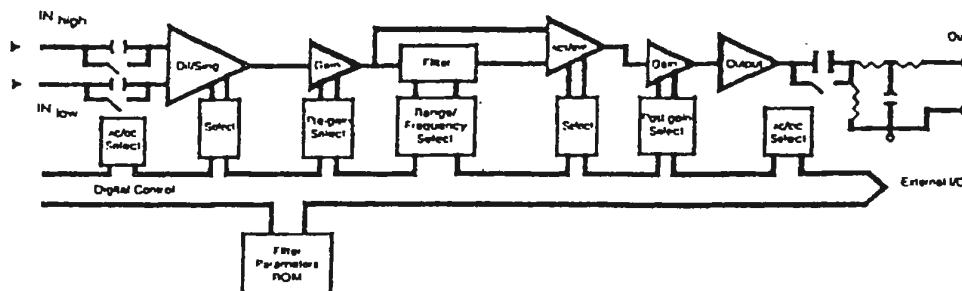
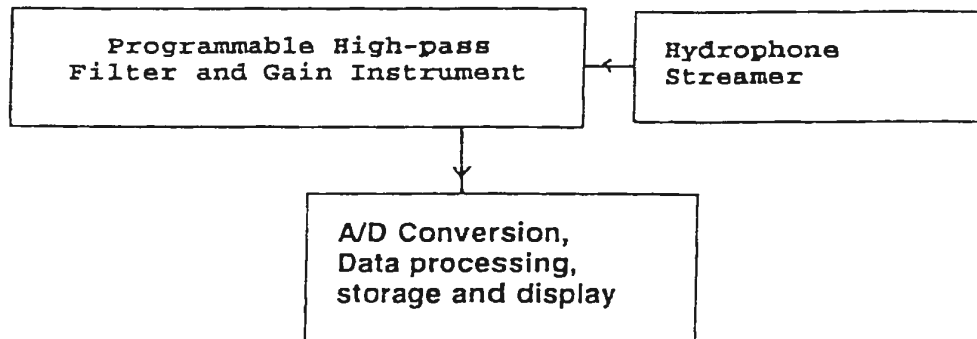
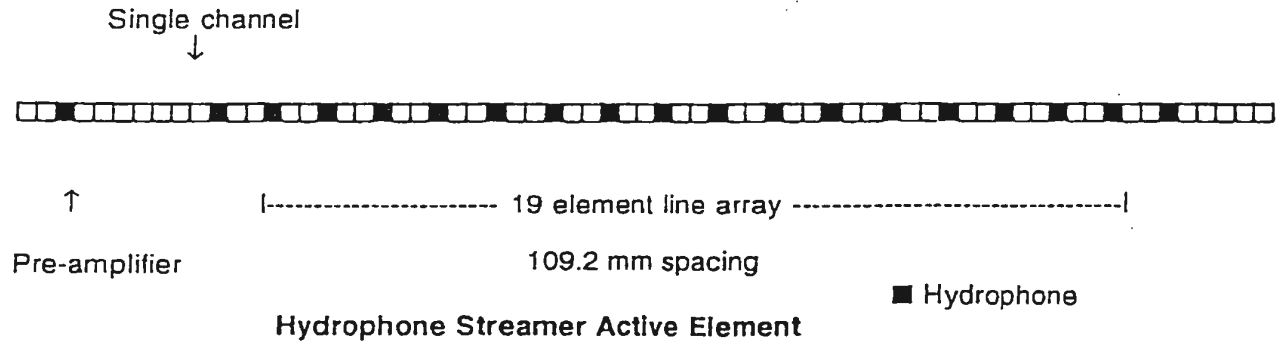


Figure 2.6 (Top) Schematic of hydrophone streamer active element. (Middle) Operational assembly. (Bottom) Schematic of the programmable filter gain instrument.

hydrophones connected electrically to form a line array and provide a single output. The output of each channel is passed through a voltage preamplifier located in the head of the streamer. The streamer has a 100 m lead-in cable and a 15 m rope tail. The rope tail is used to keep the active element under tension such that it remains straight when under tow. When operated in surface towed mode the lead-in cable is fitted with buoyancy devices such that the active element remains approximately 0.25 metres below the water/air interface. When operating in deep-tow mode a fairing constructed of 9 mm nylon rope is used to reduce the effect of strumming in the cable. The two-channel configuration was chosen to allow the streamer to be adaptable to both modes of operation and a variety of different water depths.

2.3.1 LINE ARRAY

The line array in the HI-DAPT II hydrophone streamer is an equally weighted line array. The array consists of 19 hydrophones of equal sensitivities and a uniform spacing of 109 +/- 5 mm connected electrically to provide one output. The line array provides a better signal to noise ratio than does the single channel by canceling random noise as well as preferentially receiving signals whose wavefronts are propagating vertically. A wave approaching the array in the vertical direction will affect each hydrophone simultaneously and constructively. Waves approaching at angles other than vertical will affect each individual hydrophone at different times and hence cause a degree of destructive interference. The degree of destructive interference will depend upon the angle of incidence and the frequency

of the approaching wave train.

The response of an array is shown by the means of an array response diagram. The response of a equally weighted linear array can be determined as follows:

$$R = \frac{1}{N} \frac{\sin(N\pi(\frac{d}{\lambda_a}))}{\sin(\pi(\frac{d}{\lambda_a}))} \quad (2.1)$$

Where: R = *normalized array response*
 λ_a = *apparent wavelength*
 N = *number of array elements*
 d = *array element spacing*

Figure 2.7(a) shows the normalized array response diagram for a 19 element equally weighted line array. The values of (d/λ_a) are given only up to a value of 0.25, but values of up to .50 are valid since the inverse, $(\lambda_a/d)=2.0$, is the limiting condition of two hydrophones per wavelength to avoid spatial aliasing. The diagram shows that the array response reverses sign at $(d/\lambda_a) = .05$ and $(d/\lambda_a) = .10$. The first half cycle of the curve ($0 < (d/\lambda_a) < 0.05$) is considered the pass region of the array. The portion of the curve beyond $(d/\lambda_a) = .05$ is considered the reject region. Waves for which $(d/\lambda_a) > 0.05$ will be attenuated to at least .15 of the amplitude of the signal from 19 hydrophones bunched into a single location. Figure 2.7(b)

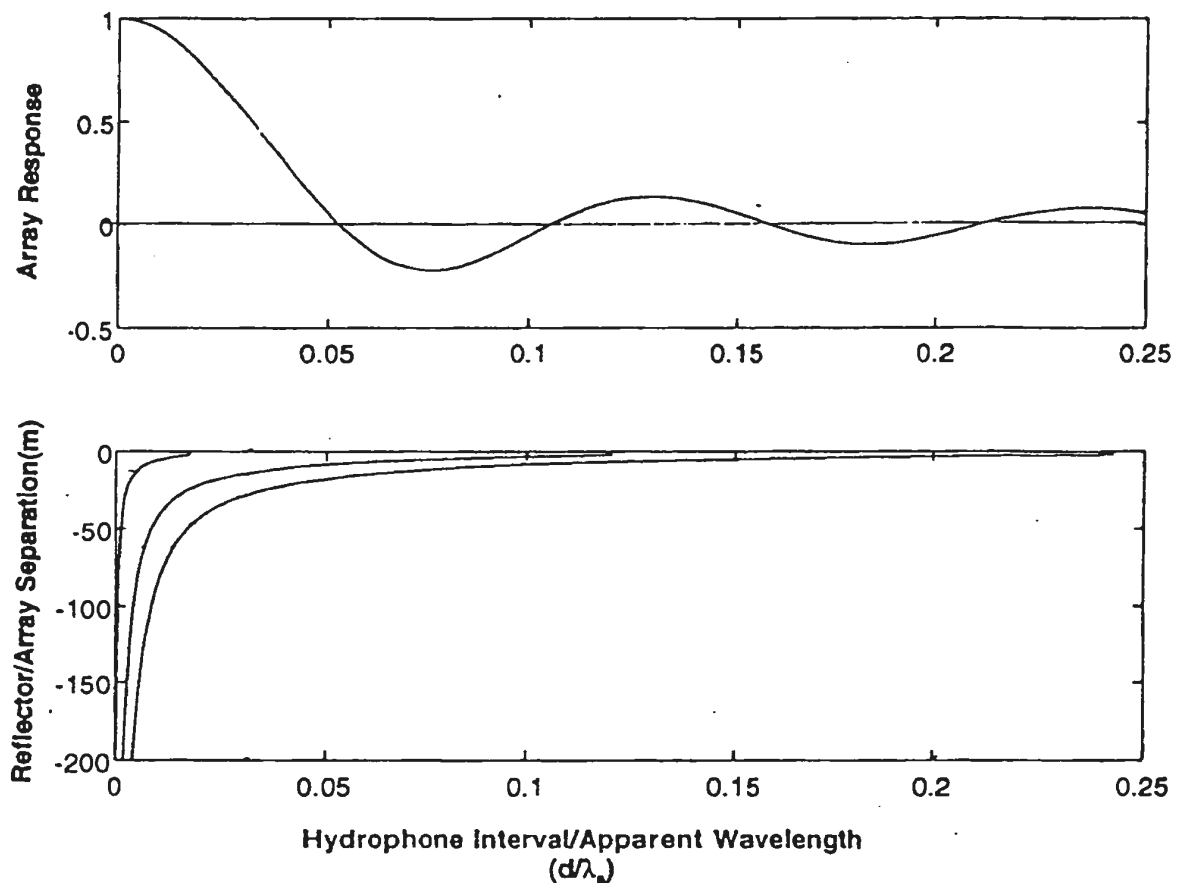


Figure 2.7 (TOP) Array response curve for a nineteen element equally weighted array. (BOTTOM) Three curves representing the ratio of hydrophone interval to apparent wavelength for increasing depths at frequencies of 300 Hz (left curve), 2000 Hz (middle curve) and 4000 Hz (right curve).

shows three curves representing ranges of (d/λ_s) for seabed reflections from increasing depths, observed with a 109.2 mm hydrophone separation and three frequency components of the sparker source. From these three frequency components, we can construct two bandwidths, 300-2000Hz (25 tip, 1080 J) and 300-4000Hz (121 tip, 1080 J). From the diagram, it is evident that at reflector depths less than 20 m the array will cause a degradation in the 4000 Hz component of the signal to approximately -3dB, thus behaving as a low pass filter.

To further illustrate the behavior of the array Figure 2.8 shows seismic records of both channels acquired with the towbody approximately 13 m below the surface and 150 m above the seabed. Figure 2.8 illustrates the benefits associated with the multi-element line array over a single hydrophone when receiver/reflector separation is large. Figure 2.8(b), data from the line array, shows much stronger images of reflectors between 200 ms and 210 ms than the equivalent data from the single hydrophone (Figure 2.8(a)). Figure 2.9 shows seismic records collected at Port de Grave, Conception Bay, Newfoundland with the towbody located at a maximum of 3.6 m above the seabed.

Examination of the records show the loss of the high frequencies in the data acquired with the line array in comparison to the data from the single hydrophone. A small in-filled channel evident on the single channel section can not be distinguished on the line array section.

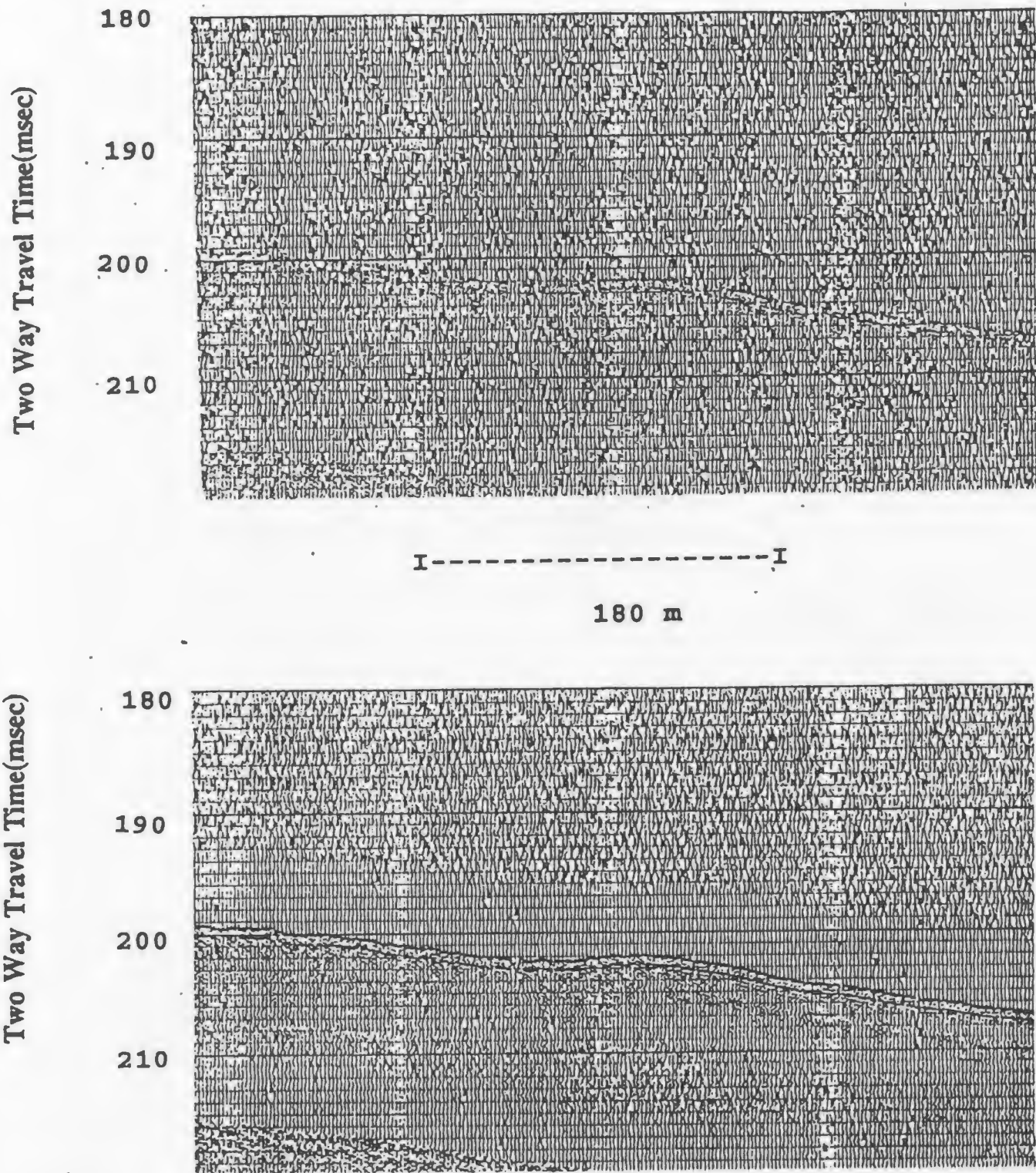


Figure 2.8 Comparison of single hydrophone (A) and line array (B) to illustrate the benefits of the multi-element line array when operating streamer large distances above the seabed. Data collected from a deep tow in the Gulf of Mexico. The source and streamer were approximately 13 m below the surface and 150 m above seabed.

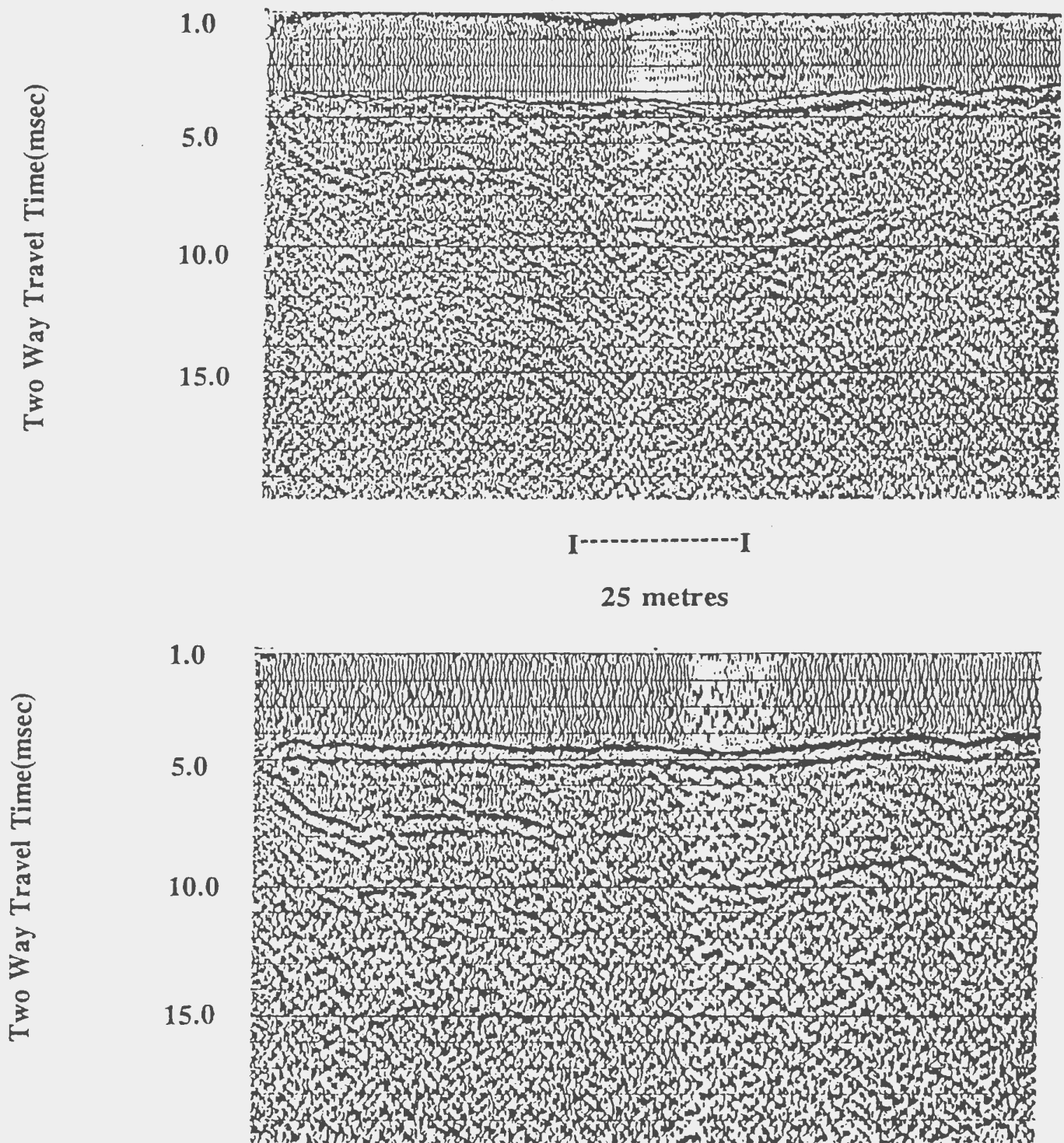


Figure 2.9 Comparison of single hydrophone (TOP) and line array(BOTTOM) to illustrate the benefits of the single hydrophone channel when operating streamer at small distances above the seabed. Shallow water seismic data collected in Port de Grave, Conception Bay, Newfoundland. Note the loss of the high frequency component in the section from the line array.

2.4 Digital Data Acquisition

Analog signals returning from the hydrophone streamer are passed through an analog high-pass filter, amplified if necessary to match the full scale sensitivity of the A/D convertors and digitized with 16 bit A/D convertors. The A/D convertors are located on the DSP board. The following sections describe the analog signal conditioning and the A/D conversion.

2.4.1 Analog Signal Conditioning

Initially the analog input stage consisted only of an analog amplifier together with adjustable blanking and clipping circuitry. The clipping circuit was set at $5 V_{p-p}$, the equivalent of the full scale sensitivity of the A/D convertors. The clipping circuit was equipped with two LED's to indicate when the signal was amplified to $5 V_{p-p}$. This arrangement would allow the direct arrival to be blanked and the seabed reflection to be amplified to a $5 V_{p-p}$ in order to retain the complete 16 bits of resolution at the seabed. The first field trials proved that signal levels in the streamer due to the ocean swell and wave induced noise were orders of magnitude larger than our seismic signals and acted as a low frequency carrier wave. When the amplitude of the carrier wave exceeded $5 V_{p-p}$ it would be clipped by the signal protection circuit and the data was lost. The analog front-end was replaced by an off-the-shelf dual-channel programmable filter instrument. This unit is a two-

channel amplifier equipped with two eight pole Butterworth high pass filters. The amplifier is capable of providing signal gain ranging from 1.0 to 13.75 in 0.05 gain increments both prior to and after filtering.

2.4.2 Analog-to-digital conversion

The HI-DAPT II processing system is equipped with two-channels of high performance, 16 bit, analog-to-digital and digital-to-analog conversion on a daughter card mounted on the DSP board (Specifications for the DSP 96002 board are provided in Appendix A). Each channel provides phase-coherent, synchronous (within 10 ns) sampling of the two-channels. The convertors themselves are connected to the DSP board by means of a high-speed serial interface. The convertor's full scale sensitivity is adjustable from 500 mV_{pp} to 5.5 V_{pp} by means of two multi-turn trimpots located on the daughter cards. The full scale sensitivity was adjusted to 5 V_{pp} using a function generator in parallel with an oscilloscope. Table 2.3 shows the A/D convertor's sampling frequencies. These values are software programmable and range from 6 kHz to 96 kHz with 16 bit resolution or from 32 kHz to 384 kHz with 12 bit resolution. The sampling frequencies available on the HI-DAPT II are listed in Table 2.3. The length of the record collected is limited only by the RAM available on the DSP board and PC. Currently record lengths of 2048 and 4096 samples are implemented.

Table 2.3 Programmable DSP 96002 Sample Rates.

Sample Rate Index	16 bit mode* Sample Rates (Kilo-samples/sec)	12 bit mode Sample Rates (Kilo-samples/sec)
0	6.000	24.000
1	8.000	32.000
2	11.025	44.100
3	12.000	48.000
4	16.000	64.000
5	22.050	88.200
6	24.000	96.000
7	32.000	128.000
8	44.100	176.400
9	48.000	192.000
10	64.000	256.000
11	96.000	384.00

* only 16 bit mode currently implemented in HI-DAPT II software.

The A/D convertors are sigma-delta oversampling devices. Prior to the advent of sigma-delta oversampling, convertors relied on either successive approximation or dual slope integration methods of pulse code modulation to encode the analog signal. Sigma-delta oversampling devices move most of the elements of the conversion process from the analog to the digital domain. The greatest benefit of the sigma-delta oversampling is the near perfect nature of the A/D's anti-aliasing filters. The anti-aliasing filter has a flat pass-band (± 0.0003 dB), excellent stop band (96 dB) and linear phase. The trade-off for the ideal filter characteristics is the group delay. This delay, inversely proportional to the sample rate, is particularly troublesome for real-time applications. In this case, the delay prevented the D/A convertor from being used to produce an external trigger for the seismic energy unit simultaneous with the onset of sampling. A software generated trigger pulse is delayed by 35 samples at the analog output of the D/A convertor. To provide a real time trigger a BNC connector was wired to a header pin for Interrupt 11 on the DSP board. This pin provides a TTL level signal which can be at either of two states, 0 V or 5 V. No interrupt handler was installed on the PC's motherboard such that the generation of an interrupt would affect the regular operation of the PC. An assembler routine was written to toggle the interrupt 11 bit high and low. This routine was used to generate the square wave pulse required to trigger the seismic energy unit. The call to the trigger routine was placed directly in front of start-up of the A/D convertors in the software to minimize the delay between source ignition and the first sample in the record.

2.5 Data Processing, Display and Storage

The HI-DAPT II system is configured to acquire two 2048 or 4096 point records per shot. The raw 16 bit data is converted to 4 byte floating point and stored in binary format on a 1 gigabyte optical cartridge in an erasable optical disk drive to allow post-processing if required. Data processors, described in detail in the next section, are selectable from a pop-up menu displayed with the data on a CRT display. All signal processing is done on a DSP chip contained on a board within the PC, which serves as an interface for the DSP board. The PC is responsible for the graphical display of the data, arranging the data in the proper format for hard copy output and the transfer of data to the optical disk drive unit. Signal processing, described in detail in the next section, includes noise spike removal, bandpass filtering, predictive and spiking deconvolution, swell compensation, first break picking, manual and automatic trace muting, horizontal stacking, automatic gain control and instantaneous attributes. Processed data can be displayed on a CRT in either wiggle trace or variable area format. A colour coded display of the instantaneous attributes is also available from the user menu. A hard copy of the data is continuously generated on the thermal plotter. Hard copy and screen display parameters are kept separate to allow a user to zoom in on an area of interest on the CRT without affecting the hard copy. Trace ID number, processing parameters and a time stamp are stored in a trace header on the optical drive.

2.6 HI-DAPT II Overview

The proceeding sections detailed the physical aspects of the HI-DAPT II sub-bottom profiling system. The system is designed be adaptable to a large number of operating environments. The sparker source, in marine applications, provides the ability to vary its spectral characteristics depending on the desired resolution and penetration depth. The flexibility in sample rates allows the use of acoustic sources of different spectral characteristics. The two-channel configuration provides two different views of the data and allows operation in shallow as well as deep water. The ability to deep-tow the system allows a reduction in the portion of the seabed insonified by the acoustic source thus increasing the spatial resolution. Processing and display of data during data acquisition yields a higher quality output than that available with conventional analog systems. The storage of raw data in digital format allows post processing to be performed.

3.0 Data Processing Software Development

Post processing of exploration seismic data revolutionized the exploration seismic industry in the 1960's. Rapid advances in digital computer technology made it economically feasible to apply processes adapted from information theory to seismic data (Telford *et al.*, 1976). Application of these techniques allowed geophysicists to increase both the coherency and the temporal resolution of the data.

In contrast to conventional exploration seismology, sub-bottom profiling still exists primarily in an analog domain. This is due mainly to the inability of the user sector to justify the additional costs associated with digital systems and the post processing of the data. The ability to process sub-bottom data during data acquisition would overcome most of the problems associated with the cost of post processing. This ability would also allow the user to select better data acquisition parameters (ie. source power level and frequency content, towing speed) based on a higher quality record than is available with an analog system. Until the recent development of low cost digital signal processing (DSP) technology it has not been economically justifiable to process single channel seismic data in real time.

The following sections describe the implementation of conventional seismic data processing techniques on a DSP embedded in a PC chassis to enable the processing of single channel sub-bottom data in real time. The first section describes the software development

environment. The second section describes each processor together with a list of its user selectable parameters. In some cases, the benefits of the processing are illustrated by means of example. The last section briefly describes the CRT and hardcopy display utilities.

3.1 Software Development Environment

To understand the software development environment a brief description of the general operation of the DSP within the PC is required. The DSP is an I/O mapped peripheral that uses eight consecutive I/O addresses . All data transferred to and from the DSP use these I/O ports. Once running, the DSP drives the HI DAPT II system with the PC providing the link between the DSP and user. All requests for data are generated by the DSP. An executable routine running on the PC downloads a file to the DSP that contains the desired instructions and then waits for requests from the DSP.

There are two distinct programming environments within which the HI-DAPT II software was developed. The executable routine which runs on the PC services requests from the DSP, displays the processed data on a CRT and handles the transfer of data to the plotter and disk drives. This program was written in the C programming language. The processing software, which runs on the DSP board is also written in C and compiled with a special compiler/assembler which has the ability to optimize the code for the parallel nature of the DSP chip. The fast Fourier transform (FFT) was written in assembler language to optimize

execution time since data must be processed between successive shots. The external trigger algorithm was written in assembler to enable access to the DSP's interrupt service.

3.2 HI-DAPT II Data Processors

Each processor on the HI-DAPT II was designed with a specific purpose. However, the overall objectives are to increase the signal-to-noise ratio and to improve the temporal resolution in the processed data. Figure 3.1 gives a flow diagram which illustrates the order of the processors available on the HI-DAPT II. The majority of processors in the flow can be either included or excluded by switching a flag available from the user menu. The following sub-sections describe each of the processors together with its associated user selectable parameters.

3.2.1 Convolutional Model for a Seismic Trace

Seismic data processing techniques have evolved since the advent of digital computers. The basic model for a recorded seismic trace is known as the convolutional model. The building blocks for the convolutional model as described by Robinson and Treitel (1980) are given in equation 3.1.

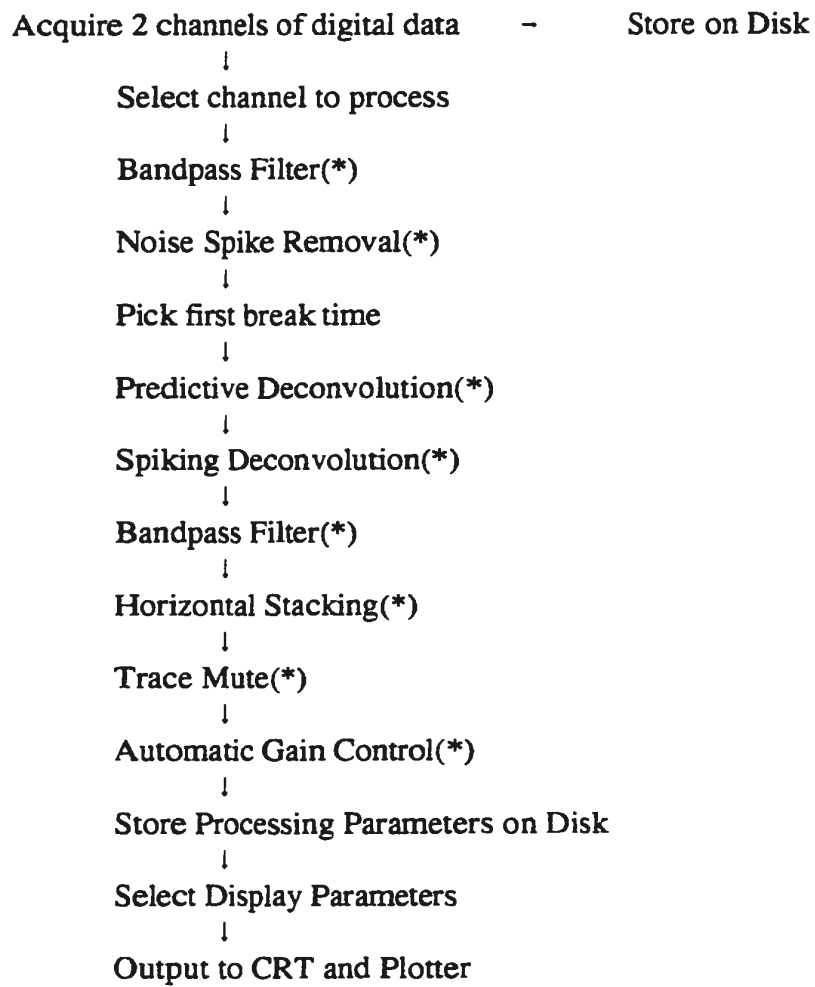


Figure 3.1 Flow chart illustrating the processing flow for HI-DAPT II data process.
* user menu selectable.

$$x(t) = w(t) * e(t) + n(t) \quad (3.1)$$

Where: $x(t)$ = *recorded seismic trace*
 $w(t)$ = *source wavelet*
 $e(t)$ = *earth response*
 $n(t)$ = *random noise*

There are a number of implicit assumptions in the model. They are that the earth is composed of homogenous horizontal layers that acoustic energy impinges upon these layers at normal incidence thus not generating shear waves, and that the source wavelet is known and does not change with its passage through the earth. In general an acoustic source generates a pressure wave which passes through the earth and is reflected from boundaries with differing acoustic impedances. This reflected energy is recorded by receivers which also record environmental noise and even generate their own noise. The basic seismic wavelet is modified as it passes through the earth causing the reflected signal to differ from that which was input. In marine work the basic seismic wavelet can be measured in the water column but not at any intermediate point of its travel through the solid earth. Hence, the basic seismic wavelet is not known. Environmental noise is assumed to be random. However, in many cases noise is coherent and can exist in the same frequency band as that of the source signal. The success

of processing depends upon the degree to which the assumed system properties are valid. The experience is that in spite of the limitations of these assumptions, digital processing does enhance the data.

3.2.2 Bandpass Filters

A seismic signal is composed of primary reflections, multiple reflections, random noise and coherent noise. In cases where the frequency content of the noise is within the bandwidth imposed by the sampling frequency and outside the bandwidth of the seismic source signal, bandpass filtering can be used to remove this noise. Caution should always be exercised when applying such a filter because a reduction in the bandwidth of a signal also means a reduction in the temporal resolution. As seen in the data processing flow diagram, bandpass filters are available immediately after data acquisition and again after the application of the deconvolution processors. These zero phase filters are designed and applied in the frequency domain. The user specifies four values to design the filter. These values (low cut, low pass, high pass and high cut) represent the pass band and reject bands for the filter. The amplitude spectrum of the data to be filtered is modified while the phase spectrum is retained. The amplitudes of frequencies between the high and low pass portions are multiplied by a value of one. The amplitudes of frequencies between the pass and cut values are multiplied a linear ramp extending from a value of one at the pass frequency to a value of zero at the cut frequency. Amplitudes of all other frequency components are multiplied by zero. The

resulting amplitude spectrum and the original phase spectrum are passed through an inverse fast Fourier transform routine to obtain the filtered data. The user is cautioned that the corner frequencies are defined at -0 dB and not the conventional -3 dB as with Butterworth filters. Care must also be taken not to make the cutoff slopes too sharp and possibly introduce ringing known as the Gibbs effect (Yilmaz, 1987). Figure 3.2 depicts the operation of the bandpass filtering routine.

3.2.3 Deconvolution

The ultimate goal of seismic data processing is to enhance the seismic data to aid in the interpretation of geology of the region. Through data processing an attempt to learn something of the reflectivity of sub-bottom sediments is made. This in turn can be used to infer, based upon reflection strength and a general knowledge of sedimentary processes and physical properties, stratigraphic boundaries and the likely nature of sub-bottom sediments. To obtain the reflectivity at each sample point would require a source of infinite bandwidth. While such sources are not physically realizable, there is a large number of broad-band sources available for use in sub-bottom profiling. The usable bandwidth of these sources is severely modified as the seismic energy propagates throughout the Earth: higher frequencies experience a much higher degree of attenuation than lower ones do. This narrowing of the signal band-width results in an increase in the length of the seismic wavelet and hence a reduction in the temporal resolution of the data. Primary reflections in a data set are

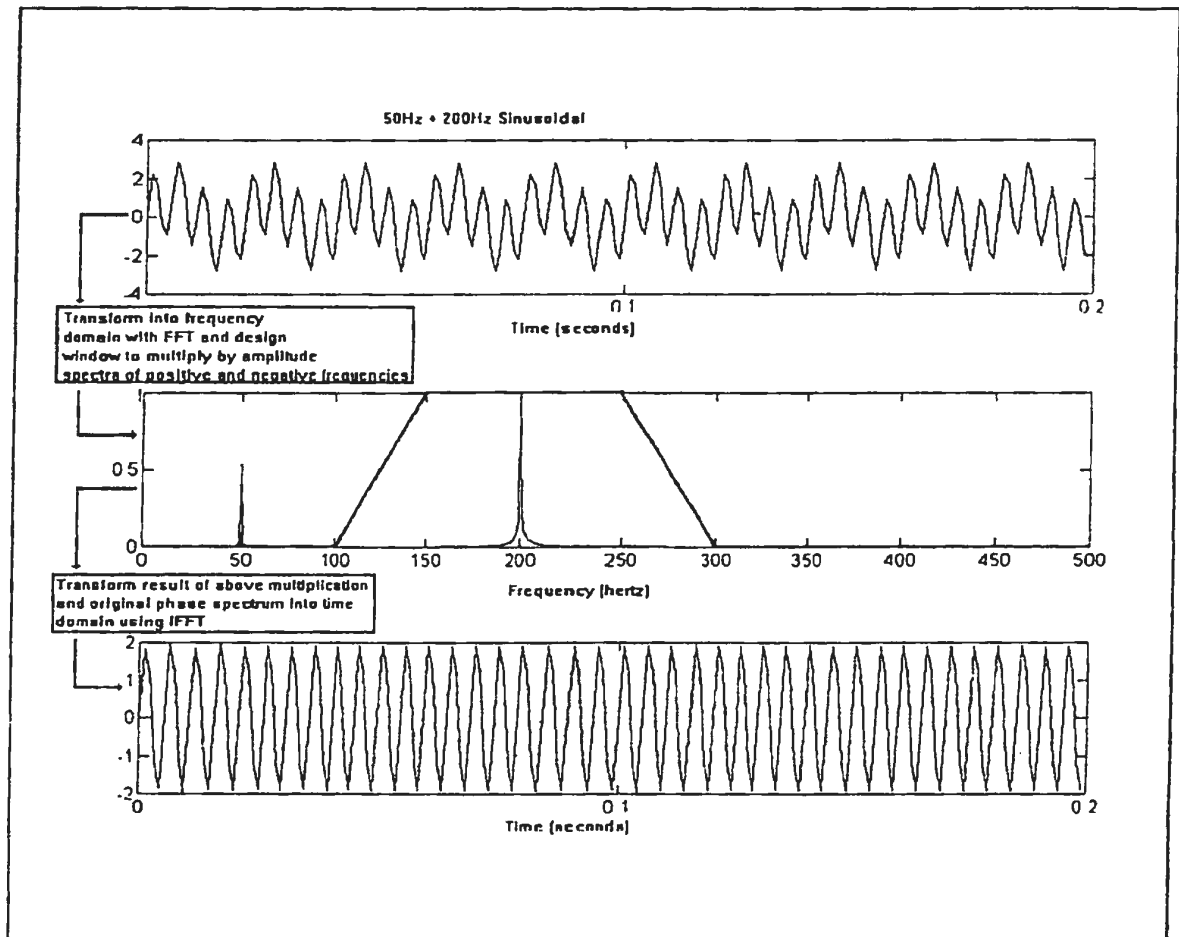


Figure 3.2 General operation of a bandpass filter designed and applied in the frequency domain.

sometimes masked by multiple reflections and interbed reverberation and source ghosts. Deconvolution in the form of least squares inverse filtering is implemented to help overcome both of these problems. Spiking deconvolution is aimed at compressing the basic seismic wavelet to a zero lag spike. This processor is used to help overcome the effects of absorption and increase the temporal resolution of the data. Predictive deconvolution is used to predict a time series at a future time $t + \alpha$ where α is the prediction distance. The predictable component of a seismic trace are multiple reflections with a periodic rate of occurrence. Predictive deconvolution is used to remove multiple reflections. A complete theoretical description of least squares inverse filtering can be found in Robinson and Treitel (1980). The two basic approaches using least squares inverse filtering included in the processing flow, spiking and predictive deconvolution, are described in the next two sections.

3.2.3.1 Spiking Deconvolution

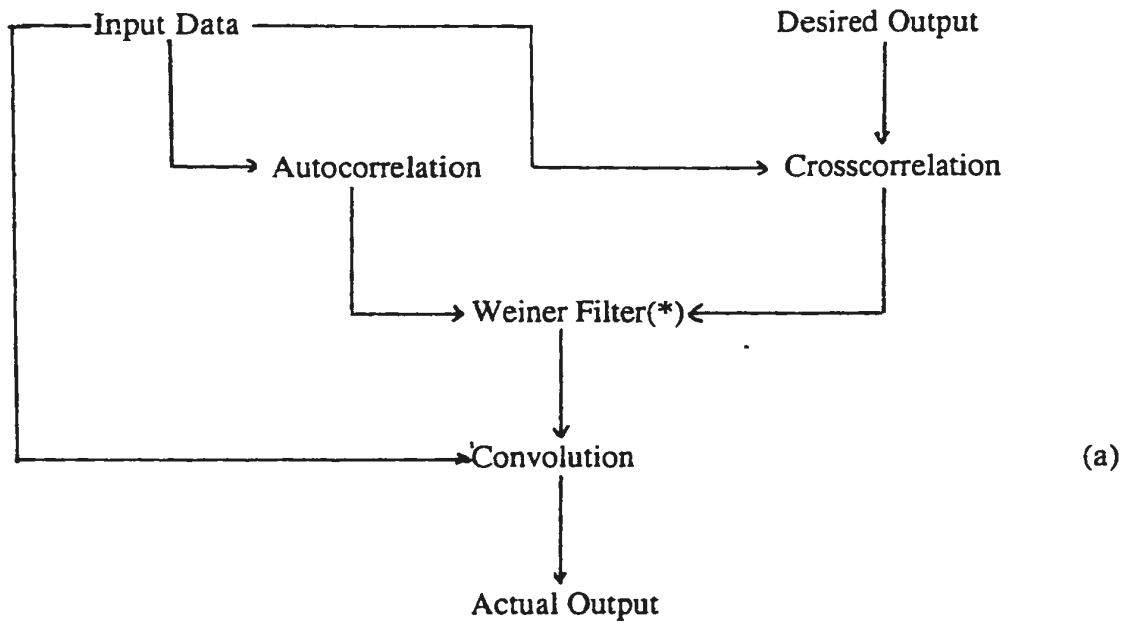
The basic goal of spiking deconvolution is to compress the seismic wavelet thus improving the temporal resolution of the data set. The theoretical model on which deconvolution theory depends makes a number of assumptions. Lindseth (1982) lists the following assumptions:

- Source signal is known;
- Transfer function is known;

- Source signature is minimum phase;
- Output signal is broad band;
- Noise is random(white);
- Earth's reflectivity is a random process;
- Source signature is stationary.

In reality, all of the above assumptions are violated at some time to a certain extent. In particular, the source signature is not stationary because of dispersion in subsurface sediments. However in most cases, the zone of interest in high resolution sub-bottom surveys is confined to the upper 50 m of the sedimentary column. In cases such as this, dispersion is not as serious a problem as that encountered in conventional exploration seismology where large travel times occur. The source is not truly minimum phase because physical systems require a finite time to be excited. However, impulsive sources, such as sparkers and boomers, are very much front end loaded, that is, most of the energy occurs near time zero. Hence these sources are a close approximation to minimum phase. In some sedimentary environments (e.g. deltaic settings) reflectivity is not random but sometimes periodic with seasonal variations in sediment loading(Lindseth, 1982). Finally some noise (e.g. cable strumming, source generated noise and ship generated noise) is coherent. Despite all these discrepancies between assumed and actual properties of the system, spiking/statistical deconvolution is a common practice in seismic data processing and, with the correct choice of the parameters, can yield satisfactory results .

Spiking deconvolution developed for the HI-DAPT II uses the Wiener-Levinson (Robinson and Treitel, 1980) algorithm. This approach, assuming a minimum phase source wavelet, derives the source signature from the autocorrelation function of the recorded seismogram. In doing so, the system response does not need to be determined since it is also present in the recorded seismogram. When the Earth's reflectivity series is random, the autocorrelation of the seismogram is equivalent to that of the source signature. The general procedure is to choose a section of the seismogram on which to calculate the autocorrelation function. This design window should be chosen to include the section of the trace which contains reflections from sub-surface boundaries of interest. The length of the filter, n , is determined from an examination of the autocorrelation. Generally, the portion of the autocorrelation function extending from zero-lag to the second zero crossing is representative of the source signature. Figure 3.3(a) depicts the general procedure to perform spiking deconvolution in the time domain using the Weiner-Levinson technique. Figure 3.3(b) shows the form of the matrix equation for a filter of length n . The square matrix on the left is filled with the autocorrelation lags, r_n as shown in figure 3.3(b). The column matrix a_n represents the filter coefficients required to produce the unity matrix on the right hand side of the equation. The autocorrelation matrix, a special type of symmetric matrix known as a Toeplitz matrix, can be solved by Levinson recursion (Robinson and Treitel, 1980). To provide numerical stability during computation, a small amount of white noise is added to the time series. This prewhitening is accomplished by adding a small percentage of the energy to the zero lag component of the autocorrelation function.



$$\begin{bmatrix} r_0 & r_1 & r_2 & \dots & r_{n-1} \\ r_1 & r_0 & r_1 & \dots & r_{n-2} \\ r_2 & r_1 & r_0 & \dots & r_{n-3} \\ \vdots & \vdots & \vdots & \ddots & \vdots \\ r_{n-1} & r_{n-2} & r_{n-3} & \dots & r_0 \end{bmatrix} \begin{bmatrix} a_0 \\ a_1 \\ a_2 \\ \vdots \\ a_{n-1} \end{bmatrix} = \begin{bmatrix} 1 \\ 0 \\ 0 \\ \vdots \\ 0 \end{bmatrix}$$

* solve for filter coefficients using equation below

Where: $r_i = i^{\text{th}}$ lag of autocorrelation
 $a_i = i^{\text{th}}$ filter element

Figure 3.3 (a) General procedure for implementing spiking deconvolution in the time domain.(b) Matrix equation to solve using Levinson's recursion (Yilmaz, 1987) to provide spiking deconvolution operator.

3.2.3.2 Predictive Deconvolution

The recorded seismic trace includes primary reflections which result from acoustic impedance contrasts in sub-surface sediments, the response of the recording equipment, random noise and multiple reflections. These multiple reflections have different origins as shown in Figure 3.4 and discussed below. The most common multiple in marine work is the multiple from the water/air interface. This boundary, with a reflection coefficient of essentially -1 causes the whole data set to be repeated with a period equal to the two-way travel time from the seabed to the water/air interface with a phase inversion. Primary reflections which exist in this zone are masked by the water/air multiple. Another source of multiple reflections, common when using a sparker source, is the collapse of the bubble generated by the sparker. This collapse causes a second pulse to occur with the same phase with the lag determined by the depth of the source and the size of the initial bubble. This collapse is essentially analogous to firing a second shot a short time after the initial shot. All primary events appear as occurring twice in the recorded section. The third common source of multiple reflections results from energy which is reflected within a particular stratigraphic layer. These interbed multiples (peglegs) manifest themselves as events occurring later in time than the primary at some factor of the two-way travel time in that particular layer.

The aim of the predictive deconvolution processor is to remove the multiple reflections from the seismic record without affecting primary events. The predictive

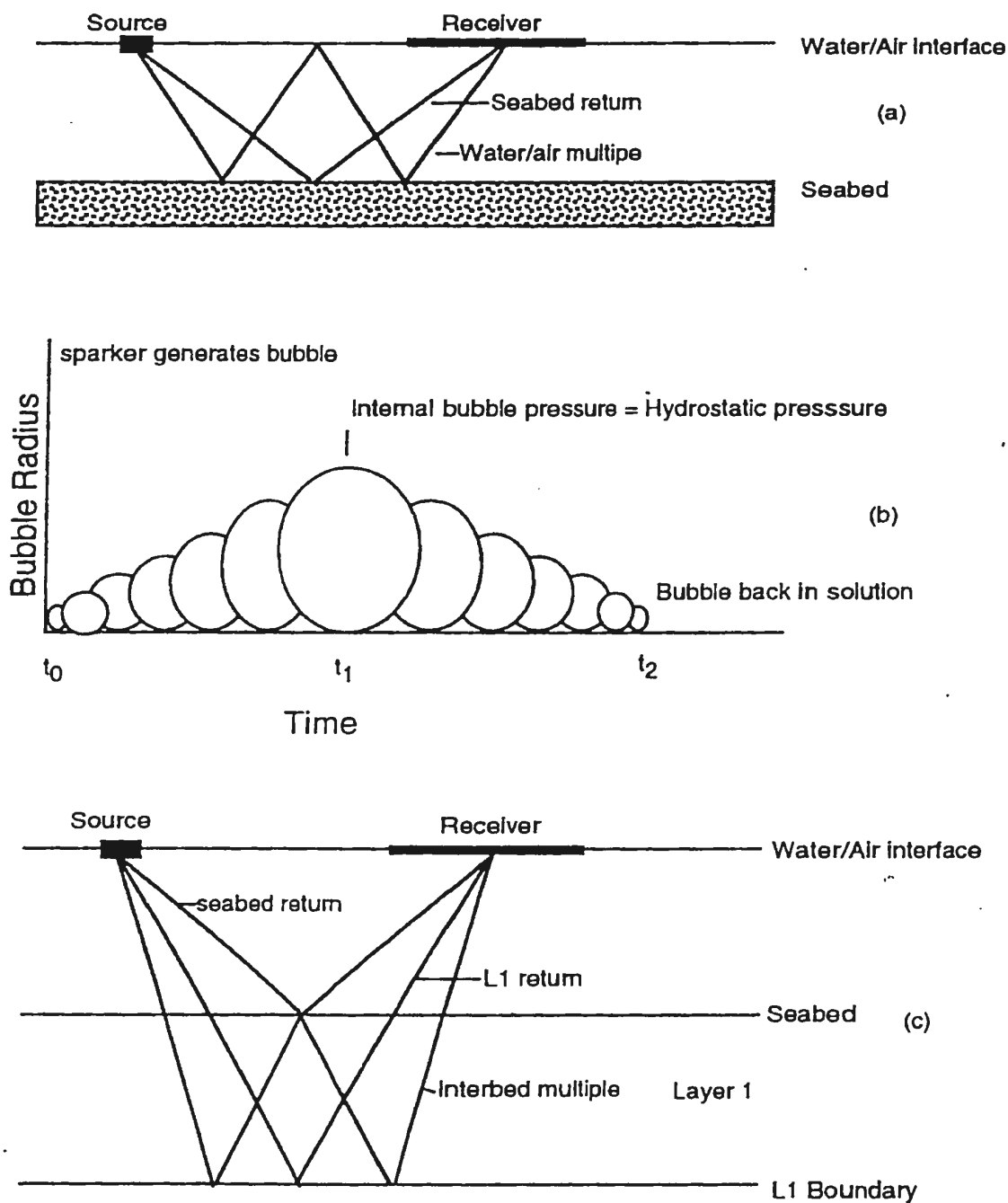
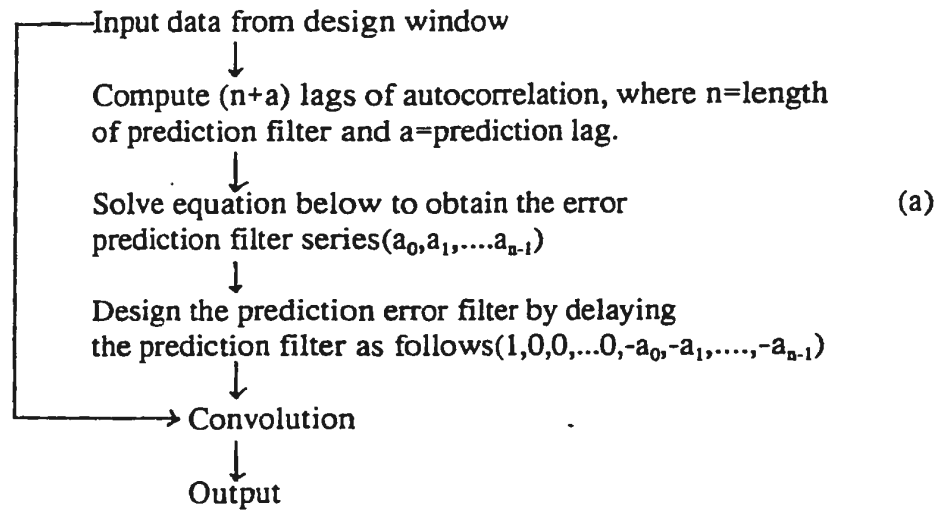


Figure 3.4 Common sources of multiple reflections in marine sub-bottom data are (a) water/air multiple, (b) Bubble collapse ghost, (c) interbed multiples.

deconvolution processor, also based on the Weiner-Levinson deconvolution algorithm, is depicted in Figure 3.5. The difference is in the design of the actual operator. Multiple reflections manifest themselves in the autocorrelation as isolated packets of energy at a lag equal to the period of the multiple. In the case of predictive deconvolution two parameters are chosen from the autocorrelation: operator length n and prediction lag or gap α . The gap time is chosen to include the entire autocorrelation up to the onset of the isolated energy which results from the multiple. In the case of the water/air multiple the gap is equal to the two way travel time from the sea surface to the seabed. When the automatic bottom tracking (described in next section) is enabled, the gap time is automatically obtained from this auto-tracking routine. The operator length is chosen to include only the isolated energy which results from the multiple. The filter series operator is then obtained from the equation as shown in Figure 3.5. This operator (with a phase reversal to account for the phase inversion at the water/air interface) is then delayed by the prediction lag and convolved with the recorded seismogram to remove the multiple reflections and leave only primary events.

3.3 Bottom Tracking and Swell compensation.

The ability to map the seabed and sub-bottom reflectors depends, in part, on the stability of the source and streamer as it is towed through or upon the water column. In cases where the source and streamer are towed at the surface, a periodic static shift is often



$$\begin{vmatrix} r_1 & r_0 & r_1 & \dots & r_{n-2} \\ r_2 & r_1 & r_0 & \dots & r_{n-3} \\ \vdots & \vdots & \vdots & \dots & \vdots \\ r_{n-1} & r_{n-2} & r_{n-3} & \dots & r_0 \end{vmatrix} \begin{vmatrix} a_1 \\ a_2 \\ \vdots \\ a_{n-1} \end{vmatrix} = \begin{vmatrix} r_{\alpha+1} \\ r_{\alpha+2} \\ \vdots \\ r_{\alpha+n-1} \end{vmatrix}$$

(b)

Where: $r_i = i^{\text{th}}$ lag of autocorrelation

$a_i = i^{\text{th}}$ filter element

Figure 3.5 (a) General procedure for implementing predictive deconvolution in the time domain. (b) Matrix equation to solve using Levinson's recursion to provide prediction error series (after Yilmaz, 1987).

imposed on the seabed as a result of surface waves upon the water body. This effect must be removed to correctly map the surficial sediments and subsurface reflectors. This can be accomplished when the time of the bottom return is known. The ability to measure this time is also essential for real-time water/air multiple suppression.

The three algorithms implemented to accomplish the foregoing are a first break time picking routine, an automatic bottom tracking algorithm and a swell compensation filter. The first routine is used to pick the first break time in a user specified window. When auto tracking is enabled, the second routine controls the length and position of the portion of the record in which the first break picking utility operates. The swell filter is used to correct the seabed position based, statistically, upon a user defined number of previous traces. The operation of each of these routines is described in the following three sections.

3.3.1 First Break Picking

The first break picking algorithm consists of two adjacent sliding windows of user defined lengths. The windows move sample by sample down the trace over a user specified search window. At each location, the mean power of the forward and rear looking windows is calculated and the ratio of the two determined and stored in a temporary array. Upon completing the slide the maximum ratio and its position in the array is calculated. The routine works best when a rear-to-forward window length is on the order of the source pulse length

and the rear looking window is approximately a factor of three larger. In most cases the timing of the first break of energy on the seismic trace (excluding the direct arrival), the seabed return, is calculated with an accuracy of ± 2 samples. These first break times are corrected to account for post shot recording delay and stored in the trace header.

3.3.2 Automatic Bottom Tracking

An automatic bottom tracking routine is included to relieve an operator of the task of continuously adjusting the first break picker search window. The routine defines the first break search window based on the median bottom time of the previous five returns. The median of the five previous terms was chosen to reduce the chances of the search window being displaced by outliers in the first break picks. The search window is confined to 1.5 ms before and after this time. When the automatic bottom tracking is enabled, the prediction gap time and automatic trace mute time can be obtained from the first break picking algorithm.

3.3.3 Swell Compensation

The swell compensation filter predicts the current position of the seabed reflection based upon a least squares fit of a user-defined number of previous returns. The time difference between the actual seabed pick and the predicted seabed location is used to apply

a static shift in the required direction. When seabed topography shows little relief a large number of traces can be used in the prediction. However in places where irregular topography exists (in Newfoundland, for example) smoothing of the seabed reflections will result from the use of a long prediction window. Despite the chances of smearing real features the routine works well with a careful choice of parameters. Figure 3.6 shows a section of data collected with a 3.5 kHz hull mount system before and after the application of a swell filter.

3.4 Trace Scaling

The type of trace scaling performed on a seismic trace will depend on the objective of the processing. Examination of amplitude variations which result from differences in acoustic impedance requires that the effects of spreading losses (spherical divergence) be removed from the data. However when examining internal structure in sub-bottom sediments, it is often useful to enhance weak reflections relative to more prominent events. This can be accomplished by applying an automatic gain correction which equalizes the energy in a user defined window shifted by a specified number of samples over the entire trace. The following two sections describe the spherical divergence and automatic gain routines of the HI-DAPT II.

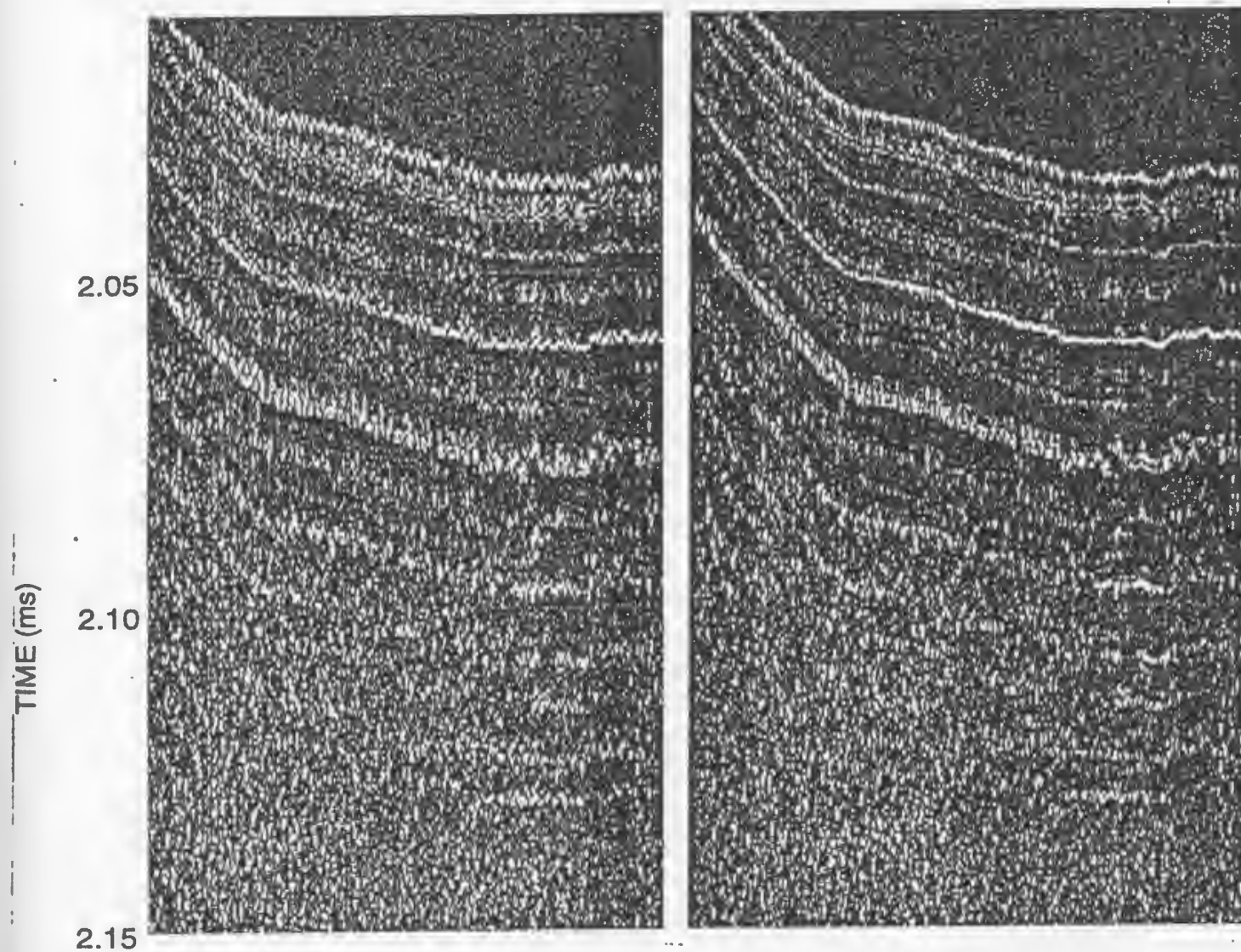


Figure 3.6 Application of a swell compensation filter to remove static shifts due to ship motion. Sea swell as seen superimposed on the seabed return (left) is removed after the swell filter is applied (right).

3.4.1 Spherical Divergence Corrections

The firing of the sparker source causes energy to flow radially outward in all directions forming a spherical wavefront. As the wavefront propagates, the energy is spread over an increasingly larger surface. Hence the energy density decreases as the wavefront expands. This decrease in energy as a function of distance from the source is known as spherical divergence. Telford *et al.* (1976) show that for a spherical wavefront diverging from a point source the energy density decreases inversely as the square of the distance from the source. Hence, the amplitude, which is proportional to the square root of the energy, decreases inversely to the distance from the source. Thus the spherical divergence correction results in scaling the trace by a factor proportional to the distance from the source. In the absence of velocity information on the subsurface and shallow reflectors, an estimate of 1500m/s, the velocity of sound in sea water, is used to correct the time series. This value is expected to be accurate to within 20% assuming a maximum compressional wave velocity of 1800 ms^{-1}

3.4.2 Automatic Gain Control

In contrast to spherical divergence corrections, an automatic gain correction (AGC) is applied to increase the relative amplitude of weak reflections to stronger events in the recorded trace. The degree to which these weaker events are enhanced is determined by the

length of the AGC window and the interval at which the window is incremented. The AGC processor consists of a sliding window of user-defined length which is incremented in user-defined steps over the entire trace. The algorithm determines the mean amplitude of the portion of the rectified trace within the window. This value is then used to scale the midpoint within the sliding window. The start position of the window is then incremented by the user-defined interval and the process repeated. Upon completion, the amplitude values between the scaled values and the start and end points are tapered linearly to the first and last scaled values respectively. The choice of parameters is dependent on the objective of the application which in turn is dependent on the sub-bottom stratigraphy.

3.5 Trace Mixing

Stacking of normal moveout (NMO) corrected common depth point (CDP) gathers to increase the signal-to-noise ratio is a well established procedure in exploration seismic data processing. Data are acquired with a single source (sometimes an array of sources) and a multi-channel hydrophone streamer. Post processing first requires that these data are sorted in CDP gathers. Each gather contains traces from the same reflection point in the subsurface, acquired at different source-receiver offsets. Each gather is corrected for NMO and stacked to yield a single trace. In theory, the signal-to-noise ratio is increased by the square root of the number of traces included in the stack. In single channel sub-bottom data, one does not have the benefits of multi-trace CDP gathers. However, in cases where sub-bottom reflectors

exhibit low temporal shifts between adjacent records, trace mixing can be applied to increase the signal-to-noise ratio. This routine has the ability to stack up to a maximum of five weighted traces horizontally. Weights are applied to control the effect of surrounding traces on the mixed trace.

3.6 Miscellaneous Utilities

The following sections describe algorithms which were developed to alleviate problems sometimes encountered in data collection and processing. The first, noise spike removal, helps remove spurious events such as electrical spikes and random environmental noise of anomalously large amplitudes. The second, trace muting, is useful to remove noise in a processed section prior to the seabed return. The third, instantaneous amplitude, allows the calculation of the magnitude of the complex representation of a seismic trace. These processors have been useful in certain situations throughout the development but have not been required most of the time.

3.6.1 Noise Spike Removal

Noise, common in all seismic data, originates from a variety of sources. In cases where the frequency content of the noise is not within the bandwidth of the seismic source, frequency filtering can be applied to remove it. Trace mixing, as described in section 3.5, is

effective in enhancing coherent events and attenuating random noise. This algorithm is designed to attenuate noise spikes in recorded data. The algorithm operates by obtaining the mean amplitude in a cone-shaped window which diverges from a particular sample over the previous three traces. If the value of the sample at the apex of the cone exceeds the mean amplitudes of the values within the cone by a factor of the user-supplied threshold, it is scaled to the mean amplitude. This window is incremented over the entire trace. In cases where the sample in question is part of a coherent event the mean amplitude is large and hence no scaling is applied. If the value in question's amplitude is at a level equal to that of the noise then no scaling is applied. In cases when the amplitude of the sample in question represents a spurious noise spike which exceeds the mean amplitude in the window, the sample is scaled down to the level of the other samples in the window. The conical window was chosen so as not to affect dipping events.

3.6.2 Trace Muting

The trace muting algorithm essentially zeros samples prior to a user-defined time in each record. When the automatic bottom tracking is enabled the trace mute time can be obtained from the first break picking algorithm. This utility is useful mainly for display purposes, to remove noise which appears in the water column as a result of the application of automatic gain recovery.

3.6.3 Instantaneous Amplitude

When considered as an analytical signal (in the mathematical sense), a seismic trace can be expressed as a complex function (Yilmaz, 1987). The seismic trace itself makes up the real part of the complex function. The imaginary portion or quadrature is merely a 90° phase shifted version of the real part. The quadrature is obtained by taking the Hilbert Transform of the recorded signal. The instantaneous attributes (instantaneous phase, frequency and magnitude) can be readily calculated once the complex trace is formed. Instantaneous amplitude provides a measure of reflection strength. However, care must be taken to preserve amplitude information in processing prior to calculation of the instantaneous amplitude in order to extract any meaningful information. Another useful application of the instantaneous amplitude is in the display of data from pulse-driven piezoelectric transducers. When displayed in the time domain the signature from such transducers is that of a ramped monochromatic sinusoidal. When displayed as the instantaneous amplitude only the envelope of the pulse is displayed. The shape of the envelope is characteristic of the rise and decay of the transducer when excited. Figure 3.7 shows a section of data acquired by the HI-DAPT II in the Pygmy Basin, Gulf of Mexico using a 3.5 KHz pulse driven transducer.

3.70 Video and Hardcopy Display

The CRT and thermal plotter display software were developed at the Centre for Cold

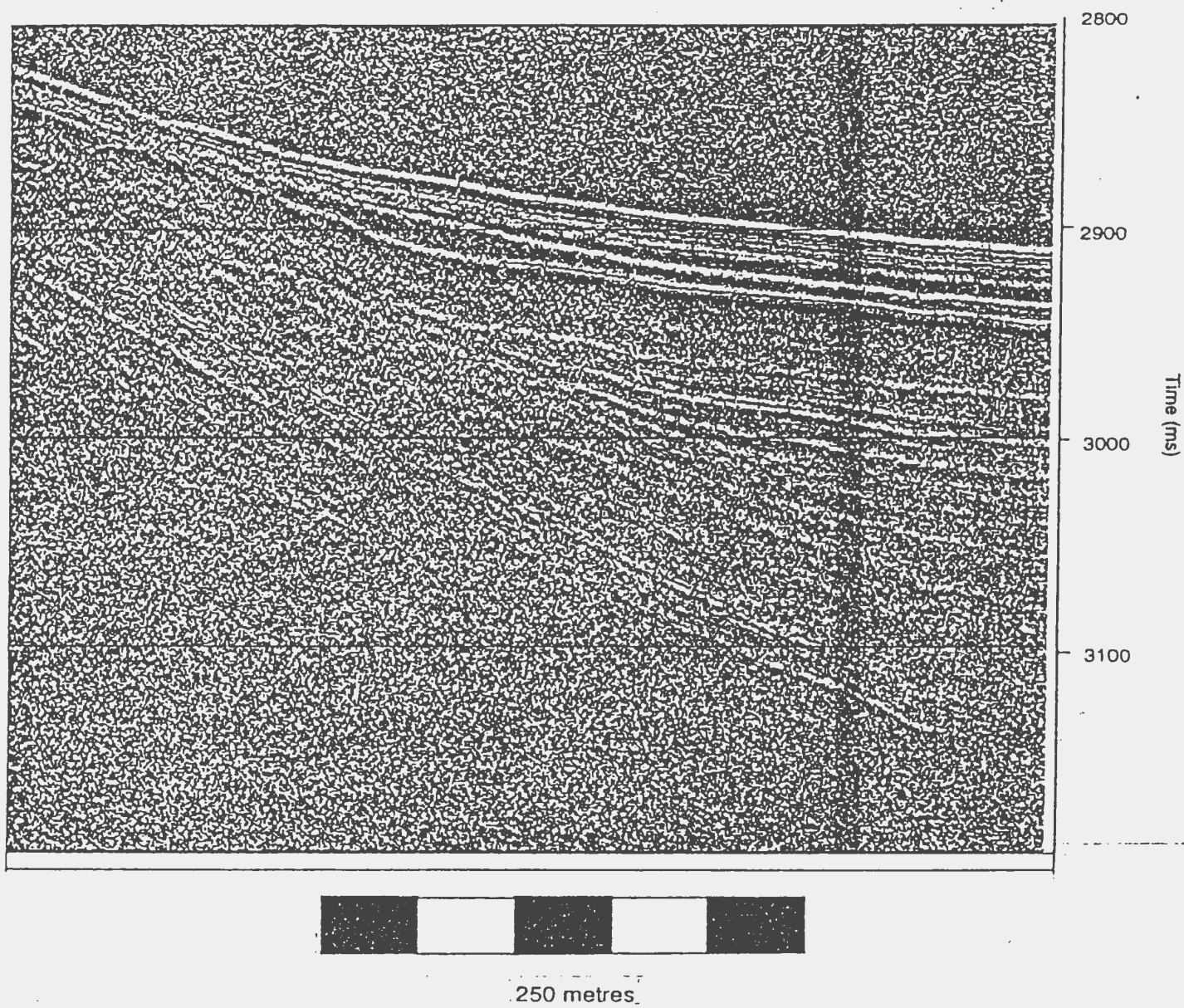


Figure 3.7 Instantaneous amplitude of 3.5 kHz data acquired at the Pygmy Basin, Gulf of Mexico from the RV Gyre, May, 1994.

Ocean Resources Engineering. The CRT display provides a real time display of processed data and the user menu from which processing and display parameters can be entered. The following section describes each of the display parameters.

3.7.1 CRT Display

Processed data can be displayed on a SVGA monitor. The screen display utility offers a large degree of flexibility in the display of the data. The following lists the available options:

- trace start/stop time
- number of traces per inch
- trace display overlap
- timing line increment
- wiggle trace/wiggle trace with variable area/variable density
- colour coded amplitude with or without wiggle trace overlay
- colour level adjustment
- 16 grey scale display
- contrast stretch

3.7.2 Thermal Plotter Display

Hardcopy of the processed data is available on a 300 dpi thermal plotter. The

hardcopy display parameters are separate from the CRT parameters to allow the user the flexibility to zoom in a section of the data without affecting the hardcopy output. The following lists the options available in the plotting menu:

- trace start/stop time
- number of traces per inch
- plot width
- trace plot overlap
- heat, a multiplier to increase amplitude
- wiggle trace/wiggle trace with variable area/variable density
- trace bias
- primary and secondary timing line interval.

The proceeding sections demonstrate the level of processing available on the HI-DAPT II system. Most of post-stack processors available in conventional processing packages have been written and implemented to run in real time. The front end menu and display package developed at C-CORE provides an excellent platform to carry out such processing.

4.0 PANAMA CITY SEA TRIALS

Sea trials of the HI-DAPT II sub-bottom profiling system were conducted over a small region of the Northwest Florida Shelf west of Cape San Blas and approximately 37 kms south of Panama City, Florida (see Figure 4.1). The sea trials were conducted as a part of the Coastal Benthic Boundary Layer Special Research Program (CBBLSRP) sponsored by the United States Office of Naval Research. The CBBLSRP addresses the physical characterization and modeling of benthic boundary layer processes and the impact of these processes on seafloor structure, properties, and behaviour (Richardson, 1994). The HI-DAPT II was one of three systems chosen to characterize the site acoustically prior to the onset of *in situ* experiments. The objective of the HI-DAPT II survey was to delineate the vertical extent of a surficial sand layer over the survey area. The other sub-bottom systems, a KleinTM 595 combination sidescan/sub-bottom profiler and a commercial prototype of the EG>M X-STAR chirp sub-bottom profiler, were used to examine detailed shallow stratigraphy in the upper several metres of the sediment column, and to measure the reflectivity of the seabed in an attempt to distinguish different bottom types based on the acoustic returns. Vessel position was obtained with Loran C. Field trials were conducted from the RV GYRE during the period from August 9, 1993 to August 13, 1993. Data were collected on a time-shared basis over a 3 day period to avoid problems associated with cross talk between the three sub-bottom systems and differences in preferred towing speeds.

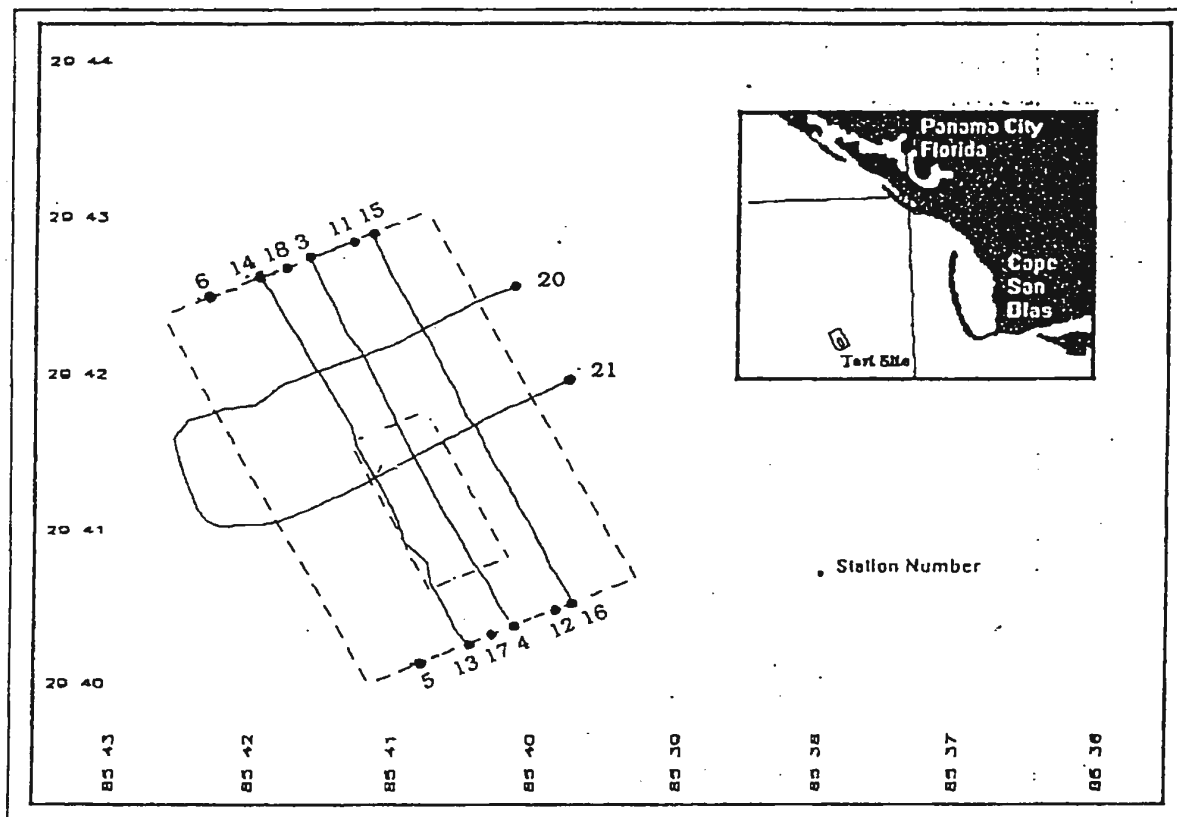


Figure 4.1 Site plan showing the location of the CBBLSRP test site.

4.1 Geologic Setting

The major structural element in the northeastern Gulf of Mexico is the Apalachicola Embayment whose axis plunges south-southwest (see Figure 4.2). The structural low of the Apalachicola Embayment is inherited from a deep water strait, sometimes referred to as the Suwannee Channel or Suwannee Straits, that existed from late Cretaceous to early Oligocene time across northern Florida and southern Georgia between the Gulf of Mexico and the Atlantic (Locker and Doyle, 1992).

The late Tertiary and Quaternary history of the northeastern Gulf of Mexico is a record of repeated marine transgressions and regressions that have veneered the inner continental shelf with fluvial sediment (Donoghue, 1989). The major source of clastic sediments to the northeastern Gulf of Mexico is the Apalachicola River. This river, the fourth largest in the northern Gulf Basin, delivers an estimated 0.7 million tons of sediment to the Gulf each year (Donoghue, 1989). The Apalachicola River is the likely source of the quartz sand sheet that extends over the study area and dominates the inner shelf of northwest Florida. Present-day features of the inner shelf bottom sediments are a product of the late Wisconsin and early Holocene fluctuations in sea level. Sediment supply to the inner shelf in northeastern Florida has been absent since late Holocene time when virtually all of the Apalachicola river's sediment load has been deposited in the Apalachicola Delta and the river's estuary.

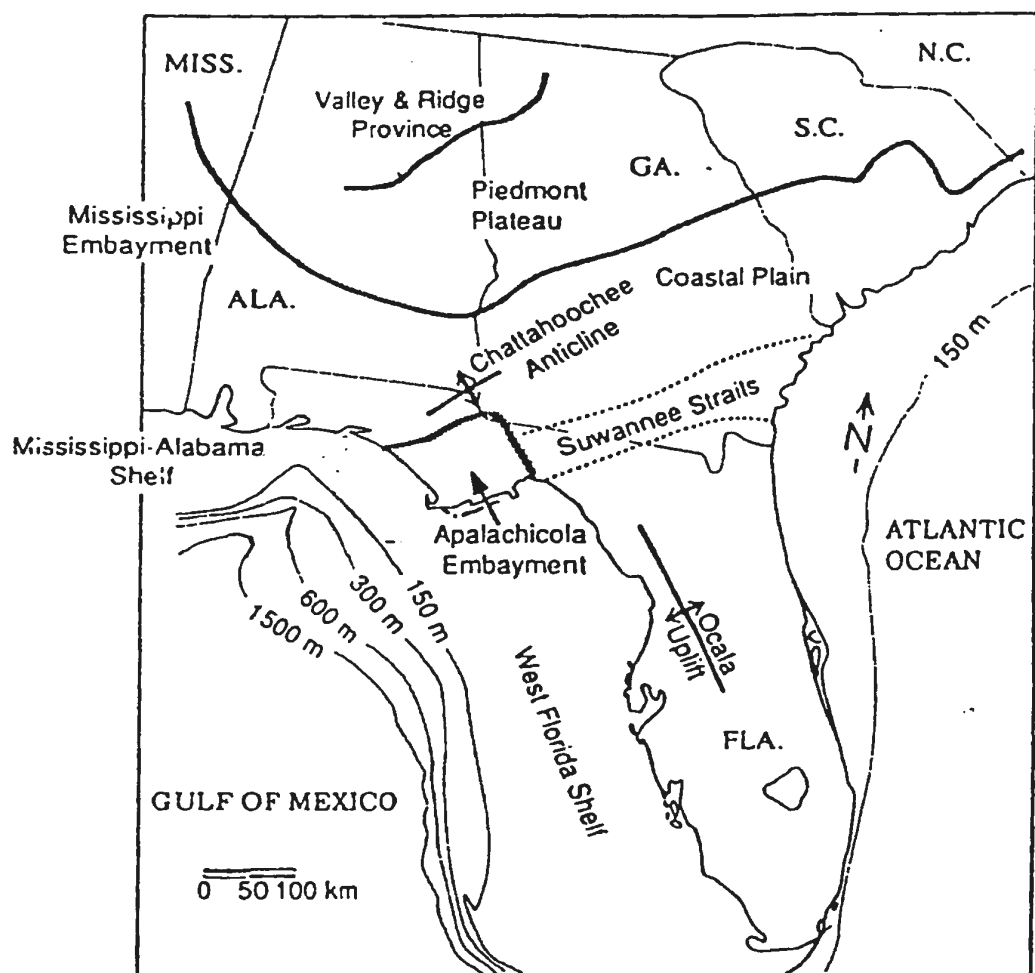


Figure 4.2 Geologic Setting in the Northeastern Gulf of Mexico.(modified after Locker and Doyle, 1992).

4.2 Methodology

Data were collected from the RV GYRE with the HI-DAPT II sub-bottom profiling system. Given the sandy nature of the seabed combined with the unknown depth of the sand body a 25 tip sparker with a power setting of 1080 J was chosen to provide a signal of sufficient amplitude and frequency content to enable penetration into the hard sand bottom. A sampling frequency of 16 kHz was used to provide record lengths of 128 ms. Data were collected during three periods on August 10, August 11, and August 12, 1993. The following summarizes each data collection period.

4.2.1 Trial One, August 10, 1993

Data collection began at 2300 hrs, August 10, 1993. Because of heavy seas it was decided to collect data in a deep-towed manner (see Figure 4.3). The hydrophone streamer lead-in cable was fitted with a fairing constructed of 9 mm nylon rope to reduce the effect of cable strumming when towing at depth. The streamer was attached to the tow body such that the first active element was located 2 m from the center of the sparker source. A 34 kg lead coring trigger weight was attached to a 2 metre chain. This chain was attached to a shackle on the end of the tow line. The tow body was attached to the same shackle by means of a 20 metre section of 12 mm nylon rope (see Figure 4.3). This method allows any vertical motion of the ship to be transferred directly to the clump weight, thus reducing the effect of the

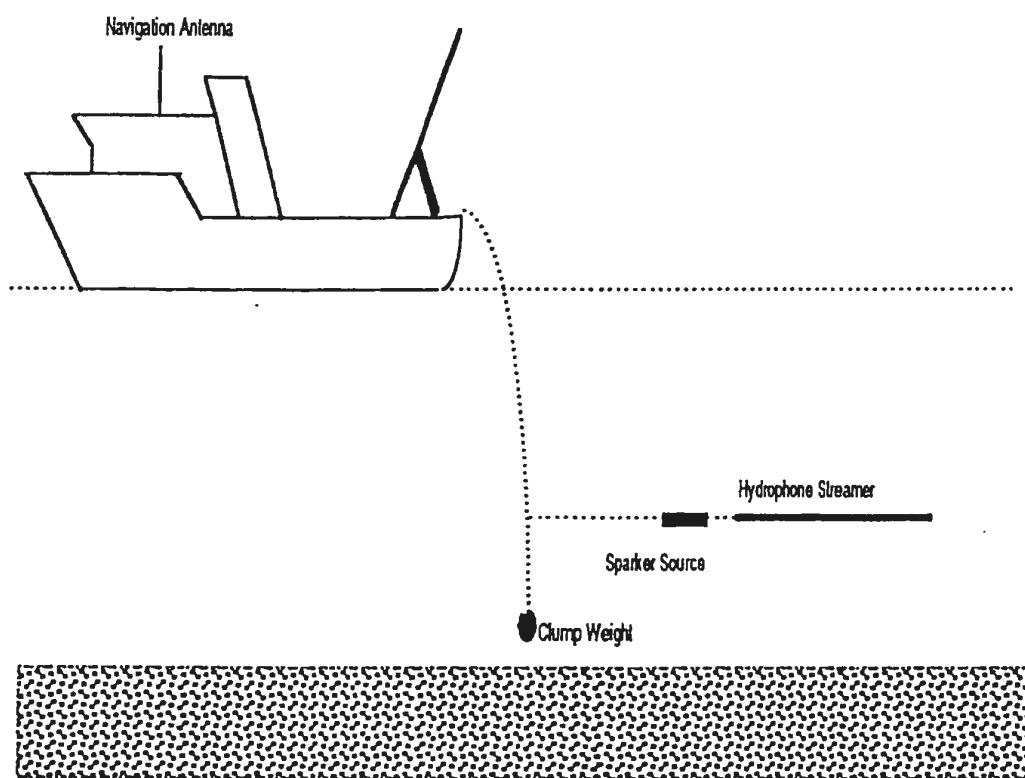


Figure 4.3 HI-DAPT II Deep Tow Configuration.

heavy seas on the towbody. The streamer, towbody and weight were deployed and data collection began. An attempt was made to tow approximately 14 m below (2/3 water column height) the sea surface to maximize the portion of the record before the sea surface ghost. Data collection began just prior to arriving on station for Profile 5-6 (see Figure 4.1). Strong winds made handling of the vessel difficult at speeds below 2 ms^{-1} . Variation in ship speed caused the towbody to rise and fall relative to the seabed. Because of the instability of the towfish and the low overrun rate attainable at 2 ms^{-1} deep towing efforts were abandoned. The system was retrieved and the weight and chain removed from the tow line. The system was re-deployed and Profile 5-6 attempted in a surface-towed mode. During the second attempt at Profile 5-6, a ghost reflection with a period of 10 ms was noticed throughout the record. The weight of the hydrophone lead in and power cables were causing the towbody and streamer to fly about 7 m below the surface. The complete system was retrieved. Floats were attached to several places on the power cable and 1 m length of foam pipe wrap insulation were secured to the hydrophone streamer lead-in cable. A third attempt was made on Profile 5-6. Data quality improved and the addition of the flotation devices removed the problem associated with the ghost reflection. At the midpoint of Profile 5-6 the trigger circuit, which converted the HI-DAPT II positive $4 V_{p,p}$ trigger pulse to the negative $15 V_{p,p}$ pulse required by the Hunttec Seismic Energy Unit failed. Lack of time and severe dampening of spirits prevented collection of any more data during this shift. The trigger from the HI-DAPT II was modified (in software) to produce a negative going square wave of $4V_{p,p}$. This trigger pulse, even though less than 1/3 the recommended voltage drop, was adequate.

4.2.2 Trial Two, August 11, 1993

Data collection began at 0200 hrs, August 11, 1993. Sea conditions had improved since the last run. It was decided to remain in a surface towed mode since discussions with the ship's mate indicated that to remain on course at a constant slow speed (1 ms^{-1}) would be nearly impossible. The system was deployed and we began to collect data along Profile 18-17 (see Figure 4.1). Approximately 5 minutes into the line the source signature changed drastically. The bubble pulse period had increased from 4 ms to 10 ms and the frequency content of the data dropped. An increase in the period of the bubble pulse could only result from the energy being discharged to a much lower number of tips. The system was retrieved and revealed that the ground cable from the Hunttec power supply was sheared off near the sparker giving the effect of a 1080 J single tip sparker. The cable was repaired and the system deployed again at approximately 0300 hrs. Profiles 18-17, 5-6 and 11-12 (see Figure 4.1), were collected during the remainder of that night. Data quality was extremely good and a strong continuous reflector could be followed on all three lines. A check of disk space on the optical drive after the shift revealed that only a small portion of Profile 18-17 had been recorded due to insufficient disk space. The software was modified to save the data file after each shot and a error check installed on the file write command to advise of insufficient disk space.

4.2.3 Trial Three August 12, 1993

Data collection began at 1900 hrs August 12, 1993. Data were collected using the same surface towed configuration as described in section 4.2.1. Conditions were excellent. The sea was very calm and there was no wind. During the night a total of 25 km of data was collected. Data were collected along Profile 13-14, Profile 3-4, Profile 16-15 and 2 cross lines to tie the profiles together (see Figure 4.1). Insufficient ship time prevented the reshooting of lines missed due to the disk write problem discussed in Section 4.2.2.

4.3 Data Processing

During the data collection procedure a minimum amount of processing was performed. A wide bandpass filter (100/300/5500/7000) and a 10 ms AGC were applied to provide an adequate display. These parameters were kept constant such that any changes in the plotted sections could be attributed to geology rather than artifacts of the processing itself. Reproductions of Profile 13-14, Profile 3-4, Profile 16-15 and the tie lines are shown in Figure 4.4 through Figure 4.7 (see Appendix B). The focus of the data processing in this case is to enhance the records with respect to the base of the sand layer. The following sections describe tests performed to select optimum parameters for the final processing of the data.

4.3.1 Preliminary Data Examination

Data are plotted in the convention of south-north and west-east as left-right. The tie line is plotted as a continuous track to illustrate the continuity of reflectors within. Preliminary examination of Figures 4.4 through 4.6 revealed the following: The seabed reflection occurs between 30 and 40 ms two way travel-time(TWT) over the entire survey area. A ghost due to the collapse of the bubble pulse can be seen at a period of approximately 4 ms. A broken reflector can be seen in places at approximately 50 ms TWT. A near continuous reflector is seen at approximately 70 ms TWT. These same reflectors, as seen on the tie lines (Figure 4.7), tend to dip to the west. The water/air multiple is evident on all records. The convoluted shape of the pulse, with its multiple peaks, make differentiation of real events and ghost reflections difficult. The hard bottom in the area also caused a large water/air multiple. This multiple makes it impossible to determine the presence of any reflectors beneath 80 ms TWT.

4.3.2 Bandpass Filter Tests

Bandpass filter panels as shown in Figure 4.8 (see Appendix B) were on performed on 50 traces from Profile 13-14 (see Figure 4.4) to determine appropriate bandpass filter

parameters for the final processed section. The panels each contain consecutively higher passbands as indicated below each panel. An examination of Figure 4.8 shows that frequency components greater than 2500 Hz were attenuated near the seabed. Based on the filter panels (Figure 4.8) a bandpass filter of 100/300/2500/5000 was selected for the final processing.

4.3.3 Predictive Deconvolution Tests

As can be seen from Figures 4.4 through 4.7, the collapse of the bubble generated by the sparker resulted in a ghost reflection with a period of approximately 4 ms. A closer examination of the seabed return reveals that there are two separate processes contributing to the distortion in the seabed return. It appears that there is a surface ghost caused by the submergence of the tow fish, as well as the collapse of the bubble. Figure 4.9 shows an enlarged section containing the seabed return illustrating this. As the tow fish sinks, the period between A and B increases because of the increase in the distance between the towfish and the surface. However, the period between A and C remains constant since it is a function of the size of the bubble which in turn is a function of the power and number of tips. This signal is on all major reflectors in Figures 4.4 through 4.7. Figure 4.10 shows a single trace (a) and its autocorrelation (b and c). As can be seen, the autocorrelation contains a significant amount of energy at lags up to approximately 8 ms. The two separate events discussed above are difficult to distinguish as separate entities in the autocorrelation. However, from

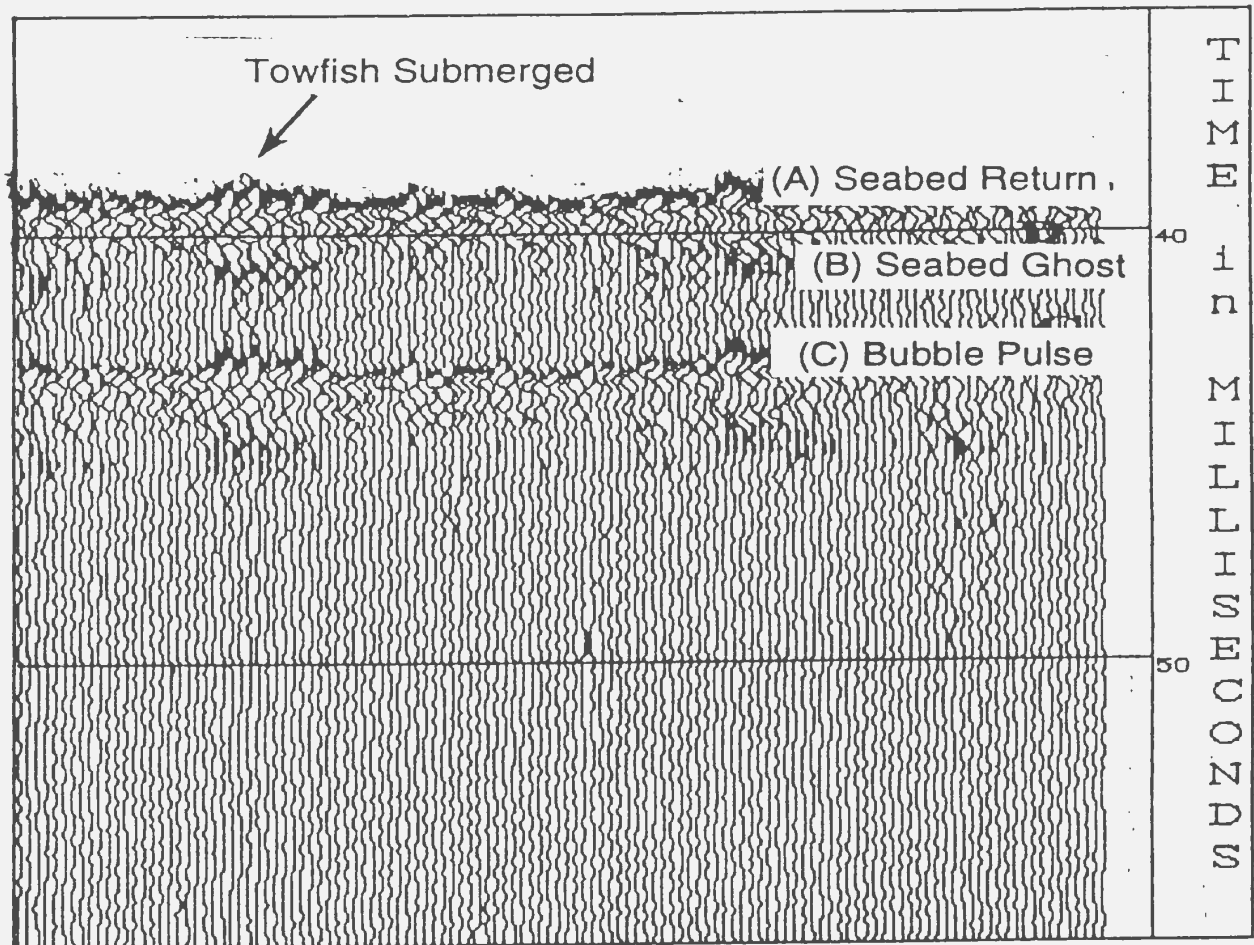


Figure 4.9 Enlarged portion of seabed return shows a combination of a surface ghost and bubble pulse. As towfish submerges, seabed return (A) occurs at earlier time. Period between A and C remains constant while that between A and B increases.

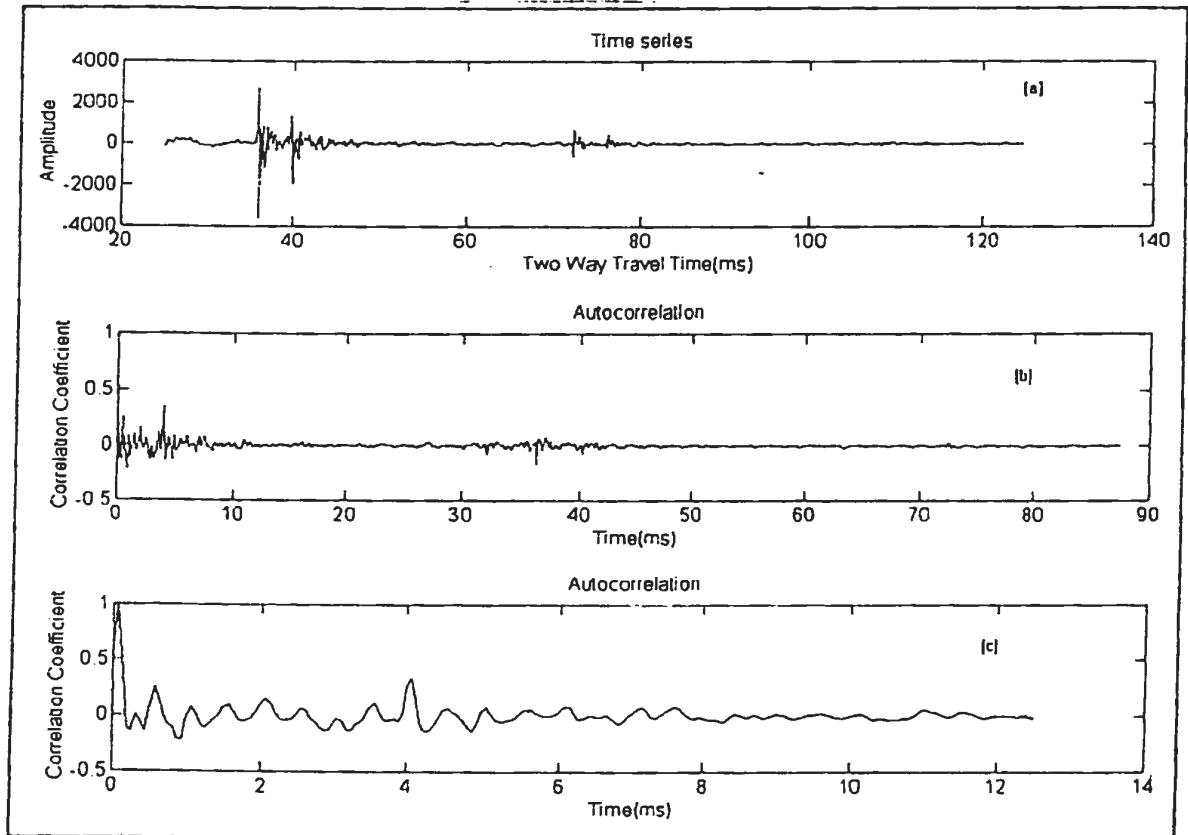


Figure 4.10 Single trace(a) and its autocorrelation(b and c).

the time sections (Figures 4.4 - 4.7) it is evident that the period of the bubble pulse is always larger than that of the surface ghost and begins at approximately 4 ms. A test panel of 100 traces (Profile 13-14 traces 100-200) was chosen to test the predictive deconvolution. These trace were chosen because of the presence of the reflectors at 51 ms and 62 ms. Given the nature of the problem, a single attack was made at both removing the reverberation and shortening the temporal duration of the source wavelet. A starting point, and limits to test the prediction gap, were determined from the autocorrelation in Figure 4.10. The gap time was chosen to begin at 0.50 ms (second zero crossing time) and increment up to 3.4 ms while the operator length was kept constant at 3 ms (see Figure 4.11 in pocket). An examination of the test panels in Figure 4.11 show that prediction gaps between 1.0 ms and 1.9 ms remove most of the reverberation and produce the sharpest seabed return. A second set of panels is shown in Figure 4.12 (see Appendix B) using a constant gap time of 1.0 ms and increasing operator length from 1 ms to 9ms. From the test panels (Figure 4.12) an operator length of 3 ms is shown to be sufficient to remove the surface ghost and bubble pulse. However, a reverberation at approximately 43 ms has become more prominent as a result of the scaling down of the collapse of the bubble pulse. At an operator length greater than 7 ms, this feature is attenuated at the expense of the reflector seen at 51 ms. A second application of predictive deconvolution with a gap of 7.5 ms and a 2 ms operator proved sufficient to remove this feature.

Predictive deconvolution was also applied to attempt to remove the water /air multiple

which can be seen in Figures 4.4 through 4.7. The prediction gap was selected by the first break picking routine to be the two way travel time to the seabed, and prediction operator length was chosen to be 3 ms. The success of the applications of predictive deconvolution can be seen in Figures 4.14 through Figure 4.18. The application of a 1 ms prediction gap and a 3 ms operator has resulted in a compression of the seismic wavelet and removal of the bubble pulse and surface ghost. The prediction filter with a 7.5 ms gap and 2 ms operator successfully attenuated the ghost reflection at 43 ms leaving the underlying 50 ms reflection. Given the success of these filters there was no need to attempt a spiking deconvolution since the prediction filter essentially accomplished the same task.

4.3.4 Automatic Gain Tests

Figure 4.13 shows a set of test panels to determine the optimum window length for the AGC processor. From the figure it can be seen how small window lengths tend to blow up noise and severely decrease the signal to noise ratio of the data. Conversely, large windows have the effect of no gain. A window length of 10 ms was chosen based on the panels of Figure 4.13.

4.3.5 Processed Seismic Sections

Figures 4.14 through 4.18 show the processed versions of Figures 4.4 through 4.7.

A bandpass filter, 100/300/2500/5000, was applied. The prediction deconvolution was applied in three steps. A prediction filter with a gap of 1.0 ms and an operator length of 3 ms was applied to collapse the seabed return and remove the bubble pulse. A second prediction filter with a gap of 7.5 ms and an operator length of 2 ms was applied to remove a ghost reflection that occurred after the amplitude of the bubble pulse was scaled down. A final prediction filter with a gap time chosen from the first break picking routine and an operator length of 3 ms was applied to remove the surface multiple. An AGC with a 10 ms window length was applied to enhance weaker events in the processed sections. A three trace mix with a trace weighting of 1:10:1 with and a one trace shift was also applied. Data are displayed in wiggle trace format with a variable area fill. The sections are plotted at 50 traces per inch with a trace overlap of 1.5. The start time was selected to be at 30 ms to avoid plotting of the water column. An automatic trace mute was applied to remove the effects of noise in the water column.

4.4 Seismic/Geologic Interpretation

Geological interpretation of seismic data is usually done with the support of sediment core information from the general area in which the seismic data are collected. In such cases, seismic events can be correlated with a change in the physical properties of the sediment core and the result extrapolated away from the core. It must be noted that the only ground truth obtained at this site was surficial grab samples. Attempts to obtain gravity cores failed

because to the inability to penetrate the hard sand bottom over the survey site. The lack of oil industry activity offshore Florida also contributes to a general lack of sub-bottom data in this region. The seismic data collected during these trials cover a relatively small region. The short length of the lines prevents interpretation of regional geological features based upon these data alone. Hence, the following interpretation is made on the basis of the seismic data itself and the work of others (Locker and Doyle, 1992, Donoghue, 1989, 1992, Schnable, 1966) in the northeastern portion of the Gulf of Mexico.

4.4.1 Seismic Characterization

The processed data as shown in Figures 4.14 through 4.18 are used in the following interpretation. The tie line shown in Figure 4.7 has been subdivided into Figure 4.17 (Profile 20-21:Shot Points 1500-1) and Figure 4.18(profile 20-21:Shot Points 1500-2790) to allow the display of each leg from west to east.

There are two main reflecting horizons evident in all of the data as shown in Figures 4.14 through 4.16. The first event, labeled S1(shaded in green), located between 48 ms and 51 ms on the south-north profiles, is characterized as a discontinuous, flat-lying, low amplitude reflector. This event is evident on the southern portion of each of the south-north profiles. On each of these profiles this reflector appears to be onlapping towards the north. This event (S1) is more prominent in the southern tie line (Figure 4.18) where it can be seen

dipping towards the southwest at approximately 0.1° (assuming a compressional wave velocity of 1800 m/s for the sand). The second event, labeled S2 (shaded in red), located between 60 ms and 70 ms on the south-north profiles (Figures 4.14, 4.15 and 4.16), is characterized as a nearly continuous, flat lying, high amplitude reflector. This interface exhibits erosional characteristics visible on southern end of each profile. This same horizon seen on the tie lines(Figures 4.17 and 4.18) between 59 ms and 70 ms dips south-southwest at approximately 0.1° . The high amplitude of this reflector indicates a strong impedance contrast considering the depth of burial and attenuation experienced by waves traveling through the overlying sand.

4.4.2 Interpretation

The event labeled S2 is thought to represent the base of the West Florida Sand Sheet and the top of weathered limestone bedrock. The event labeled S1 is believed to represent an erosional cycle during the deposition of the sand sheet. Donoghue (1993) studied well logs in the Apalachicola Bay in conjunction with high resolution seismic data. His study indicated two seismic sequences representing two erosional cycles overlying the Mio-Pliocene Intracoastal Formation. The Mio-Pliocene Intracoastal Formation is described as a sandy, argillaceous, poorly consolidated, highly microfossiliferous calcarenite (Locker and Doyle, 1992). Locker and Doyle (1987) report the same sequence from data acquired near Cape San Blas. Schnable (1966) reports two discrete sequences of Pleistocene fluvial-deltaic sediments

with a thin veneer of silt on top from a 27 m borehole on land approximately 20 km west of Cape San Blas. Donoghue (1993) reports the lower reflector to intersect the seafloor east of Apalachicola Embayment as a series of south-southwest dipping, discontinuous low ledges.

The following summarizes the interpretation in terms of the late Wisconsin-Holocene history of the study area. At the time of maximum sea-level lowering associated with the late Wisconsinan glacial stage (approx. 17000 ybp), sea level stood approximately -90 m BSL (Donoghue, 1993; Frazier, 1974). The study area, then subaerially exposed, was stripped of its marine and deltaic deposits from previous high stands in sea level and eroded to the Miocene carbonate sequence. Based upon the studies near shore and the seismic character of S2 the author believes this surface to represent the eroded Miocene limestone. Upon the beginning of the retreat of the glaciers, fluvial volumes would have increased dramatically with fluvial sediment deposited on top of the eroded limestone bedrock. Frazier (1974) indicates a still-stand in sea level during the period 10,000-7500 ybp. Still-stands in sea level during an otherwise steady transgression would probably cause a disconformity in the fluvial deposit. This is the likely nature of the event labeled S1. The establishment of the river-mouth estuary-Apalachicola Bay (3000-4000 ybp) has meant an end to the sediment supply for the northeast Gulf shelf (Donoghue, 1989). This absence of an active source would mean that the surficial sediment of the northeast gulf is a product of constant reworking. This may explain the reflection-free character within the upper portion of the sedimentary column.

Records collected by the chirp sonar during this same cruise indicated a nearly reflection-free sequence within its 5 metre penetration limit (Anderson, pers.com, 1994).

5.0 Conclusions

A new sub-bottom profiling system, the HI-DAPT II, was designed, assembled and field tested. The system is adaptable to any number of acoustic sources thus well suited to any aqueous environment. The two-channel receiver, single hydrophone and line array, offers a flexibility not available in many conventional sub-bottom systems. Data is recorded with a high dynamic range, stored on optical disk, processed and displayed both on a CRT and in hard copy. Data processors perform well and are suited to meet many of the challenges associated with the processing of high resolution sub-bottom data.

The sparker source used in the HI-DAPT II sub-bottom profiling system provided a broad band signal with sufficient amplitude for use in profiling shallow sediments with a high degree of temporal resolution. The ghost caused by the collapse of the bubble is an unattractive feature common to all sparker sources. The digital signal processing was able to reduce the effects of the bubble pulse. The amount of time required to service the source is it's main deficiency. Field tests have shown the system to perform relatively well in a surface towed mode. Problems associated with the deep tow are likely related to the hydrodynamics of the tow body itself. The surface ghost caused by the submergence of the towfish also indicates that an alternate towing vehicle needs to be found. Future research should be directed towards investigating a means of replacing the sparker tips without a complete disassembling of the source as well as designing a new tow body.

The two-channel configuration of the hydrophone streamer has been proven to be adaptable to both shallow and medium water depths. The streamer has not been used to record data from depths of 200 metres therefore it is impossible to evaluate the streamer for deep water operations.

The pipeline processing and display of data limits the shot repetition rate to a maximum of 1 shot per 1.5 seconds. In situations with shallow water and vessels which cannot maneuver at low speeds data coverage will be low. This is particularly dangerous in areas with high dipping reflectors where the risk of spatially aliasing is greater. Two alternatives are available to increase the repetition rate without sacrificing processing capabilities. The first would involve replacing the digital signal processing board with one which operates at a higher speed. The second alternative would be to move the system to a platform where true multitasking could be performed. Because the PC platform was chosen to keep the costs of such a system to a minimum, the first alternative is recommended.

The objectives of the field tests near Panama City were met. The event interpreted to represent the base of the West Florida Sand Sheet can be seen throughout the survey area. Whereas, lack of physical data prevents substantiation of this interpretation, the findings do agree with those of Donoghue (1993) and Locker and Doyle (1992). Whereas a profile from the survey site east towards Cape San Blas would have provided the data to validate the interpretation, it was beyond the scope of this program.

In conclusion, the HI-DAPT II sub-bottom profiling system offers many advantages over conventional systems which have been considered industry standards. The ability to acquire, store, process and display high quality digital data represents a great advance in comparison to analog dry paper records. The advantage of in-line processing will allow survey parameters to be based on a better quality output than previously available. The processing of high resolution seismic data in a cost effective manner will yield a better quality product for the marine geologist. The ability to remove water multiples, source ghosts and other artifacts of the data acquisition process will make interpretation of such data less difficult in the future.

Glossary

analog-to-digital (A/D): The process of converting an analog voltage to a digital number.

automatic gain control (AGC): A gain function applied in the time domain where the amplitudes of values in a user defined window are scaled to the maximum value in that window. The application of an AGC tends to equalize the amplitude values within a seismic trace.

binary format: A format of storing digital numbers which uses the binary number system.

cathode ray tube (CRT): The mechanism used in the video display of computer systems.

common depth point (CDP): The situation where the same portion of the subsurface is involved in producing reflections from different source receiver locations.

deconvolution: The process of undoing the effect of another filter. In the seismic case this filter can be earth response or an artifact of the acoustic source.

digital signal processing (DSP): A specialized computer chip, usually a parallel processor, dedicated to processing digital data.

first break: The seabed reflection on a marine seismic record.

front end: The interface from which a user controls a geophysical instrument and which analog inputs undergo signal conditioning and are digitized.

input/output (I/O): The process which refers to how information is input and output from a computer.

line array: A receiver in which a group of elements are attached in a straight line and whose outputs are summed to provide a single output.

minimum phase wavelet: A wavelet that exhibits minimum phase in the frequency domain. In the time domain this wavelet type wavelet will have all its energy concentrated towards time zero.

normal moveout (NMO): The variation in the time of a reflection due to the variation of source/receiver offset.

pegleg multiple: A multiple reflection from different interfaces such that its ray path is not symmetrical, or a multiple reflection which is reflected more than once within a certain layer.

post stack: A time interval in a processing flow which occurs after data have been gathered in to CDP gathers, corrected for NMO and stacked to form a composite record. Similar to a normal incidence profile as collected by a single channel sub-bottom profiler.

overrun rate: The rate of firing of an acoustic source relative to the distance covered. It is desirable to fire the source at an interval whereby successive footprints on the sea floor provide a minimum of total coverage.

real time: The process of processing and displaying data as it is acquired.

seismic section: A collection of seismic records displayed adjacent to each other to display a 2 D time/depth section of the subsurface.

time variant gain (TVG): A gain function applied to seismic data whereby the gain is applied as some function of time.

REFERENCES

- Donoghue, J. F., Sedimentary environments of the inner continental shelf, northeastern Gulf of Mexico, *Transactions Gulf Coast Association of Geological Societies*, Vol 39, p. 335-363, 1989. .
- Donoghue, J. F., Late Wisconsin and Holocene deposit history, northeastern Gulf of Mexico. *Marine Geology Vol. 112*, p. 185-205, 1993.
- English, J.M., Inkpen, S.T., and Guigne, J.Y., A New High Frequency, Broadband Seismic Source, *Offshore Technology Conference*, Houston, Texas, 1991.
- Frazier, D. E., Depositional episodes, their relationship to the Quaternary stratigraphy framework in the northwestern portion of the Gulf Basin, *Tex. Bur. Econ. Geol. Circ., Vol. 74, No. 1*, 28 pp., 1974.
- Lindseth, R. O., *Digital Processing of Geophysical Data: A REVIEW*, Continuing Education Program, Society of Exploration Geophysicists, Tulsa, Oklahoma, 1982.

Locker, S. D. and L. J. Doyle, Neogene to Recent stratigraphy and depositional regimes of the northwest Florida inner continental shelf. *Marine Geology Vol. 104*, 128-138, 1992.

Richardson, M. D., Costal benthic Boundary Layer Special Research Program: A Review of the First Year, Volume 1, Naval Research Laboratory Report NRL/MRI/7431-94-7099, Stennis Space Centre, MS 1994.

Robinson, E. A., and S. Treitel, *Geophysical Signal Analysis*, Prentice-Hall, Inc., Englewood Cliffs, NJ, 1980.

Schnable, J., Evolution and development of part of the northwest Florida coast., Ph.D. dissertation, Florida State University, 231 p., 1966

Schock S. G. and L. R. LeBlanc., Chirp sonar: new technology for sub-bottom profiling, *Sea Technology. Vol. 31 No. 9*, 35-43, 1990

Simpkin, P. G. and A. Davis, For Seismic Profiling in Very Shallow Water, a Novel Receiver, in *Sea Technology Vol 34 No.9*, 21-28, 1994.

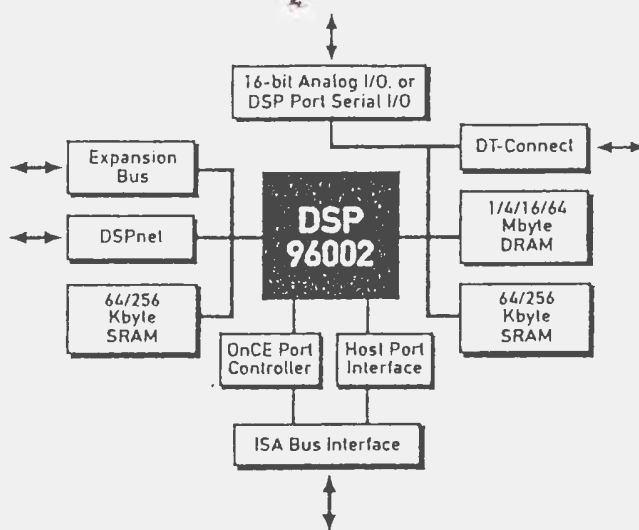
Telford, W. M., Geldart, L. P., Sheriff, R. E. And D. A. Keys, *Applied Geophysics*,
Cambridge University Press, Cambridge, 1976

Trabant, P. K., *Applied High-Resolution Geophysical Methods Offshore Geoengineering
Hazards*. International Human Resources Development Corporation, Boston,
1984..

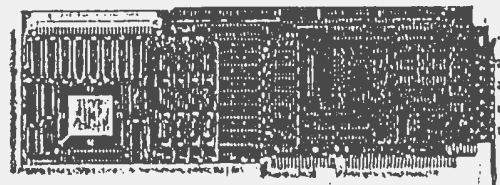
Yilmaz, O., Seismic Data Processing , *Investigations in Geophysics; Volume 2* edited by
Edwin B Neitzel, Society of Exploration Geophysicists, Tulsa, 1987

Appendix A
DSP96002 Specifications

up to 60 MFLOPS
floating-point DSP
compatible AT/ISA/EISA
I/O and serial I/O
options
up to 64 Mbytes DRAM
up to 512 Kbytes SRAM
DT-Connect and DSPnet
interfaces
Expansion bus for
multi-board systems



DSP-96
Motorola DSP96002
Floating-Point DSP



The DSP-96 brings up to 60 MFLOPS of Motorola DSP96002 floating-point power to a single ISA-bus board. Extensive processor expansion capabilities allow multimaster connection of up to 10 boards via DSPnet, or shared memory connection of up to four boards (MM-96 boards may be equally connected with DSP-96s). Up to 64 Mbytes of DRAM and 1/2 Mbyte of zero-wait-state SRAM are front-ended by CD-quality stereo analog I/O or a DSP Port high-speed serial connection to external I/O hardware such as the ProPort 656 (see page 27). And DT-Connect opens the board up for video frame grabber inputs or multi-channel data acquisition.

DSP-96 Series: 50 MFLOPS, single-processor 32-bit floating-point DSP board with signal I/O daughter card. Standard hardware includes 33 MHz processor, two 16 Kword (x32 bits) SRAM banks (32 Kwords or 128 Kbytes total), and 24 Kwords (1 Mbyte) DRAM, plus DT-Connect and DSPnet interfaces, and an Expansion Bus. Standard DSP-96 includes a channel, 16-bit analog I/O (via RCA connectors). Alternate DSP-96D version substitutes a DSP Port interface (for use with ProPort 656) in place of on-board analog I/O facilities. Bundled software includes Janus resident monitor, Bug-96 debugger, host driver, and example programs.

* DSP-96	DSP96002 Development Board with 33 MHz processor and dual-channel 16-bit analog I/O	\$4,995.00
DSP-96D	DSP96002 Development Board with 33 MHz processor and DSP Port Interface	4,695.00
40M-D96	40 MHz (60 MFLOPS) DSP96002 processor option for DSP-96 or DSP-96D	500.00
* 64X-D96	Upgrade two standard SRAM banks to 64 Kwords (256 Kbytes) per bank	375.00
* 1M-96	Upgrade standard DRAM to 1 Mword (4 Mbytes)	300.00
4M-96	Upgrade standard DRAM to 4 Mwords (16 Mbytes)	1,750.00
16M-96	Upgrade standard DRAM to 16 Mwords (64 Mbytes)	6,600.00
LHW-D96	Extended hardware warranty, DSP-96 series	500.00
ProPort 656	Pro audio-quality dual-channel oversampling 16-bit analog I/O for DSP Port (DSP-96D only)	1,595.00

Accessories for MM-96 and DSP-96

CBL-HYP	Expansion Bus Interface cable; specify which DSPs will be connected	\$100.00
CBL-DT	DT-Connect Interface cables (pair)	50.00
CBL-NET	DSPnet Interface cable	40.00

Optional PC Development Tools and Application Software for DSP96002 Products

* DSP96KCLASA	Motorola DSP96002 Assembler and Simulator	\$495.00
DSP96KCCA	Motorola DSP96002 C Compiler and Assembler	709.00
* C96KX-S	Intermetrics InterTools DSP96002 C Compiler/Assembler, with 1 year Intermetrics service/support policy	3,000.00
* D96KX-S	Intermetrics XDB DSP96002 C-Source Debugger; Includes one year Intermetrics service/support policy	2,760.00
HSA-96	Hypersignal-Acoustic software (DSP-96 only)	1,489.00
HSM-96	Hypersignal-Macro software (DSP-96 only)	1,289.00
HSRT3-96	Hypersignal-Windows RT-3 software package (DSP-96 only)	2,995.00
HSRT4-32	Hypersignal-Windows RT-4 software package (DSP-96 only)	7,995.00
DSPW-96	Momentum Data Systems DSPworks software	495.00
QED-96	Momentum QEDesign 1000 filter design software with 96002 code generator, DOS version	1,145.00
WQED-96	Momentum QEDesign 1000 filter design software with 96002 code generator, Windows 3.x version	1,145.00

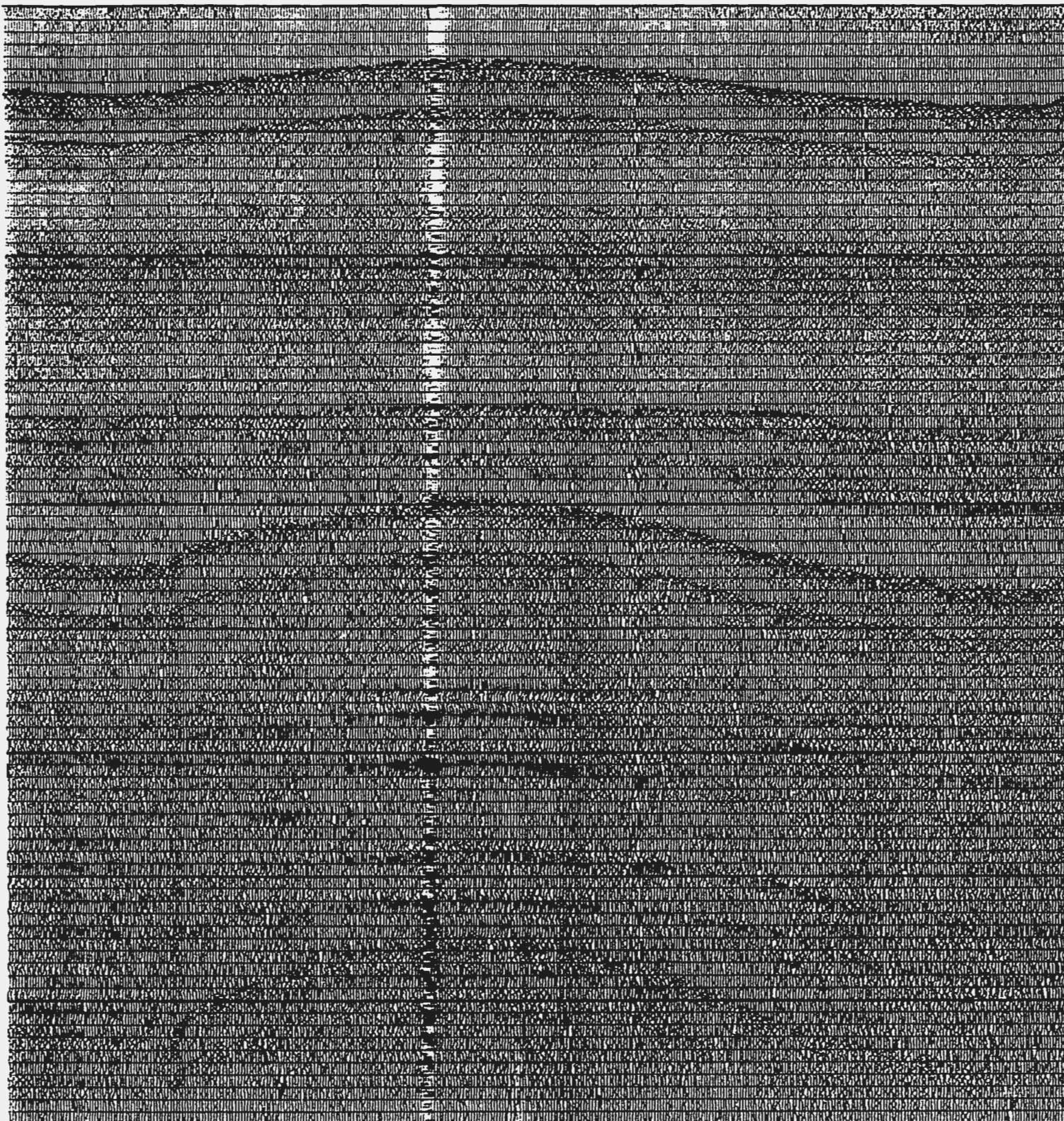
* HI-DAPT II OPTIONS

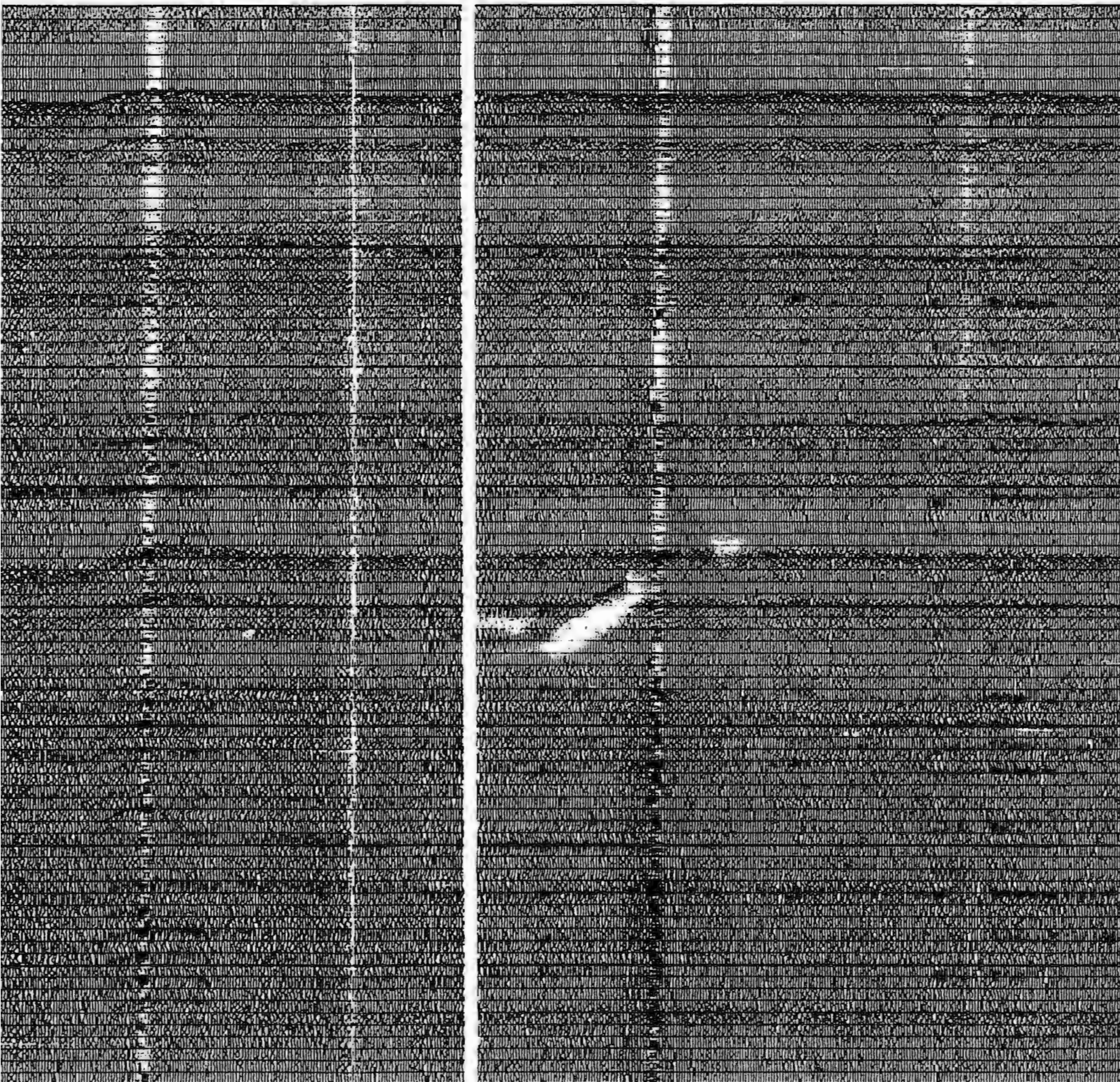
Appendix B
Seismic Sections

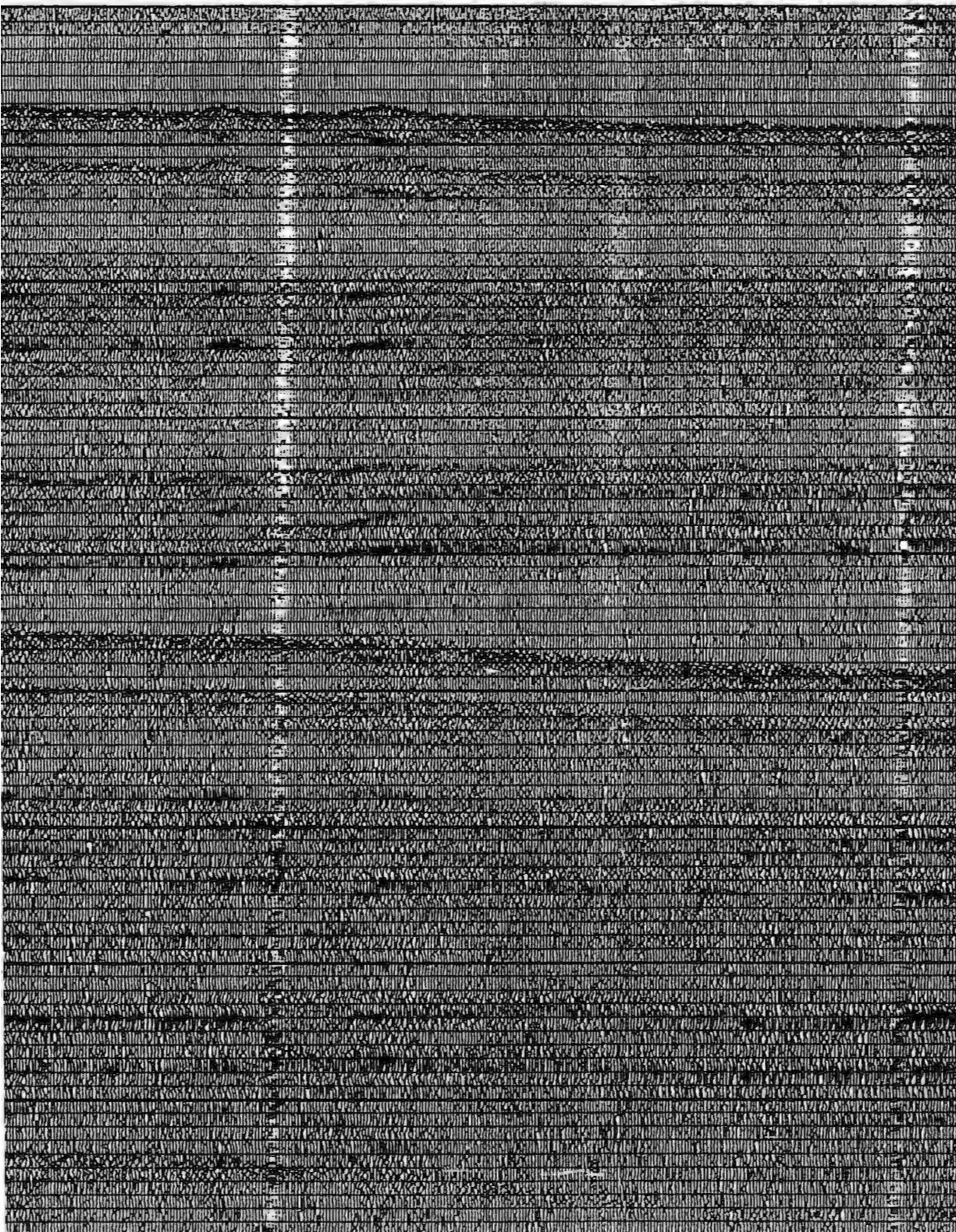
Seismic Section Legend

Horizon S1 -----

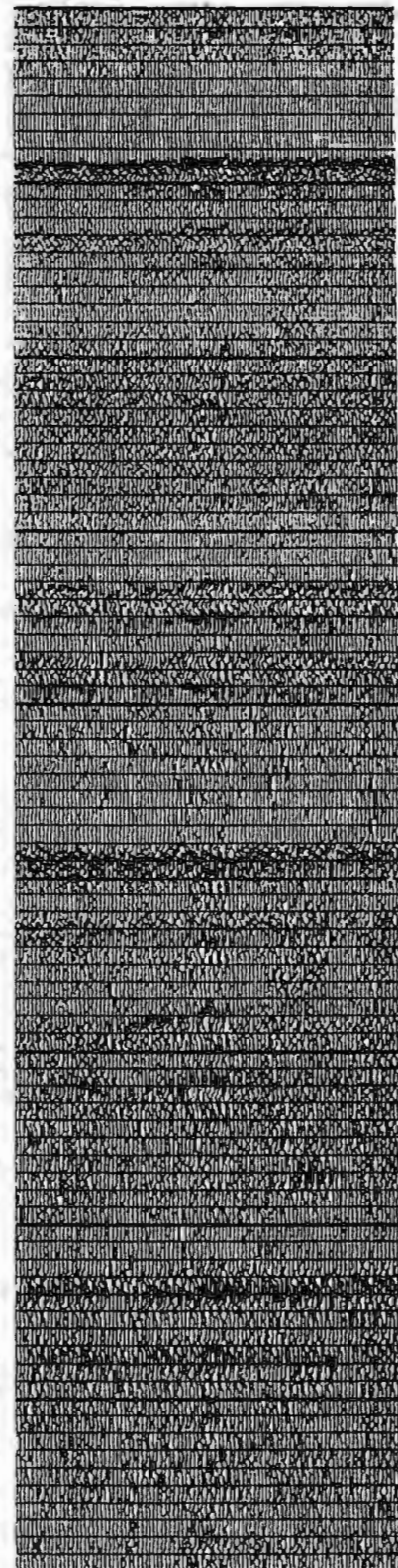
Horizon S2 ----->



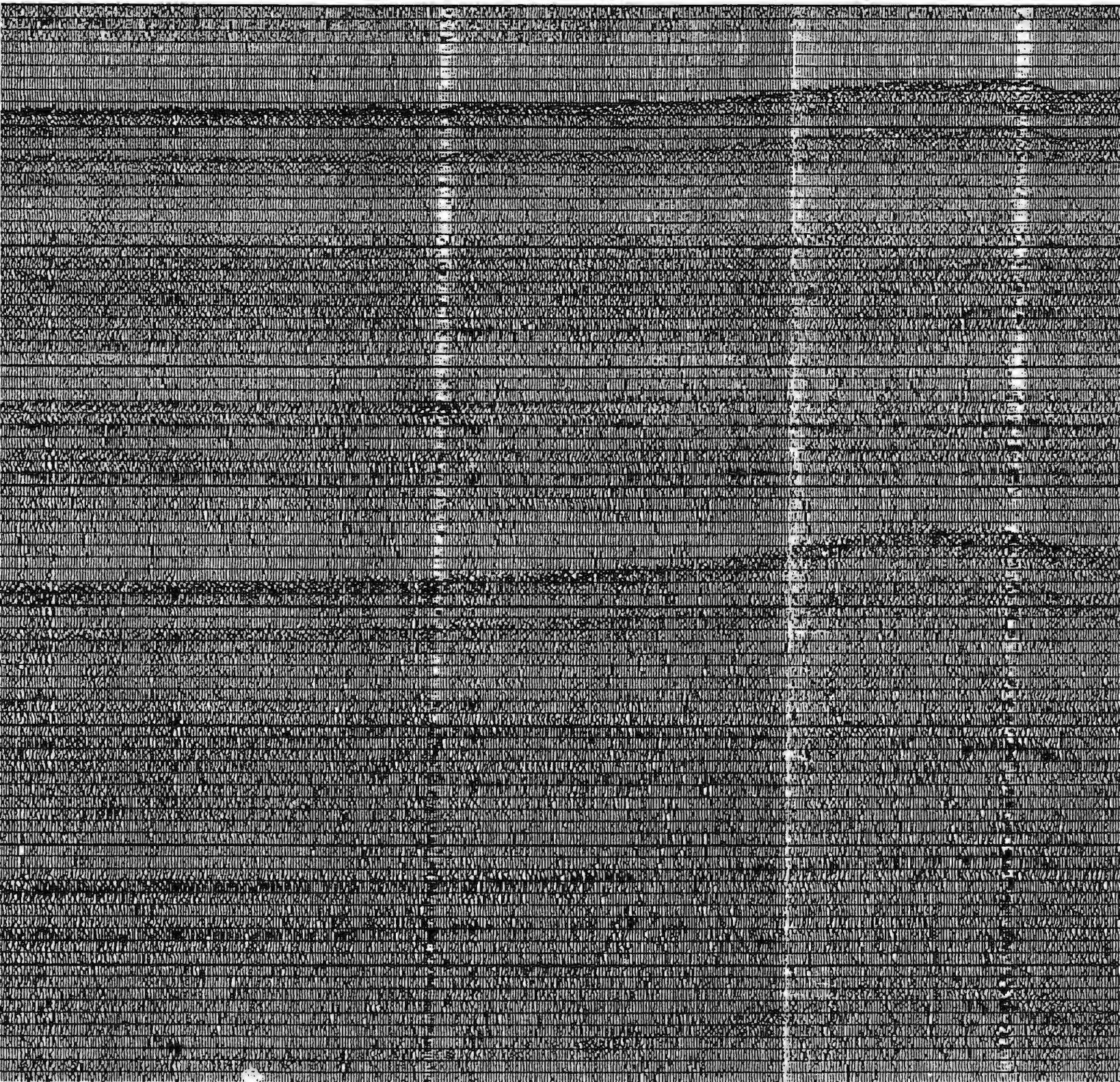




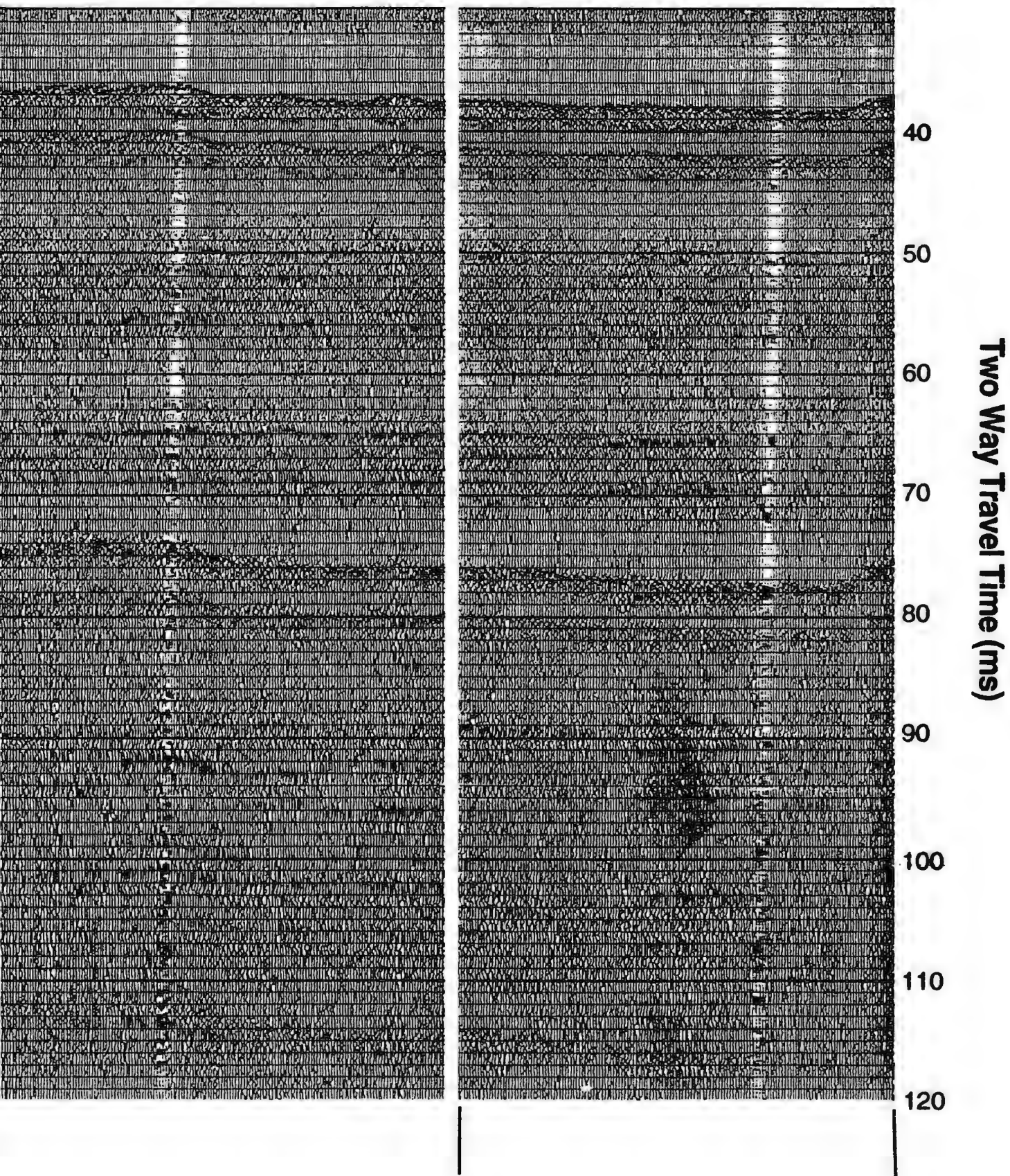
sp. 800



sp. 1000



sp. 1270



sp. 1500

sp. 1650

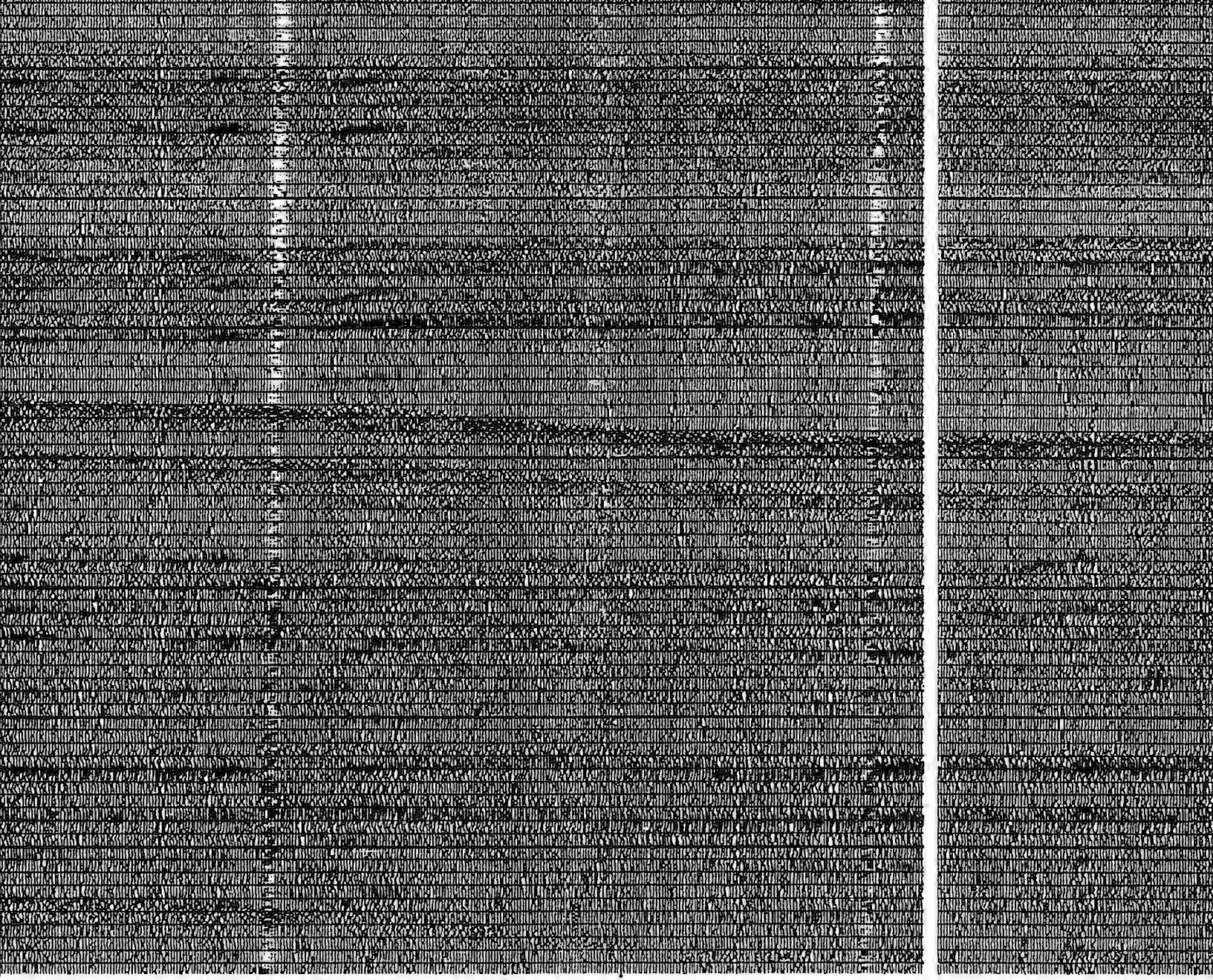
sp. 30

wp. 13



sp. 500





sp. 800

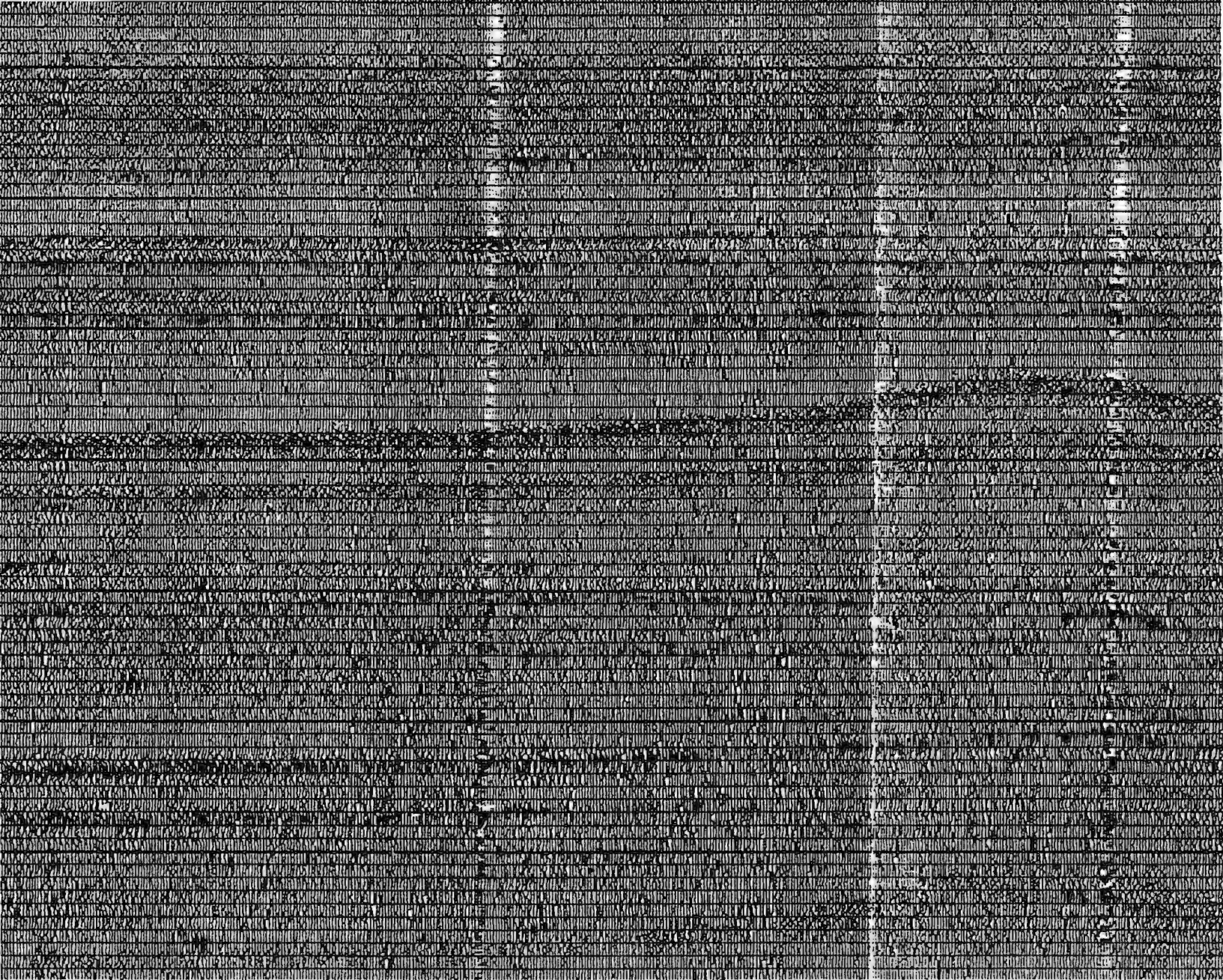
sp. 1000

Cross Tie
Profile 20-21
@ sp. 2060



1000 metres

1000



sp. 1270

Cross Tie
Profile 20-21
@ sp. 700

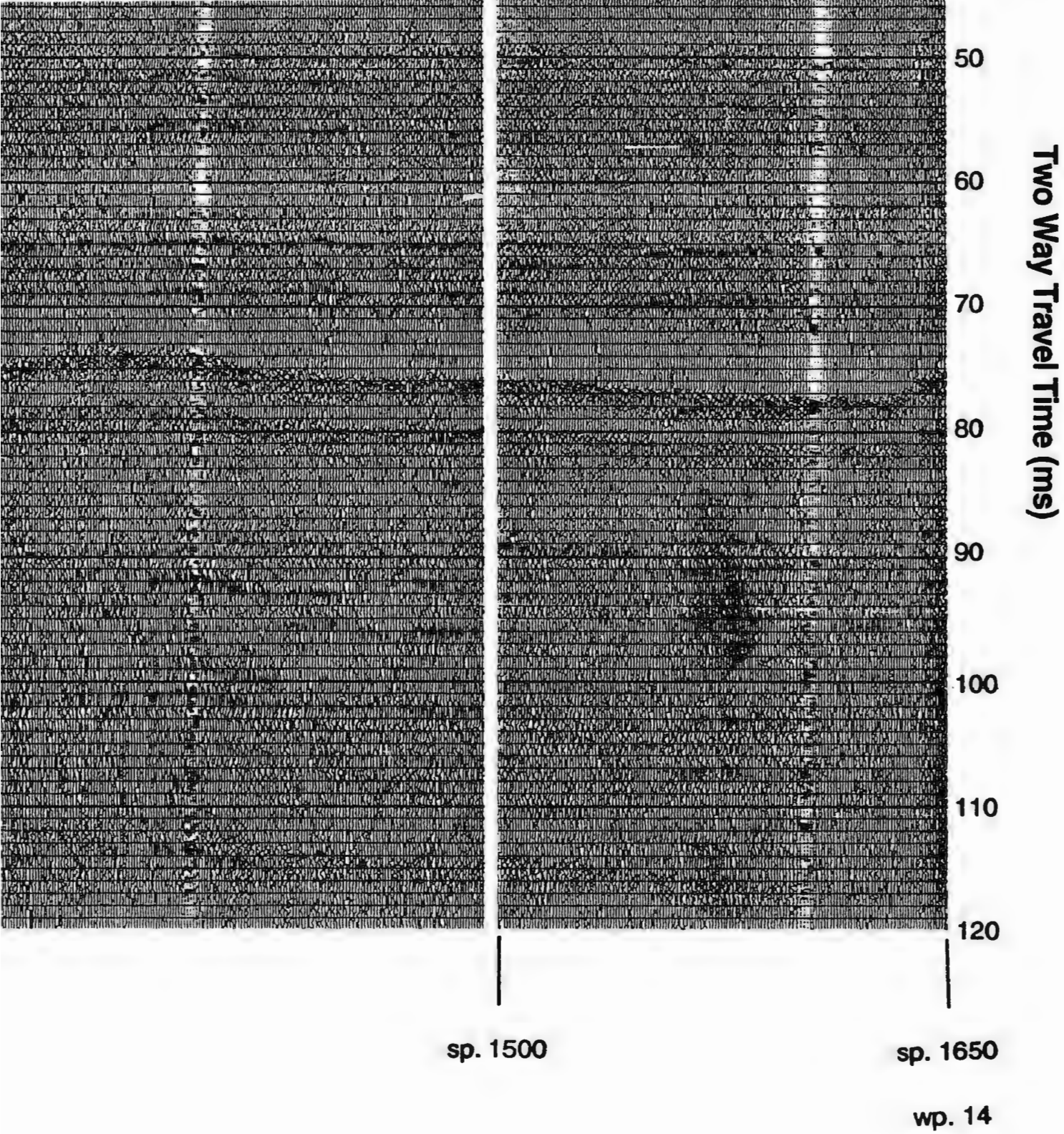
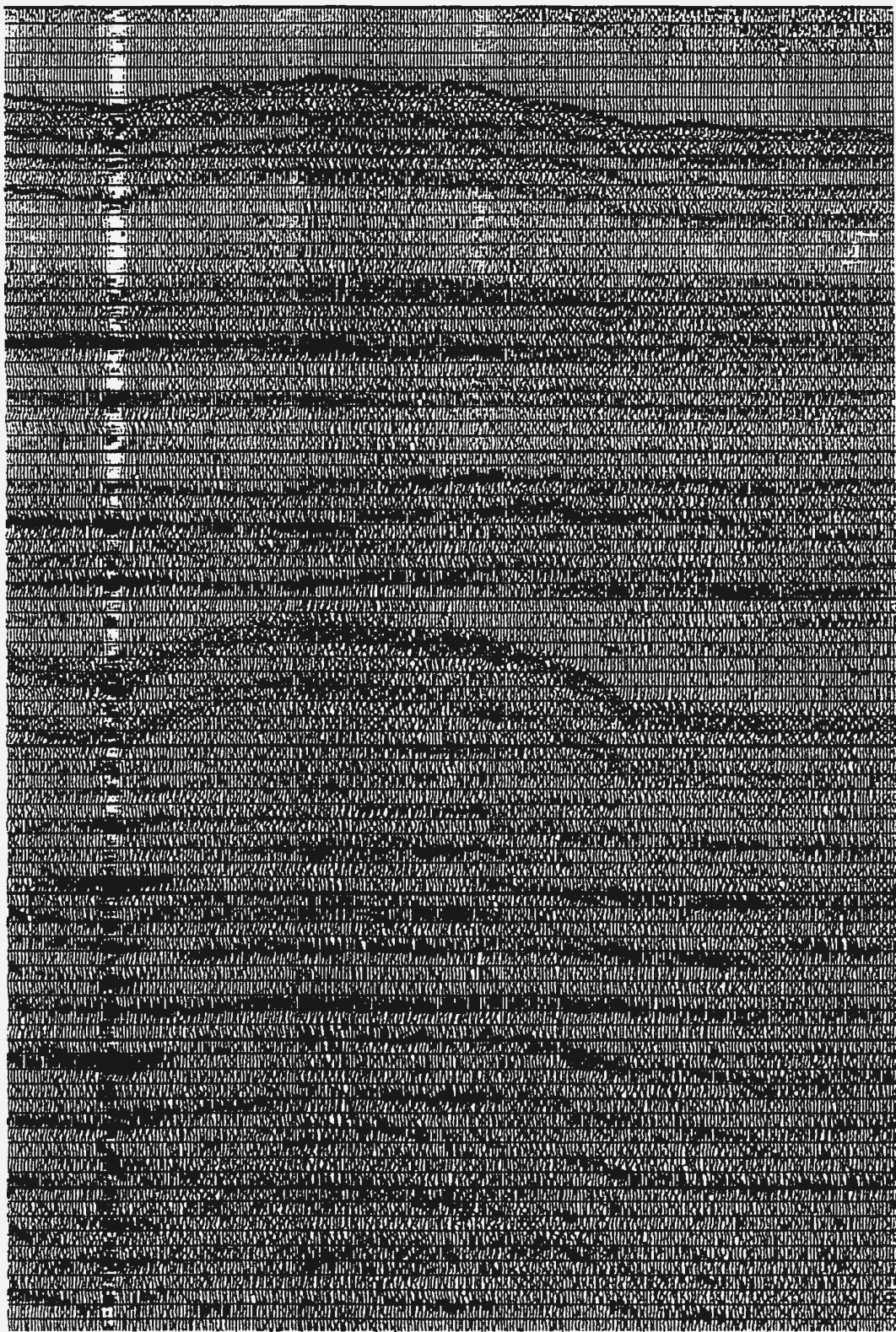


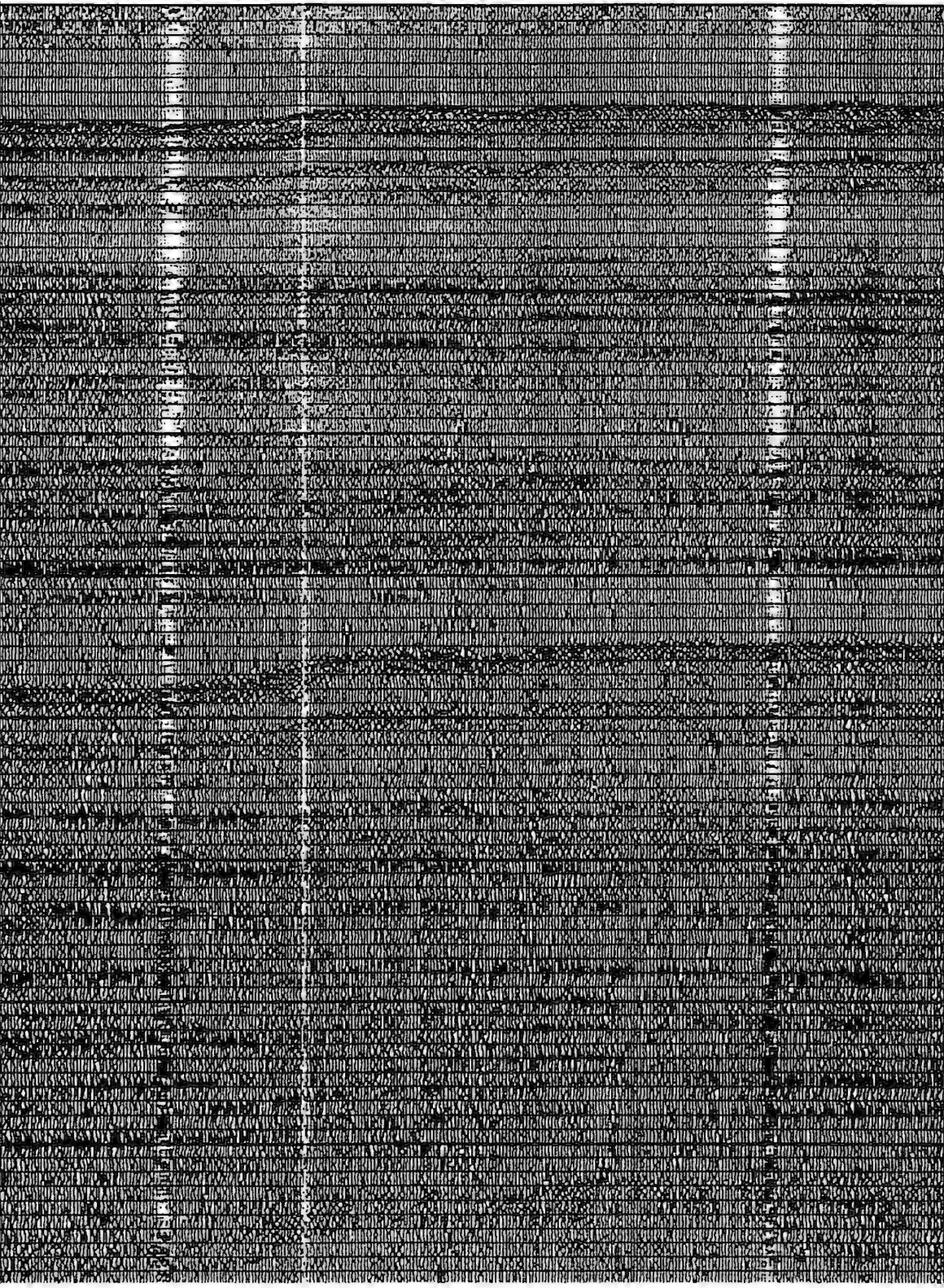
Figure 4.4 Seismic Profile 13-14



sp. 1599

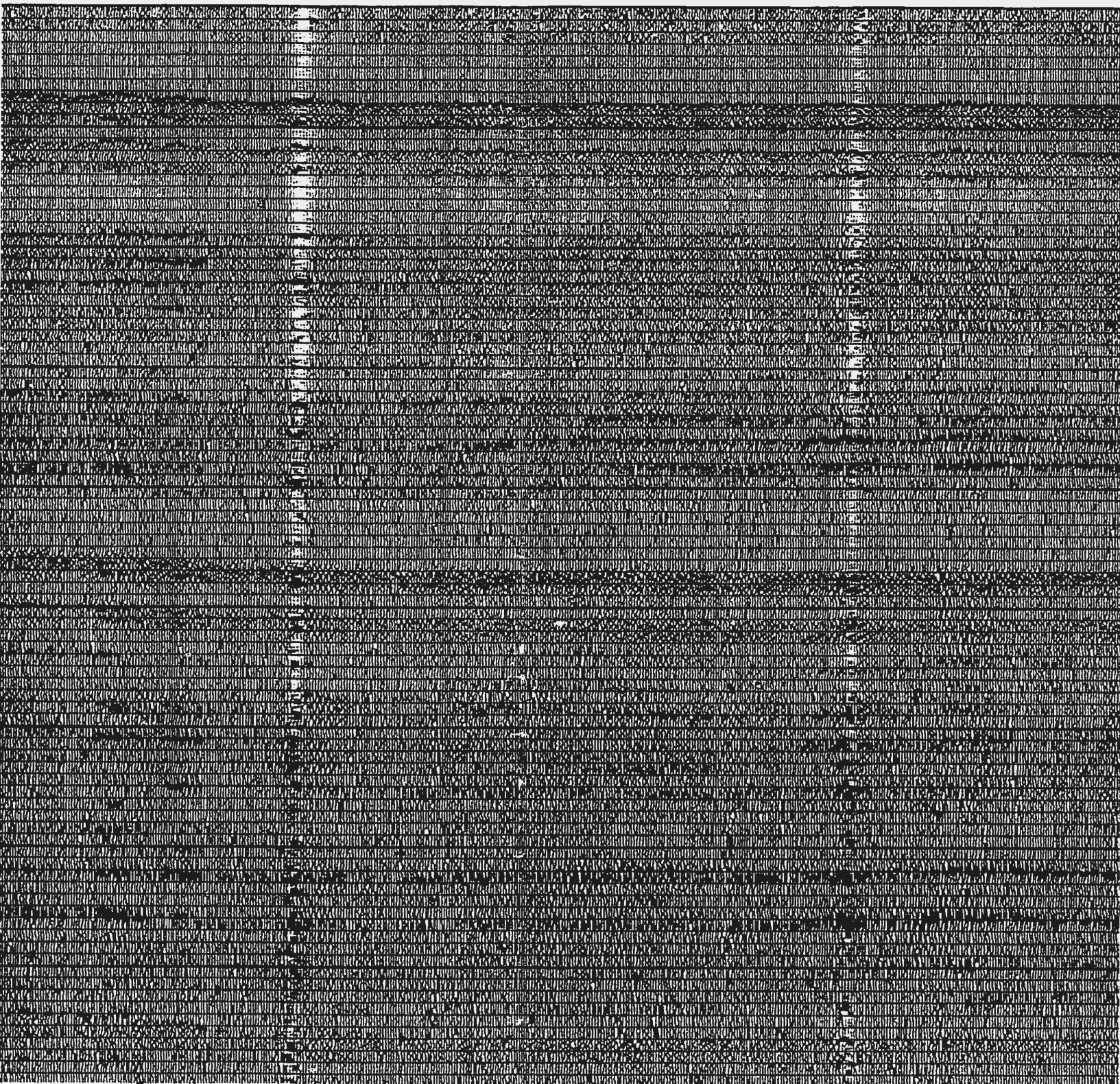


sp. 1500

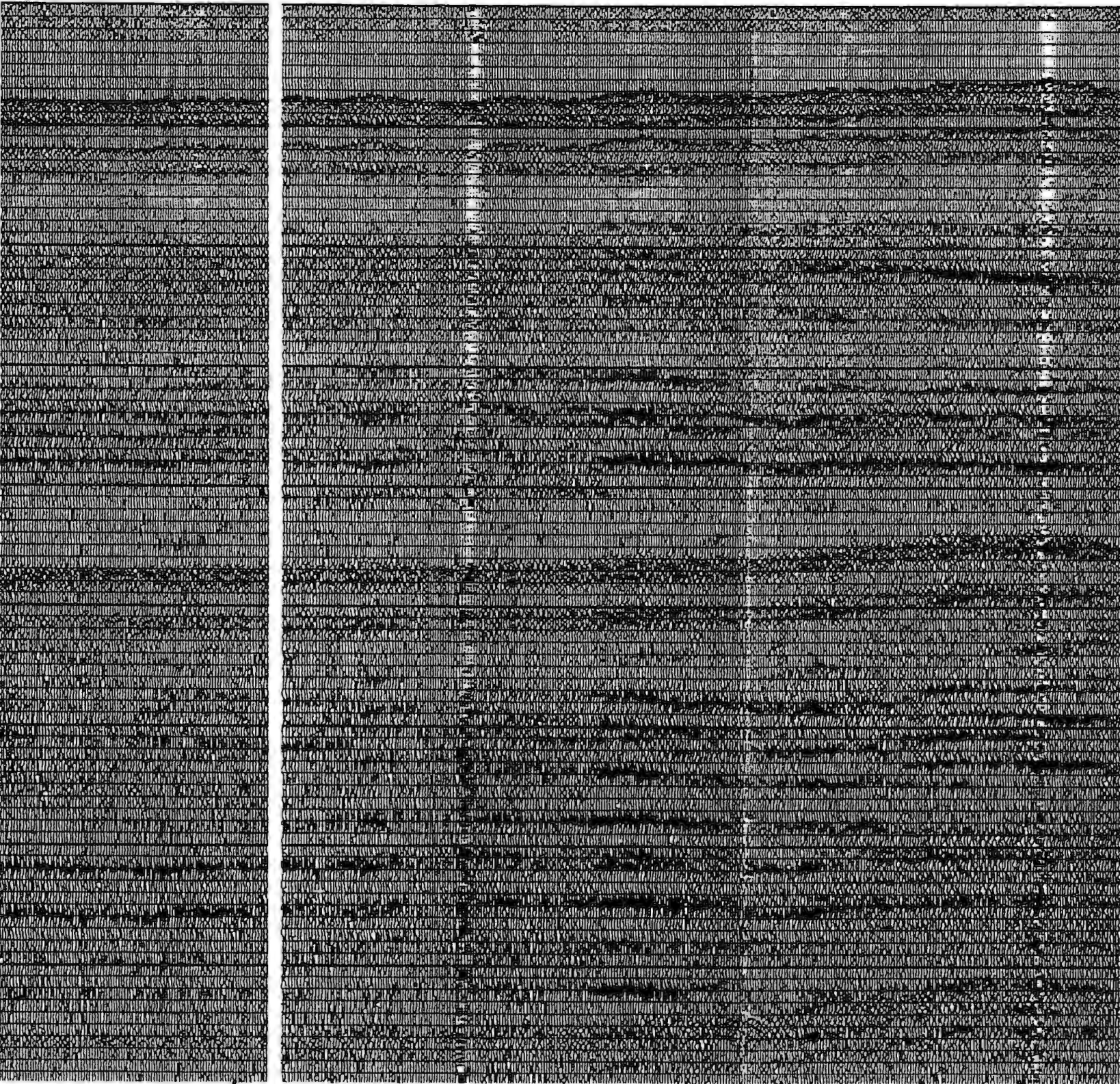


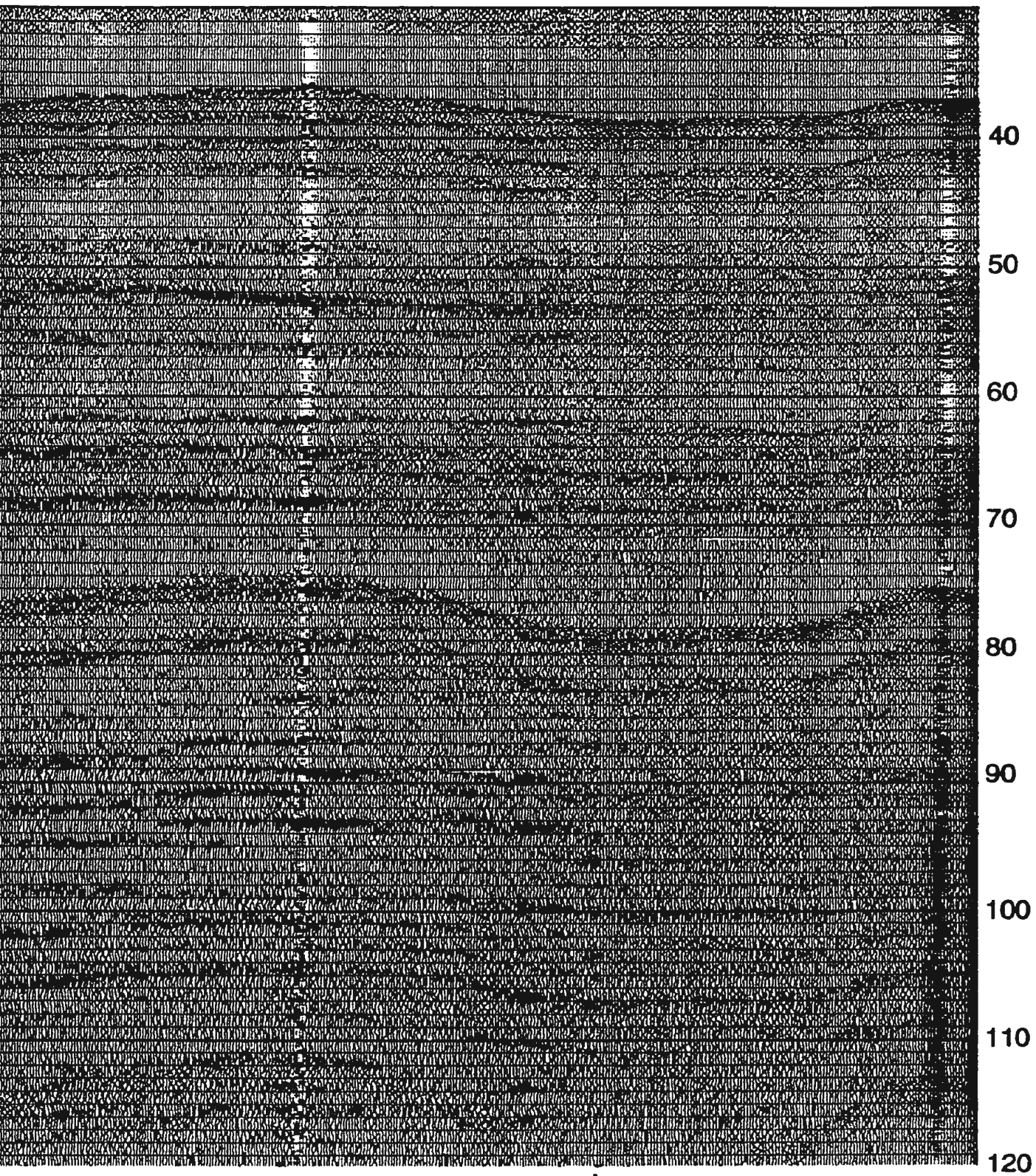
sp. 1000

sp. 90

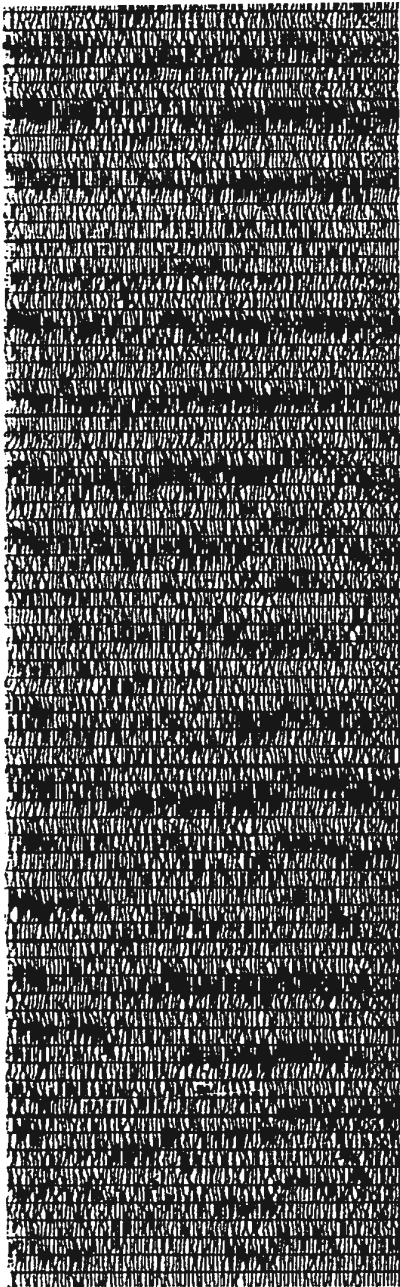


|





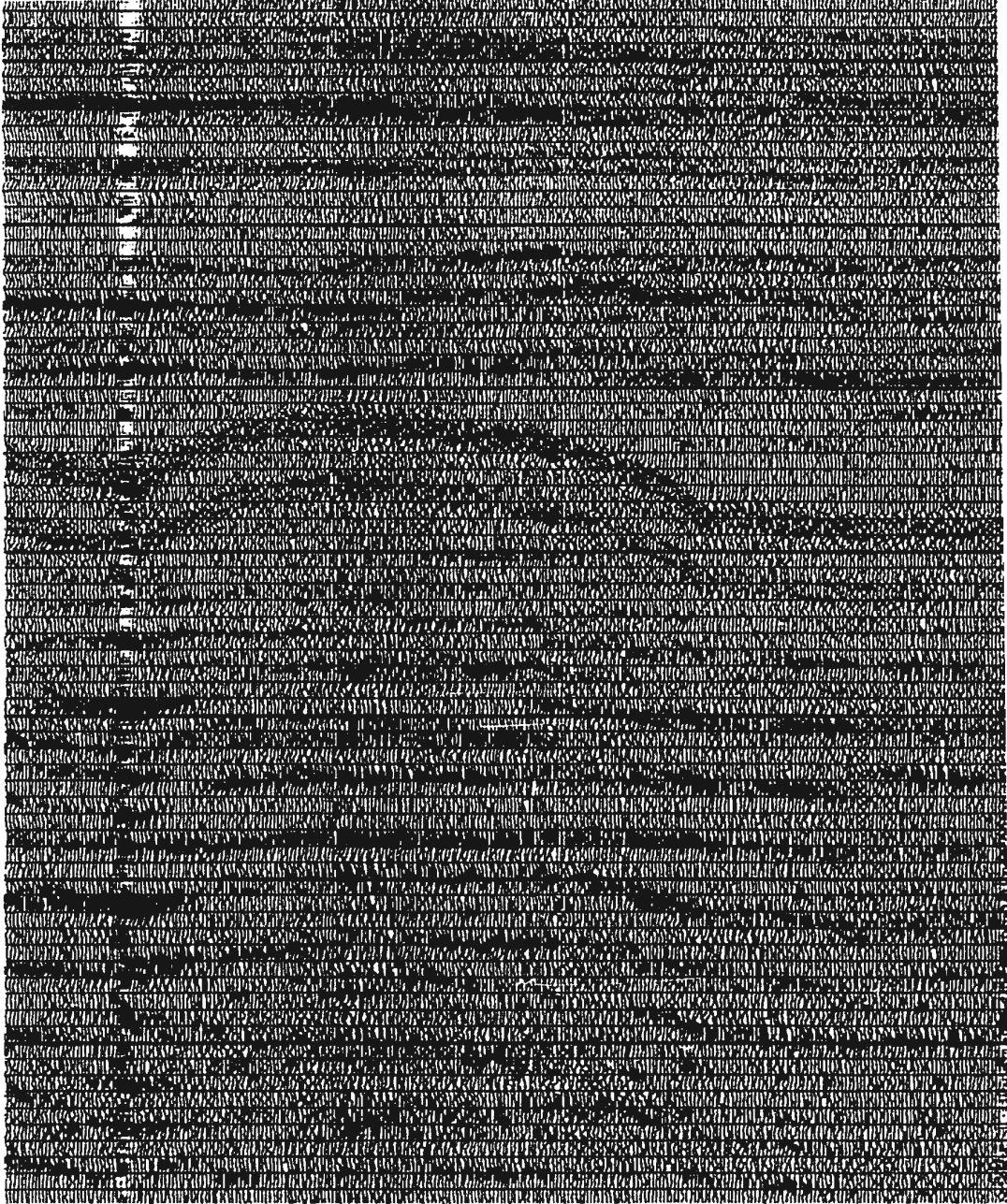
Two Way Travel Time (ms)



sp. 1599

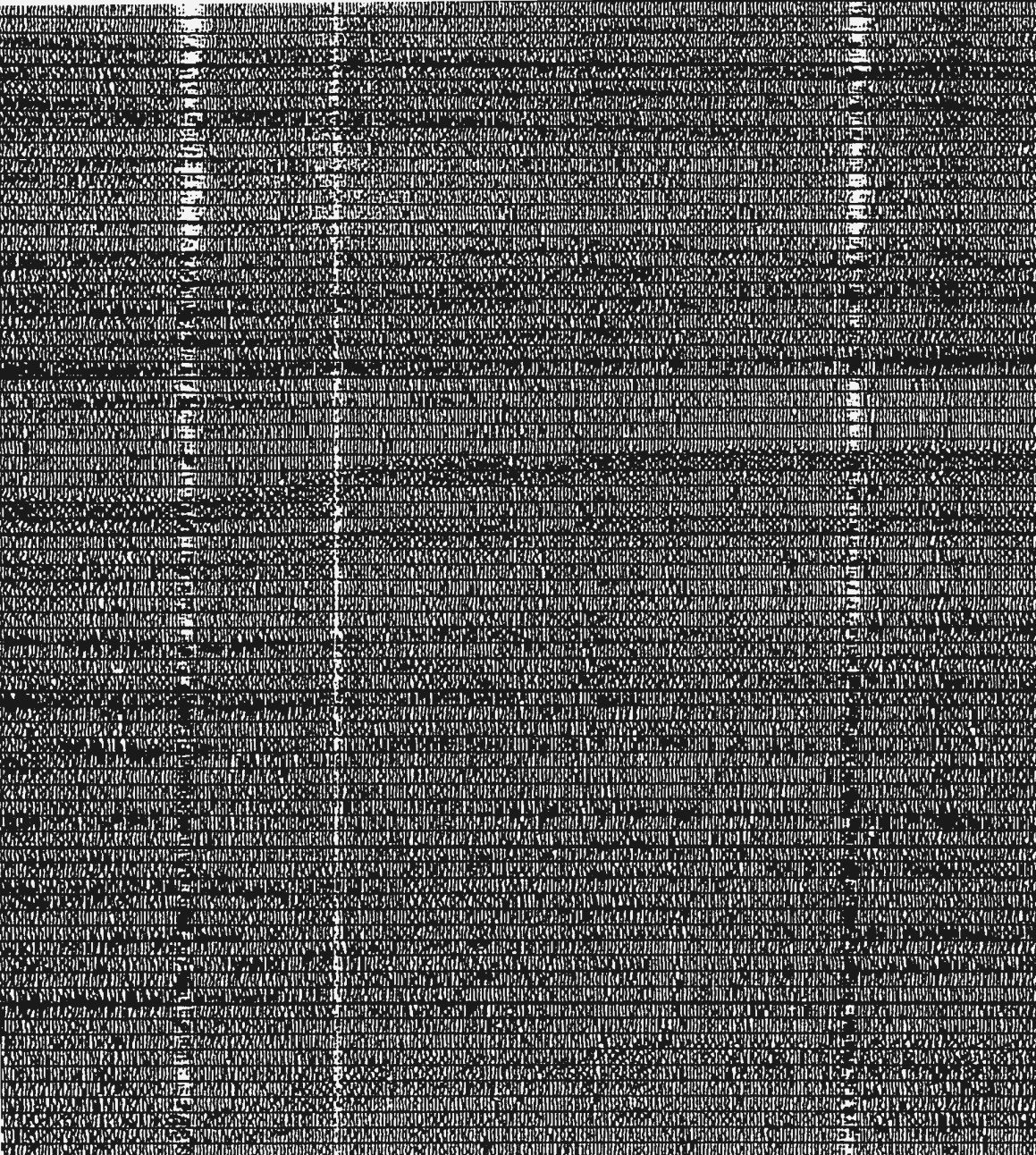
wp. 4

0ms



sp. 1500

1500

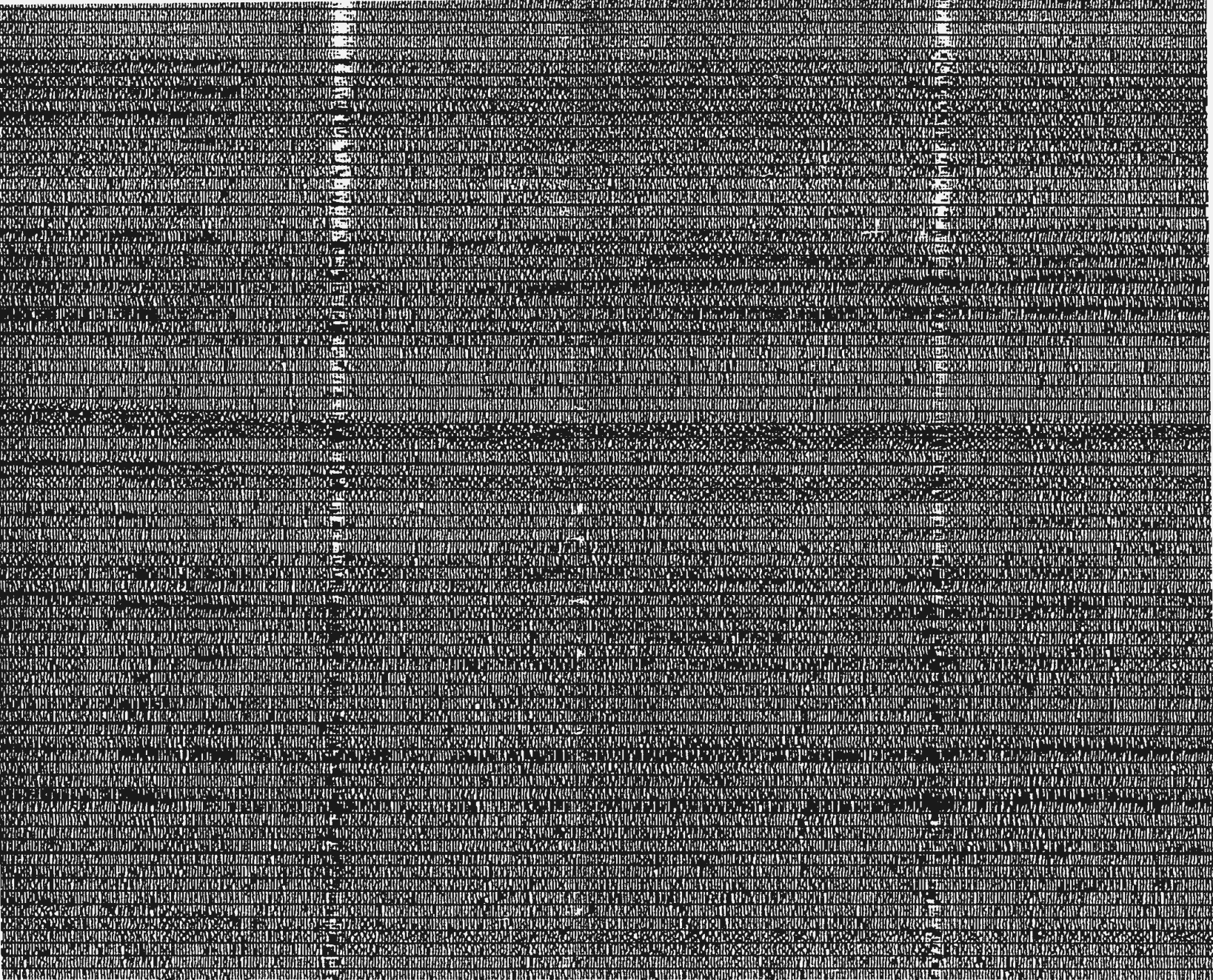


sp. 1000

sp. 900

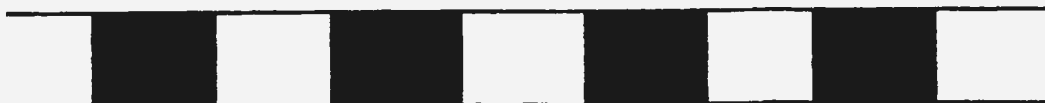
Cross T
Profile 20
@ sp. 23



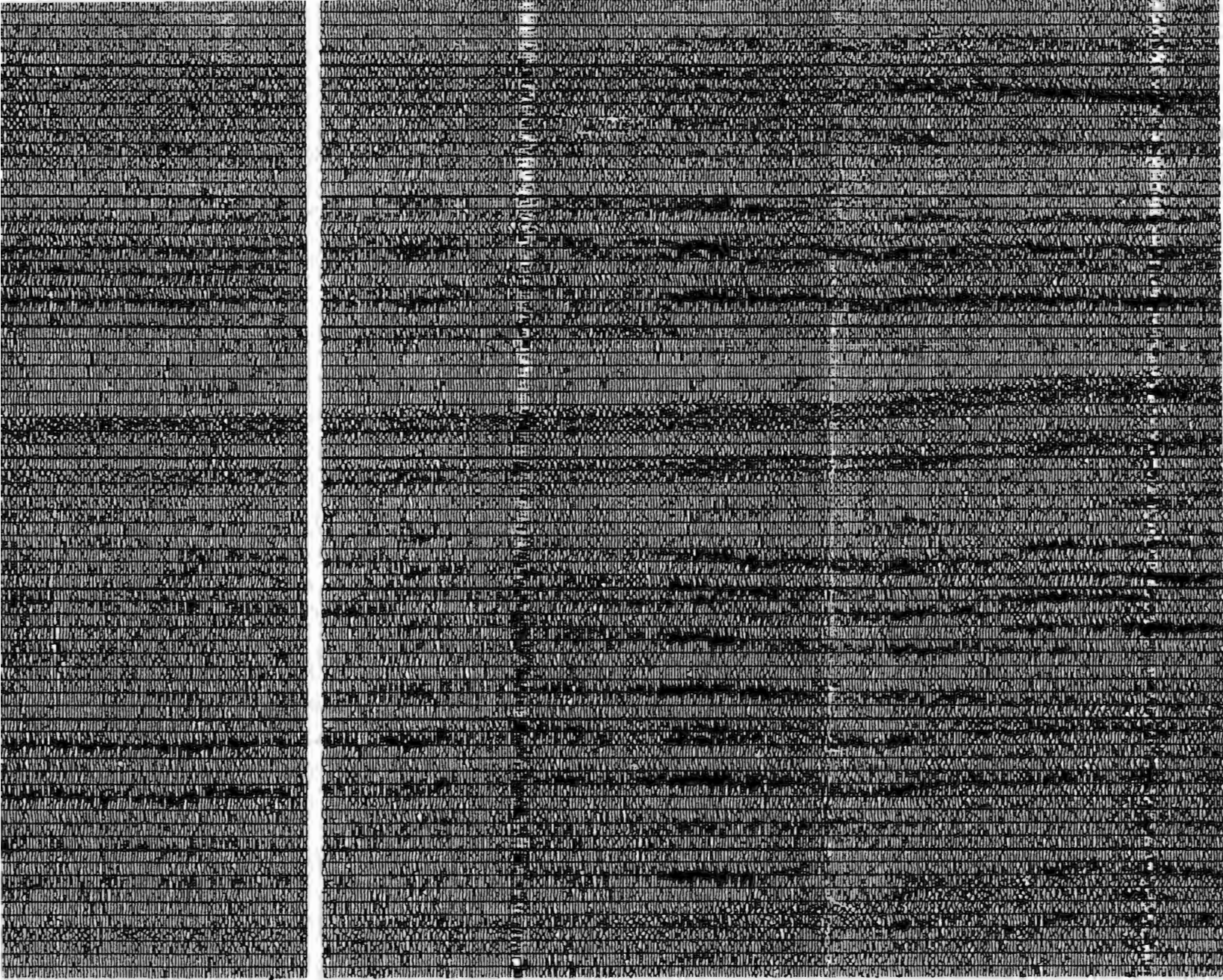


sp. 900

Cross Tie
Profile 20-21
@ sp. 2300

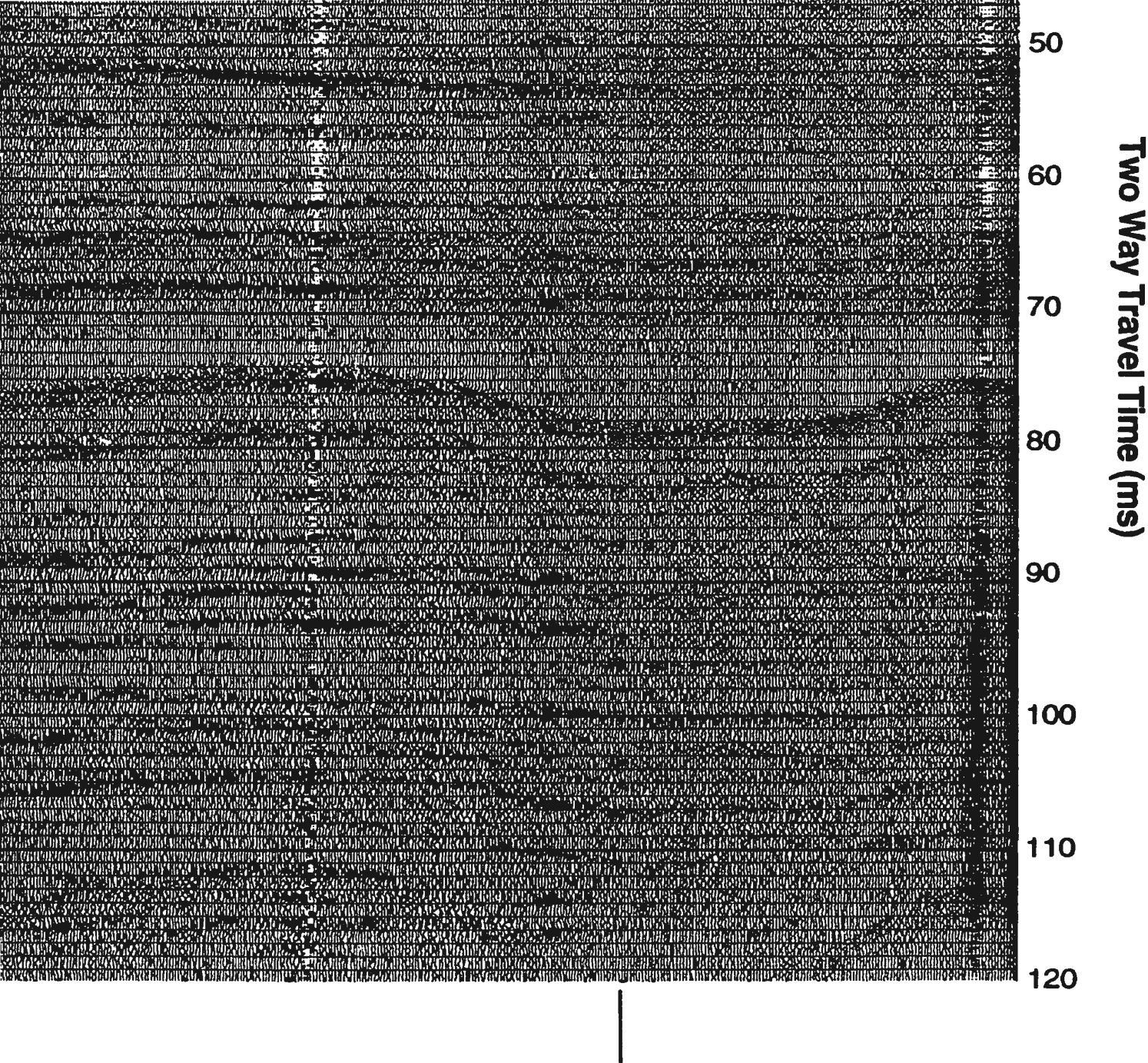


1000 metres



sp. 510

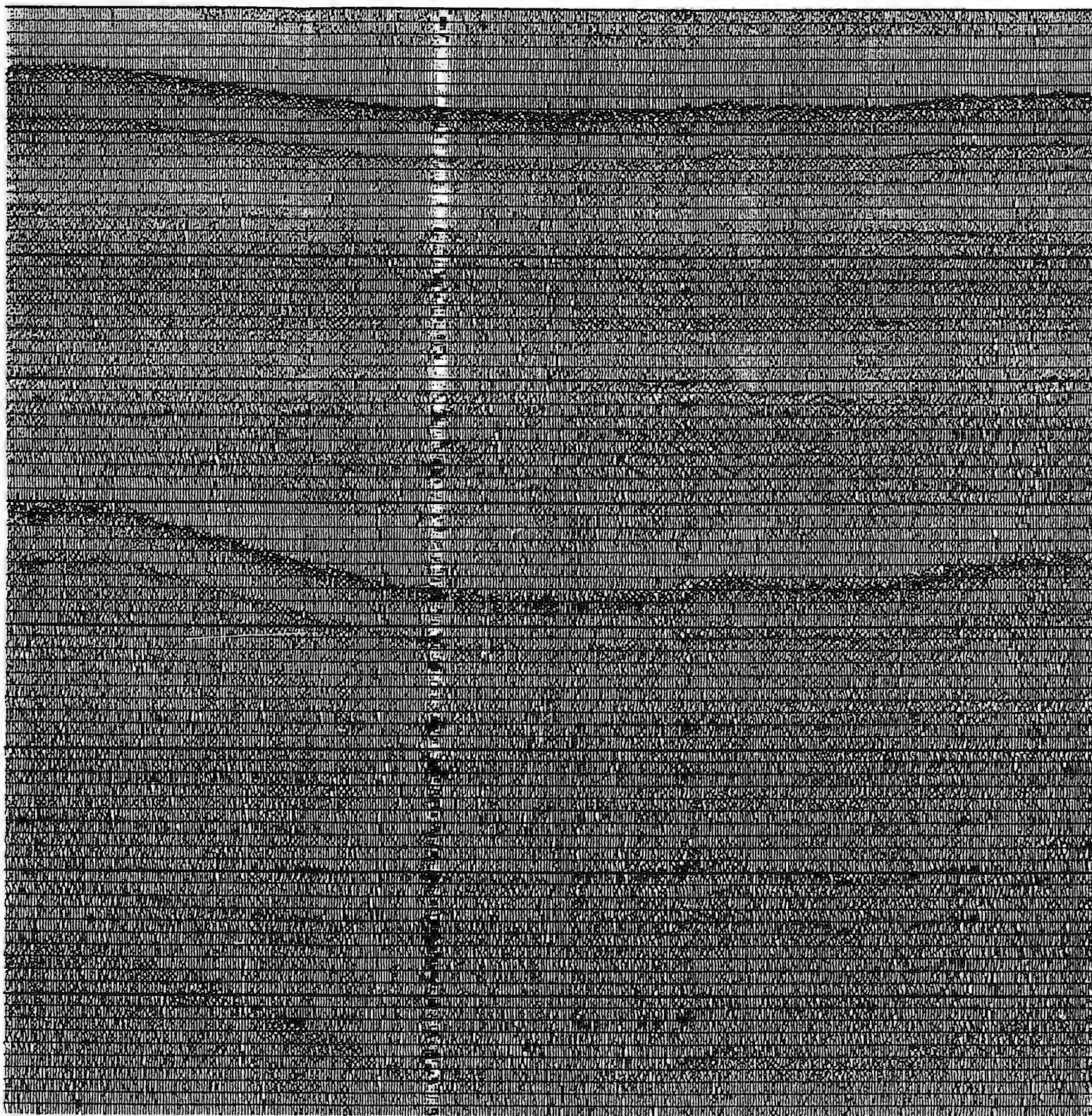
Cross Tie
Profile 20-21
@ sp. 550

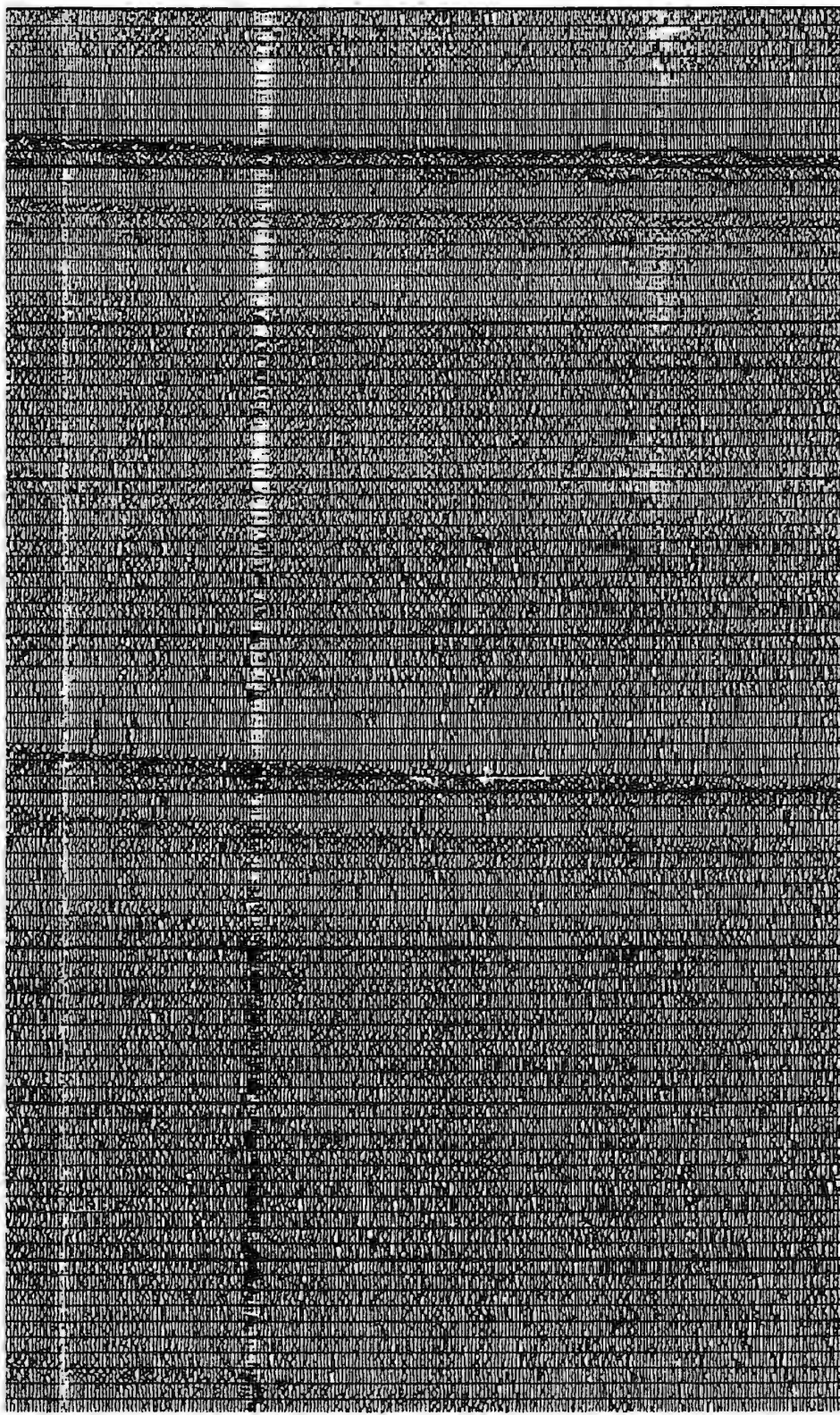
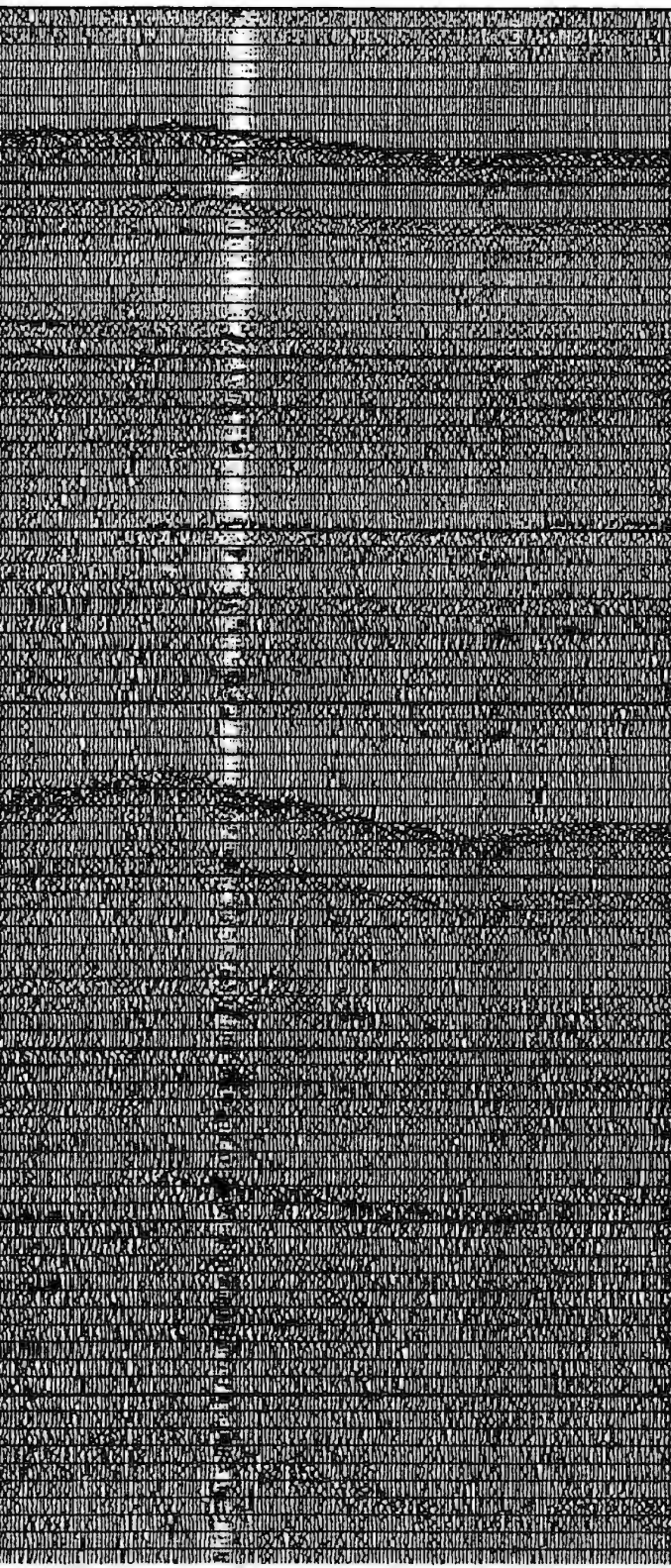


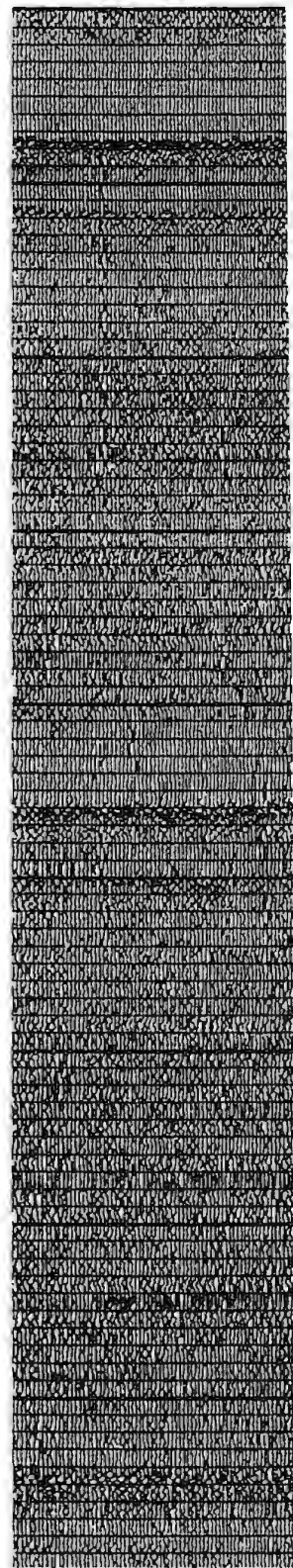
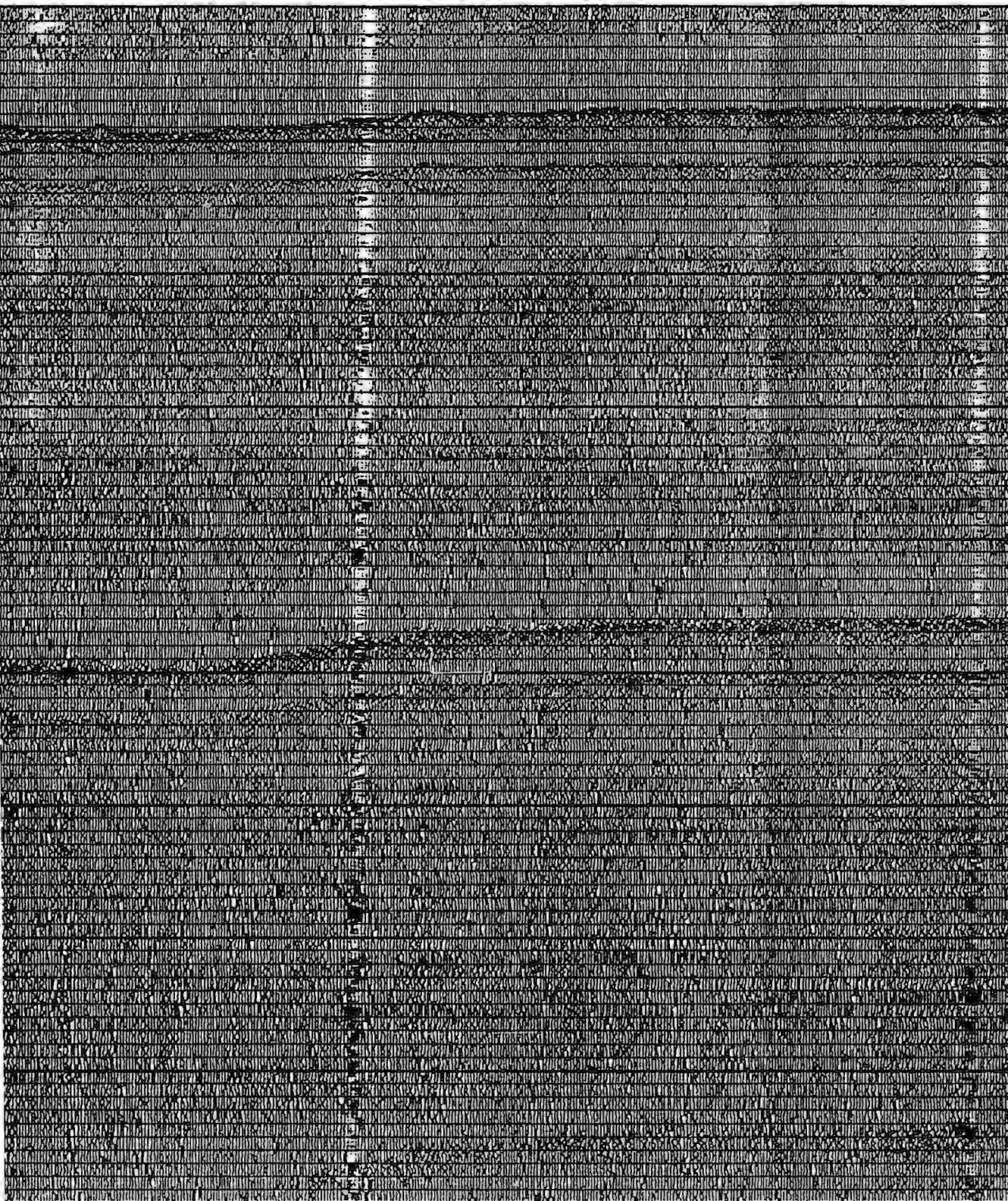
sp. 125

wp. 3

Figure 4.5 Seismic Profile 4-3

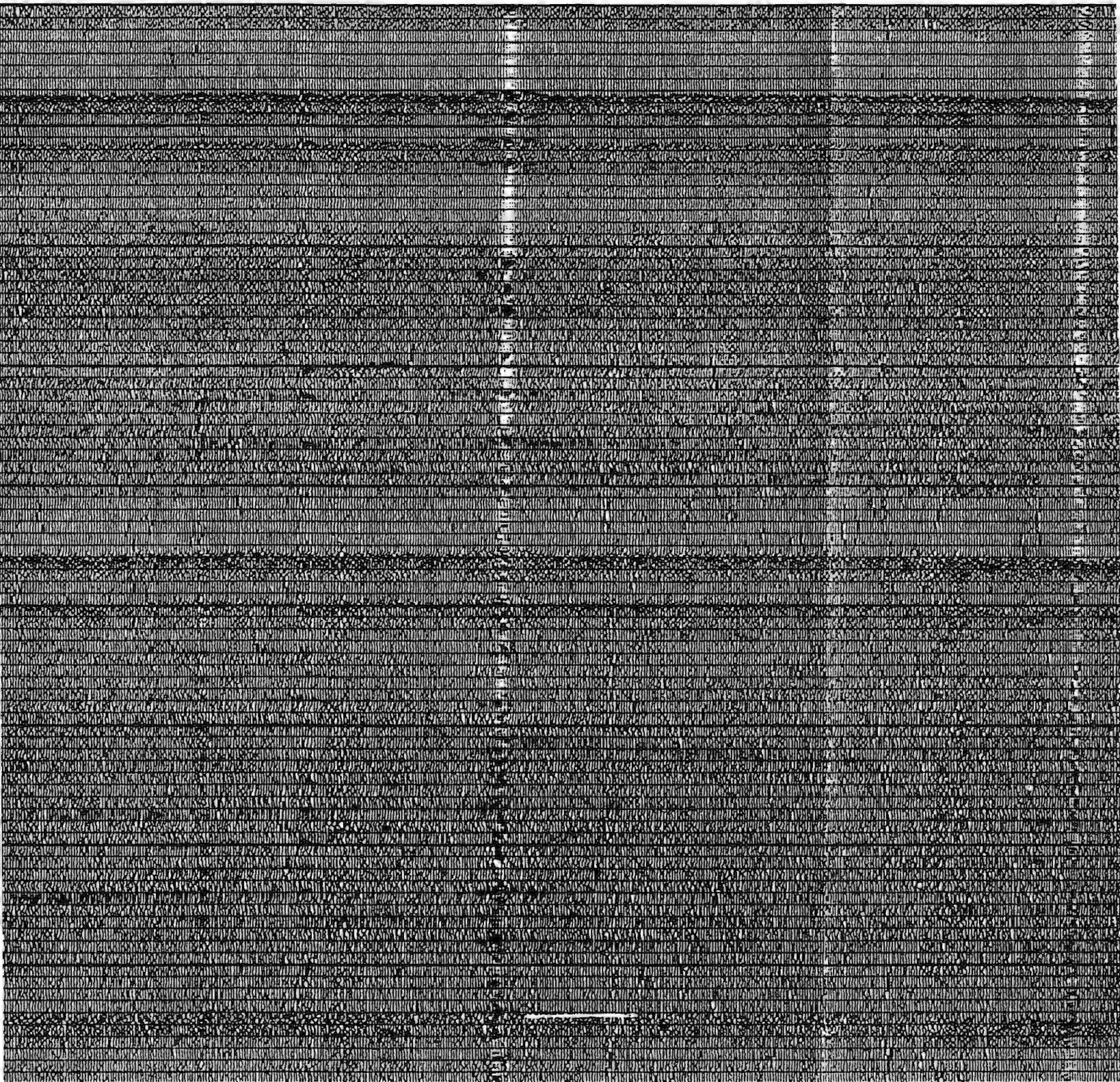




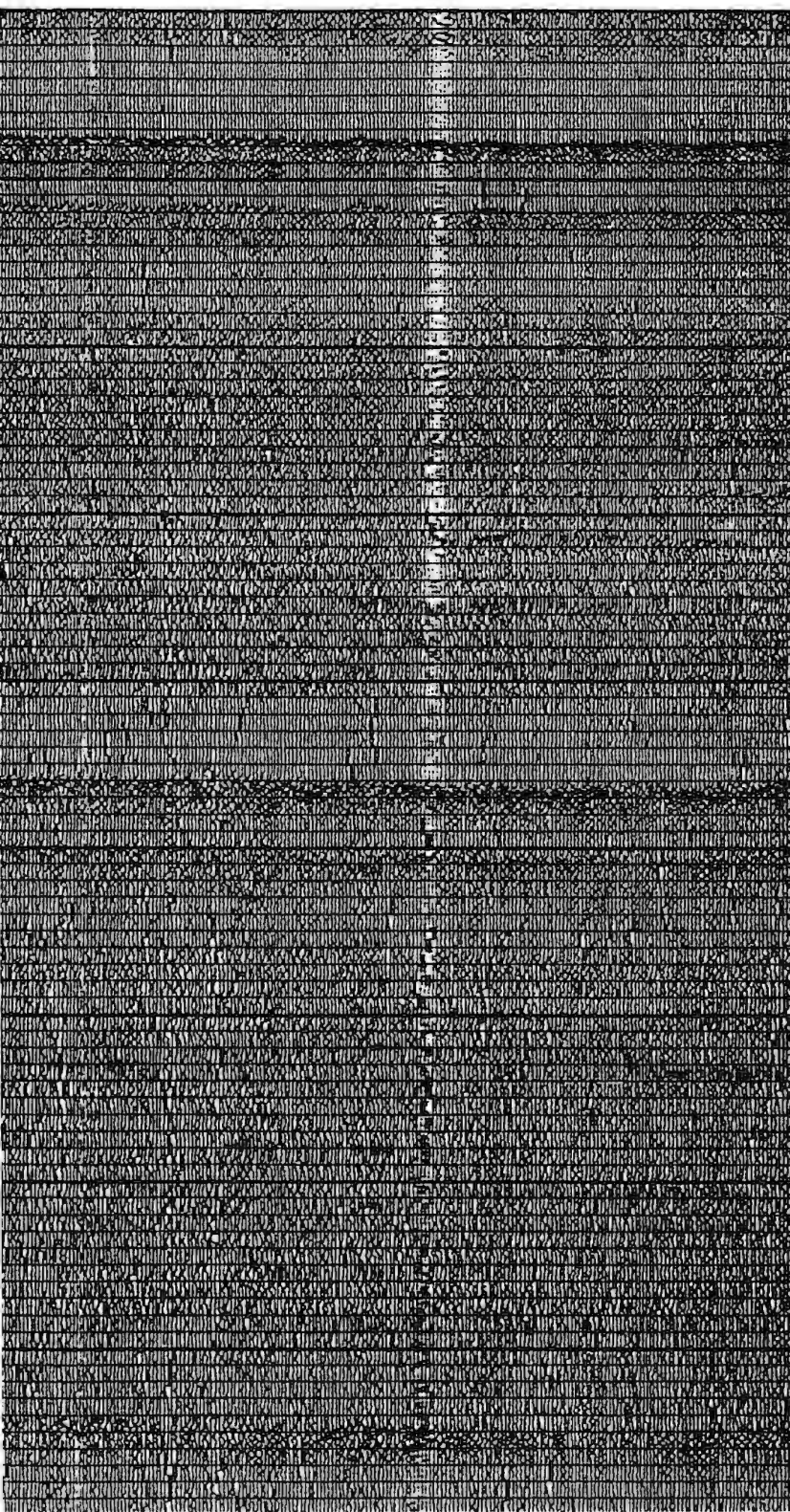


sp. 750

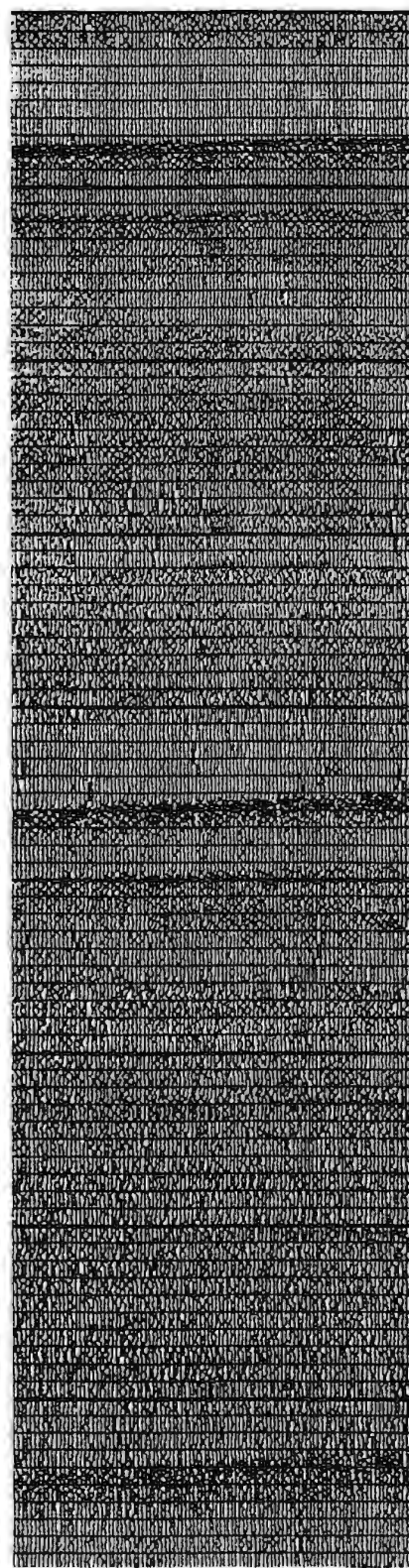
sp. 1000



sp. 1220



sp. 1500



sp. 1600

40

50

60

70

80

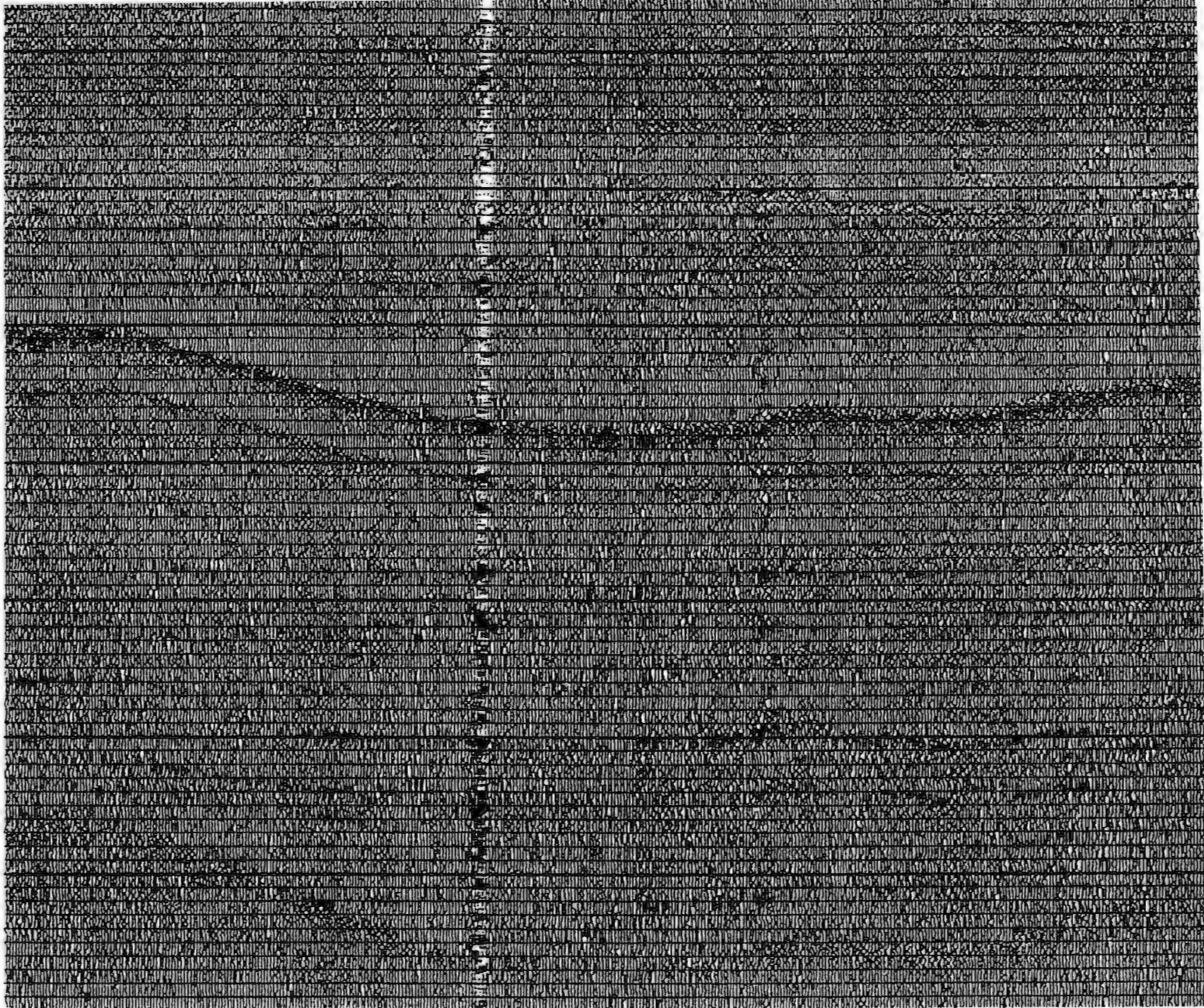
90

100

110

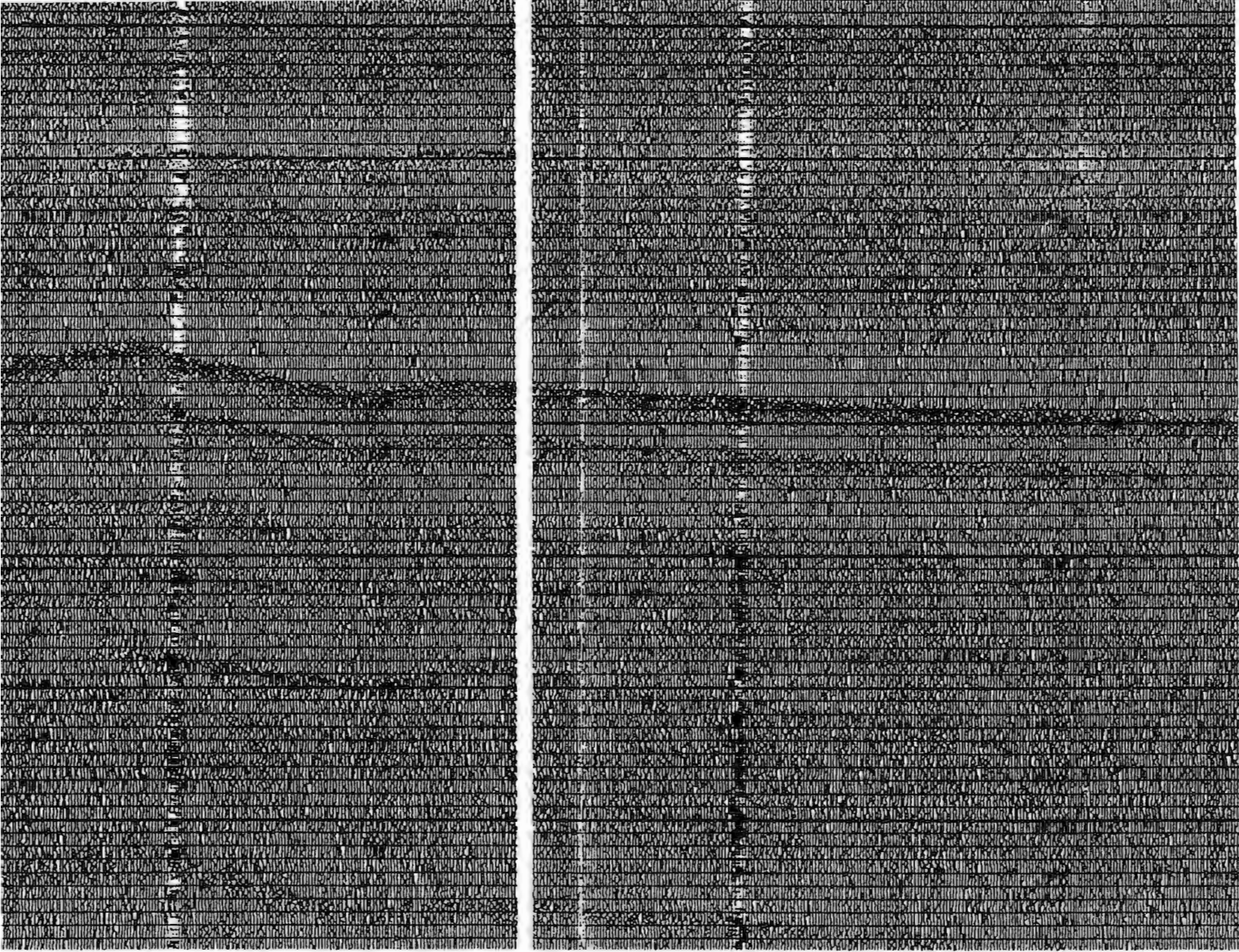
120

Two Way Travel Time (ms)

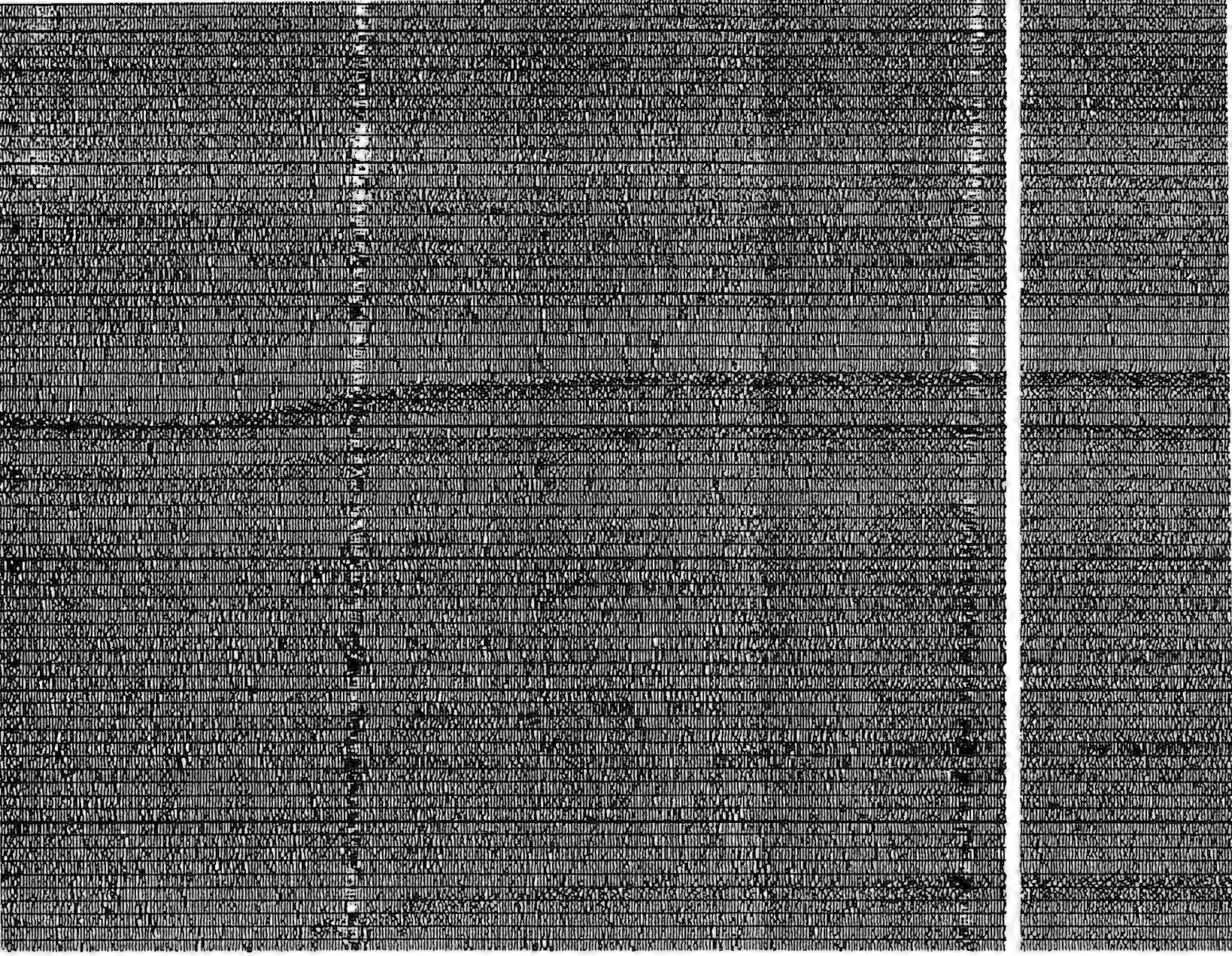


sp. 1

wp. 16



sp. 500



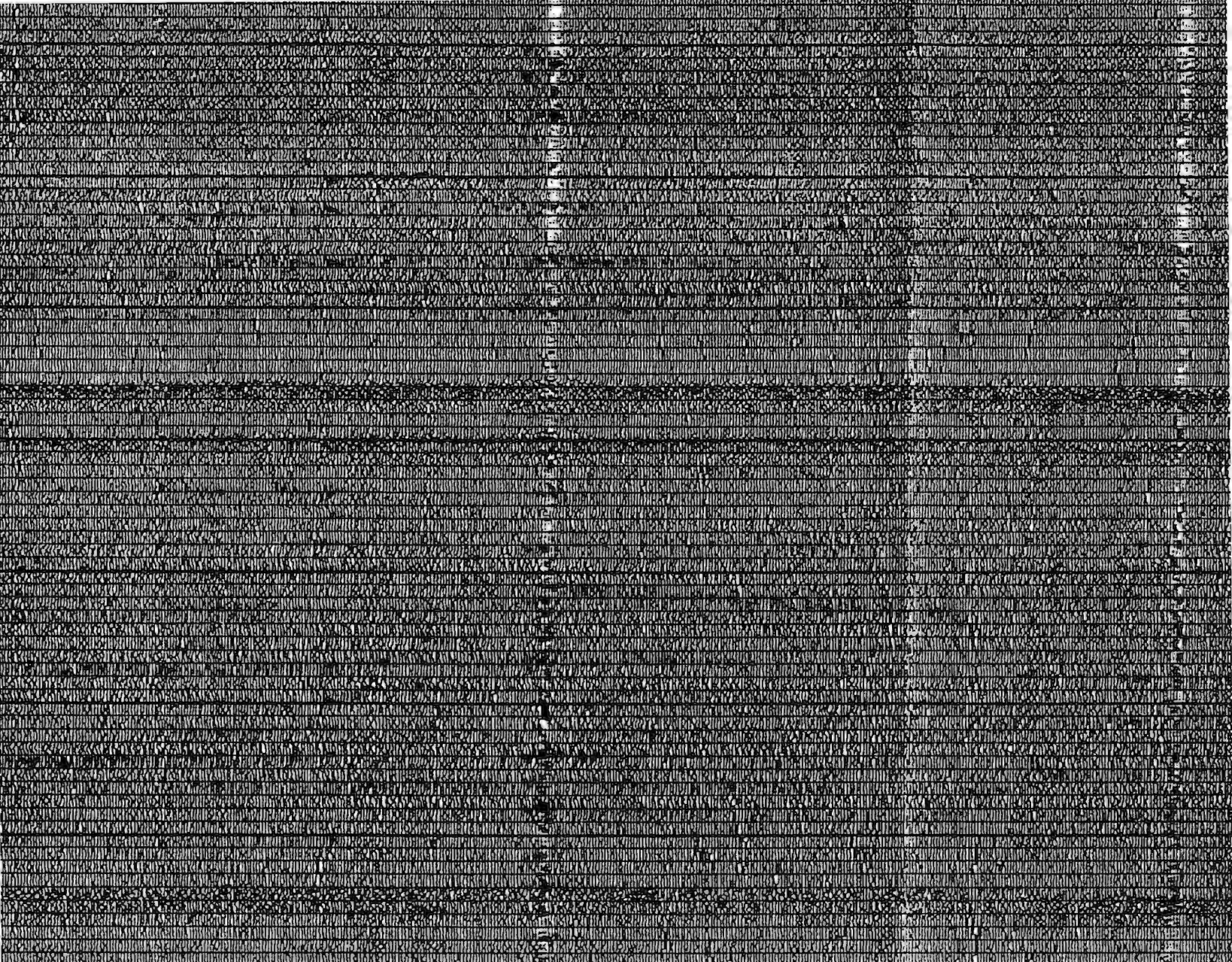
sp. 750

sp. 1000

Cross Tie
Profile 20-21
@ sp. 2590



1000 metres



sp. 1220

Cross Tie
Profile 20-21
@ sp. 330



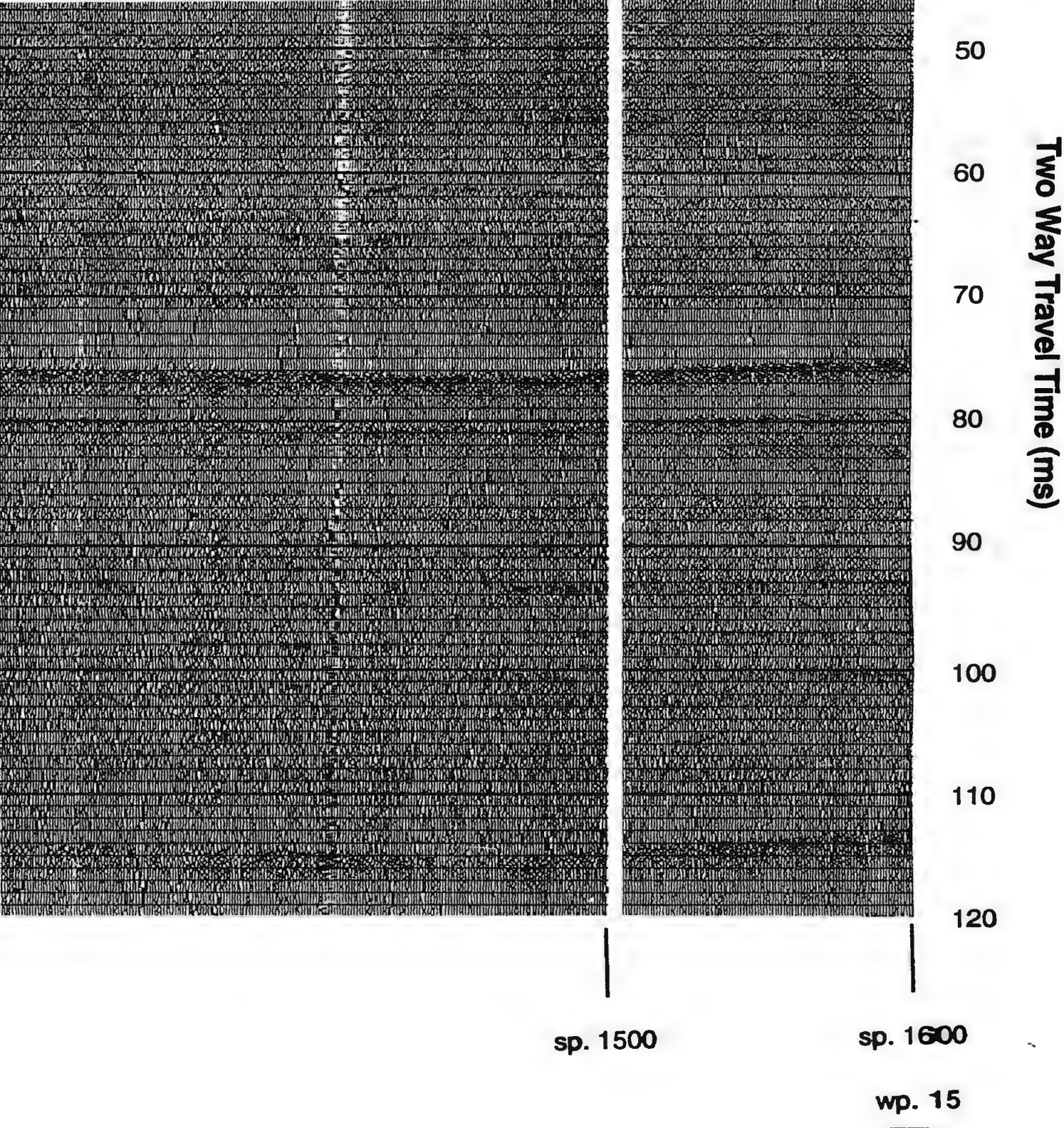
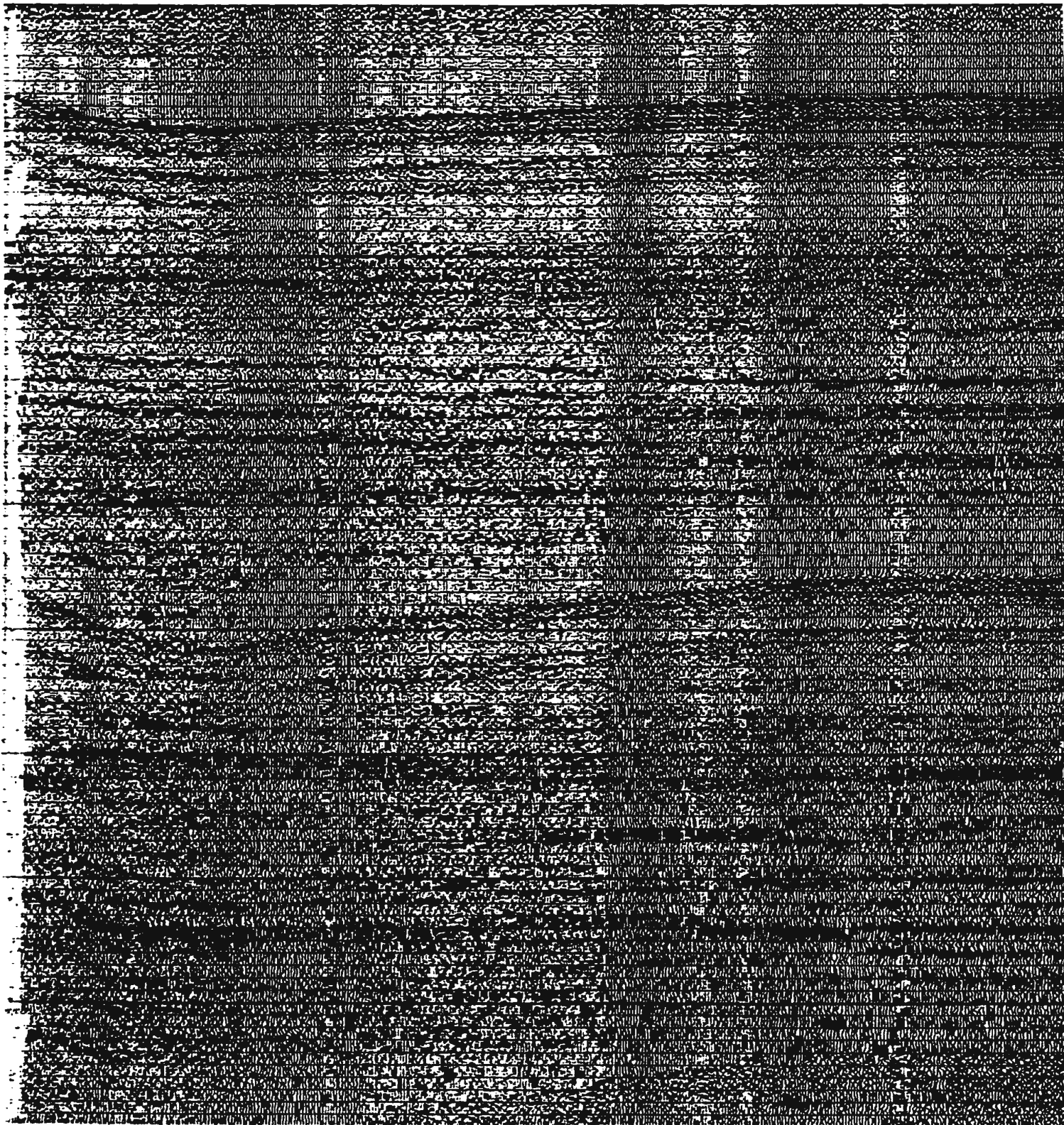
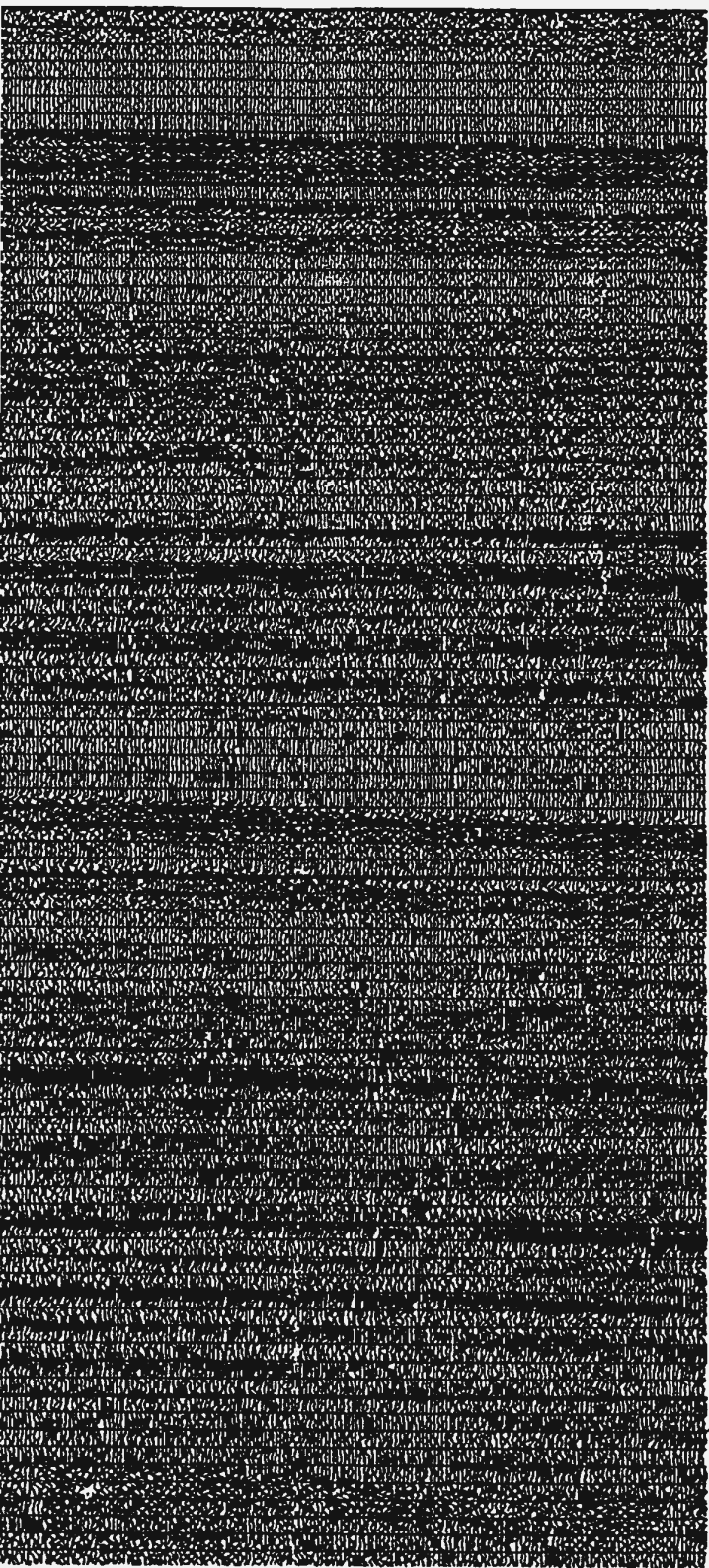
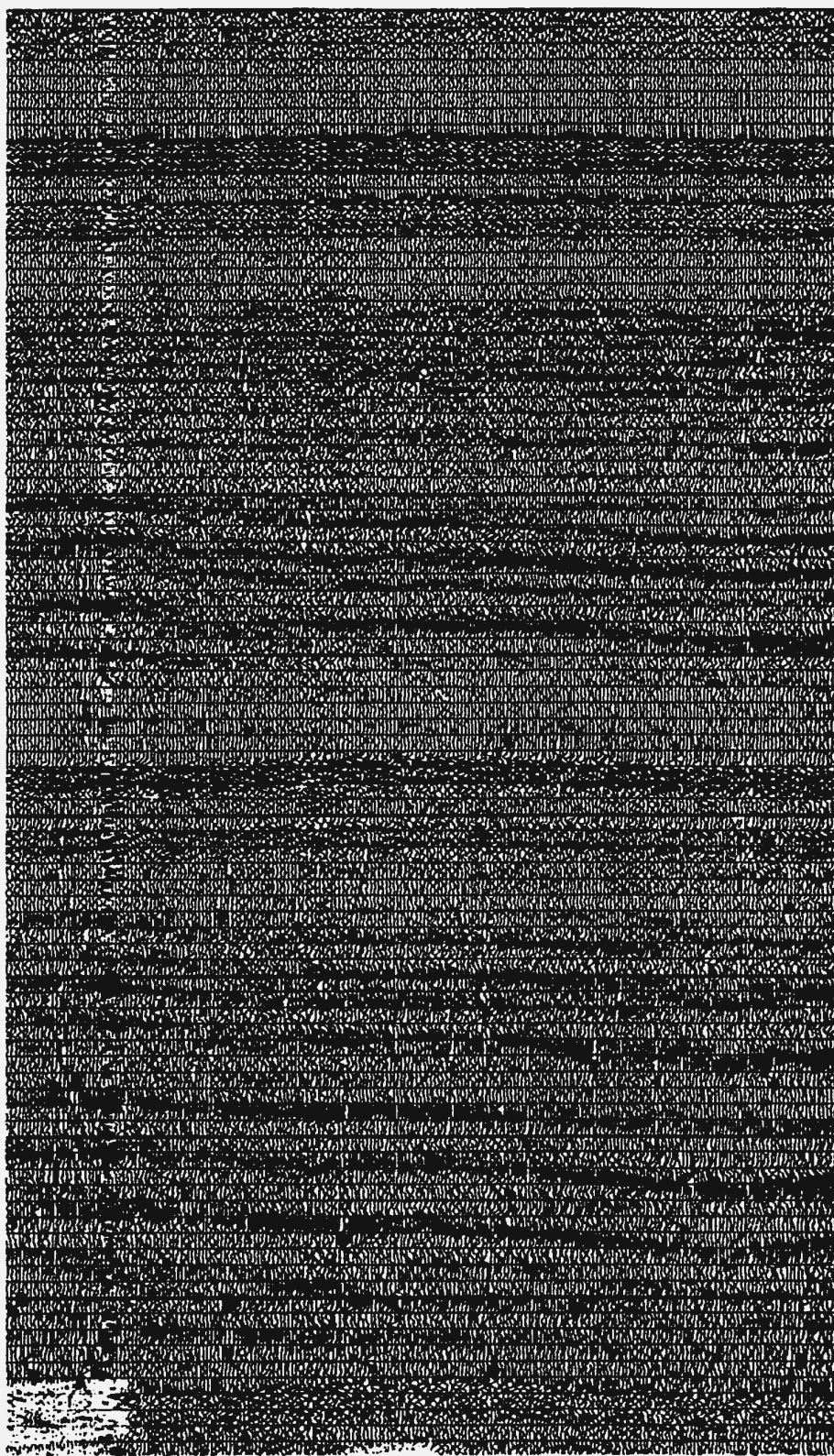


Figure 4.6 Seismic Profile 16-15





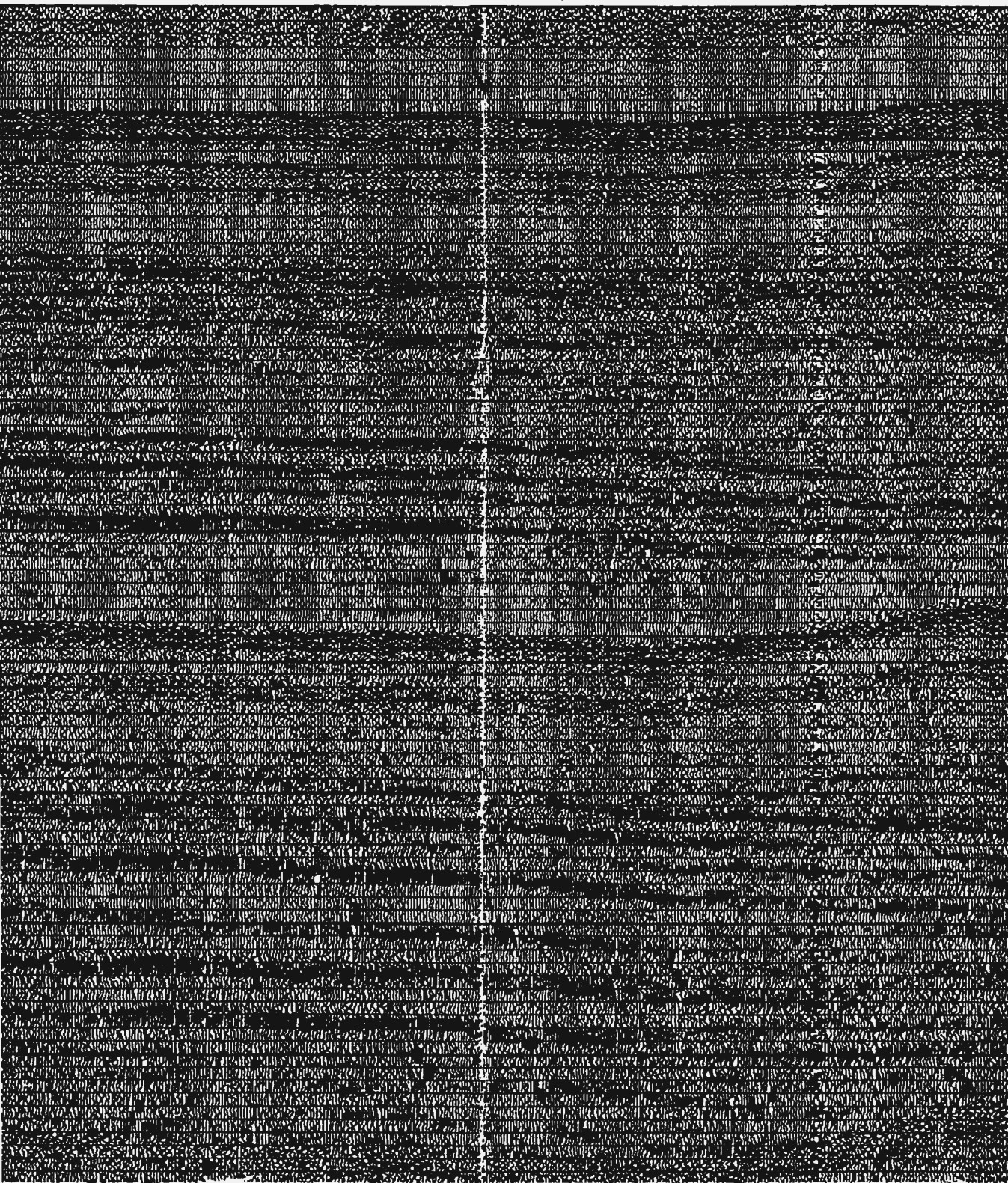
. 330



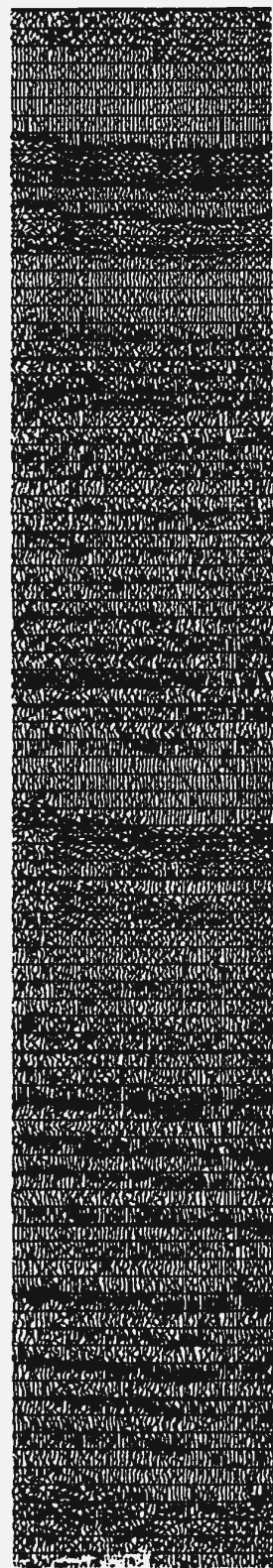
sp. 500

sp. 550

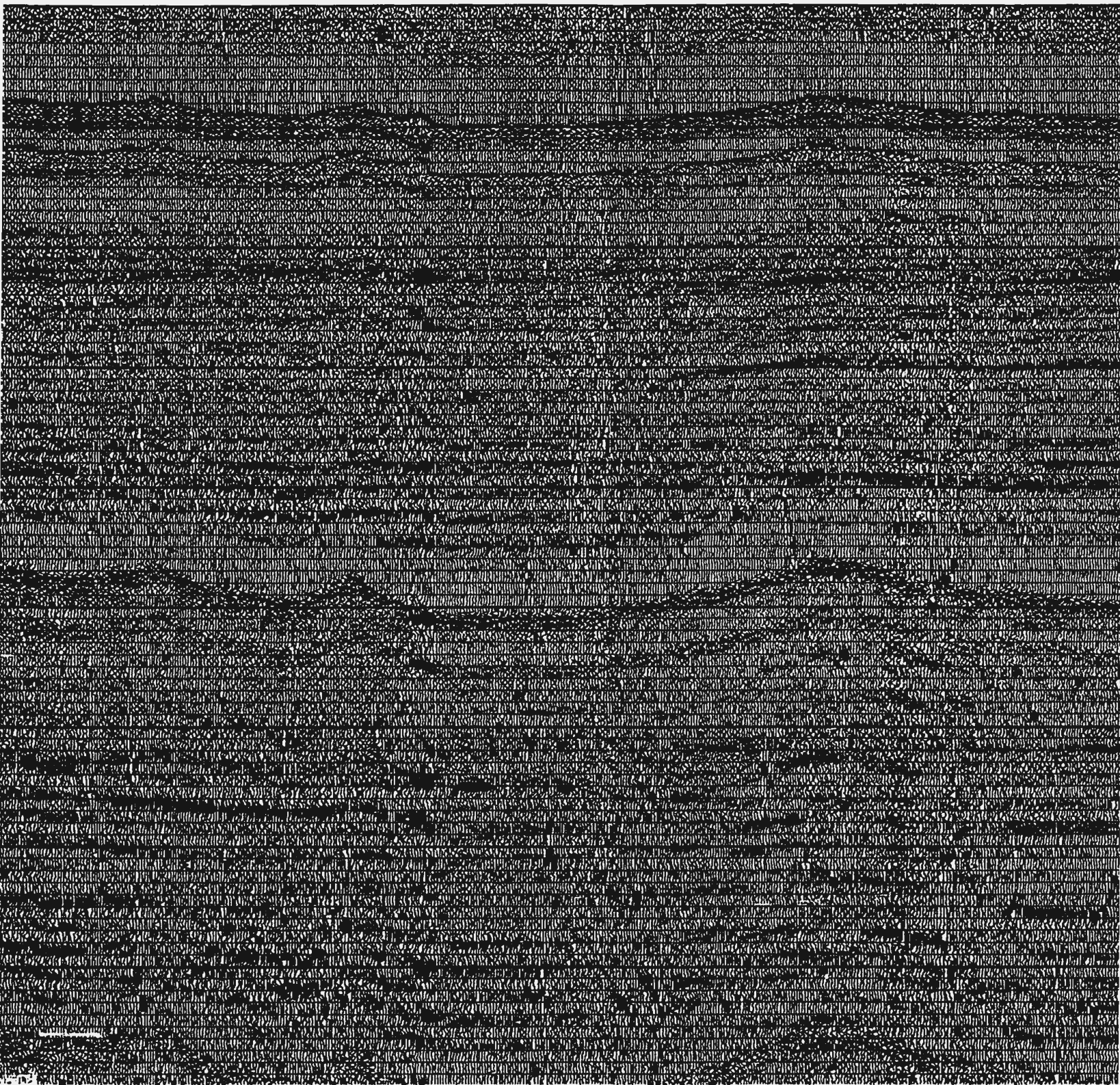
sp. 700

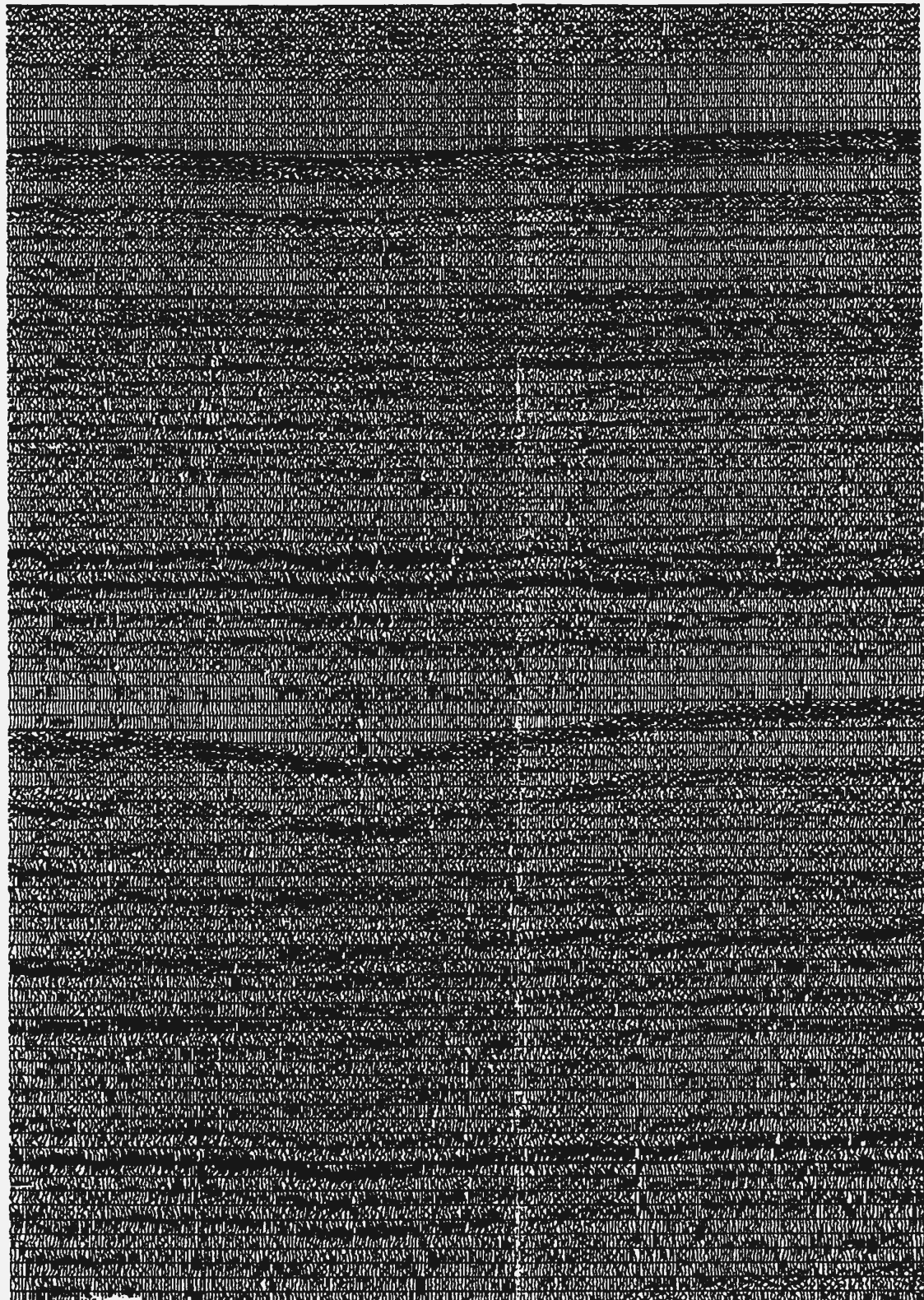


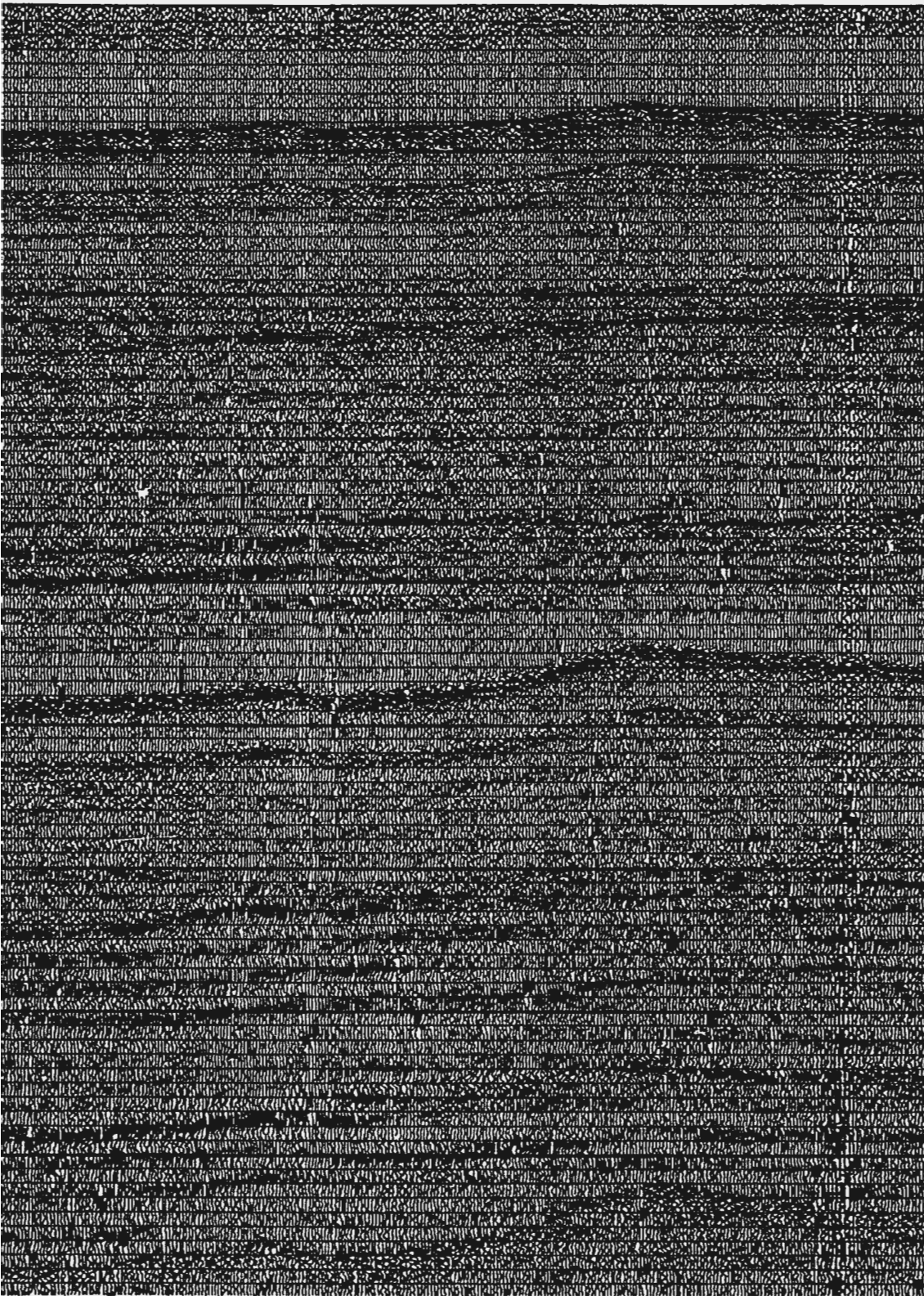
sp. 700



sp. 1000

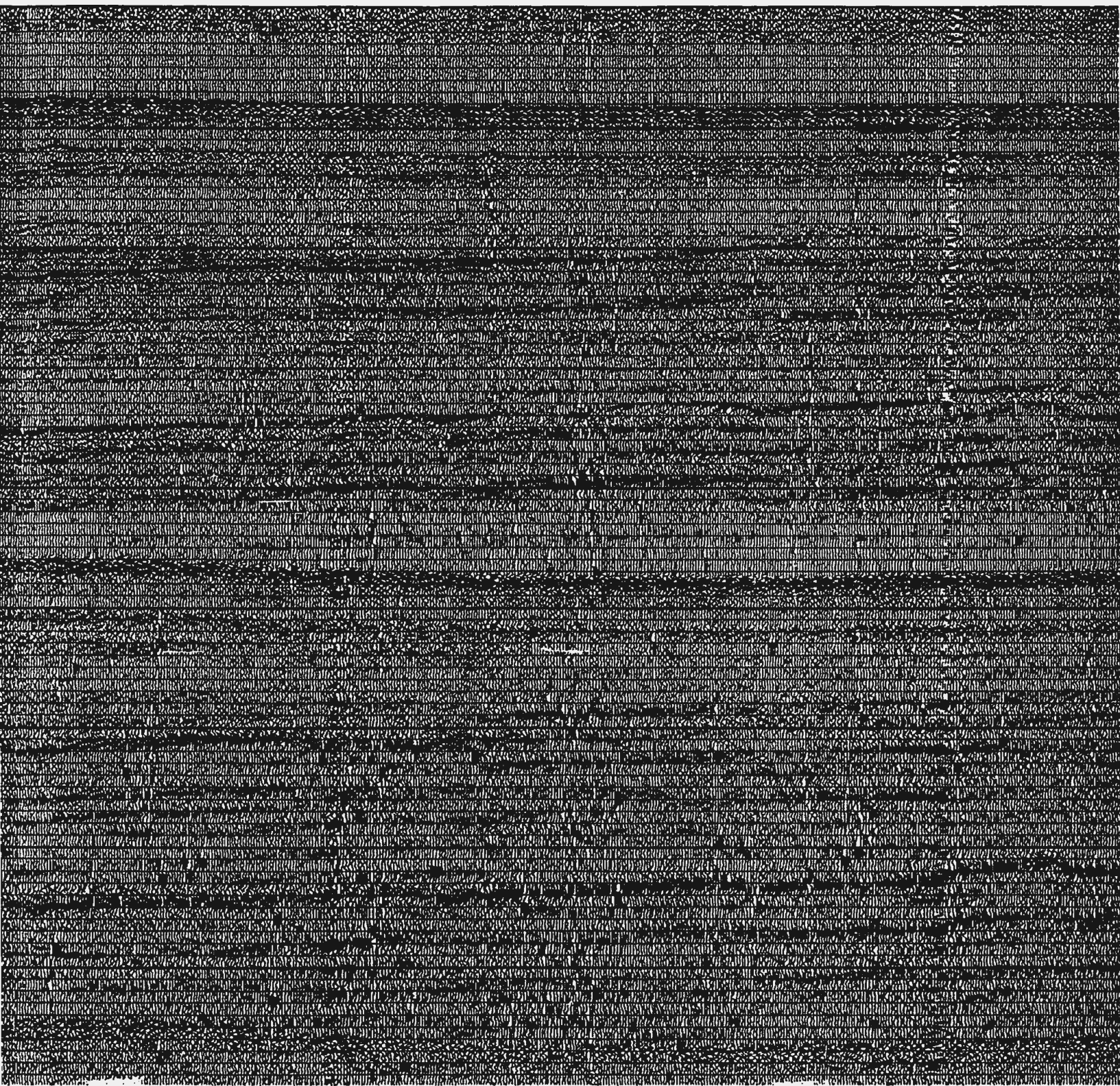






sp. 2000

sp. 2060

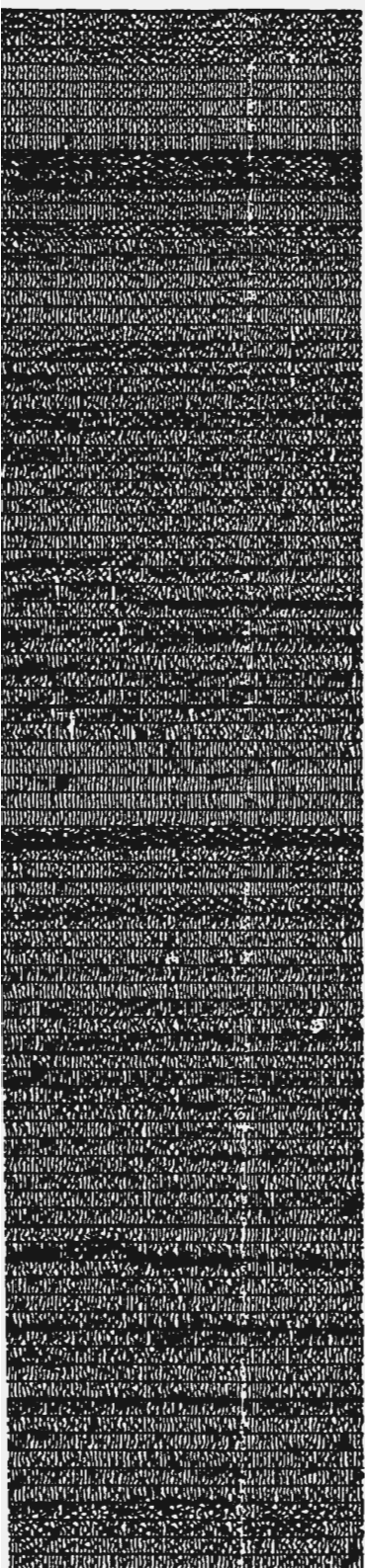


060

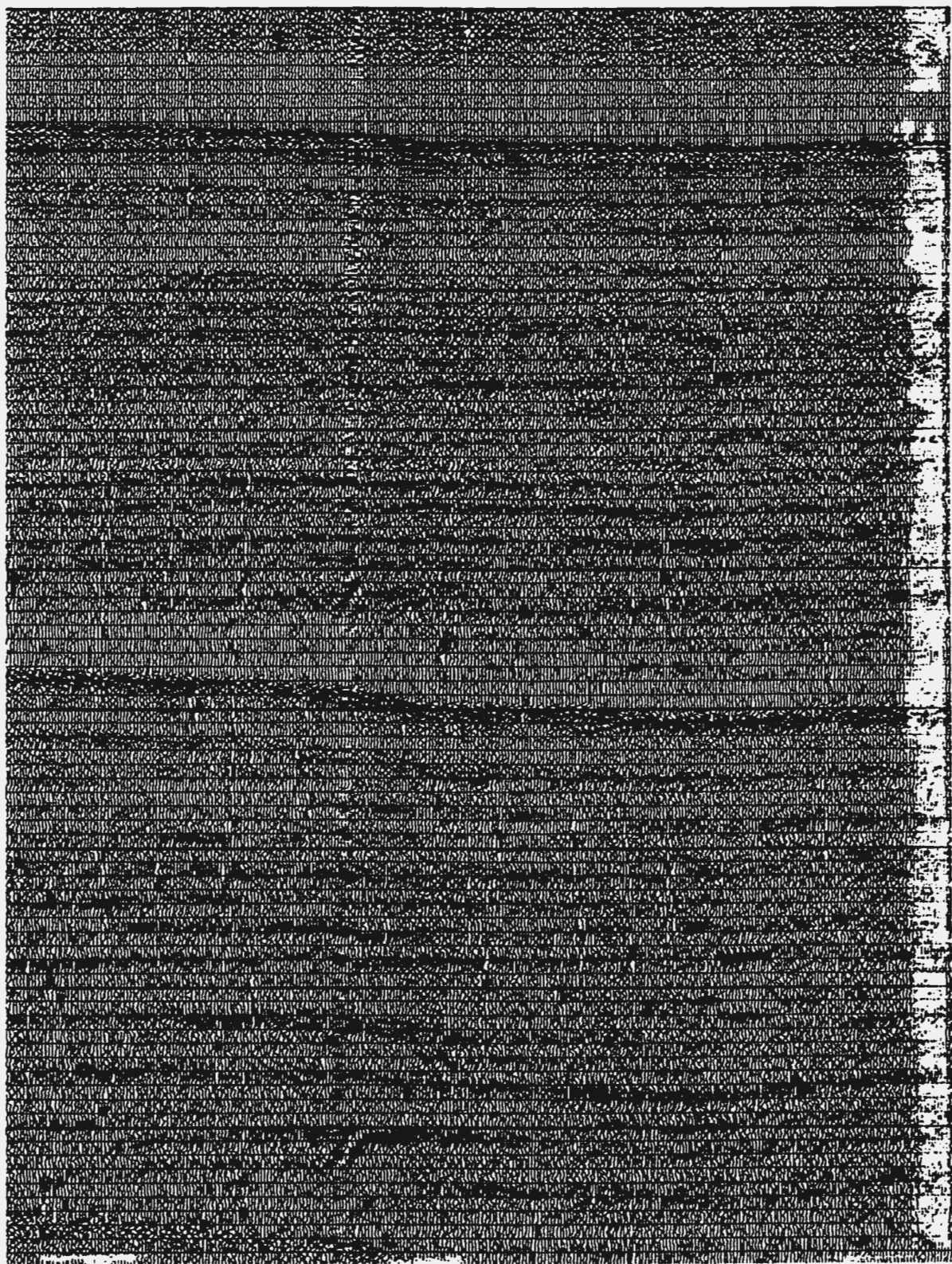
s Tie

sp. 2300

Cross Tie



sp. 2500

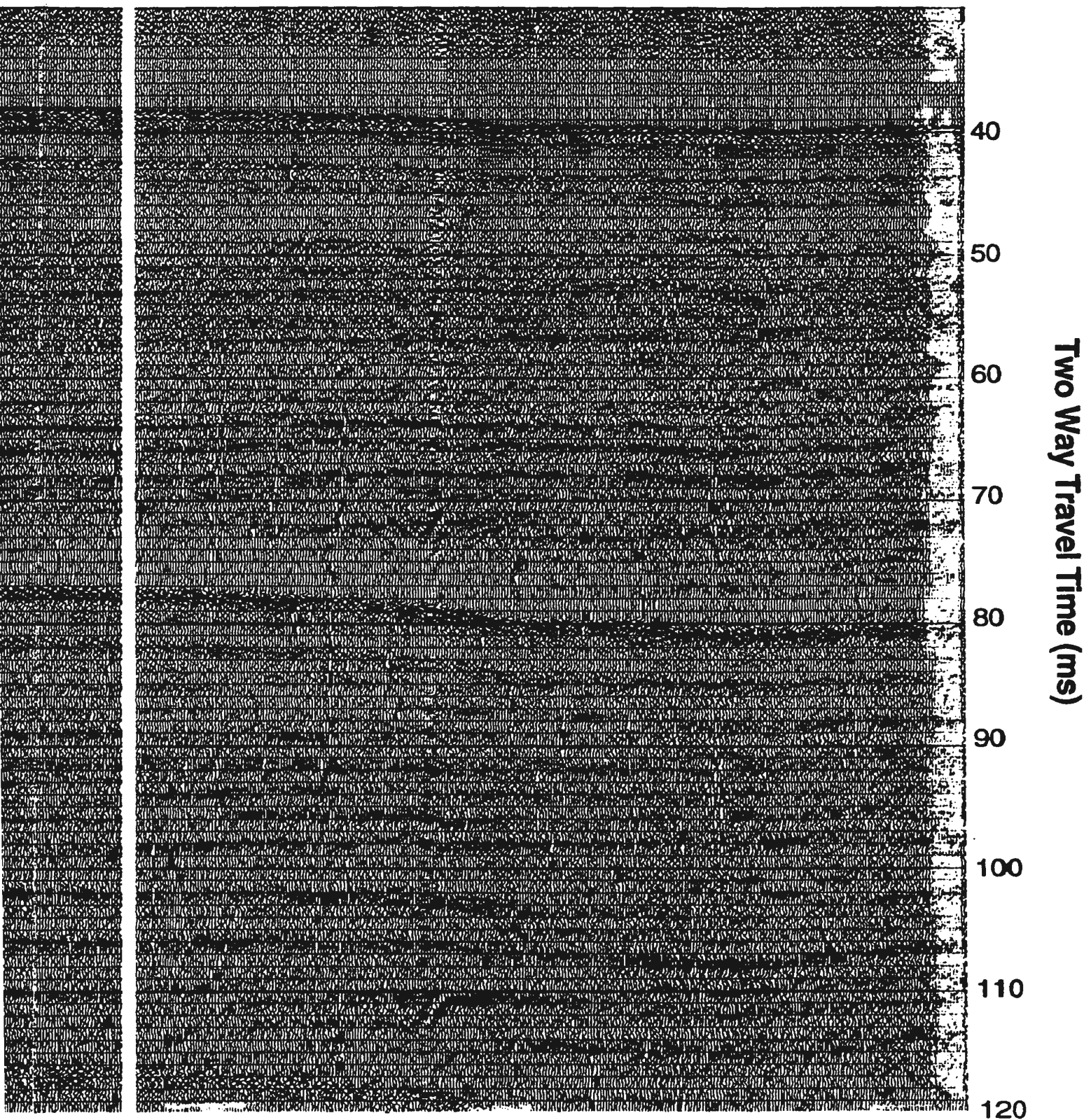


sp. 2590

Cross Tie

sp. 2790

sp. 2790



sp. 2500

sp. 2590

sp. 2790

Cross Tie
Profile 16 15

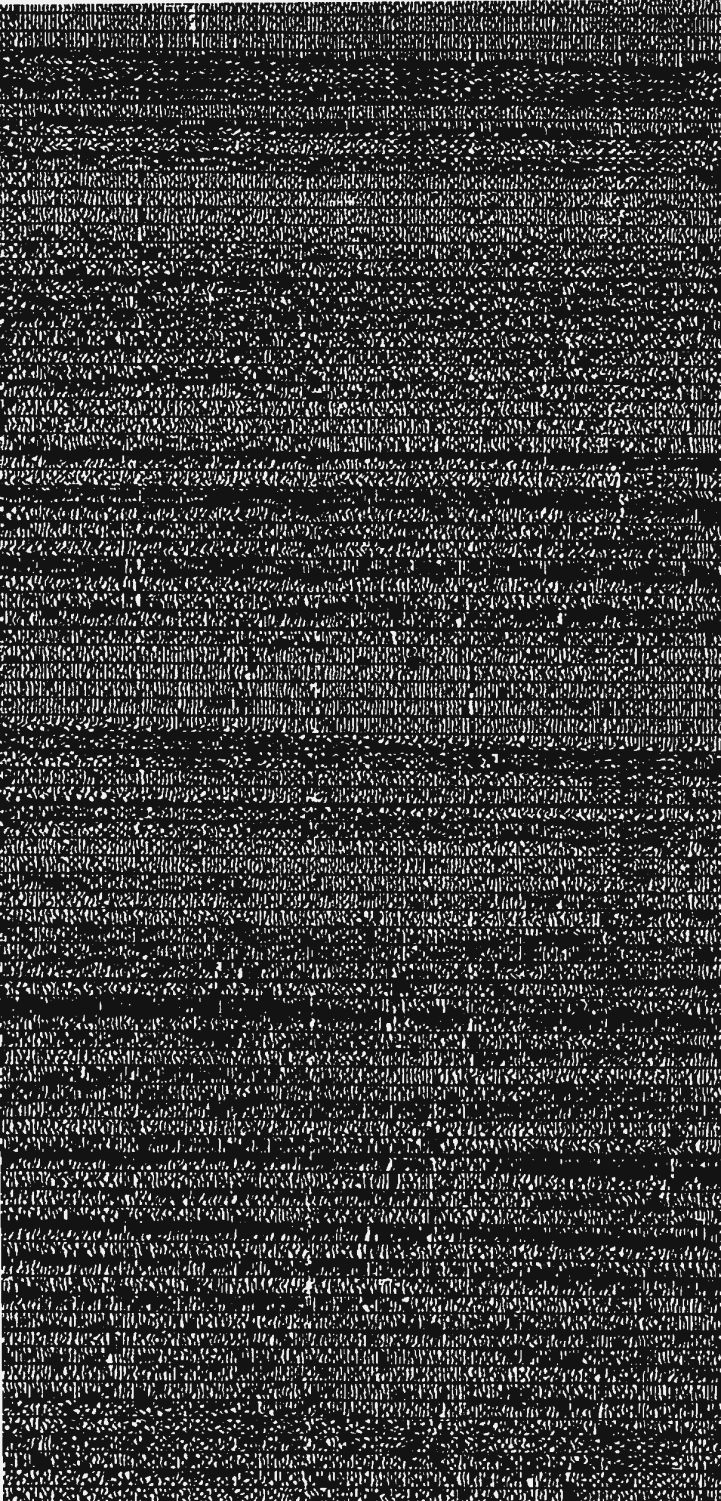
wp. 21

sp. 1

wp. 20

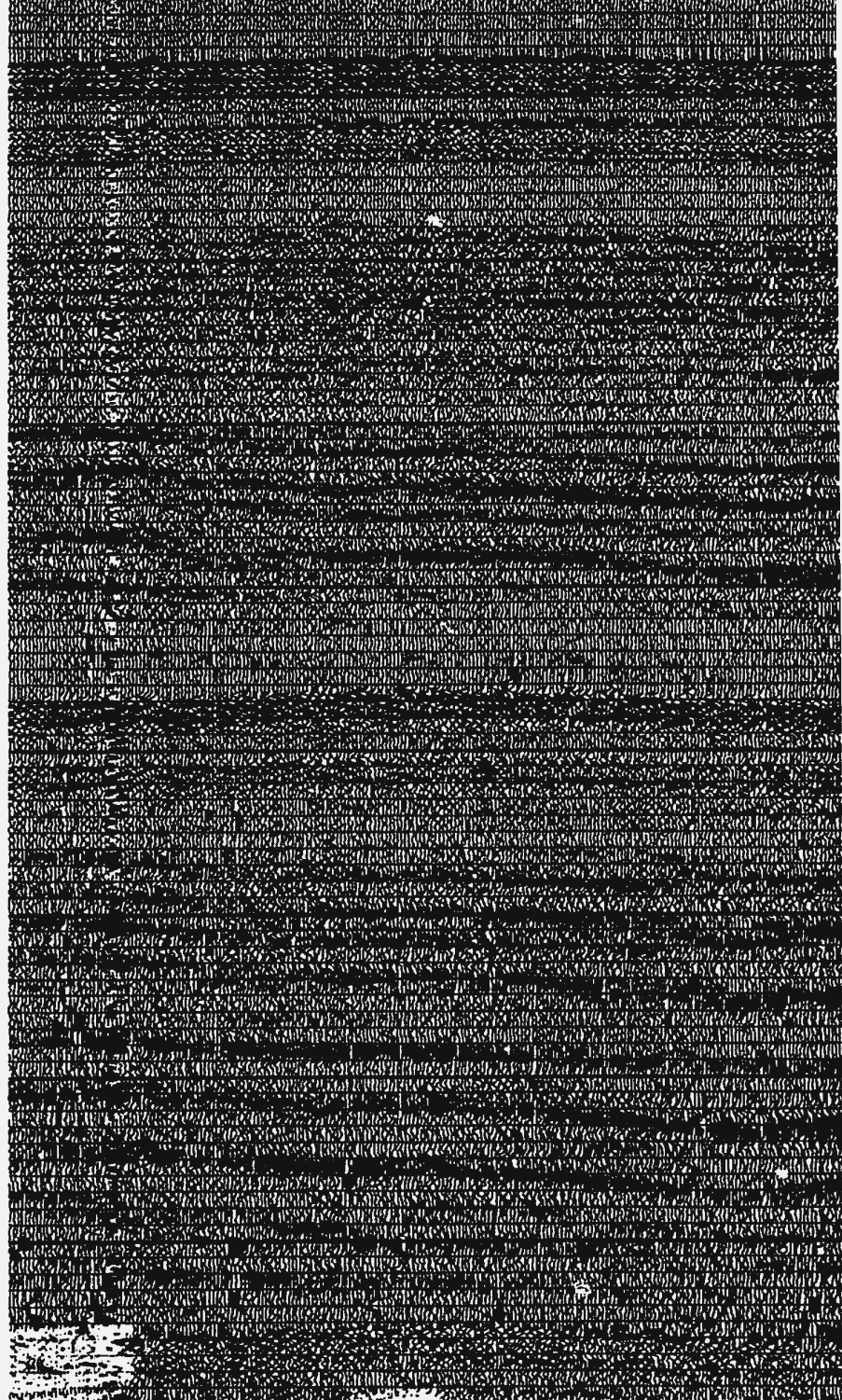
sp. 330

Cross Tie
Profile 16-15
@ sp. 1220



p. 330

Cross Tie
Profile 16-15
p. 1220



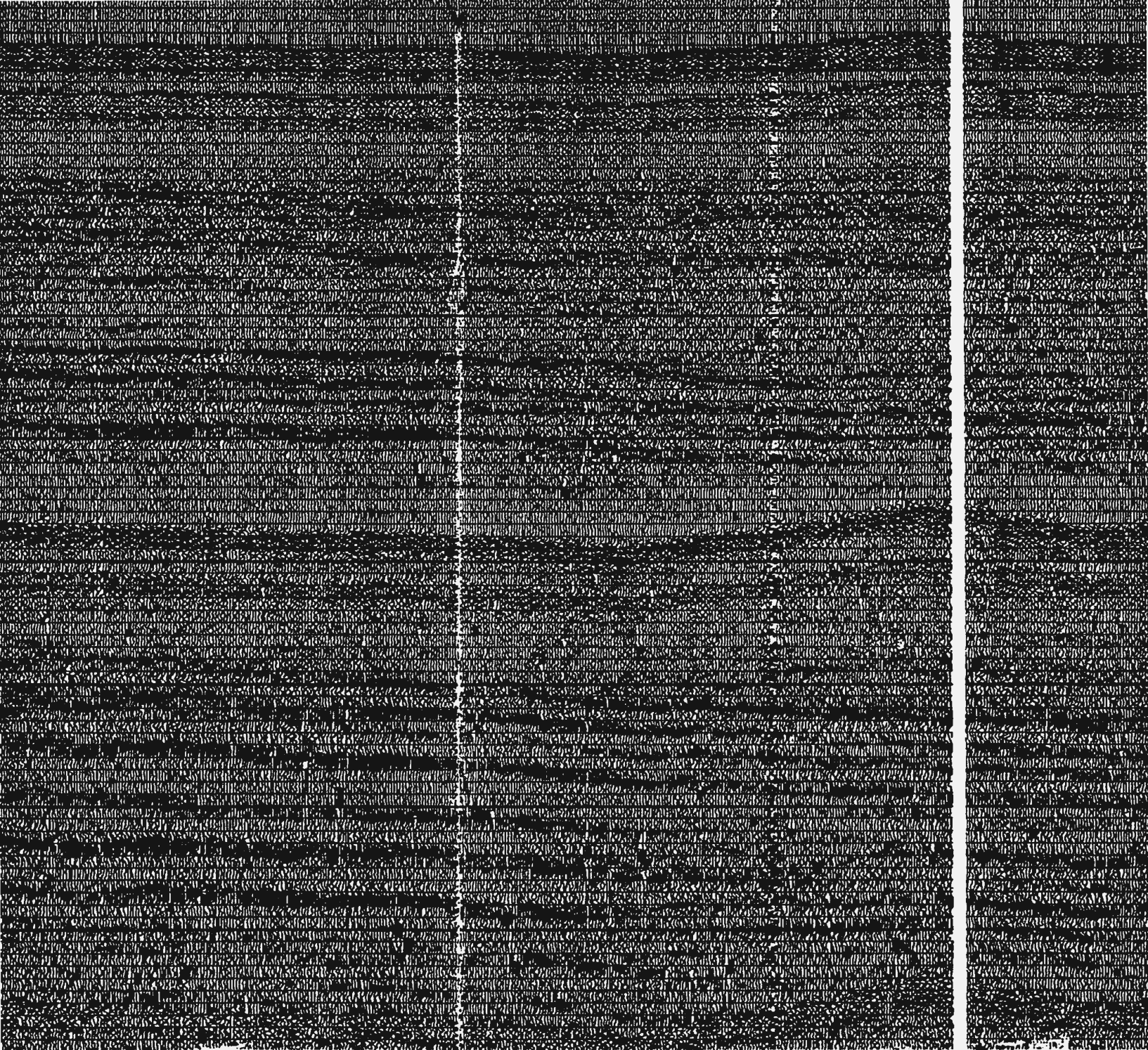
sp. 500

Cross Tie
Profile 4-3
@ sp. 1510

sp. 550

sp. 700

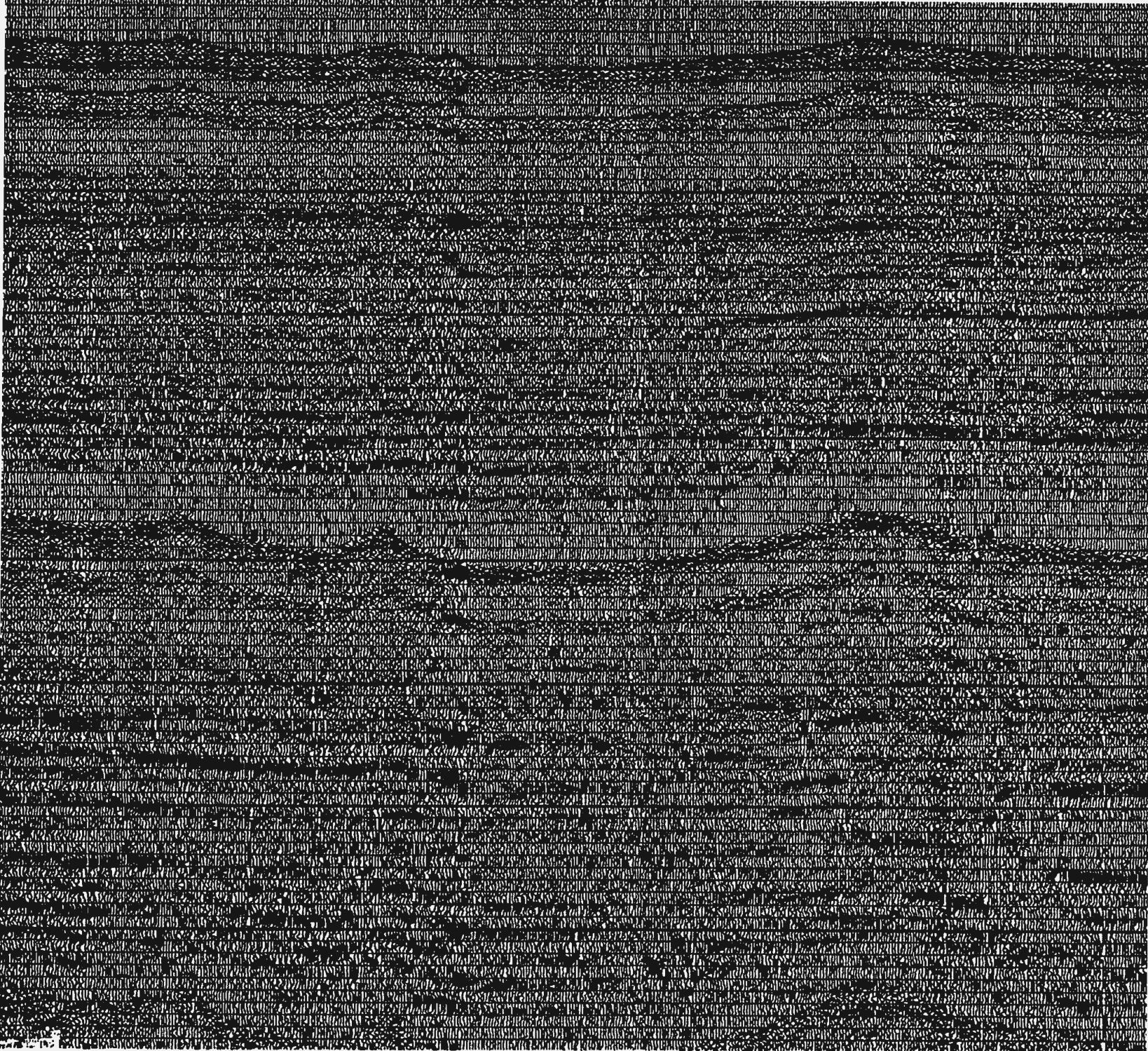
Cross Tie
Profile 13-1
@ sp. 1270

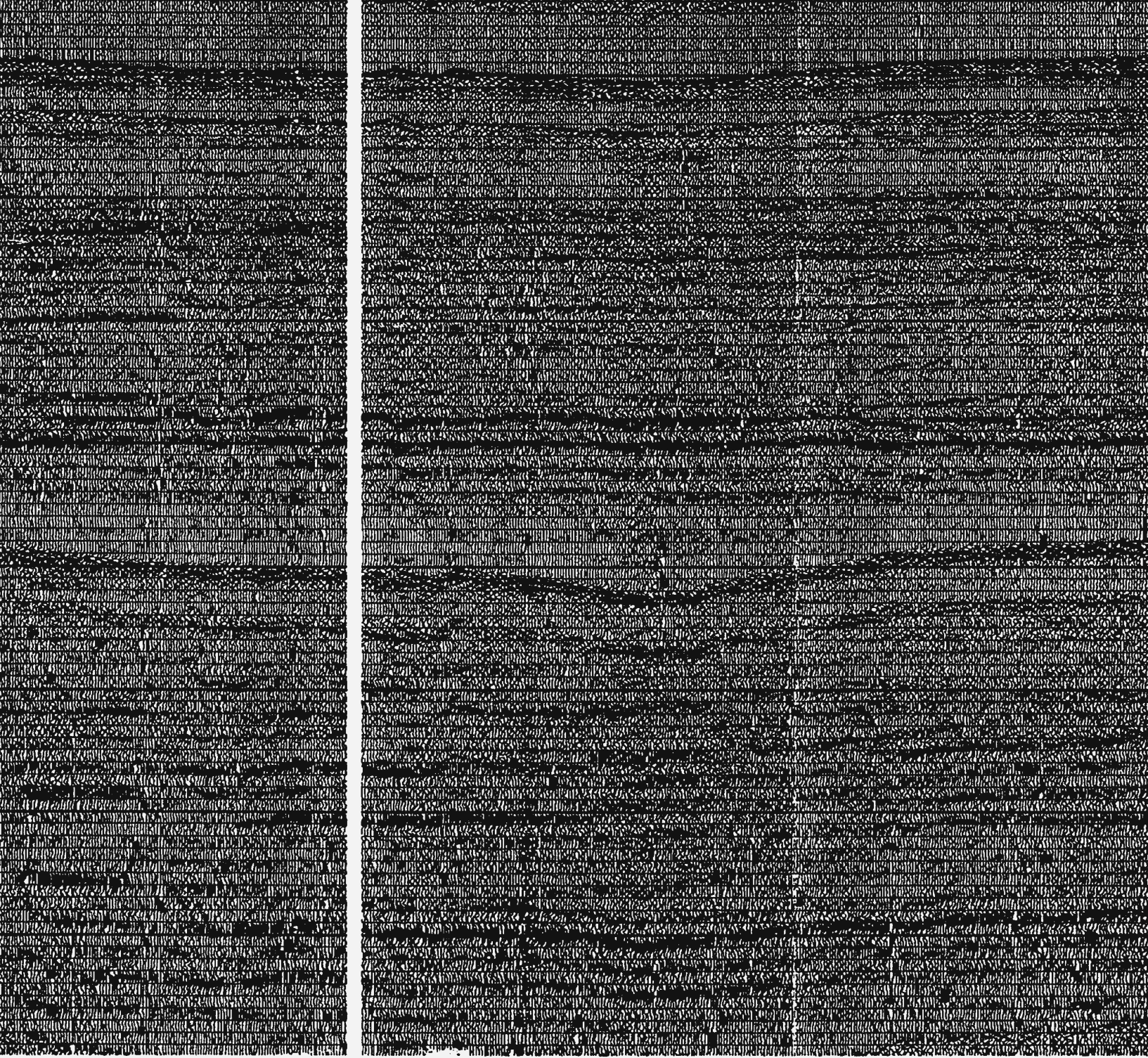


sp. 700

sp. 1000

Cross Tie
Profile 13-14
@ sp. 1270

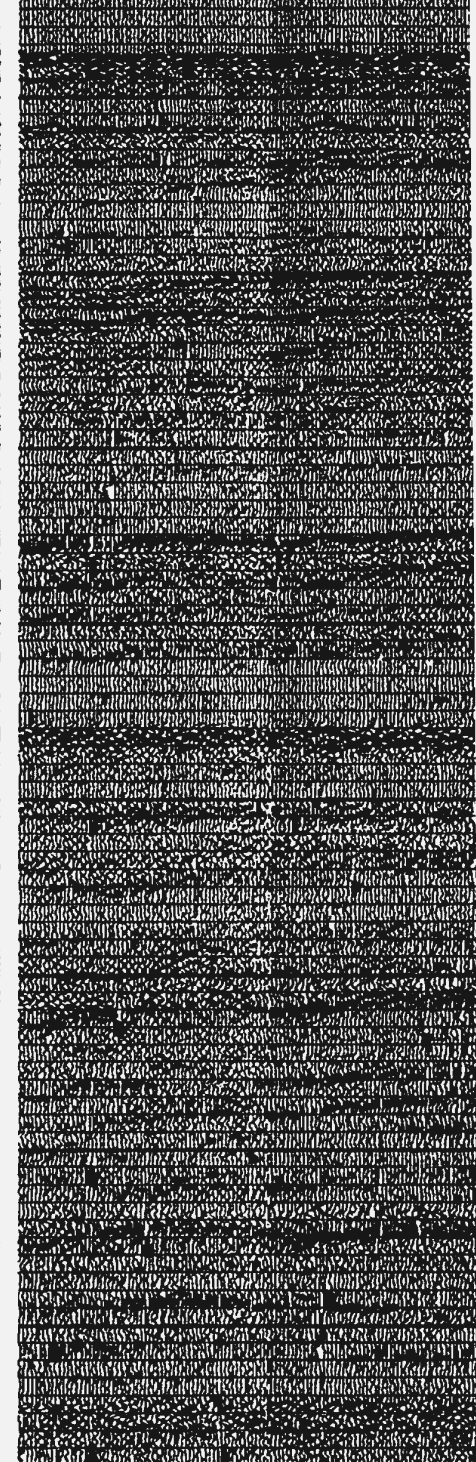
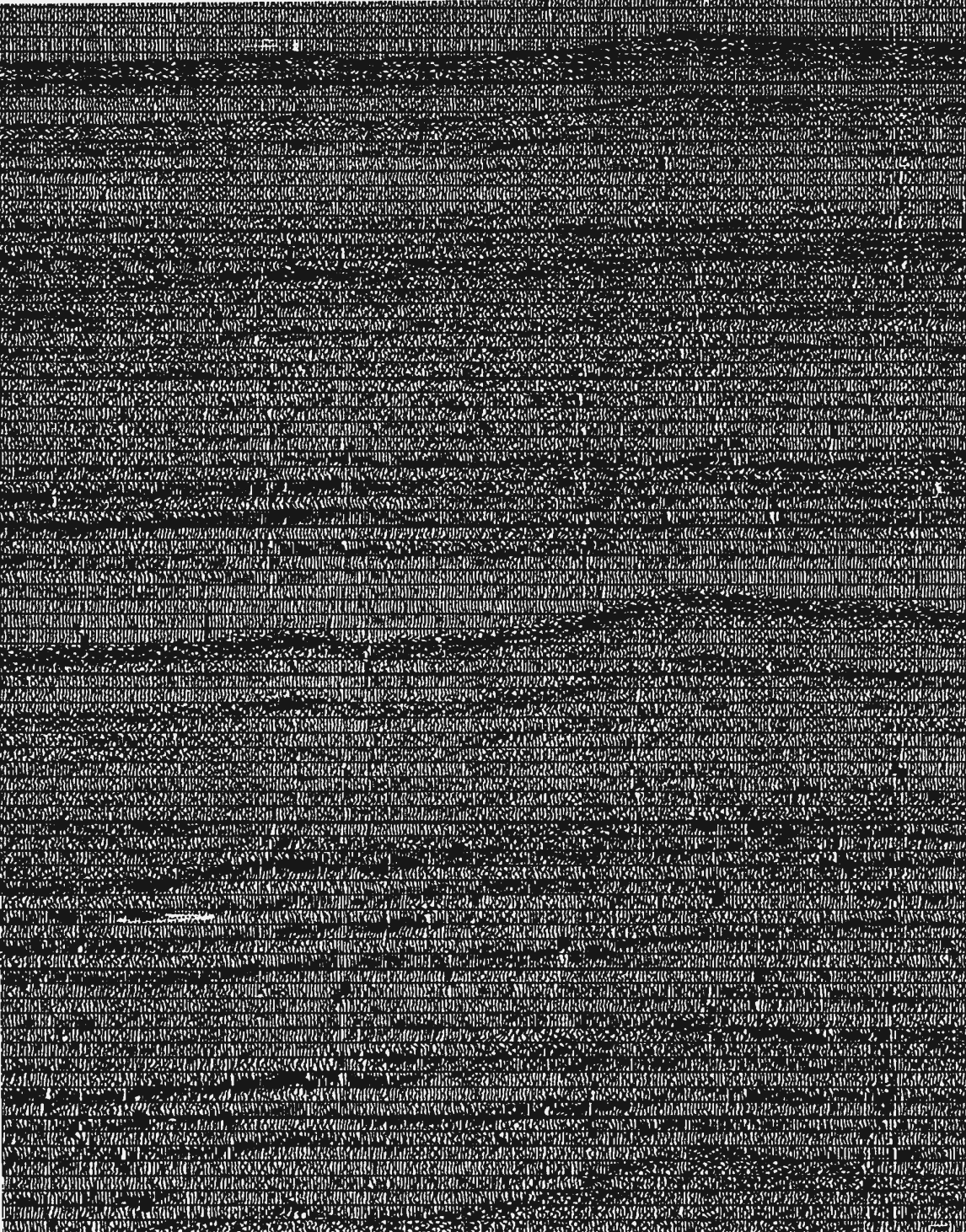




sp. 1500



1000 metres



sp. 2000

sp. 2060

Cross Tie
Profile 13-14
@ sp. 800

2060

ss Tie
e 13-14
p. 800

sp. 2300

Cross Tie
Profile 4-3
@ sp. 900

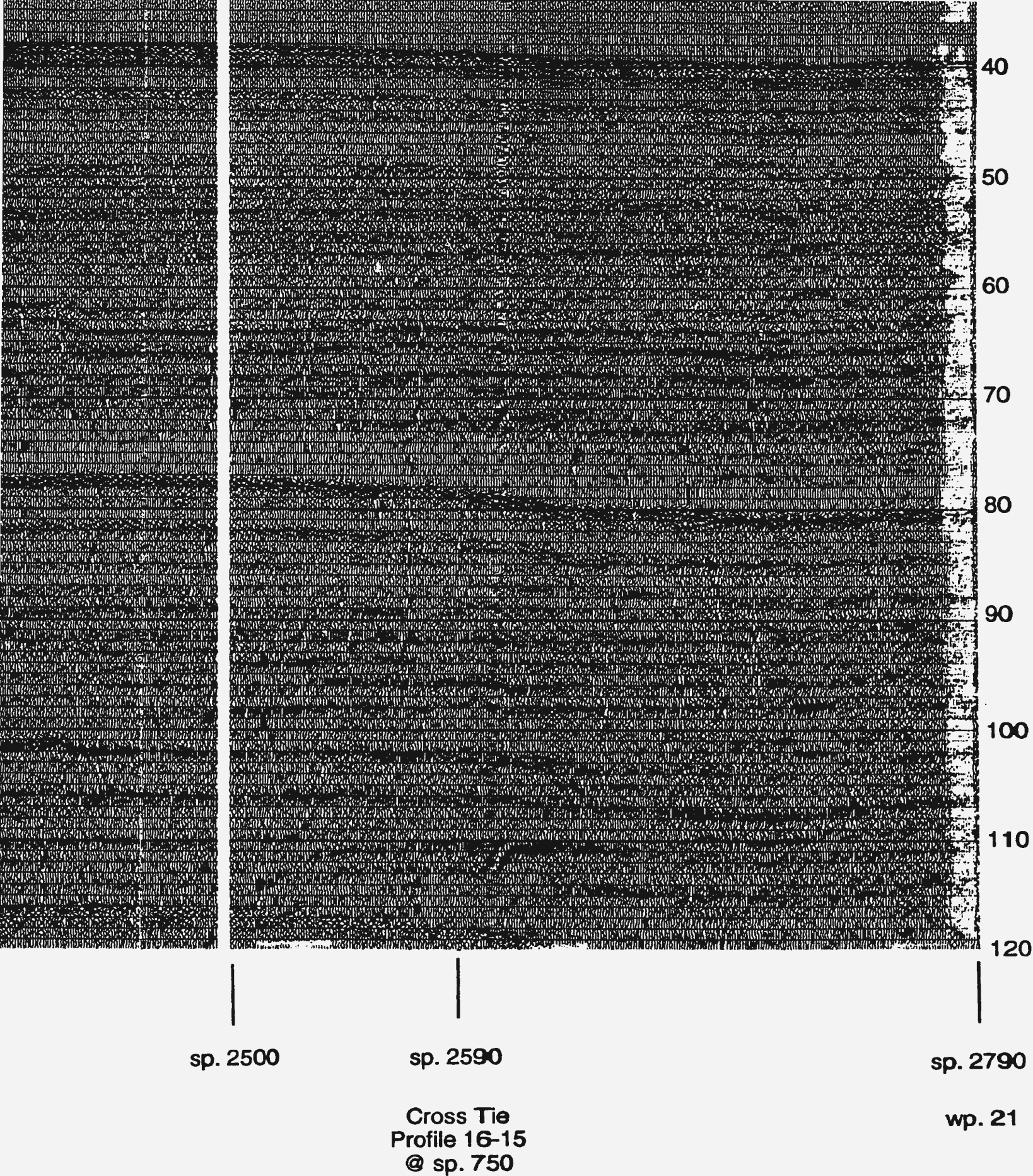


Figure 4.7 Seismic Profile 20-21 (Tie Li

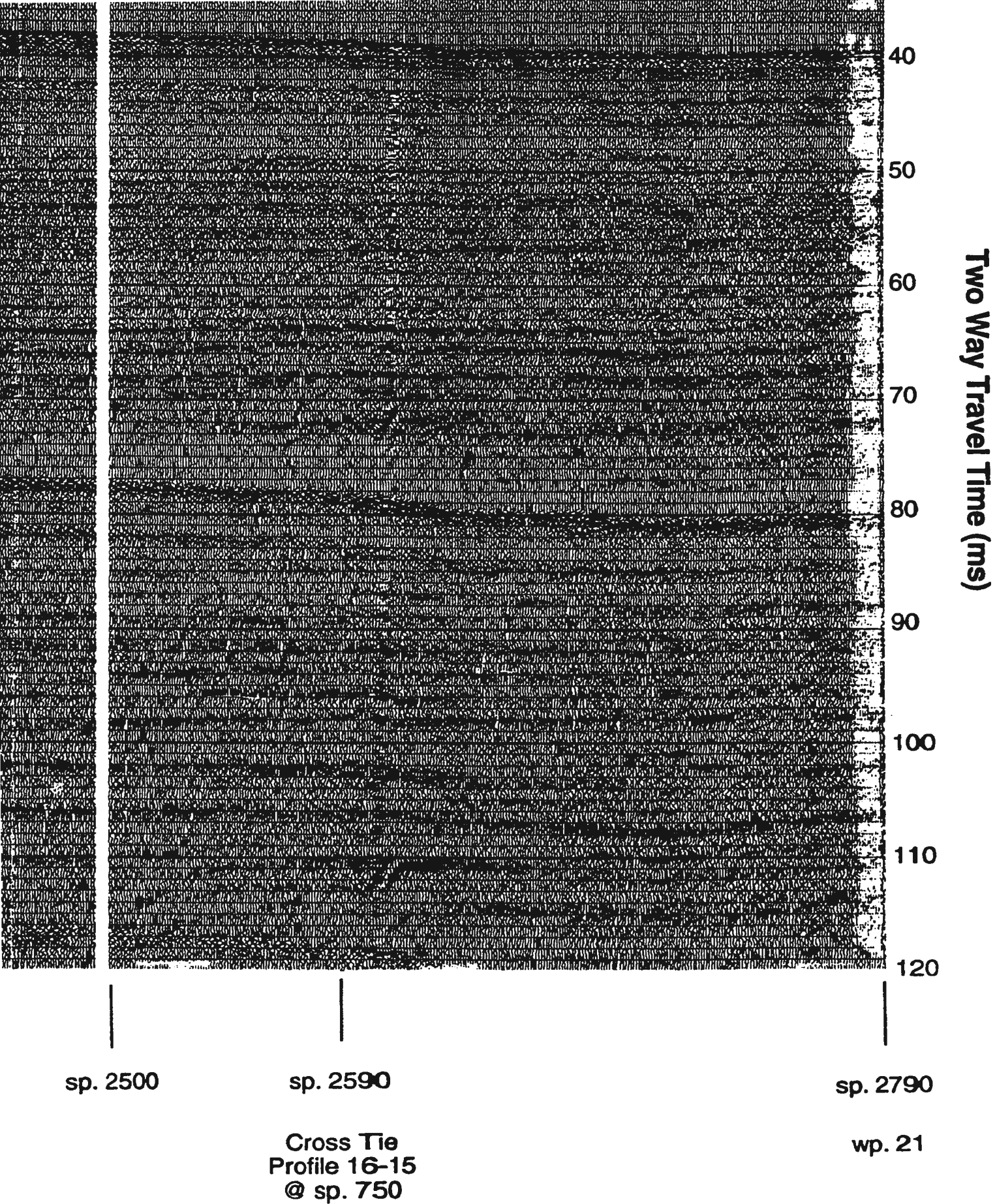
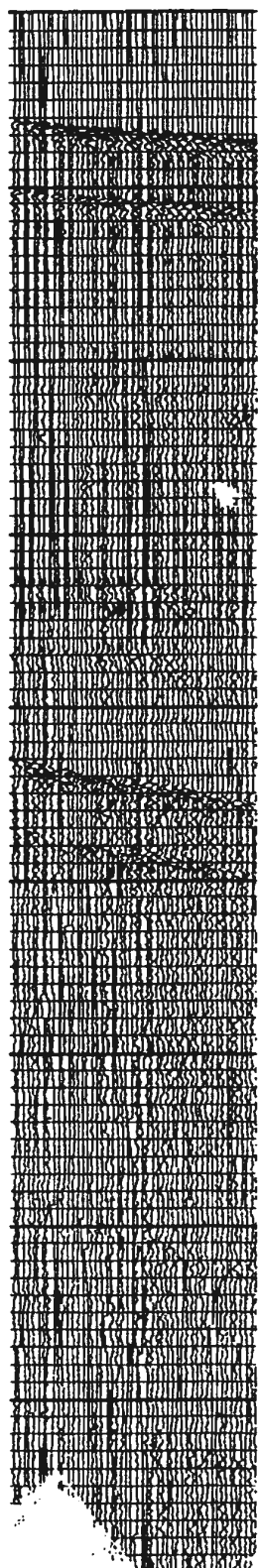
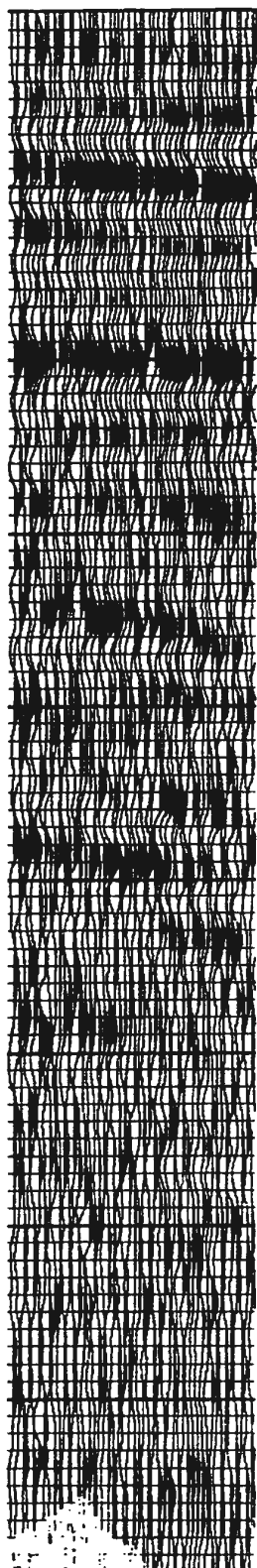


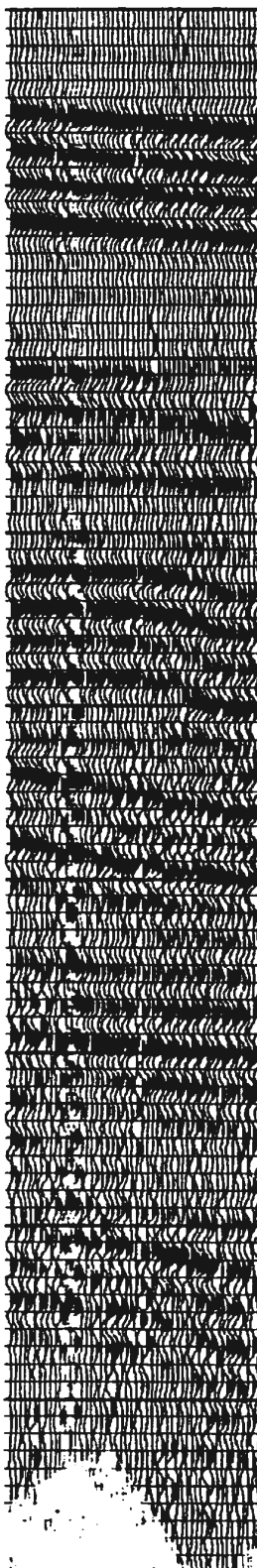
Figure 4.7 Seismic Profile 20-21 (Tie Lines)



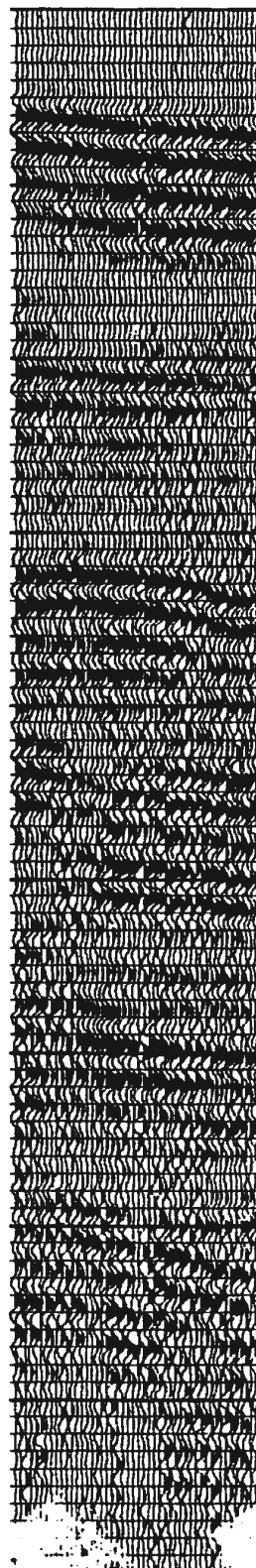
OFF



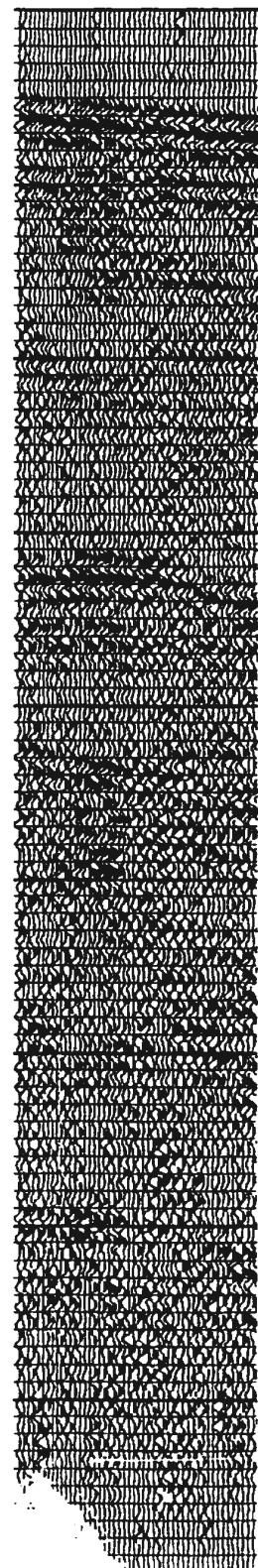
50/100/300/40



200/300/500/8



300/500/700/1



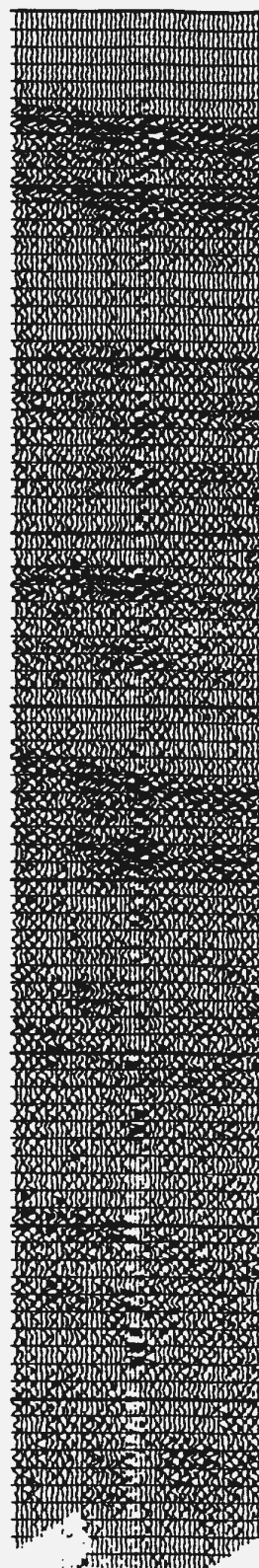
500/700/1000/



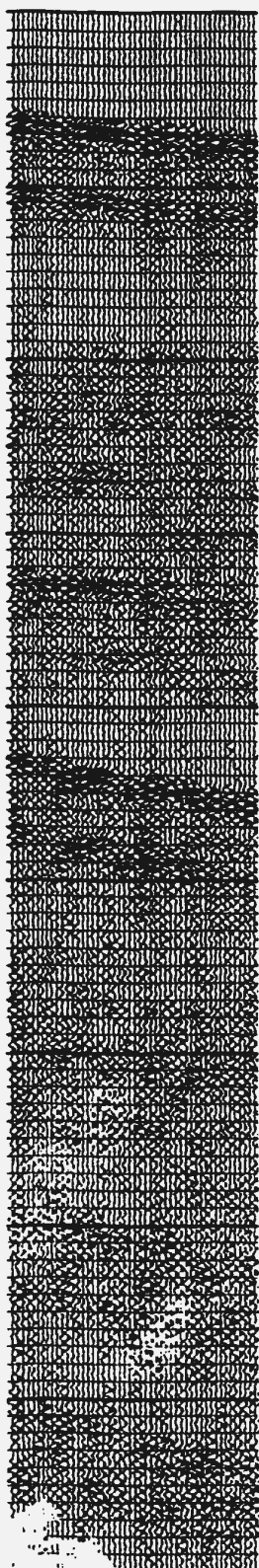
700/



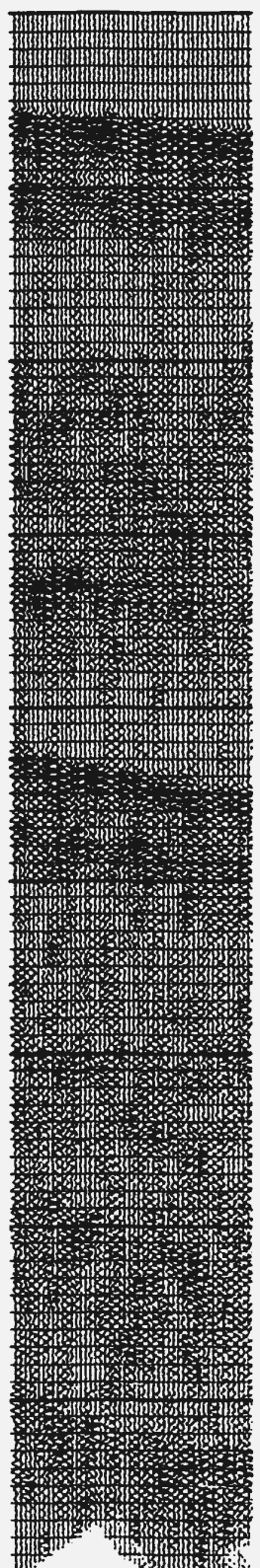
1000/1



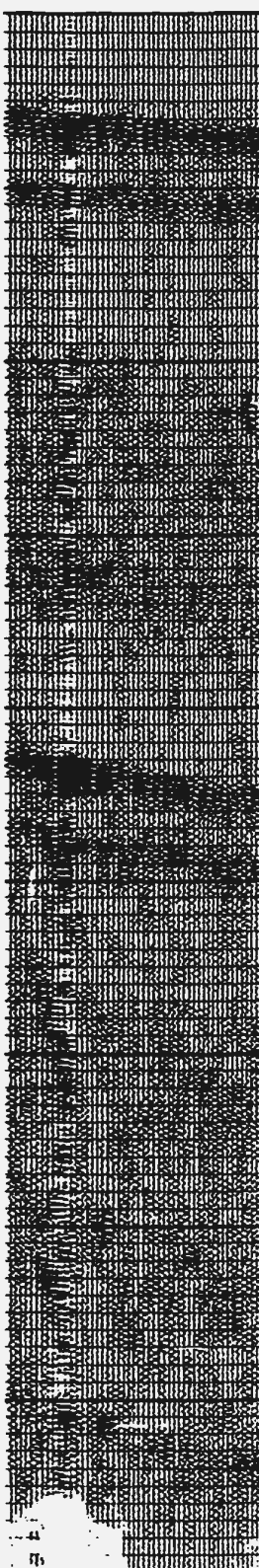
700/1000/1500/



1000/1500/200



1500/2000/250



2000/2500/300

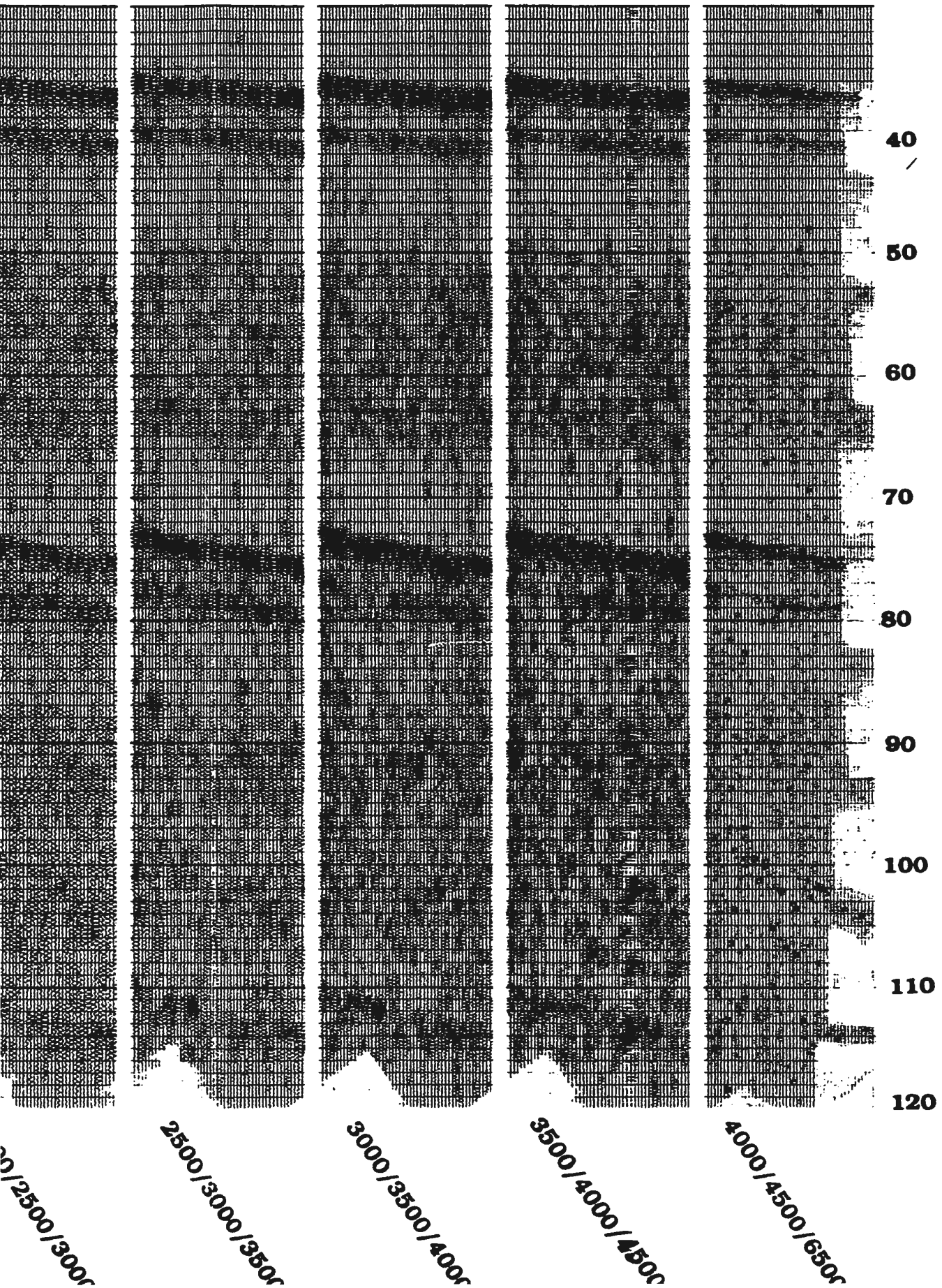


2500/3000/350



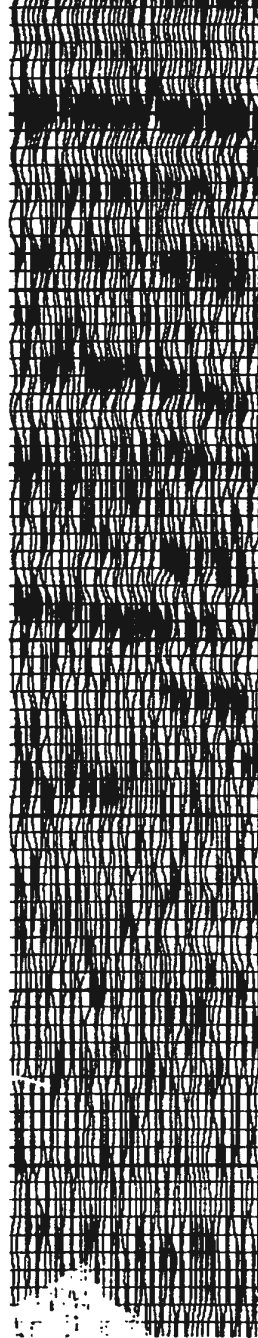
3000/3

Two Way Travel Time (ms)





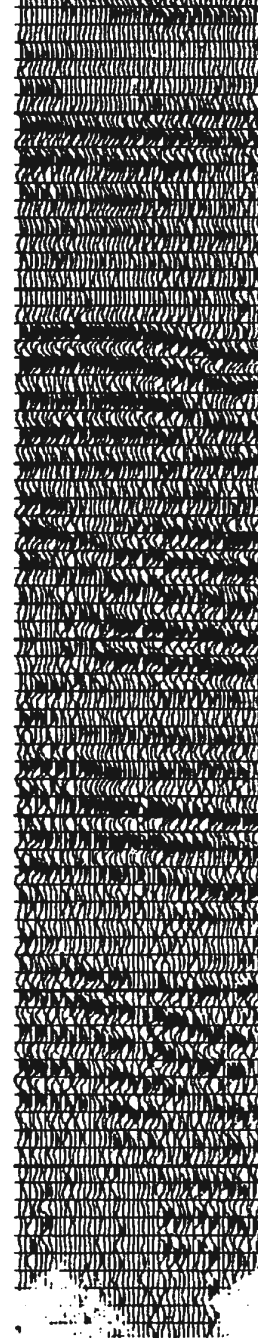
OFF



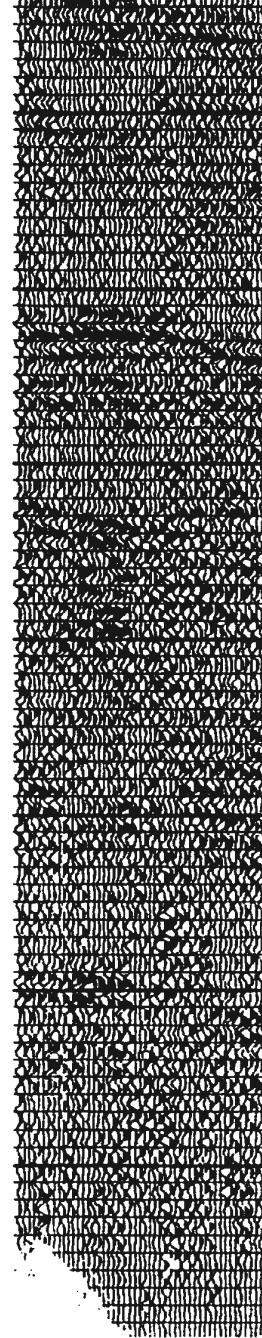
50/100/300/400



200/300/500/800



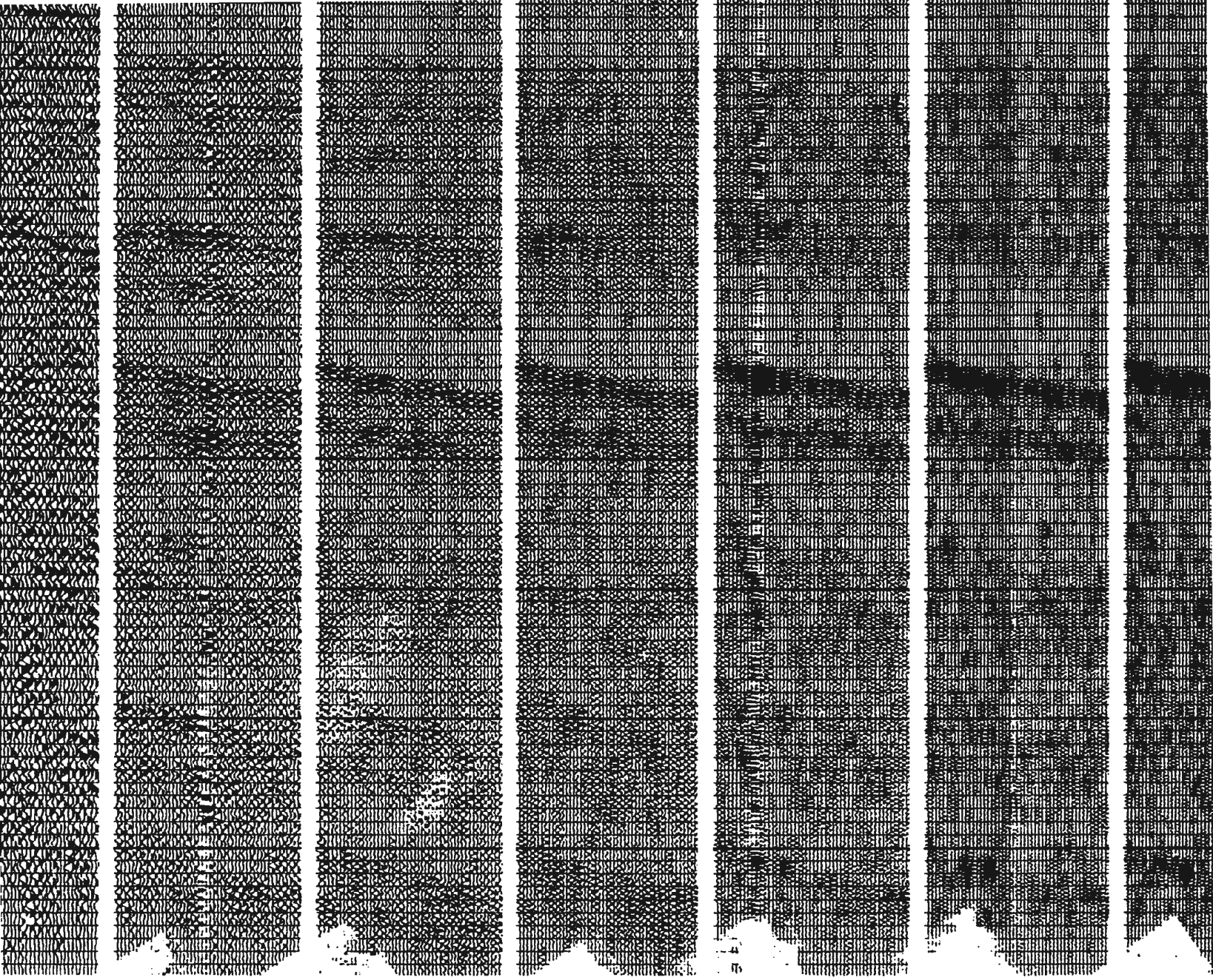
300/500/700/1000



500/700/1000/1500



700/



2/1000/1500
700/1000/1500/2000
1000/1500/2000/3000
1500/2000/2500/3000
2000/2500/3000/3500
2500/3000/3500/4000
3000/3500/4000/4500

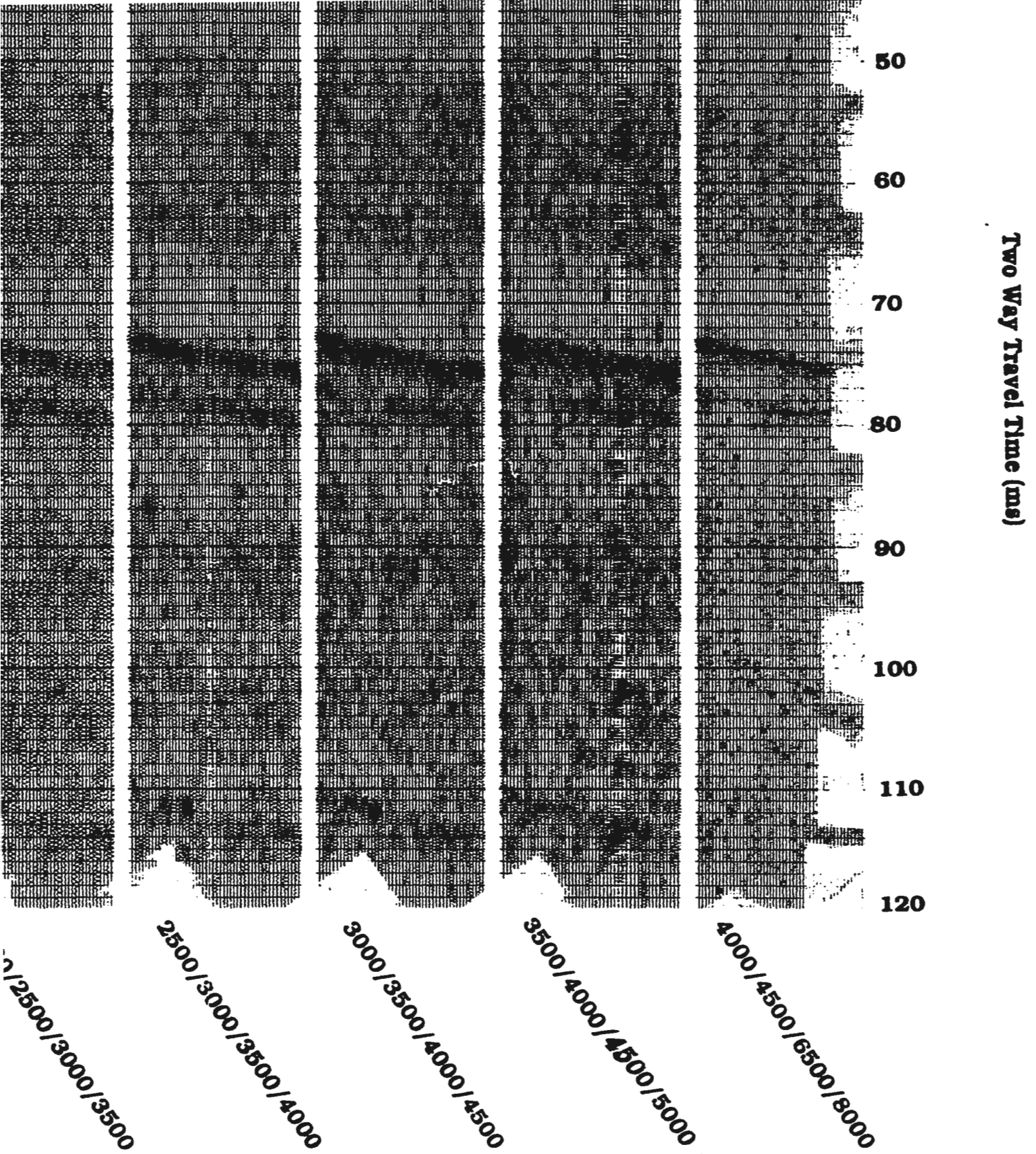
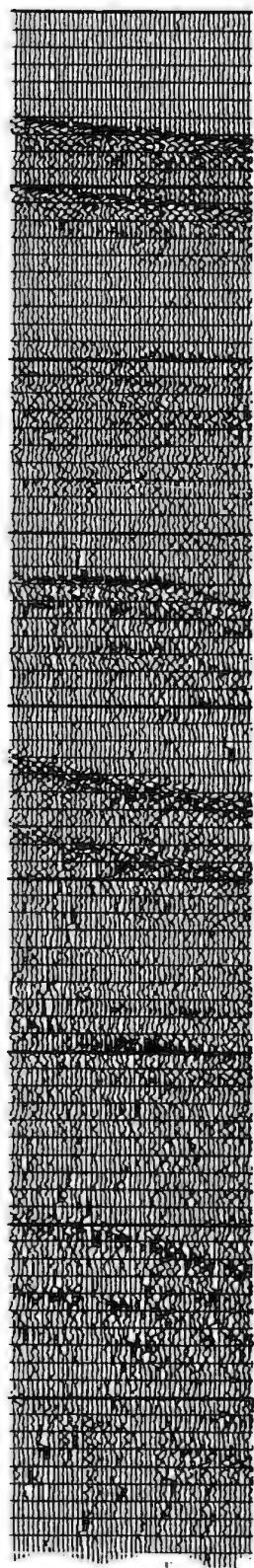
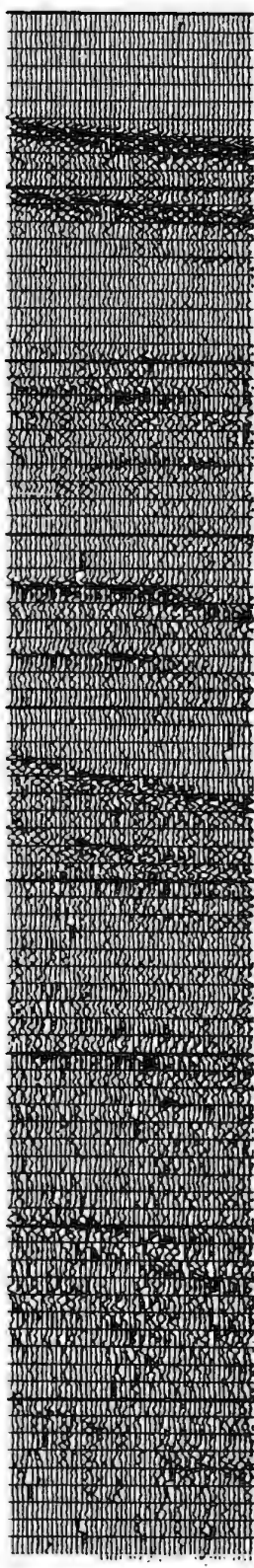


Figure 4.8

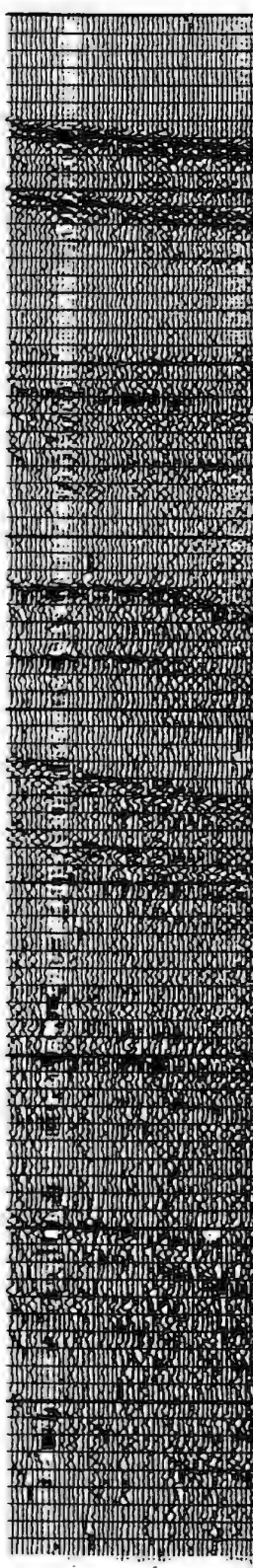
Bandpass Filter Test



0.5 ms



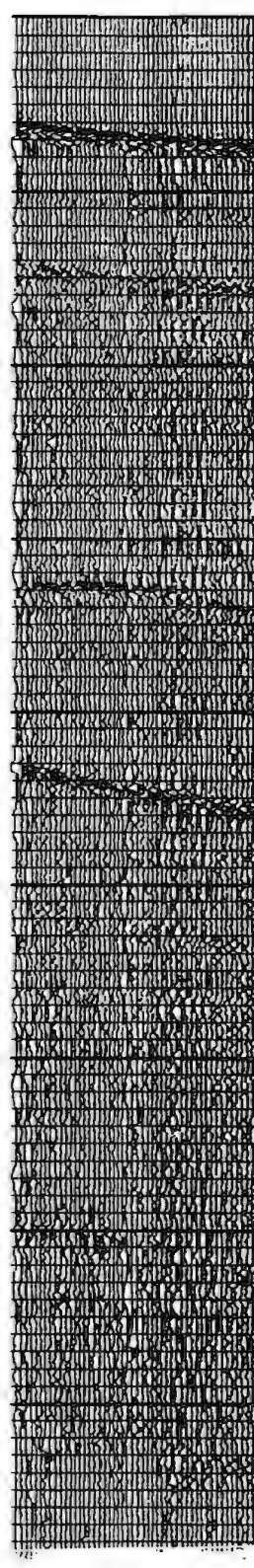
0.7 ms



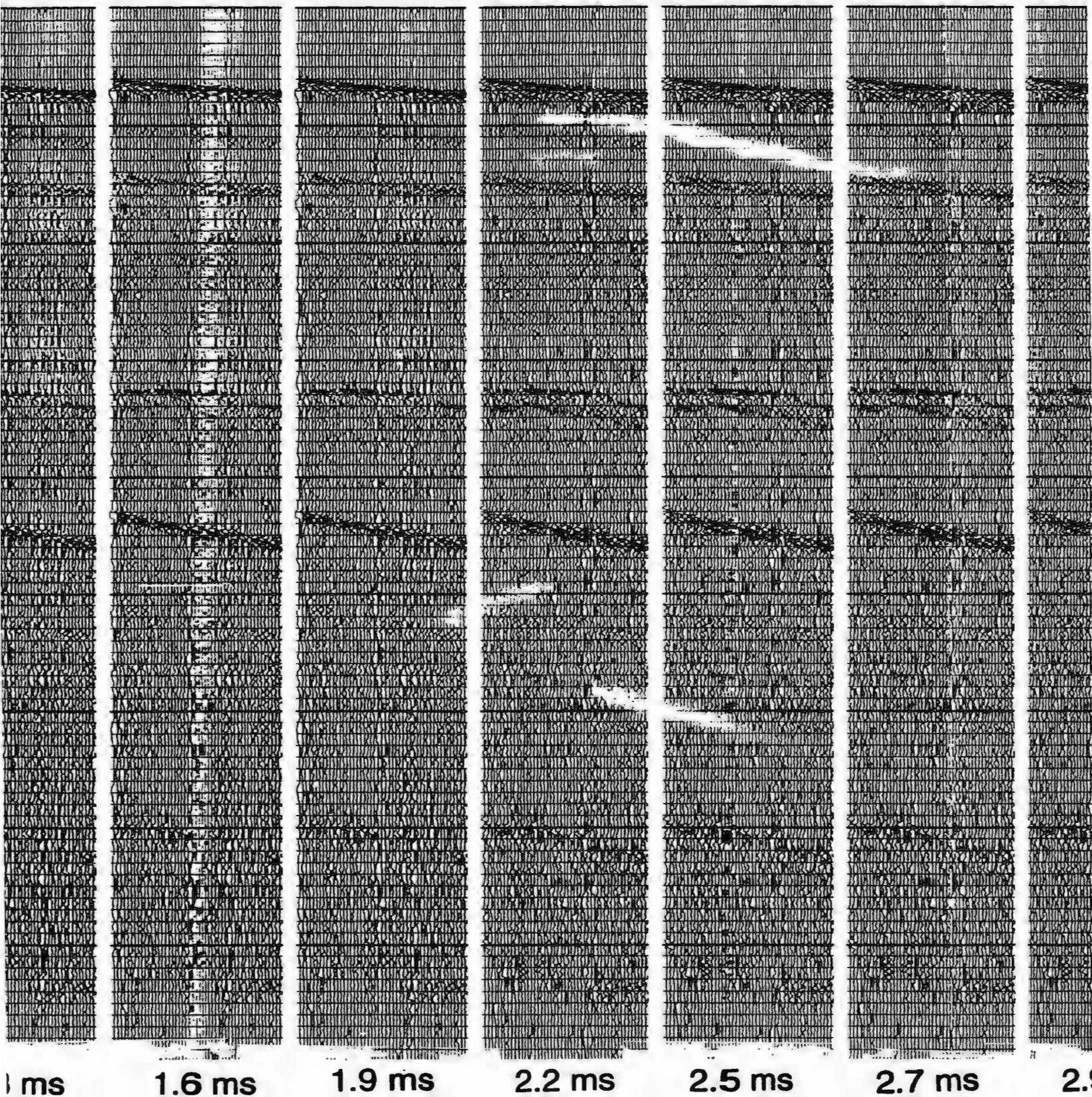
1.0 ms



1.3 ms



1.5 ms



0 ms

1.6 ms

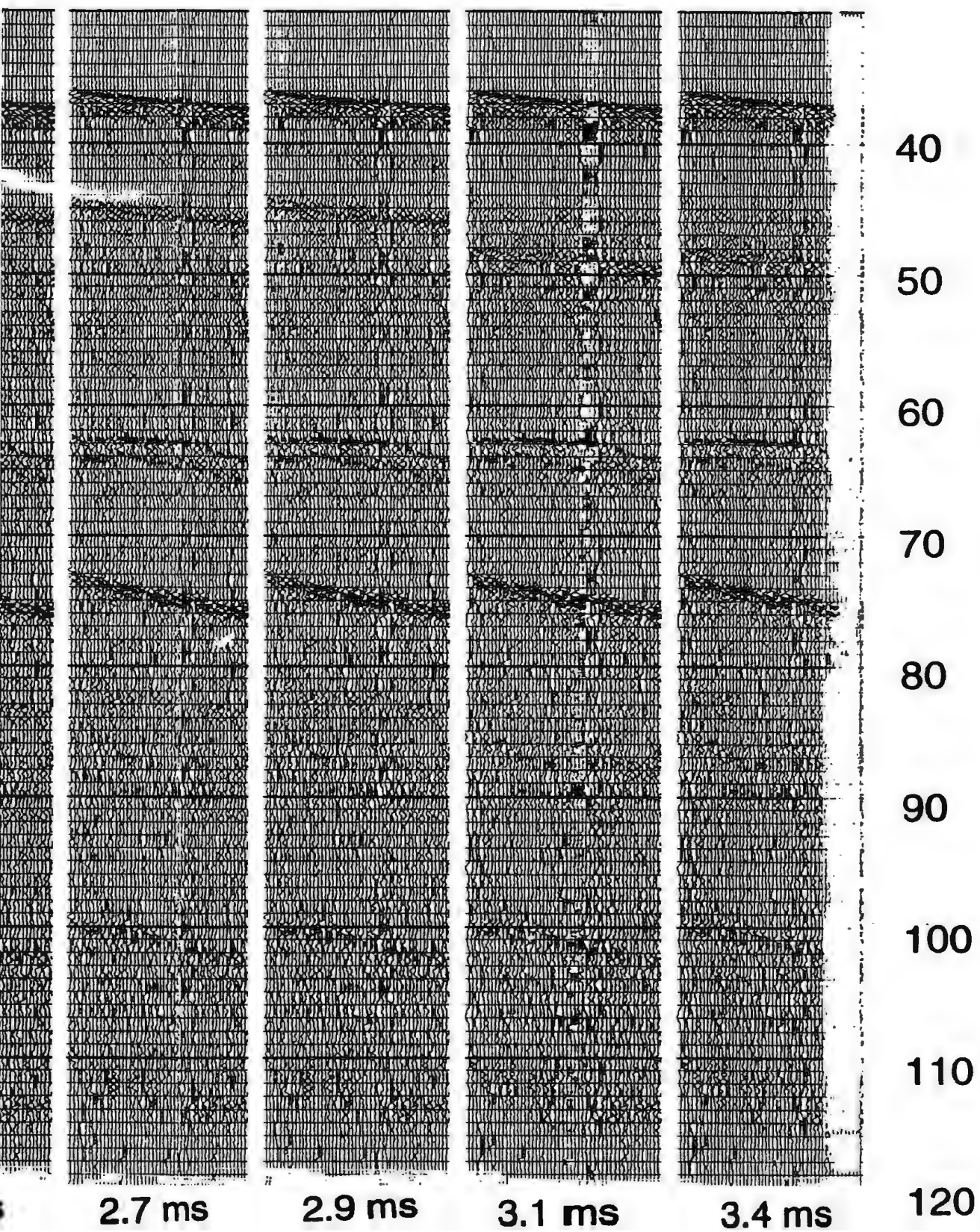
1.9 ms

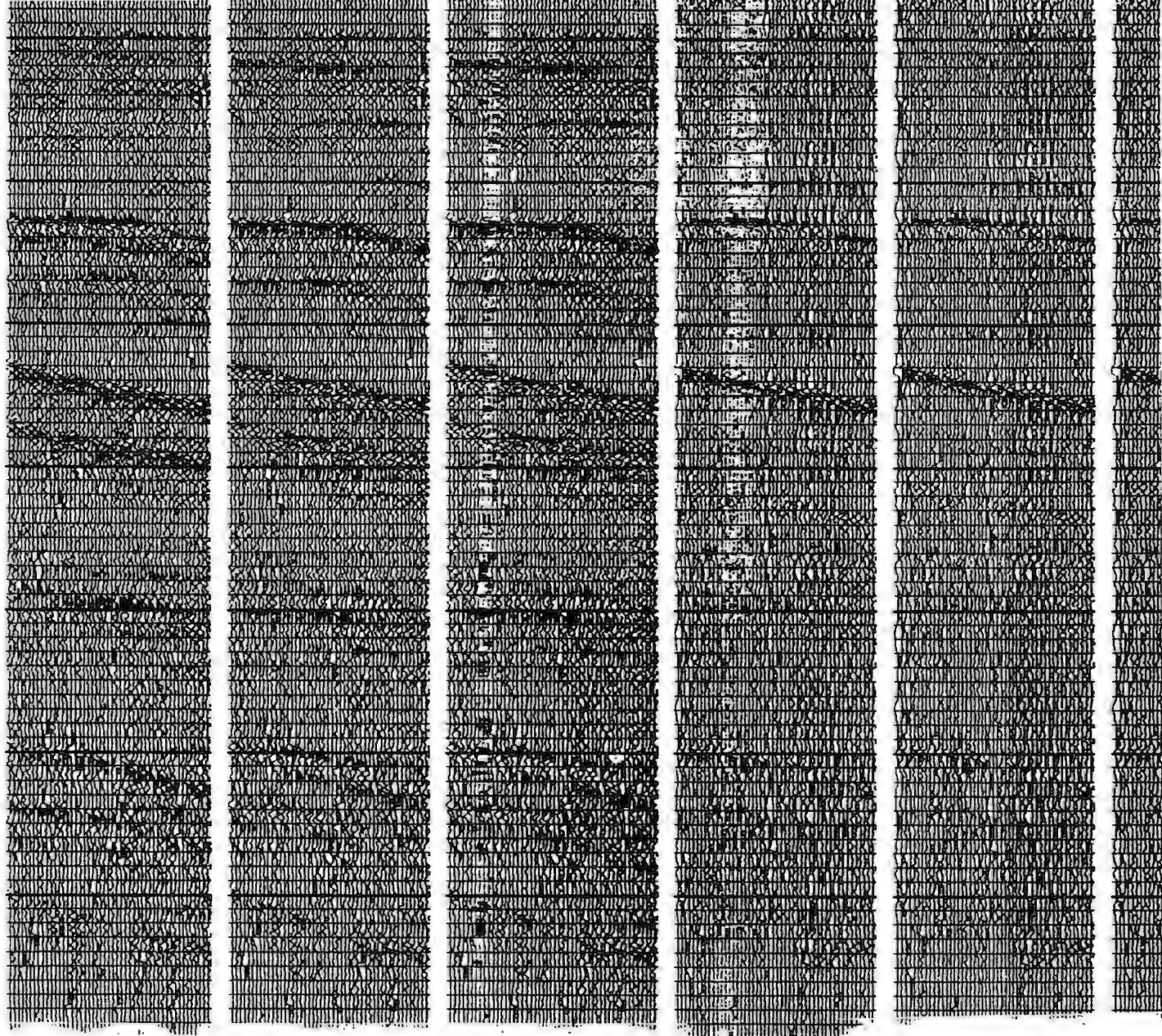
2.2 ms

2.5 ms

2.7 ms

2.9 ms





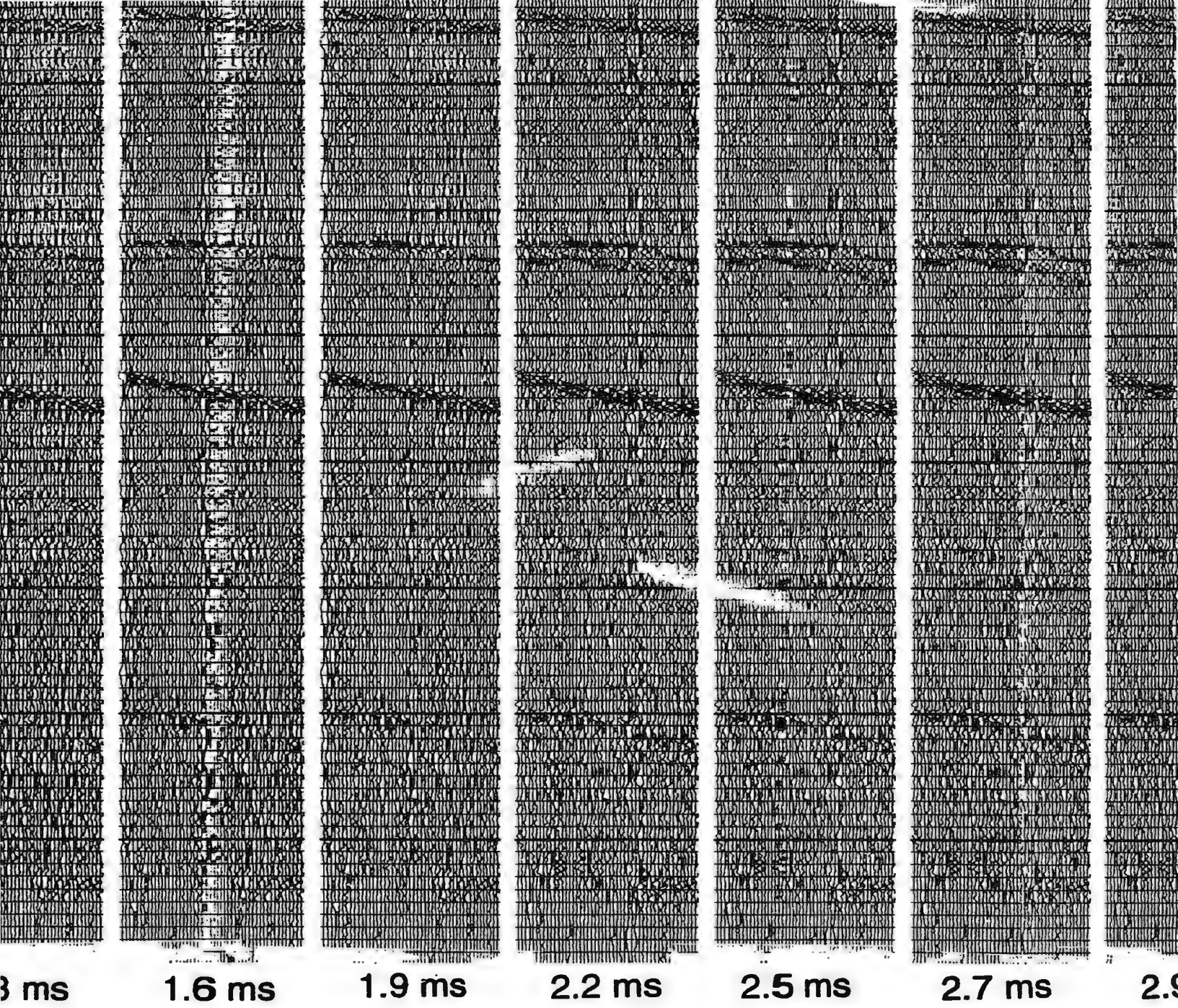
0.5 ms

0.7 ms

1.0 ms

1.3 ms

Bandpass Filter: 100/300/2500/5000
AGC Window: 10 ms
Prediction Operator: 3 ms



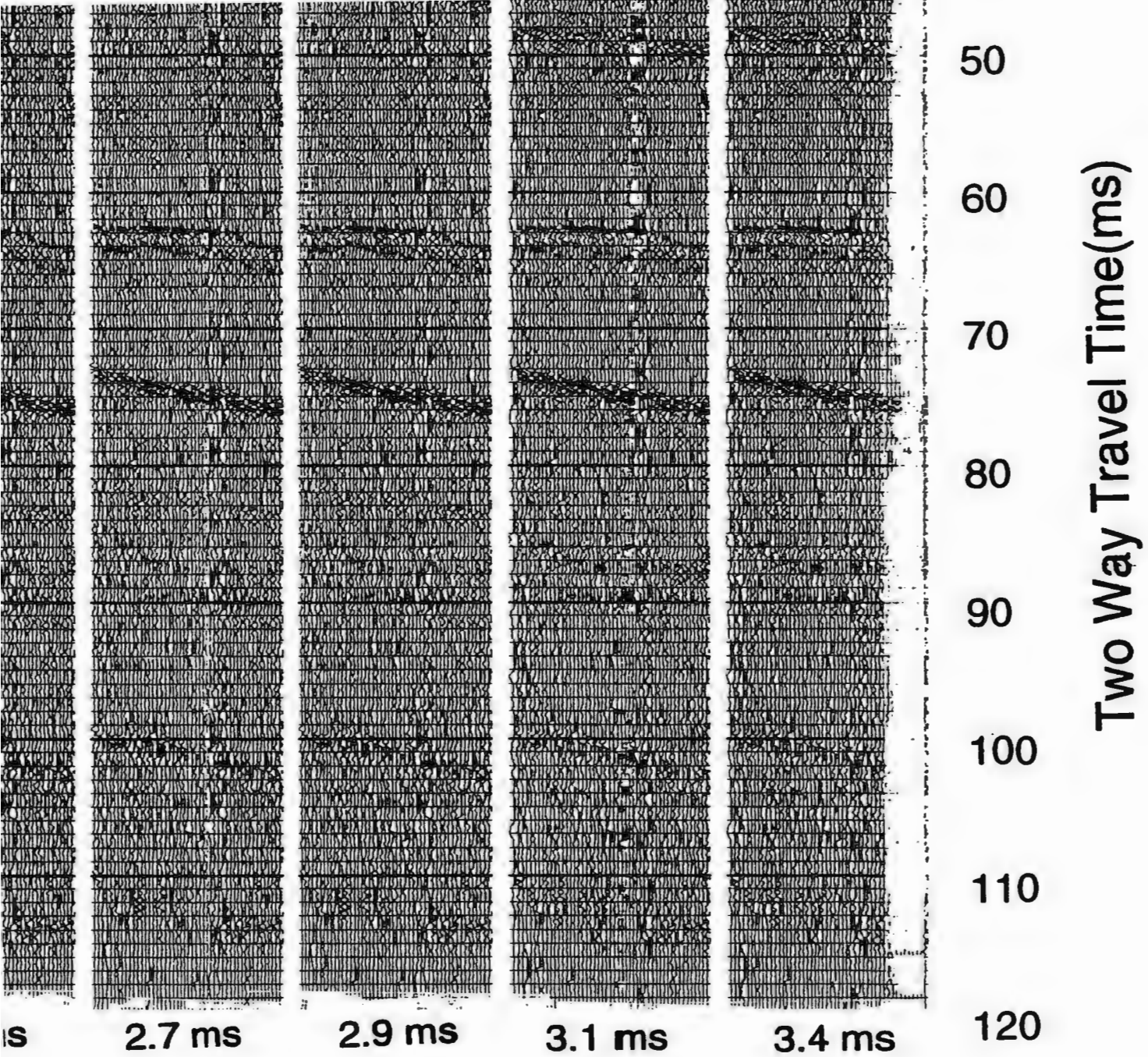


Figure 4.11 Prediction Gap Test



off



1 ms



2 ms



3 ms



4 ms



5 ms



6 ms



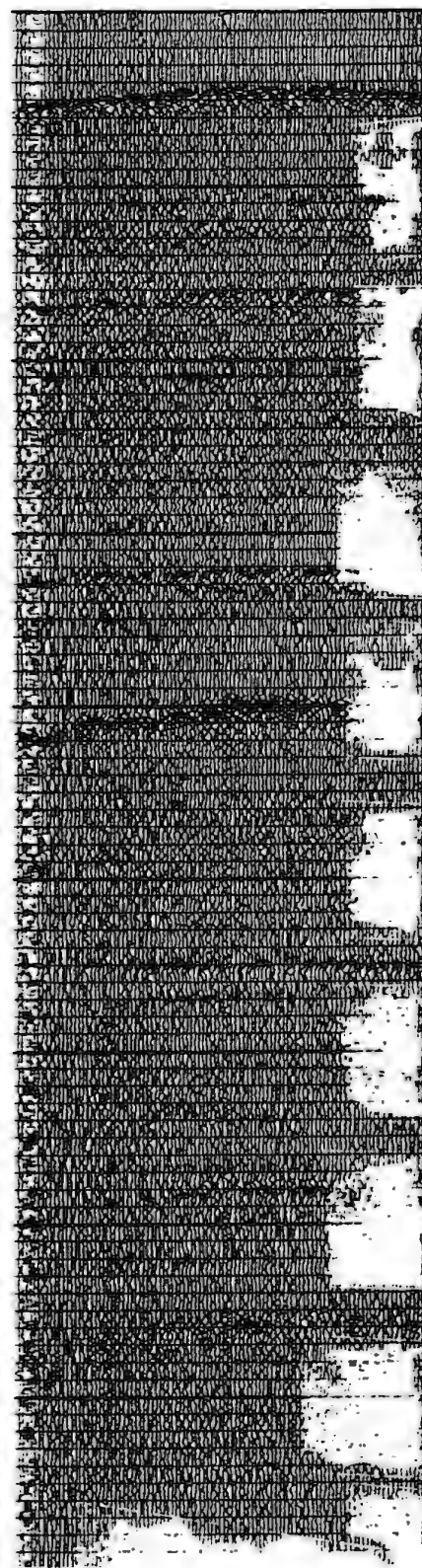
6 ms



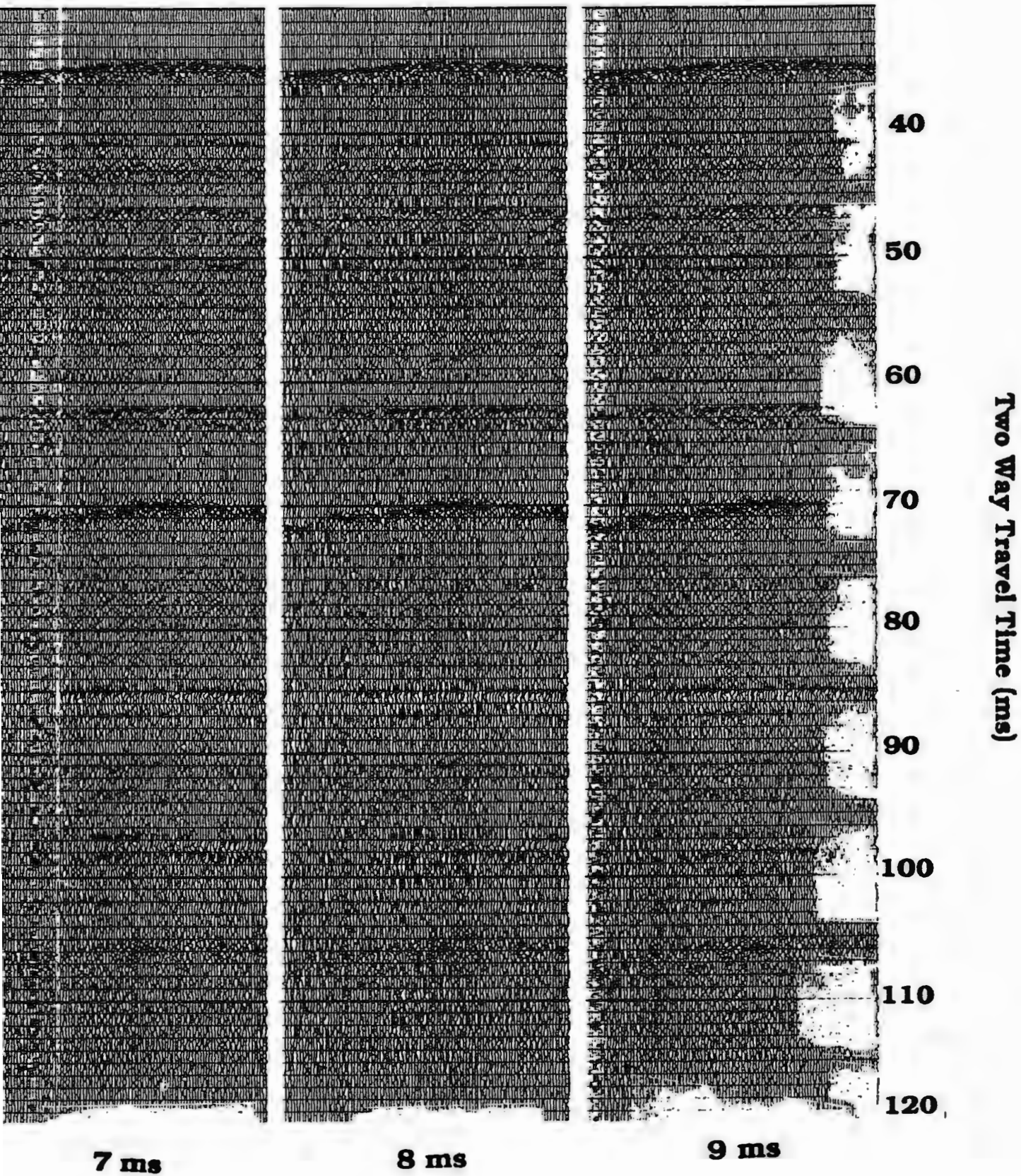
7 ms

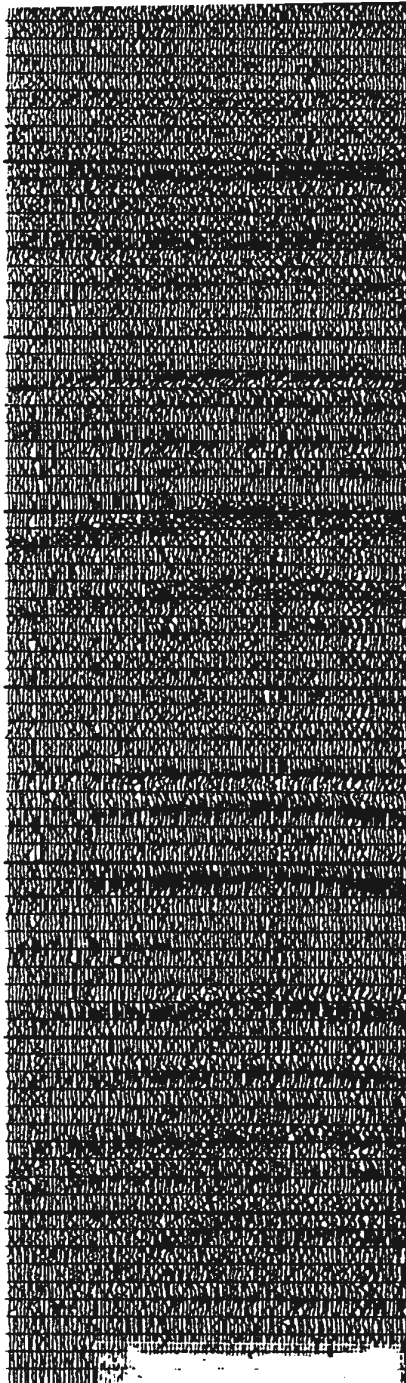


8 ms



9 ms





off



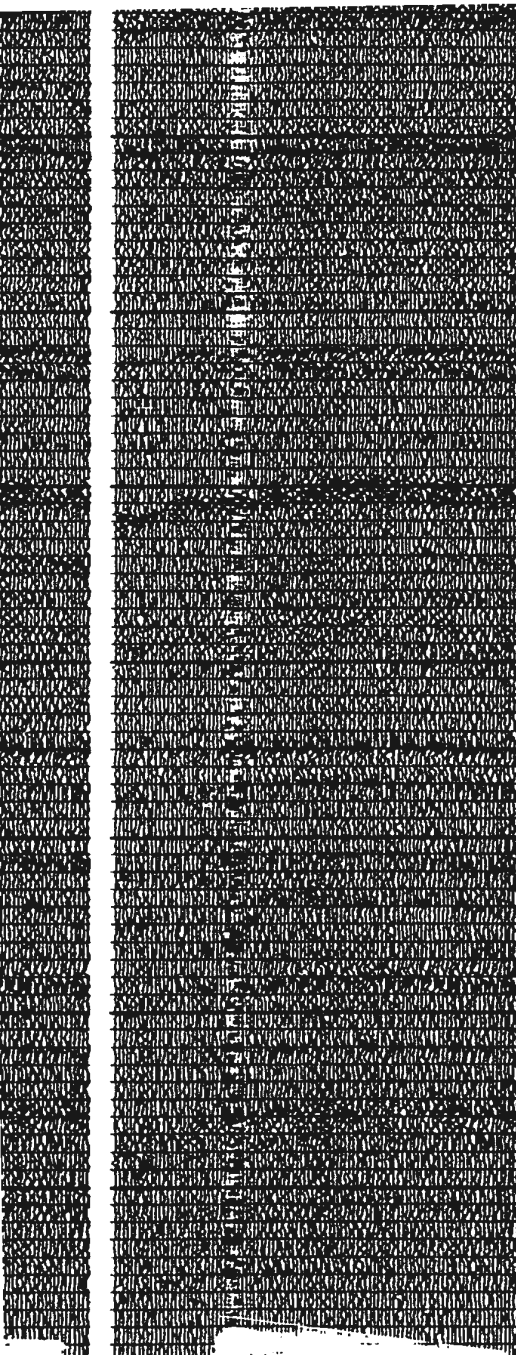
1 ms



2 ms

Bandpass Filter:
AGC Window:
Prediction Gap:

100/300/2500/5000
10 ms
1 ms



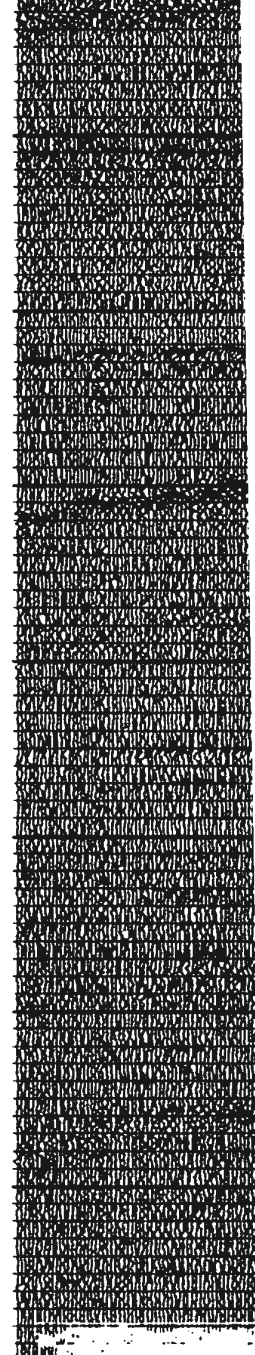
3 ms



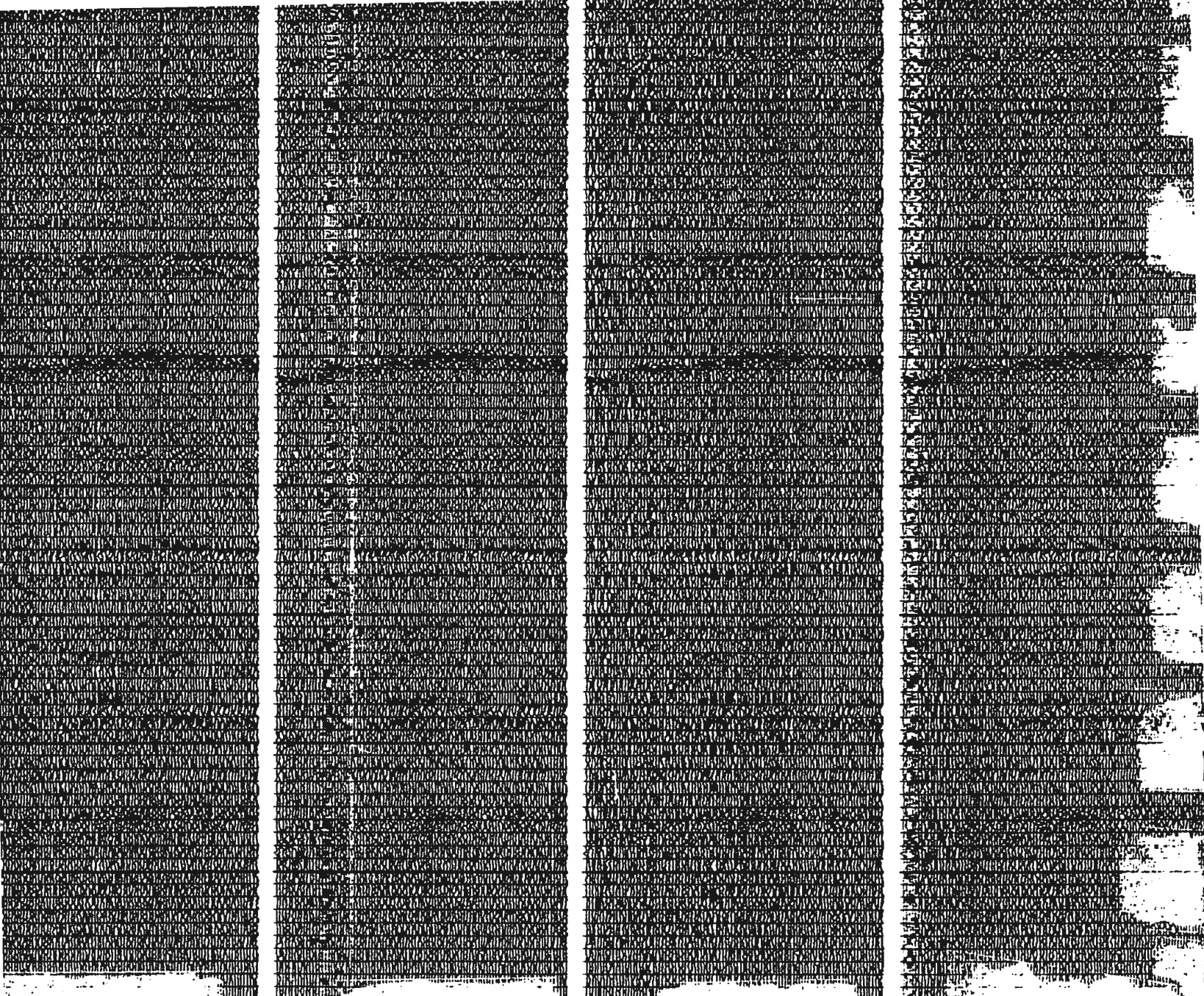
4 ms



5 ms



6 ms



6 ms

7 ms

8 ms

9 ms

Figure 4.12

Prediction Operator

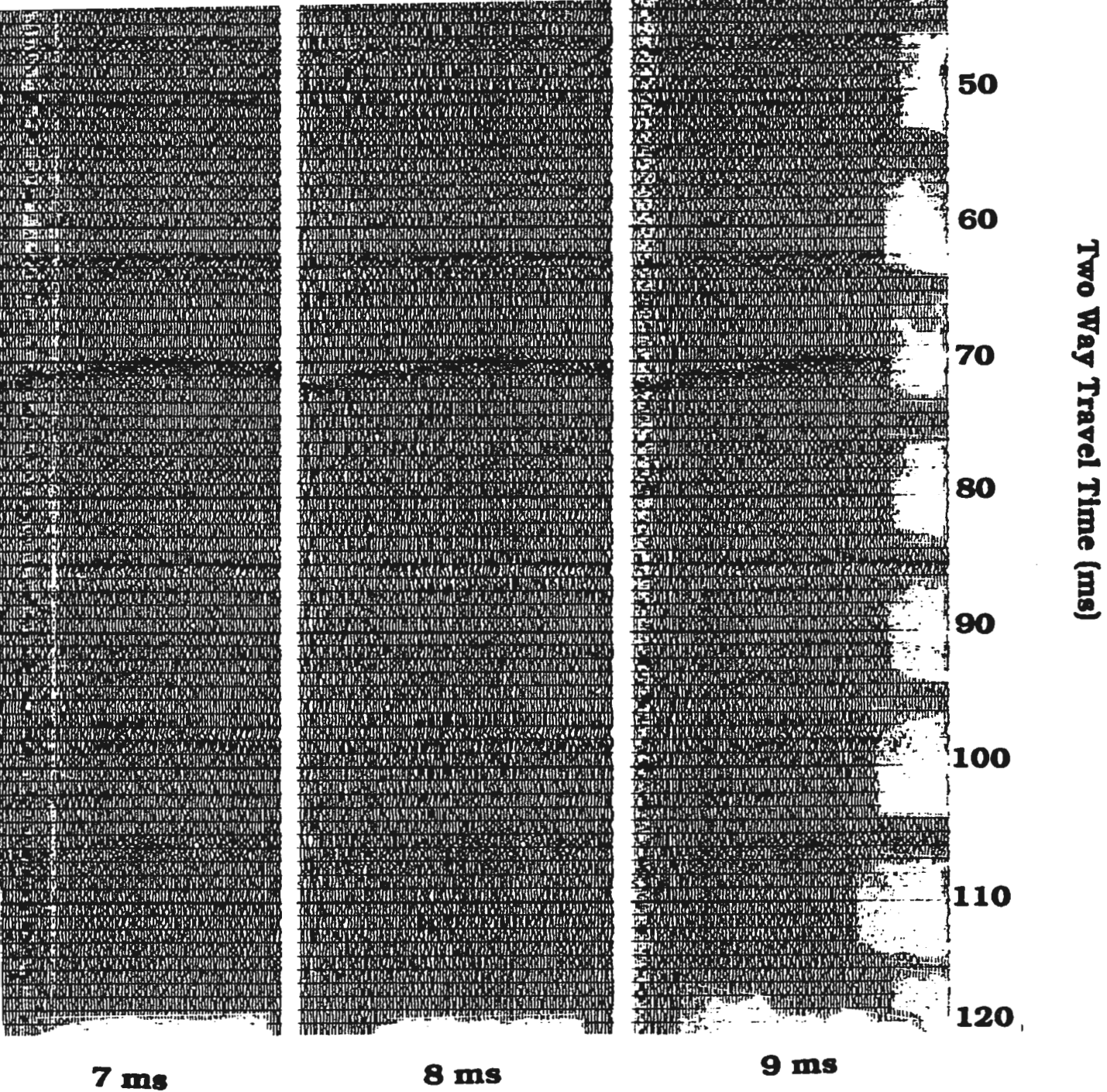


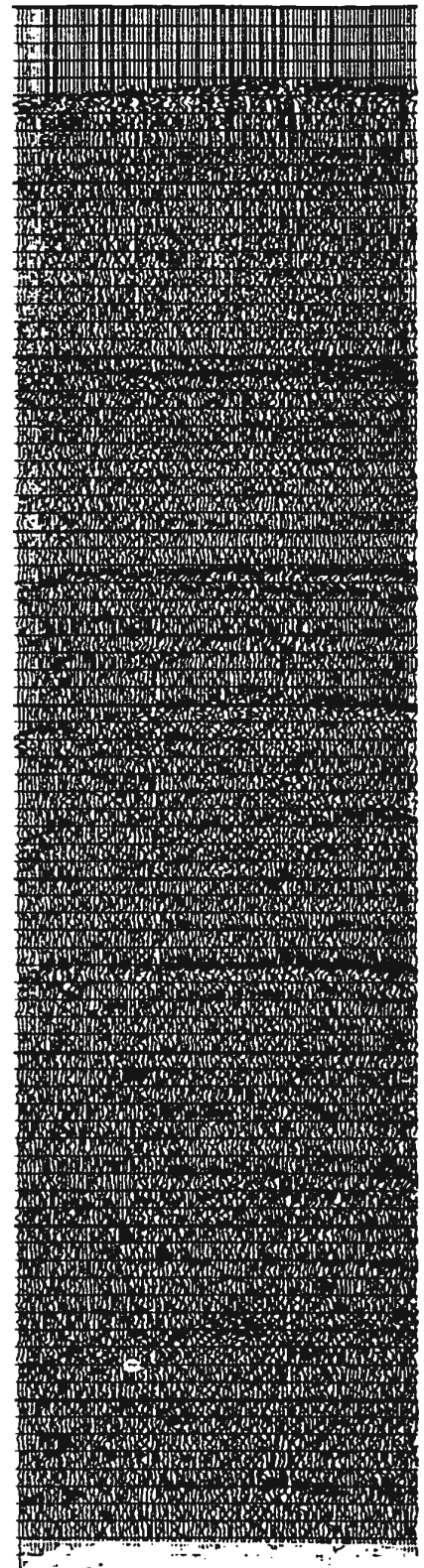
Figure 4.12 Prediction Operator Test



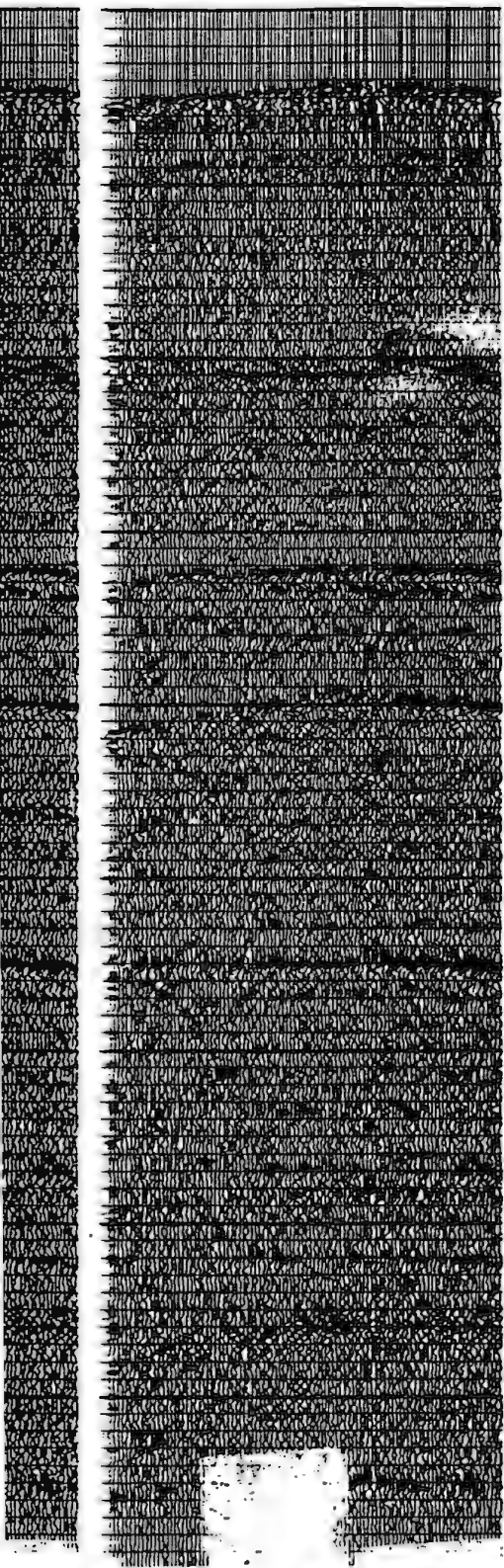
5 ms



7 ms



10ms



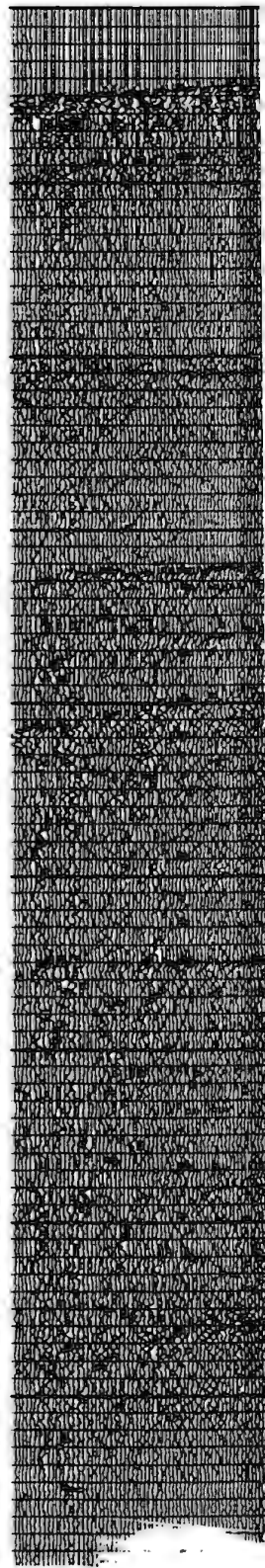
12 ms



15 ms



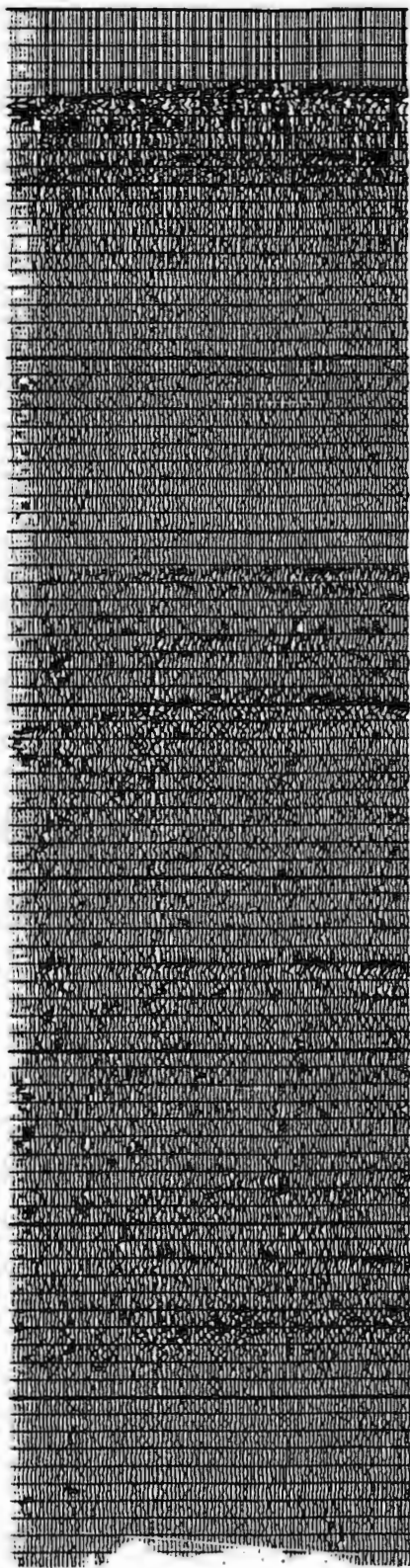
17 ms



20 ms



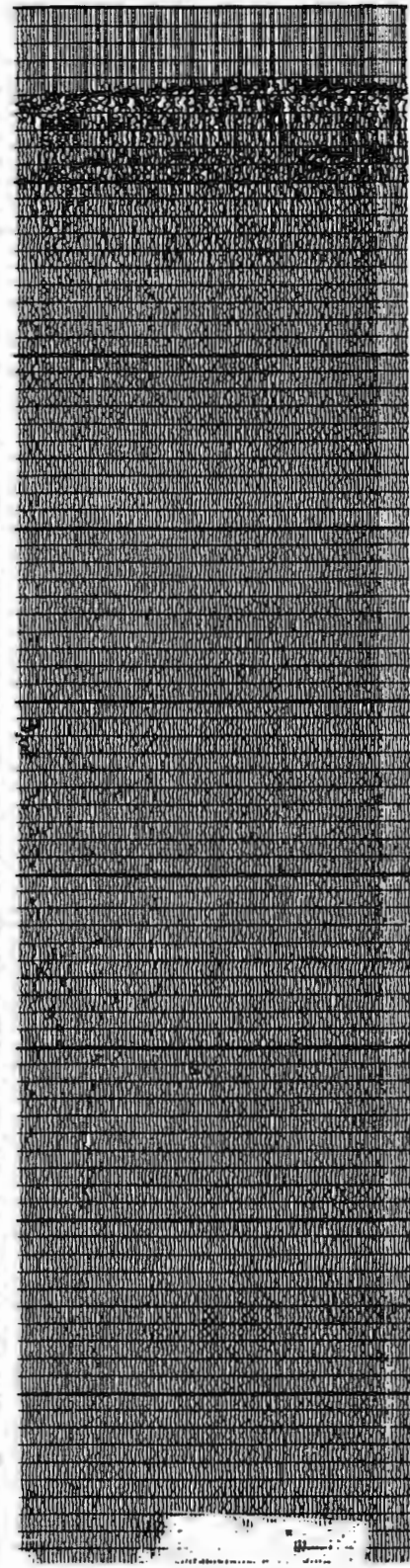
20 ms



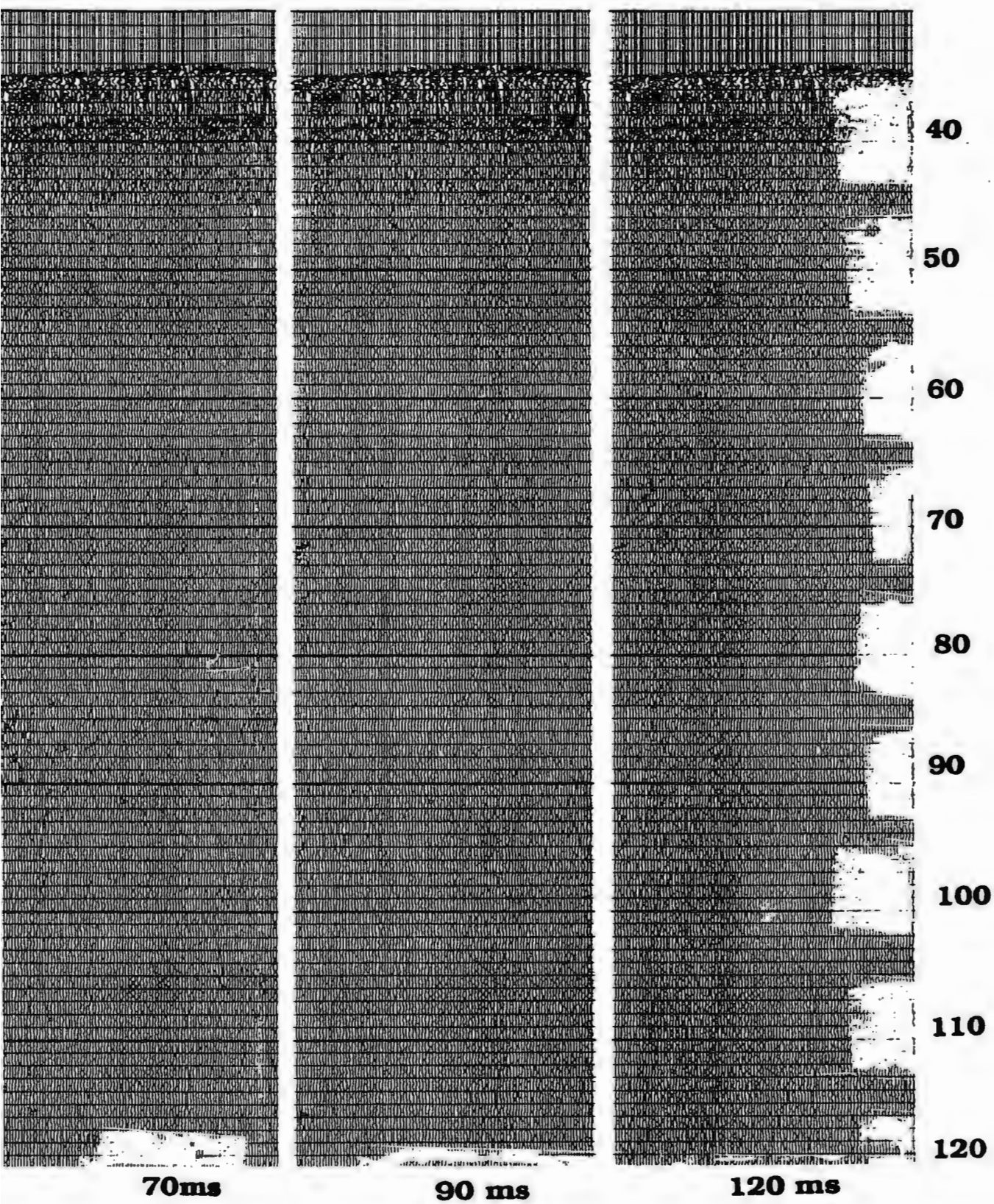
30ms



50ms



70ms





5 ms



7 ms



10ms

Bandpass Filter:
Predictive Decon:

Trace Mixing:

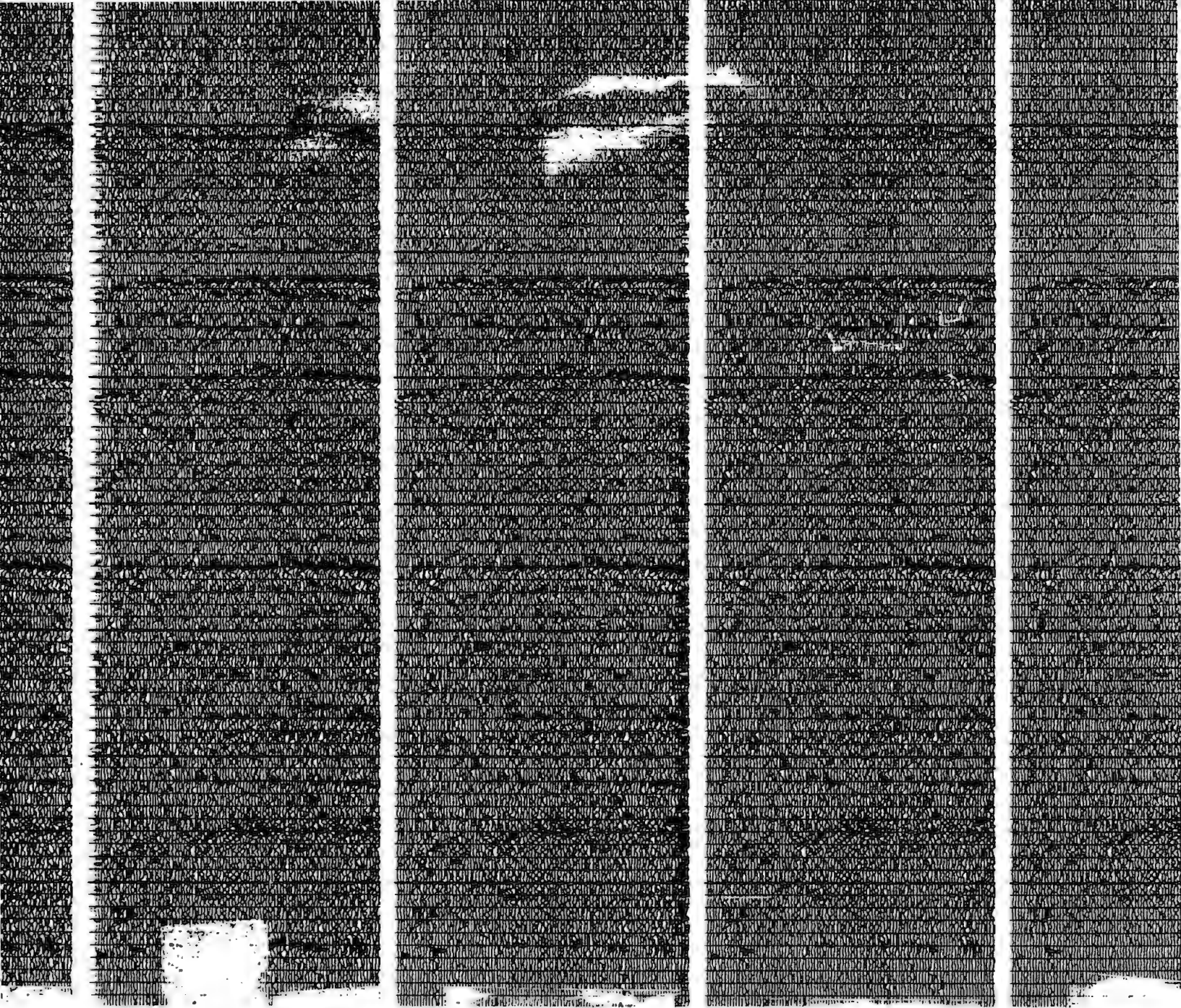
100/300/2500/5000

1) 1 ms gap: 3 ms operator

2) 7.5 ms gap: 2 ms operator

3) seabed time gap: 3 ms operator

3 trace mix with 1:10:1 weighting



12 ms

15 ms

17 ms

20 ms

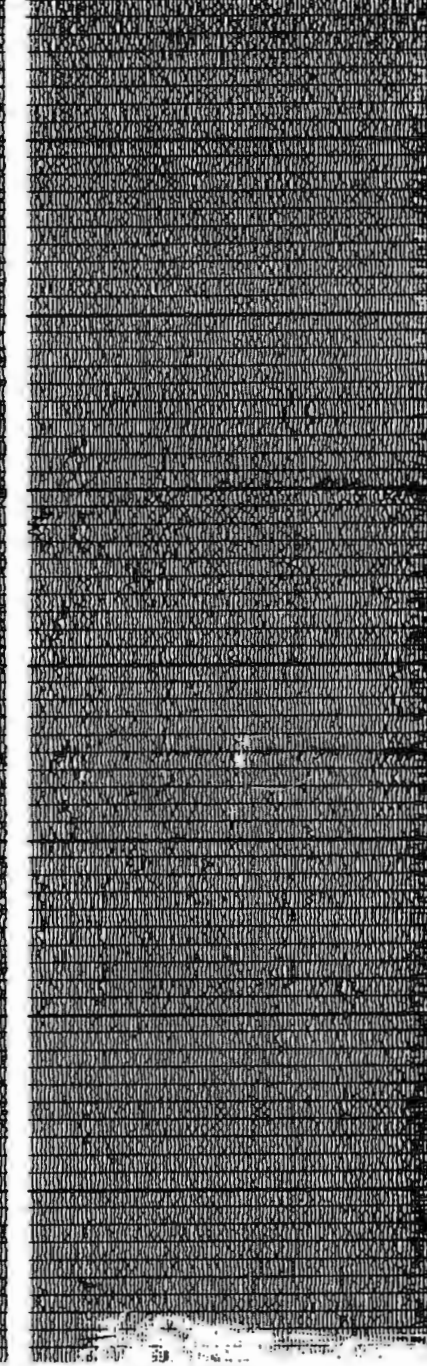
tor
ing



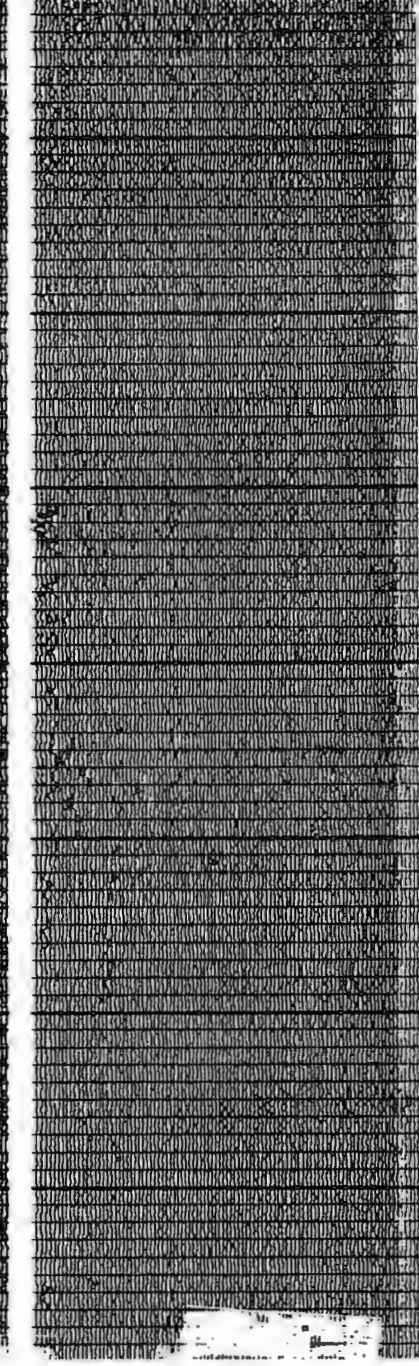
20 ms



30ms



50ms



70ms

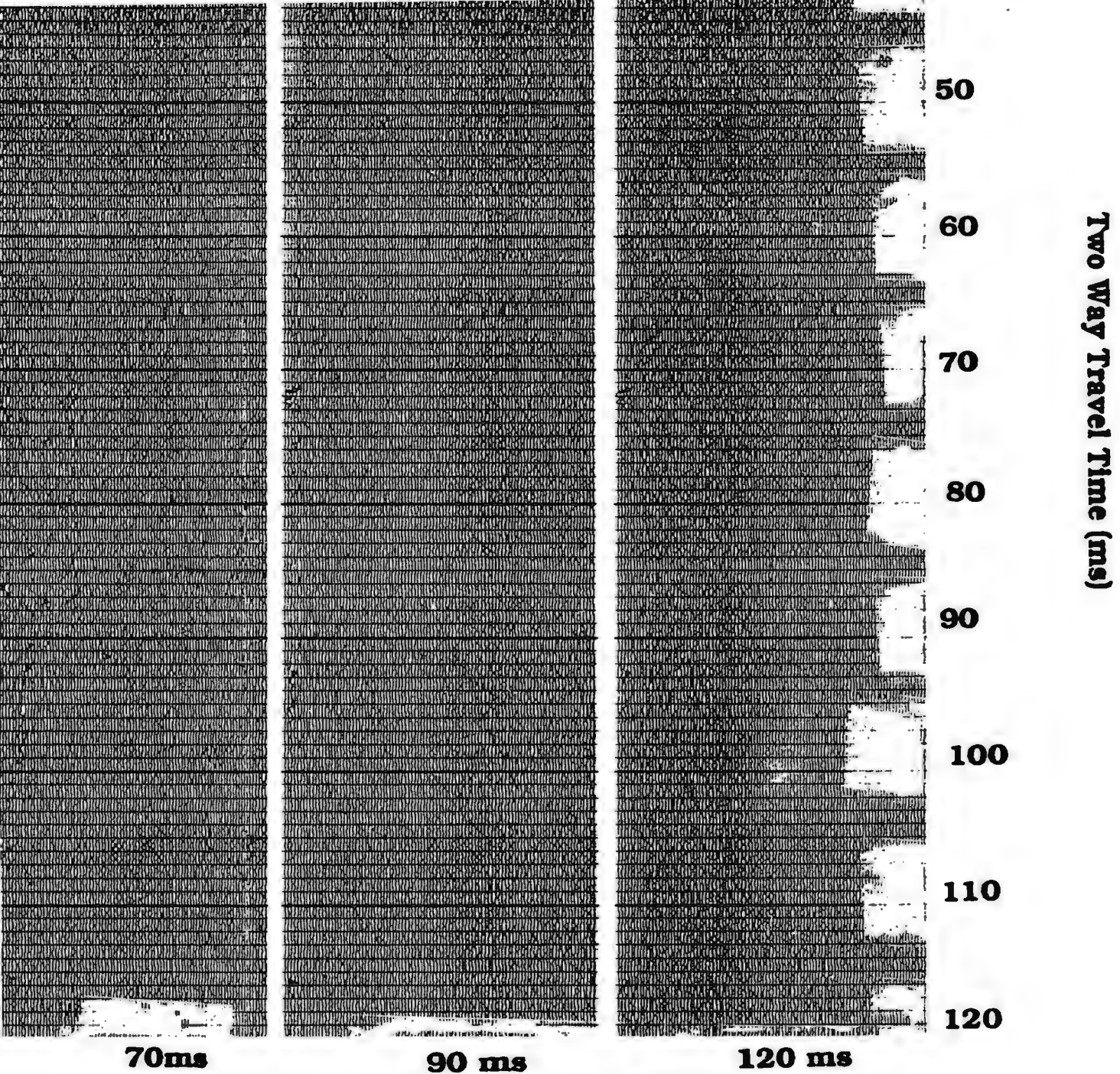
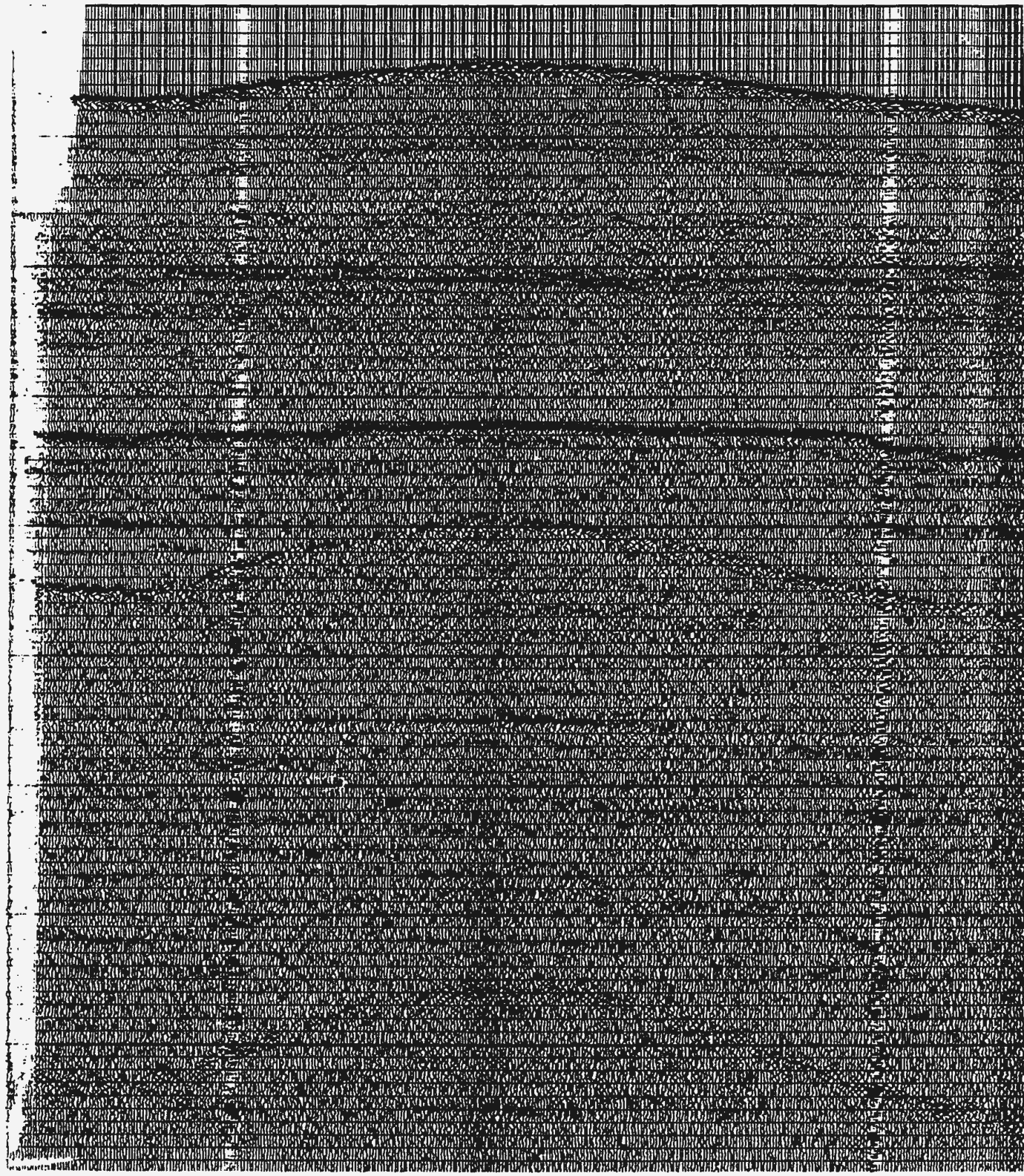
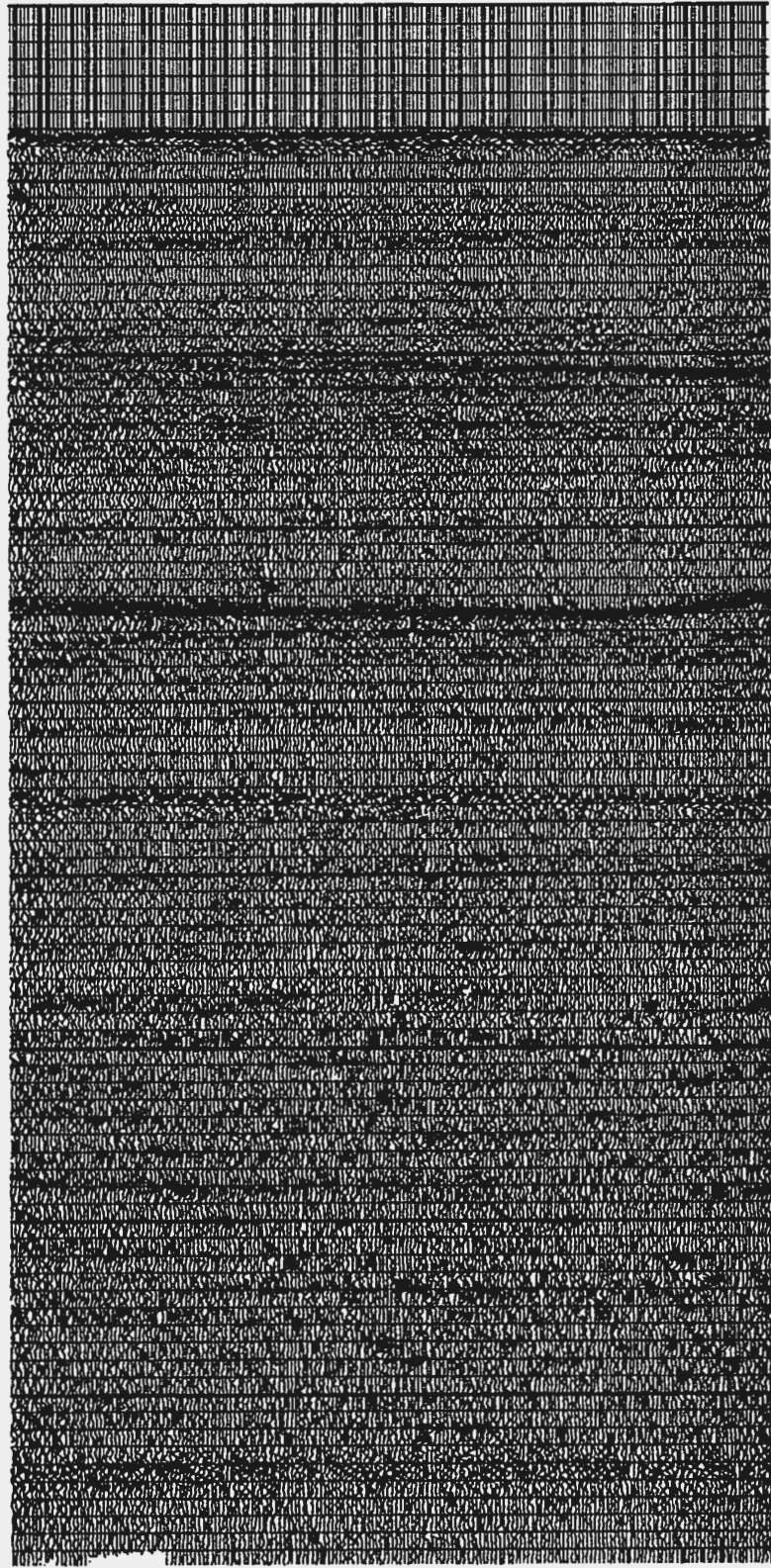
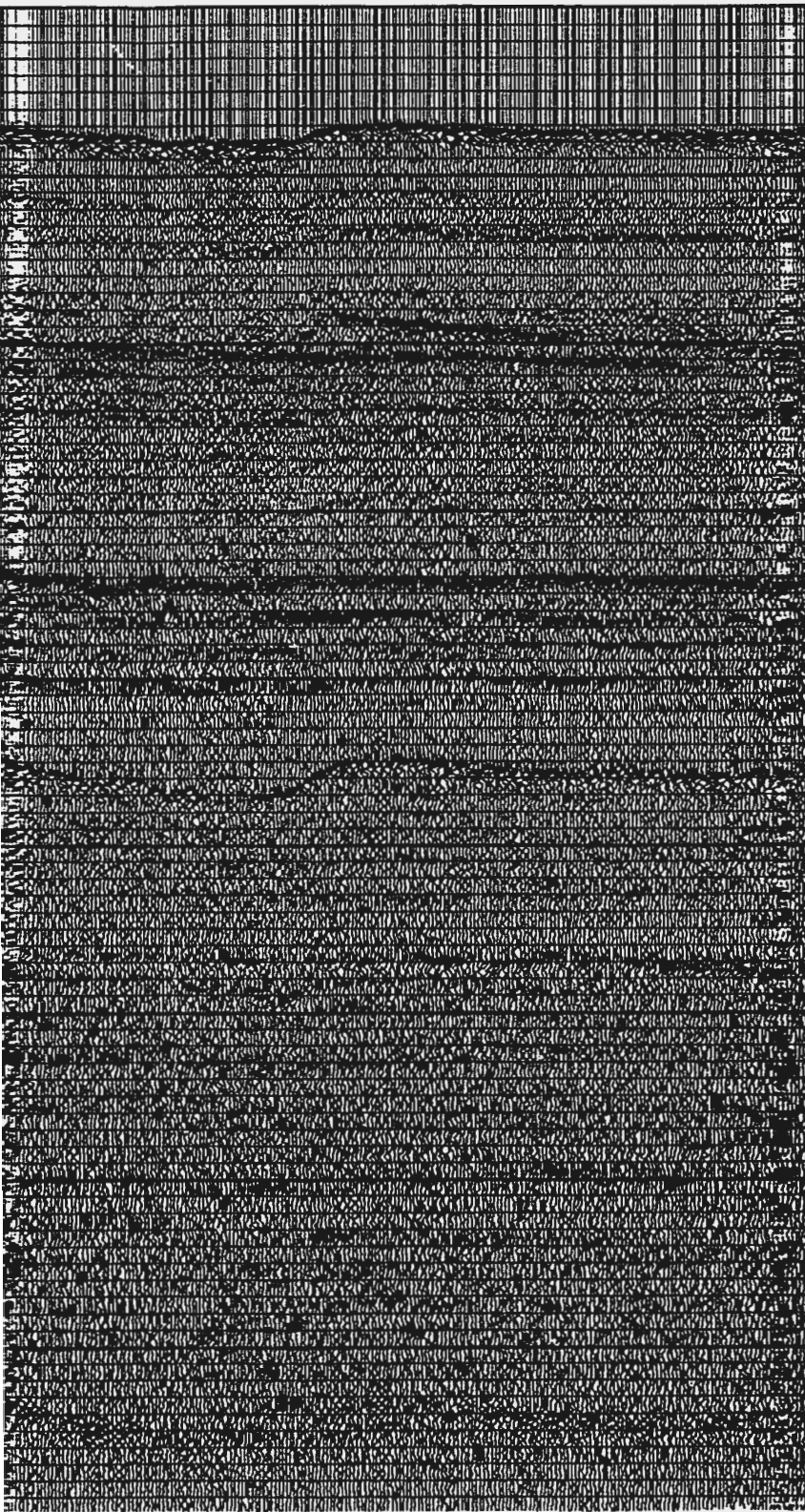
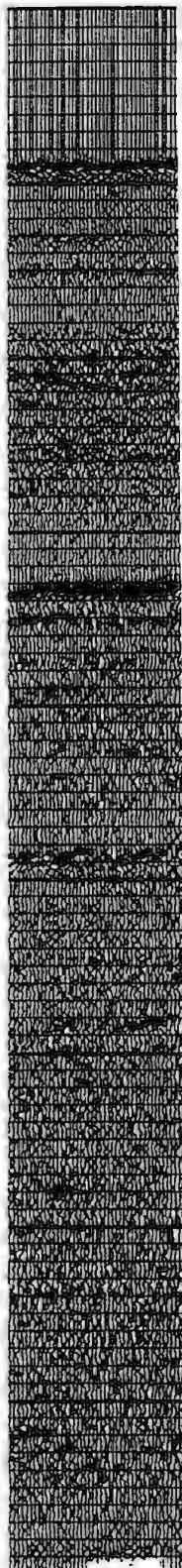
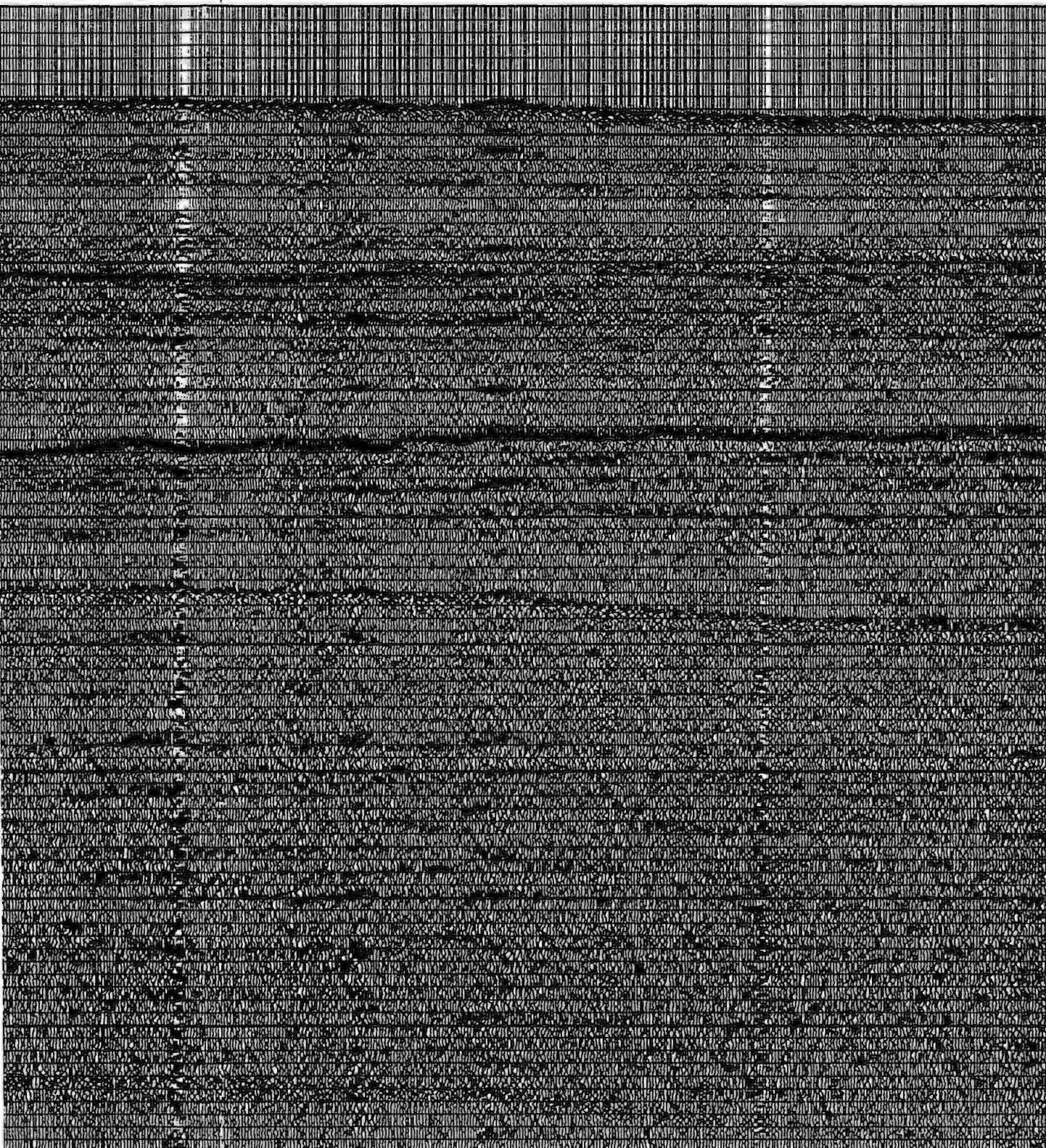


Figure 4.13 AGC Window Length Test

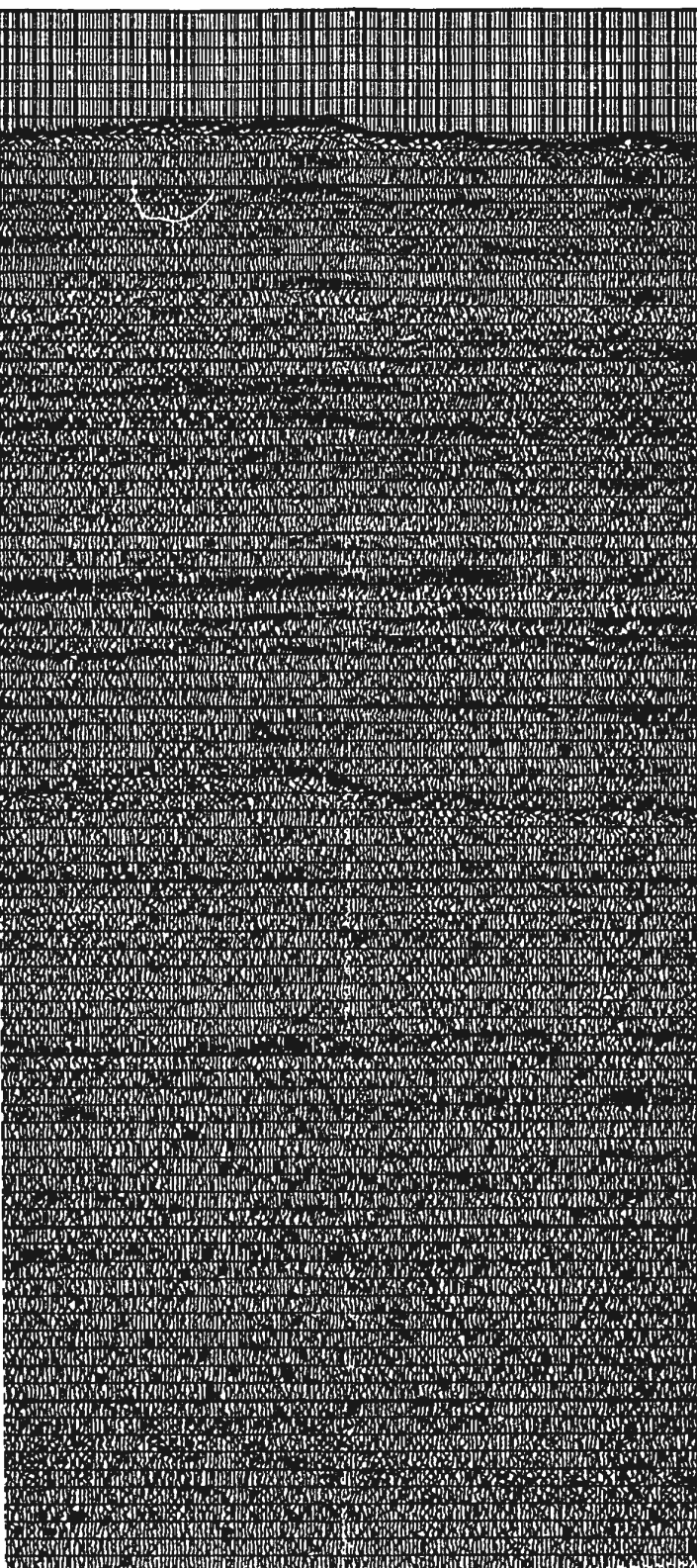




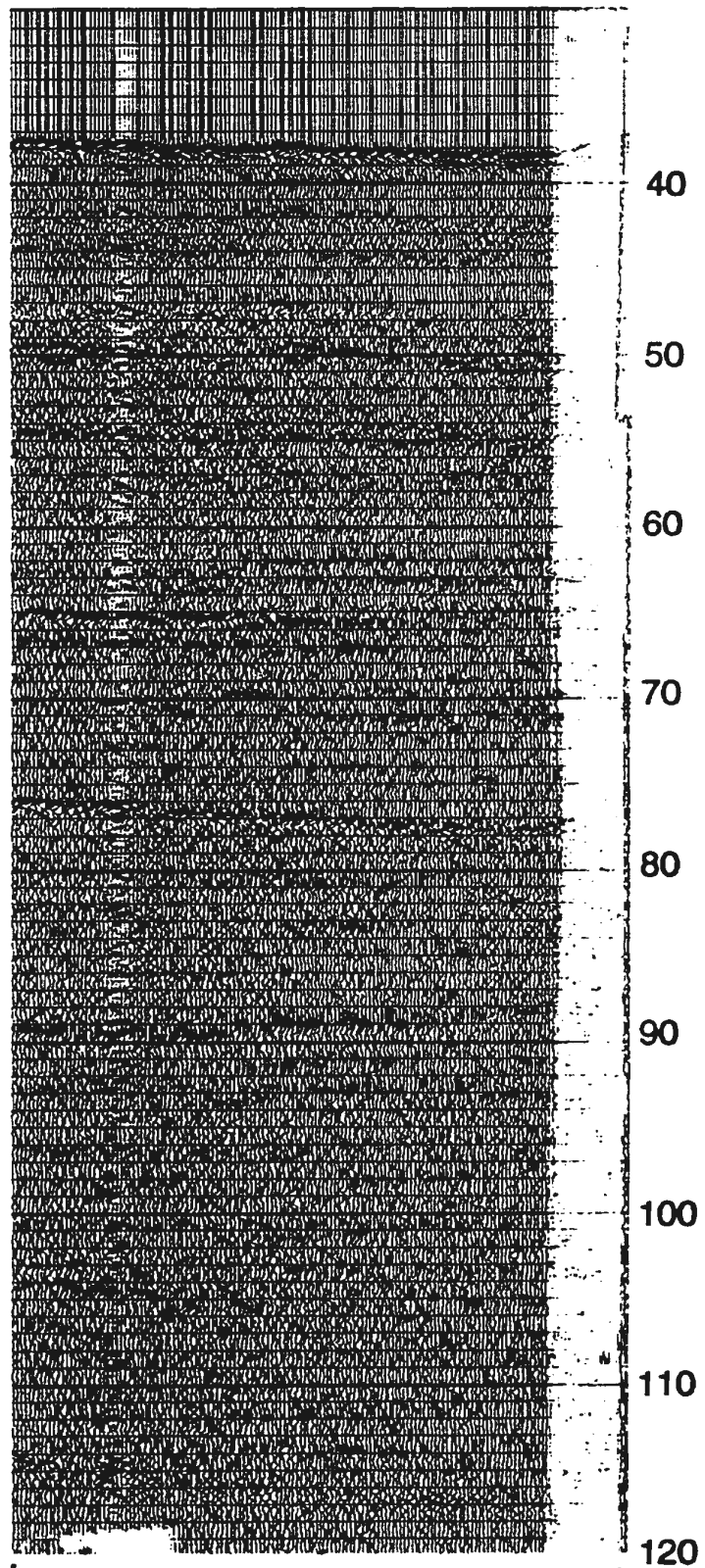


sp. 800

sp. 1000



sp. 1500



sp. 1650

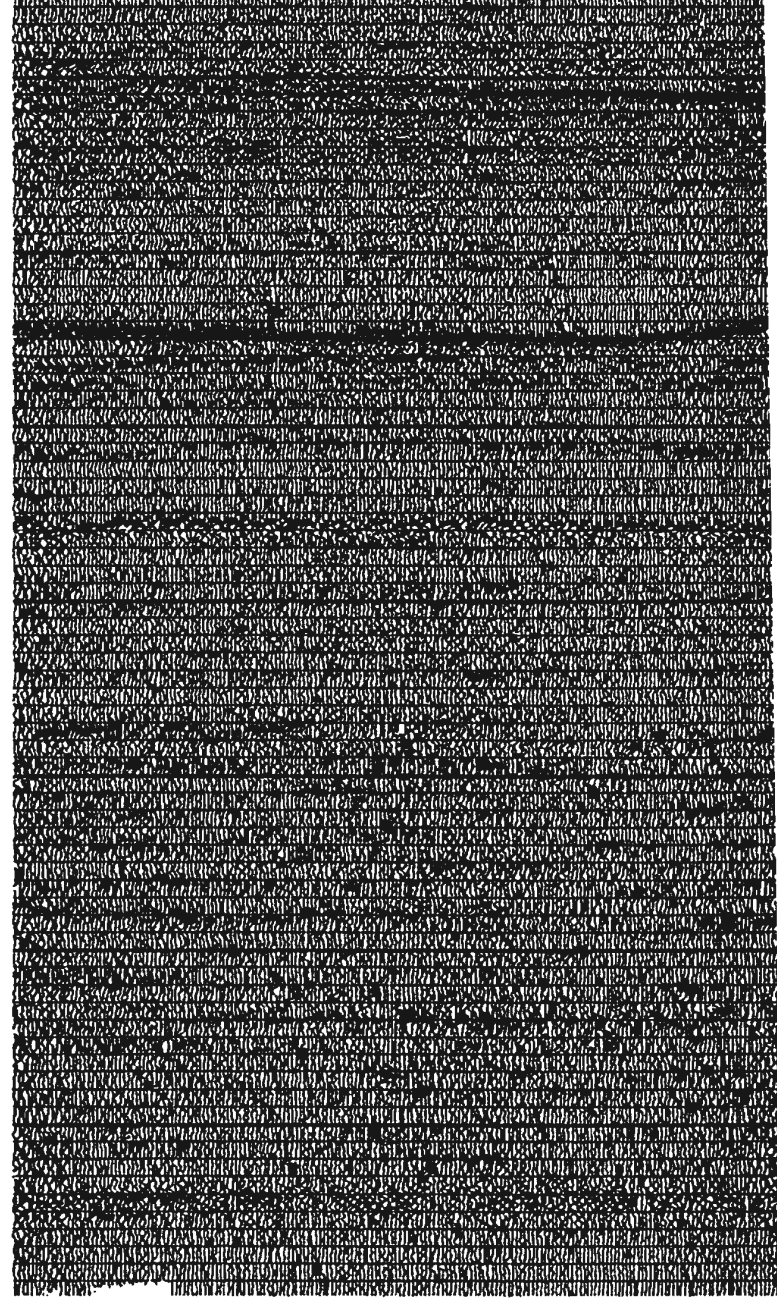
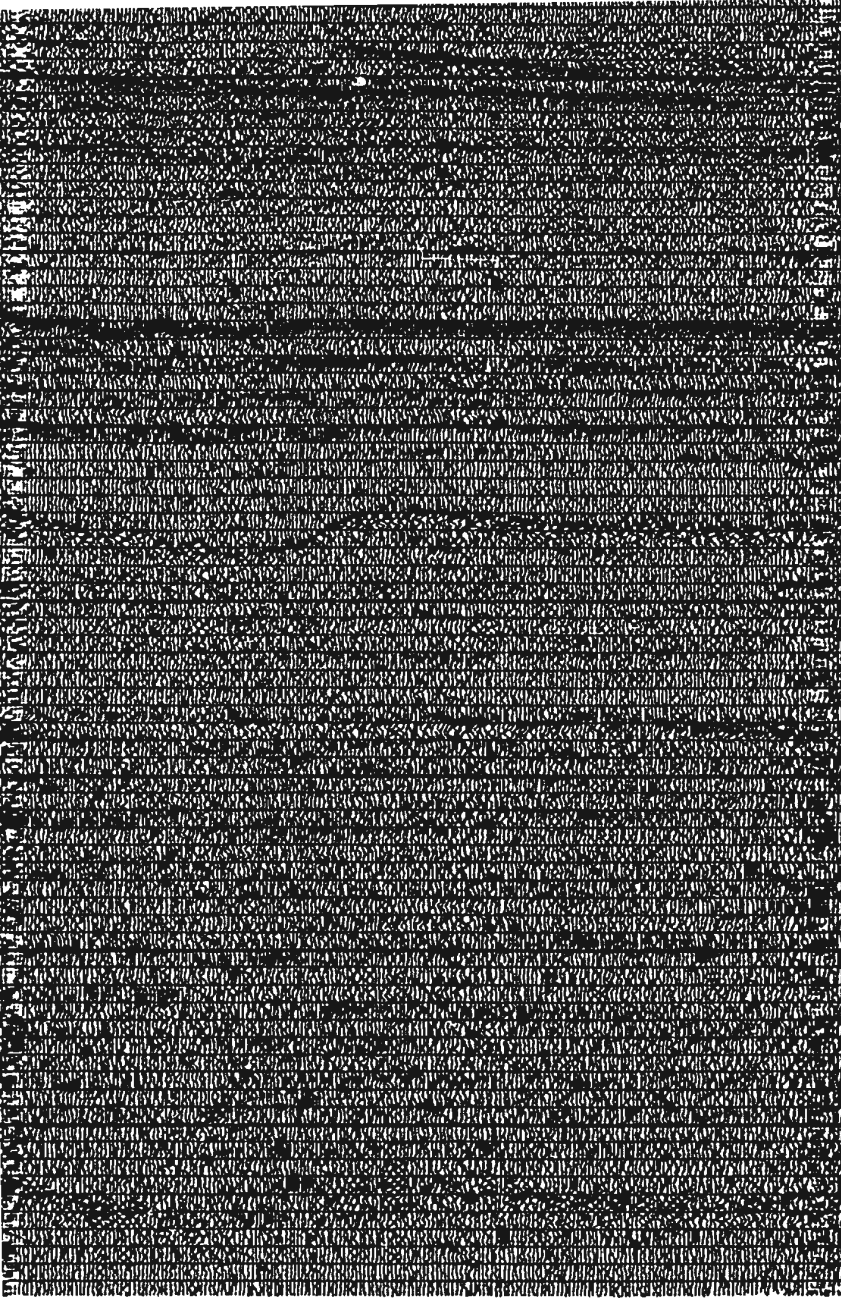
Two Way Travel Time (ms)

3

sp. 30

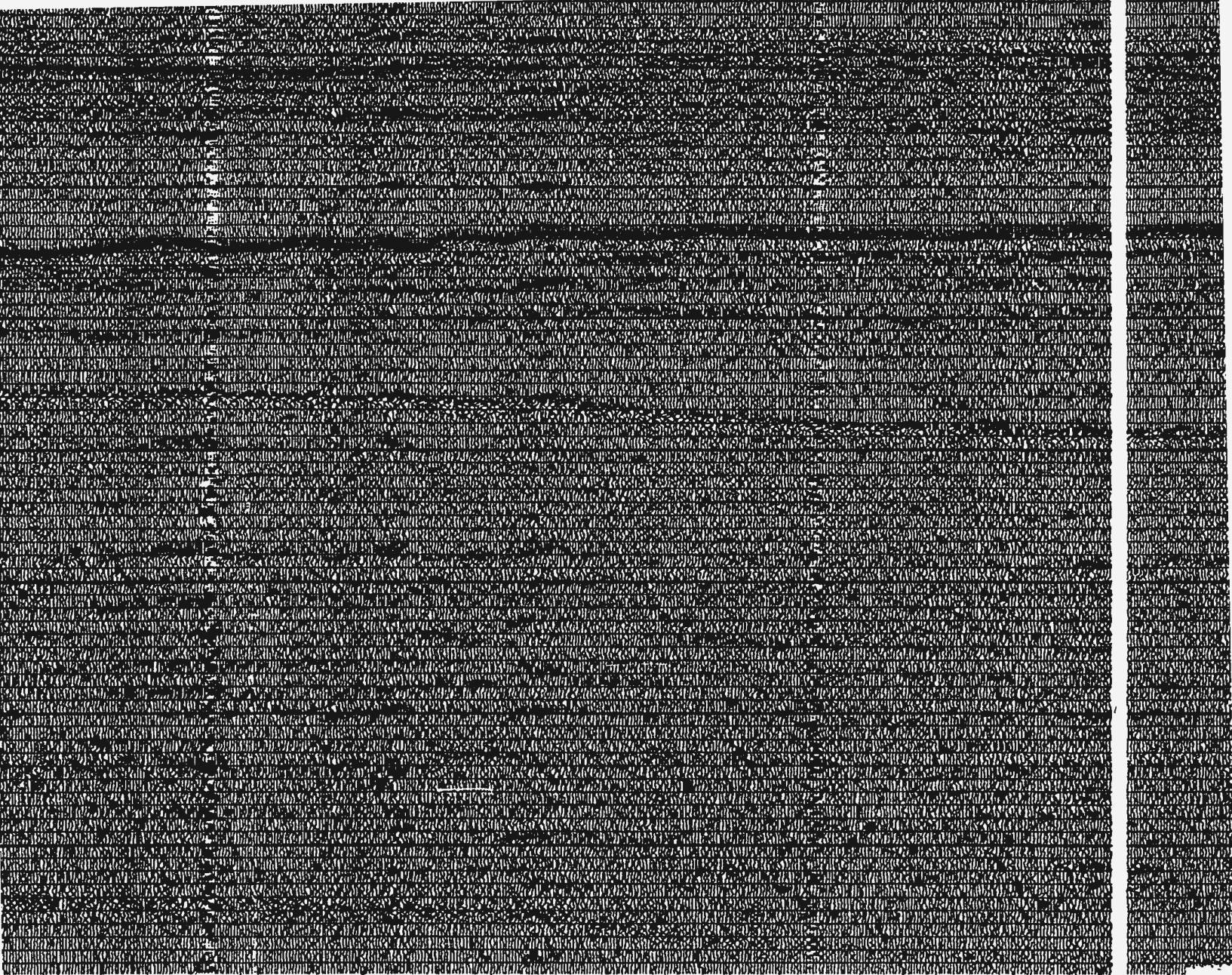
wp. 13

pan2:



sp. 500





sp. 800

sp. 1000

Cross Tie
Profile 20-21
@ sp. 2060



1000 metres

1000

1000

sp. 1270

Cross Tie
Profile 20-21
@ sp. 700

1000

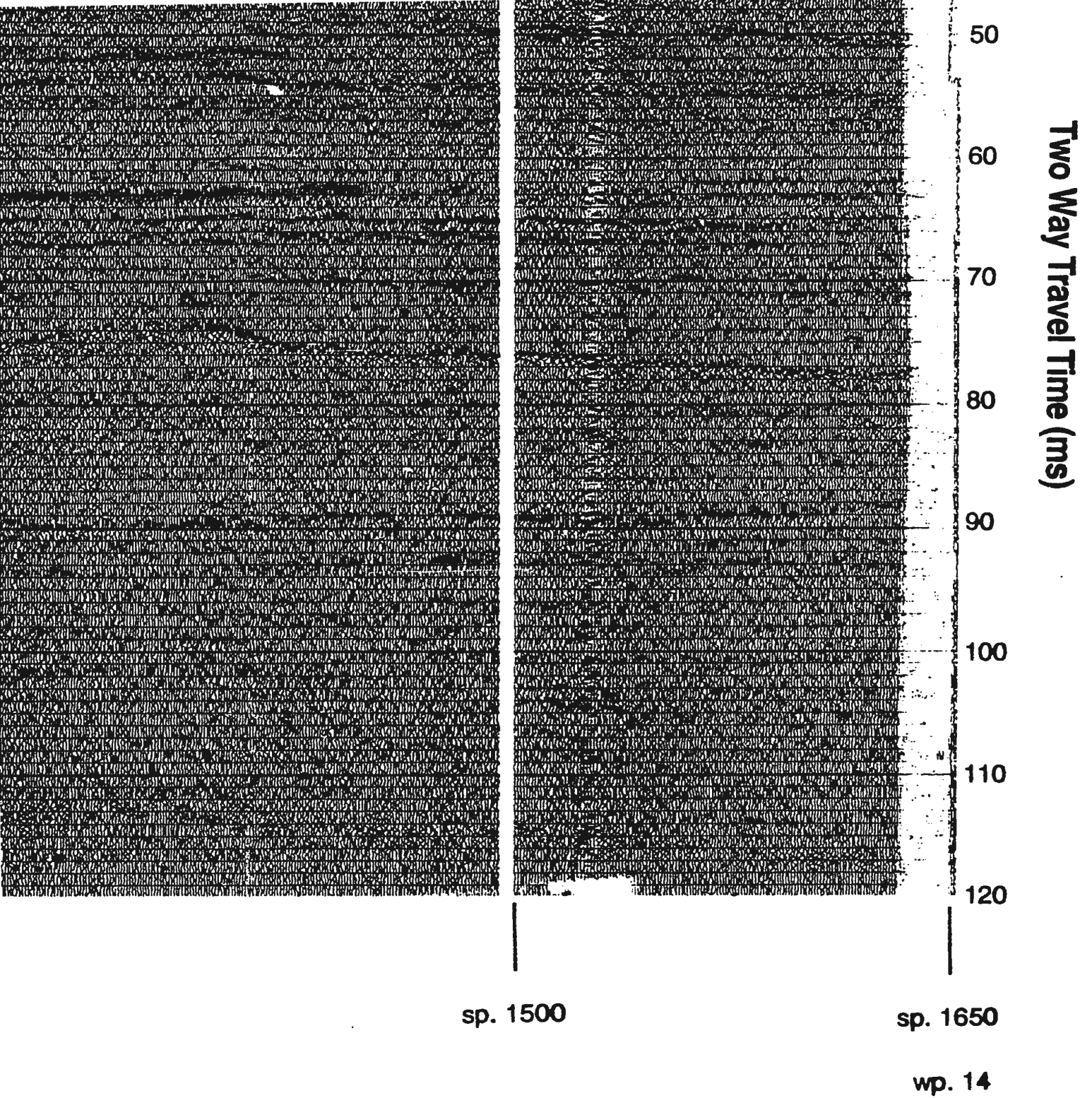
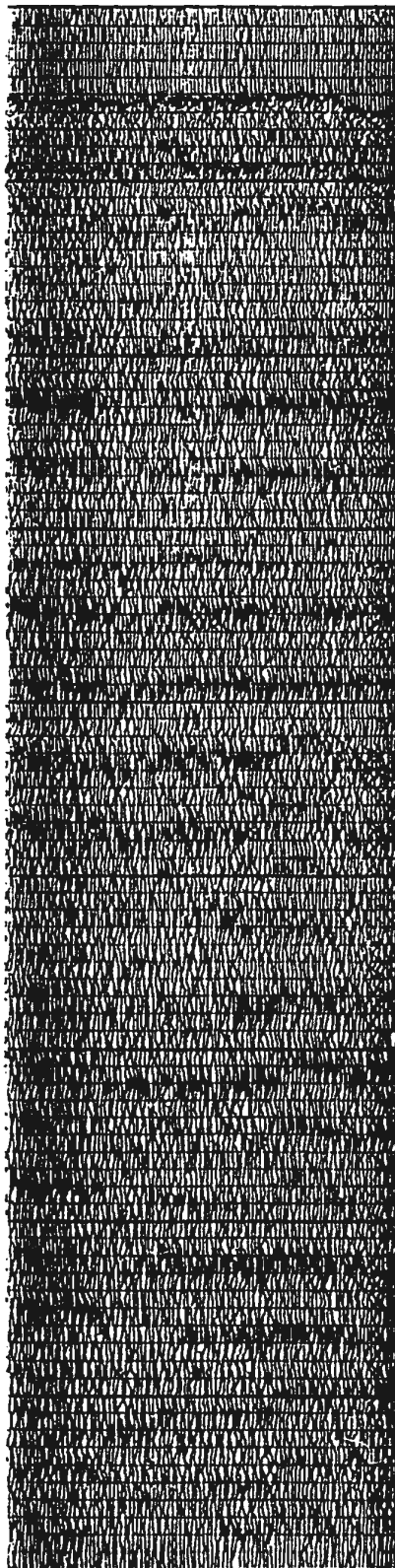
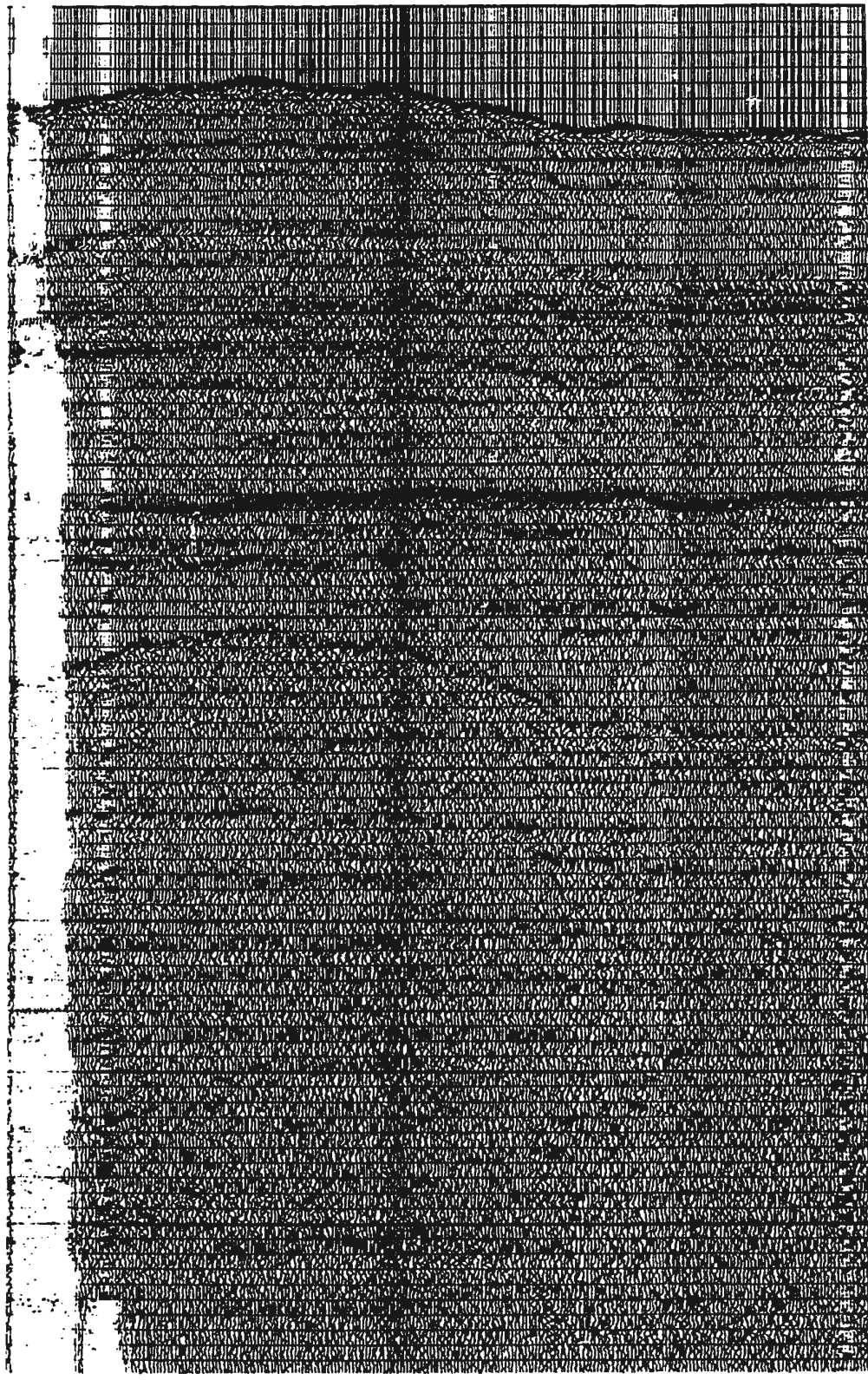


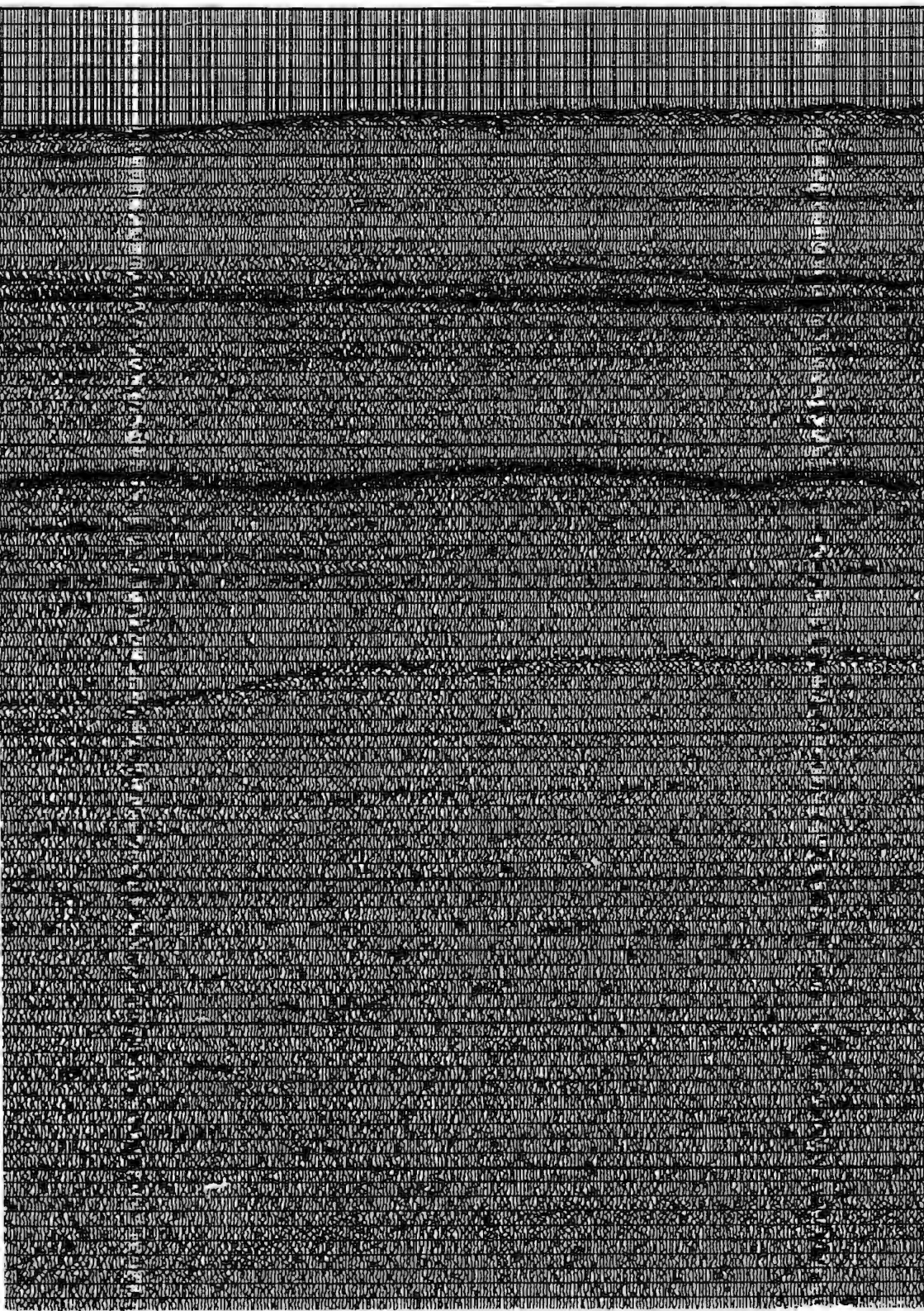
Figure 4.14 Processed Seismic Profile 13-14



sp. 1599



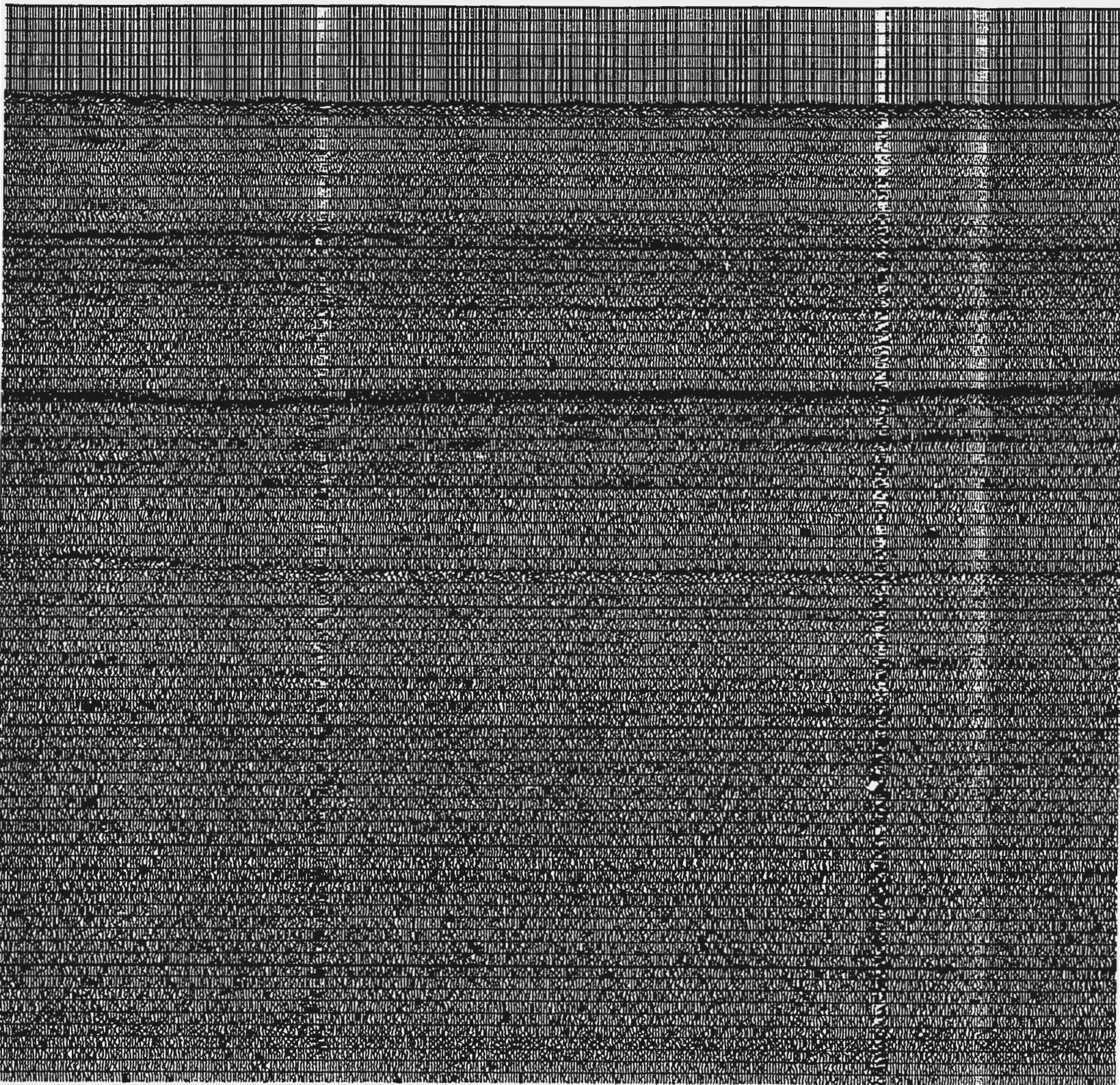
sp. 1500



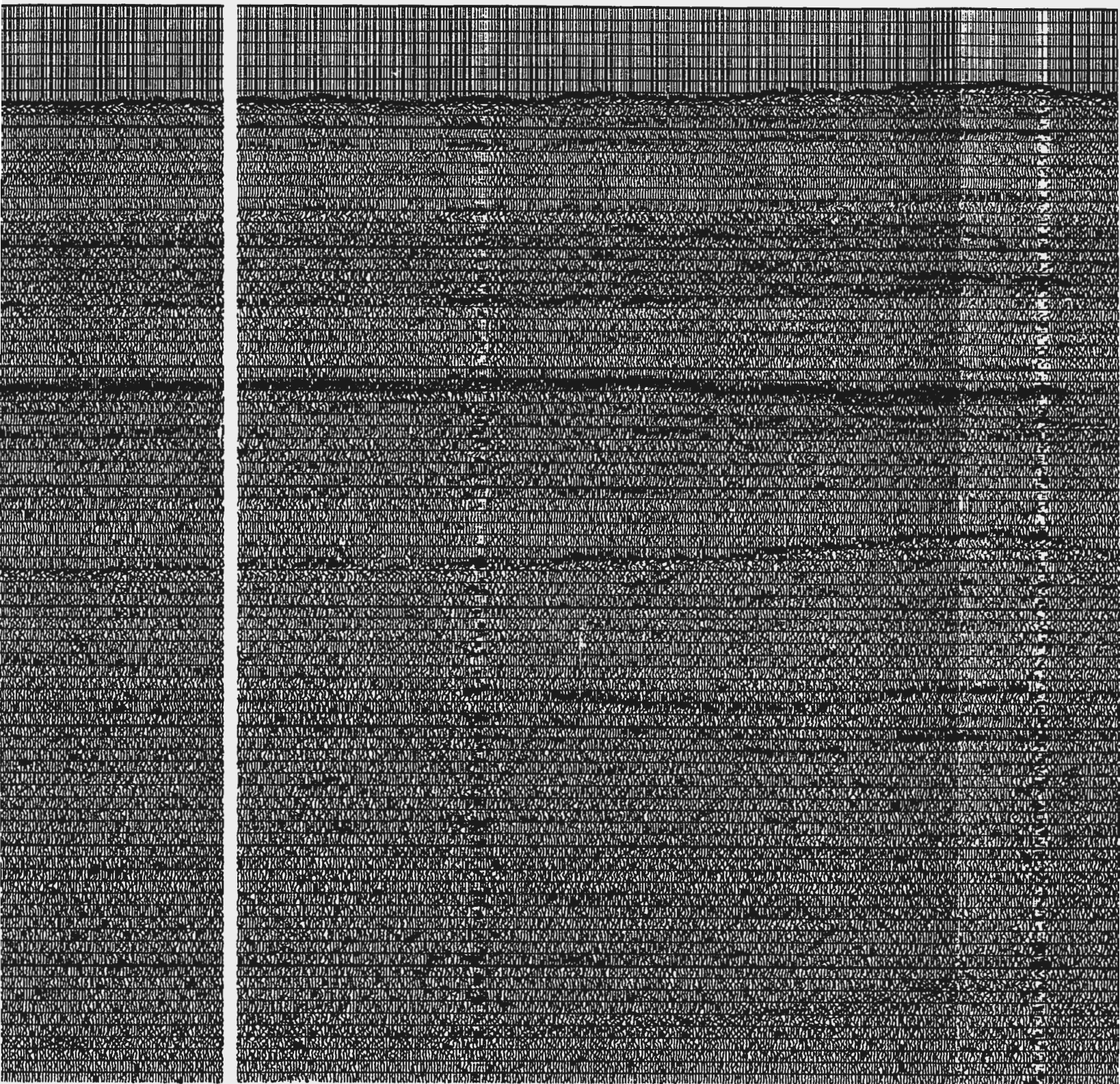
sp. 1000

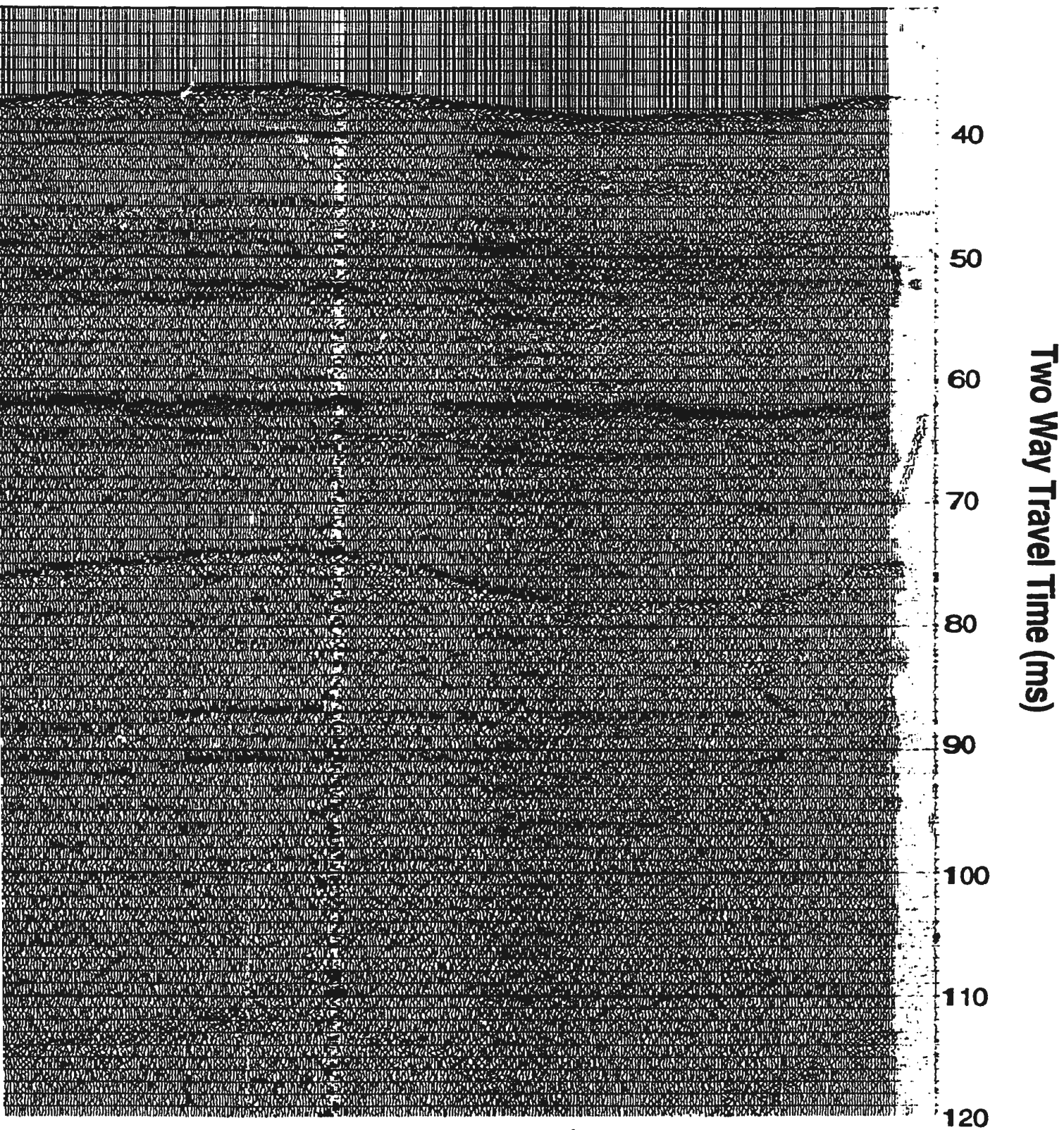


sp. 900

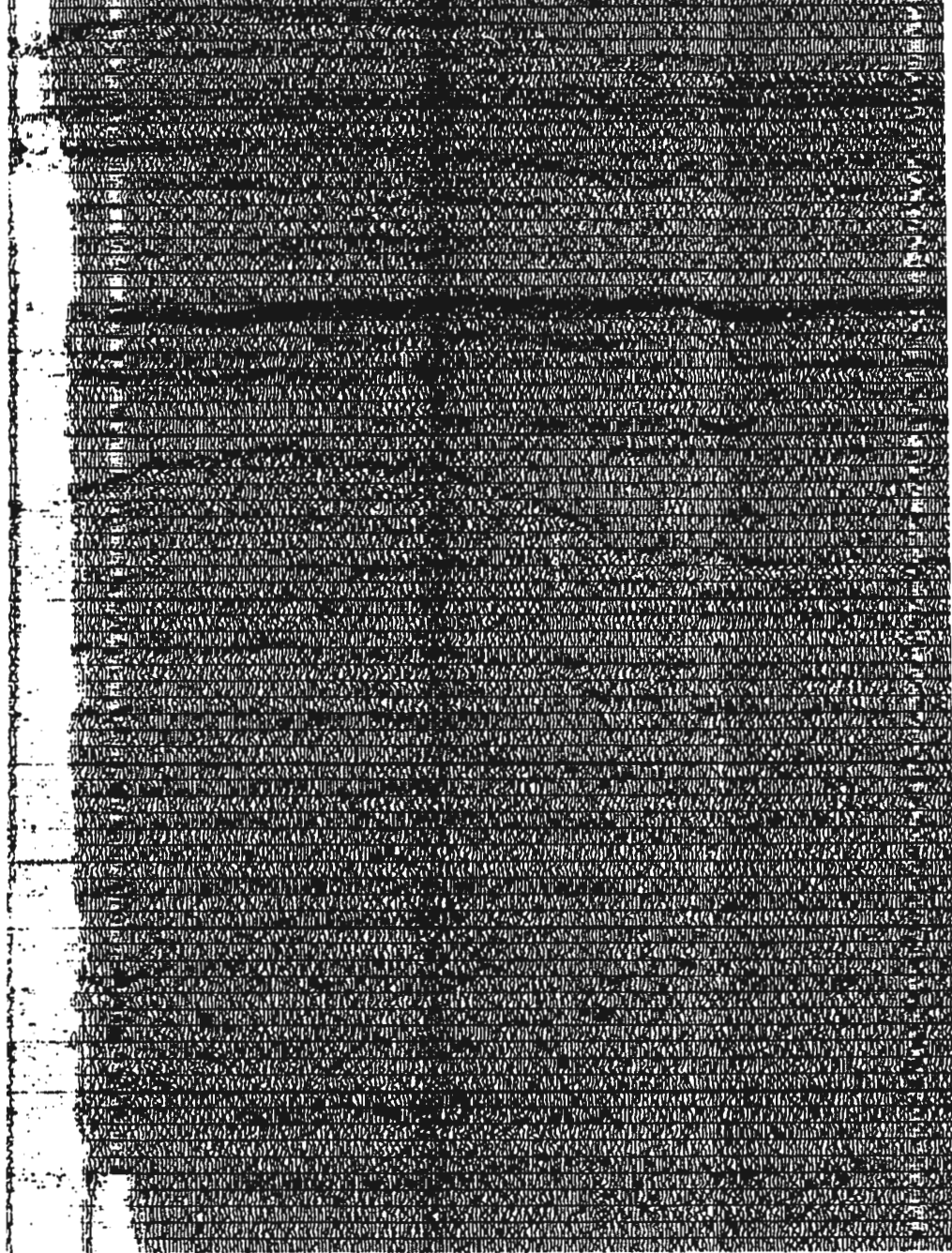
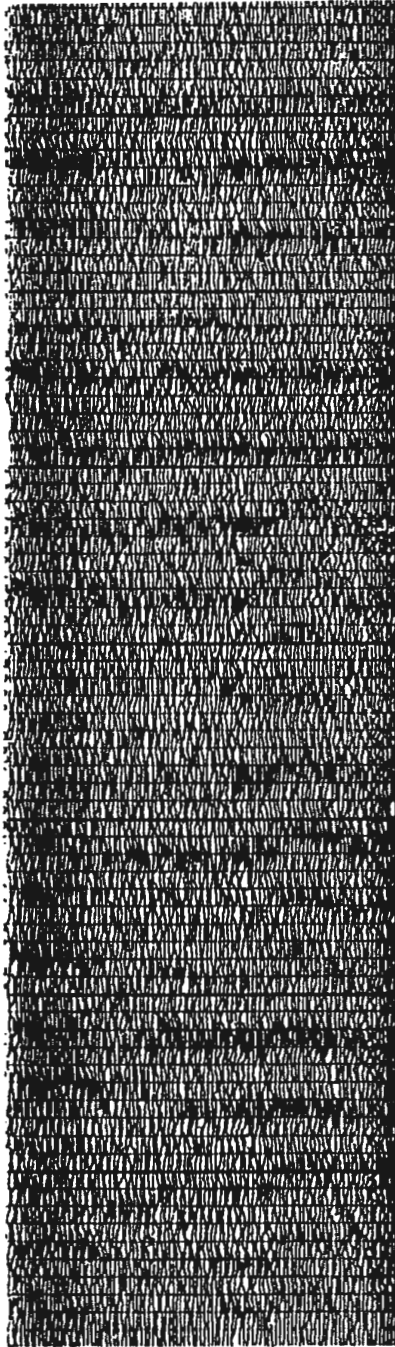


sp. 900





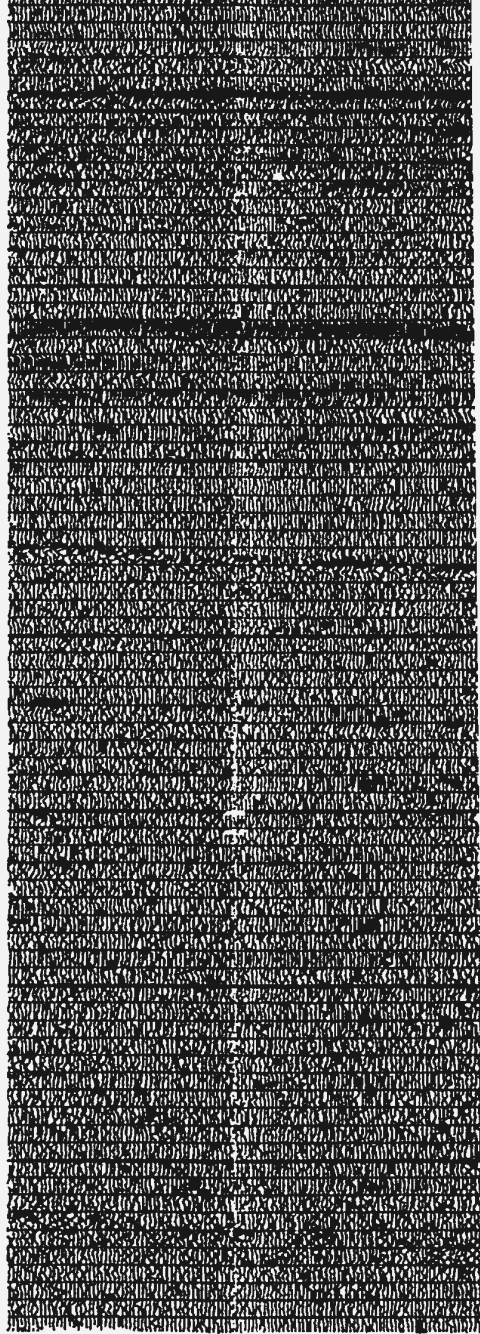
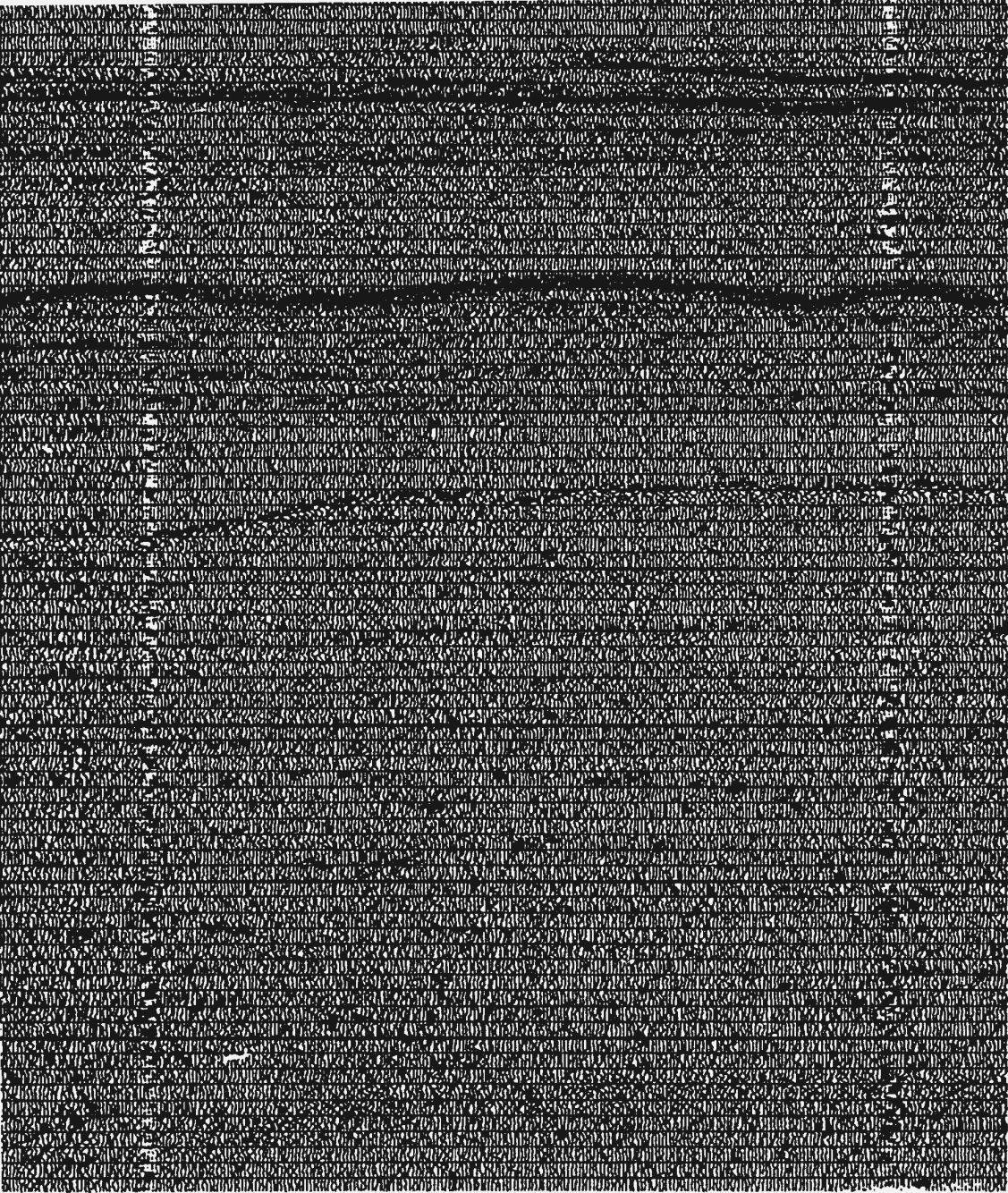
sp. 125



sp. 1599

sp. 1500

wp. 4



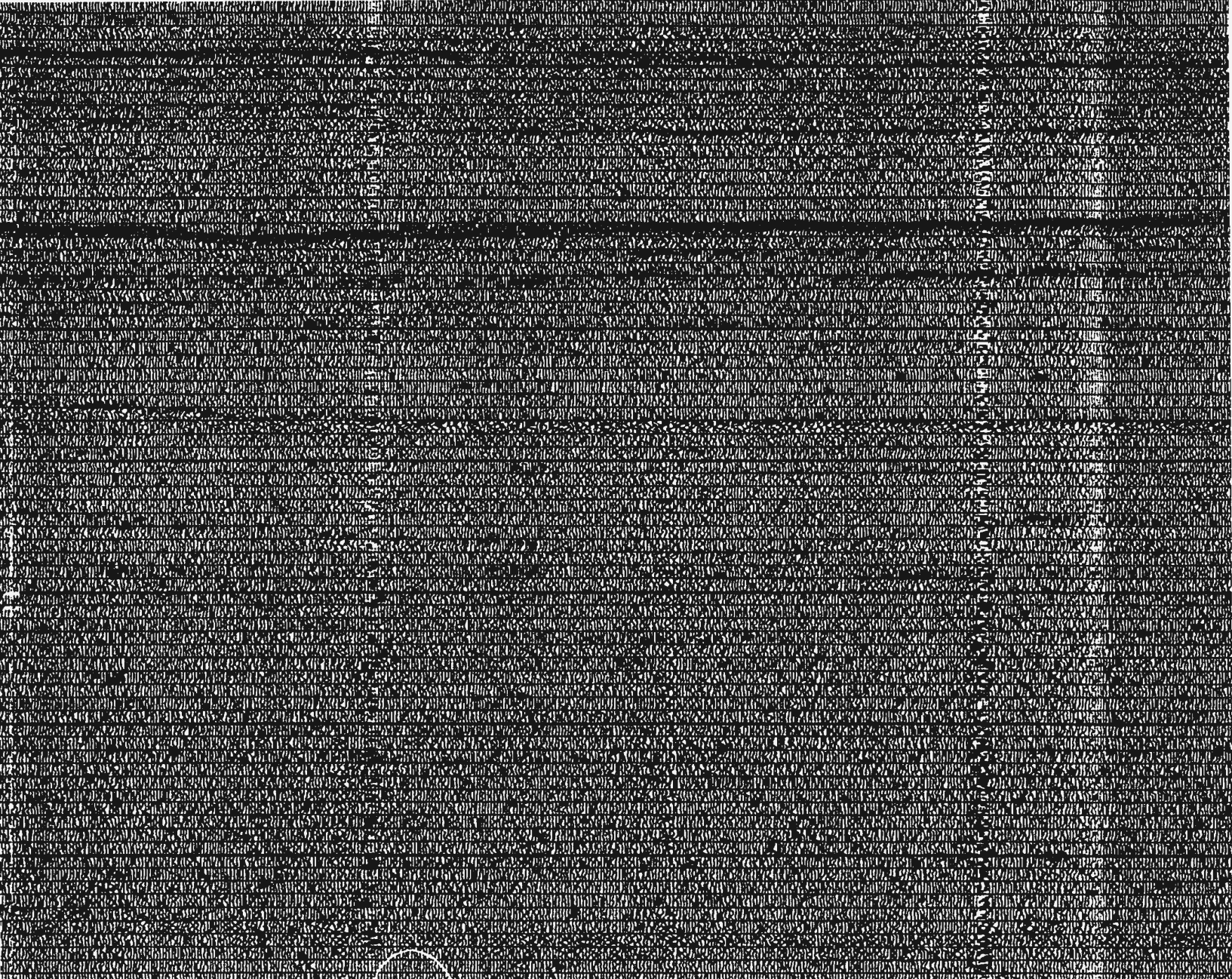
sp. 1000

sp. 900

Cross Tie
Profile 20-
@ sp. 230



1000



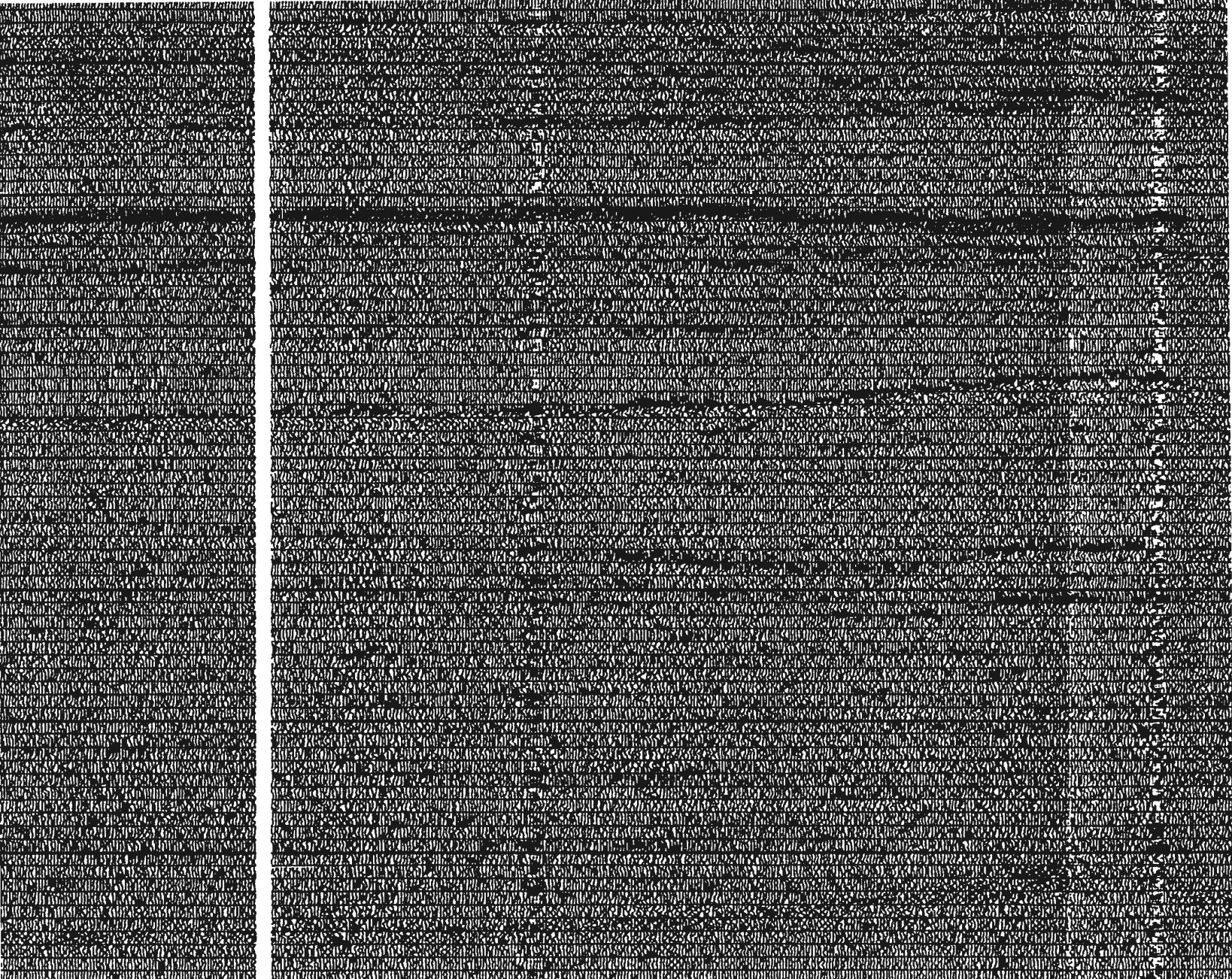
sp. 900

Cross Tie
Profile 20-21
@ sp. 2300



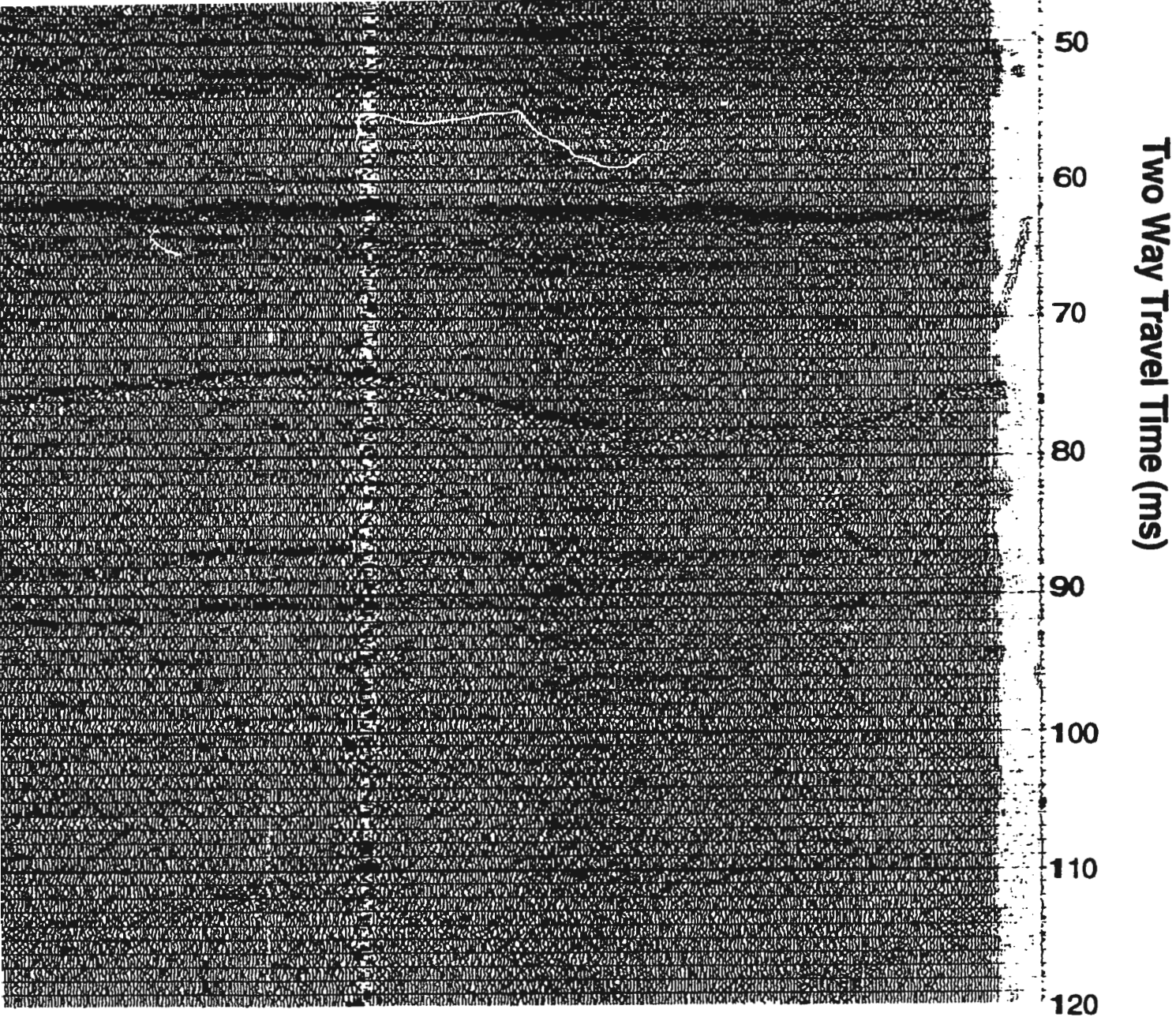
1000 metres





sp. 510

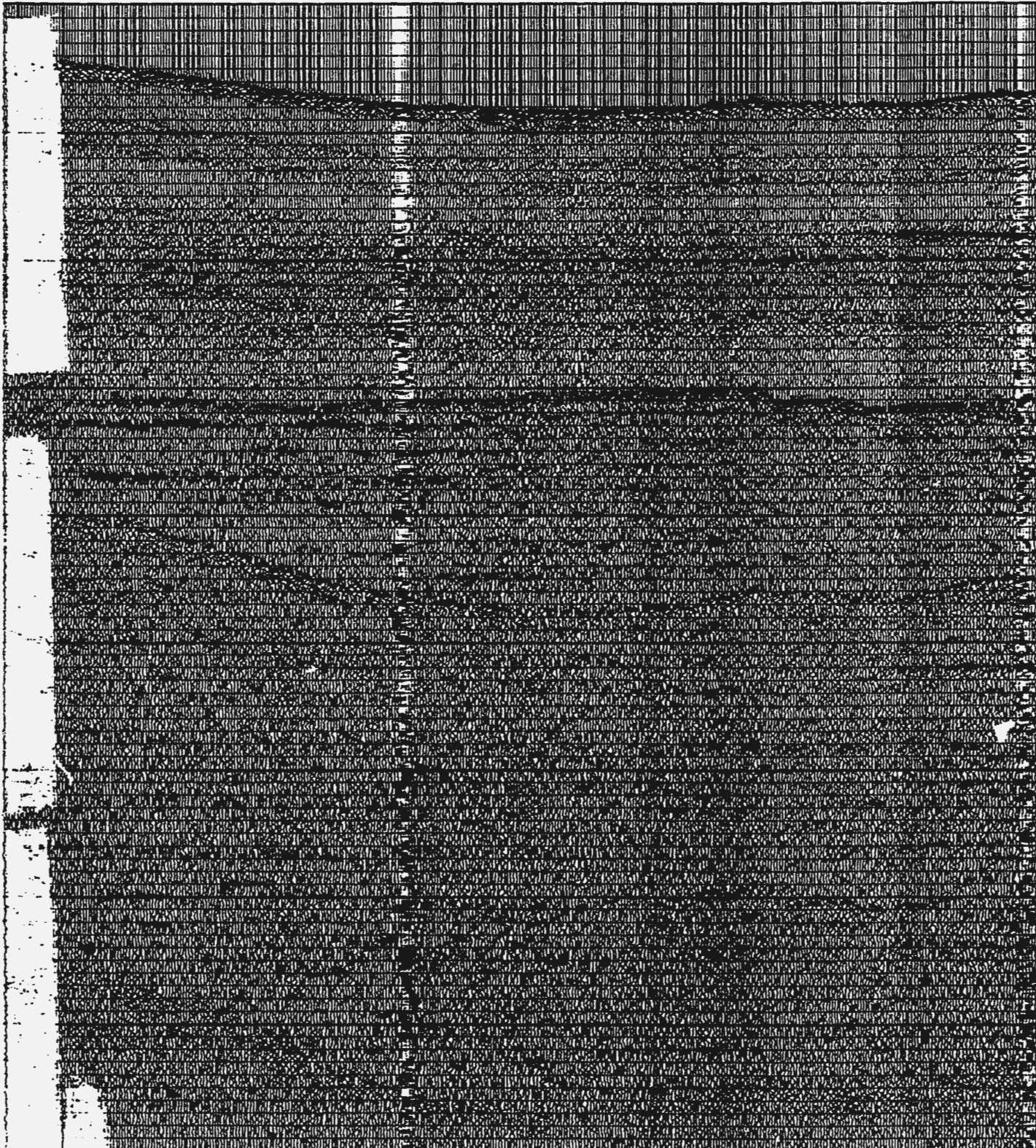
Cross Tie
Profile 20-21
@ sp. 550

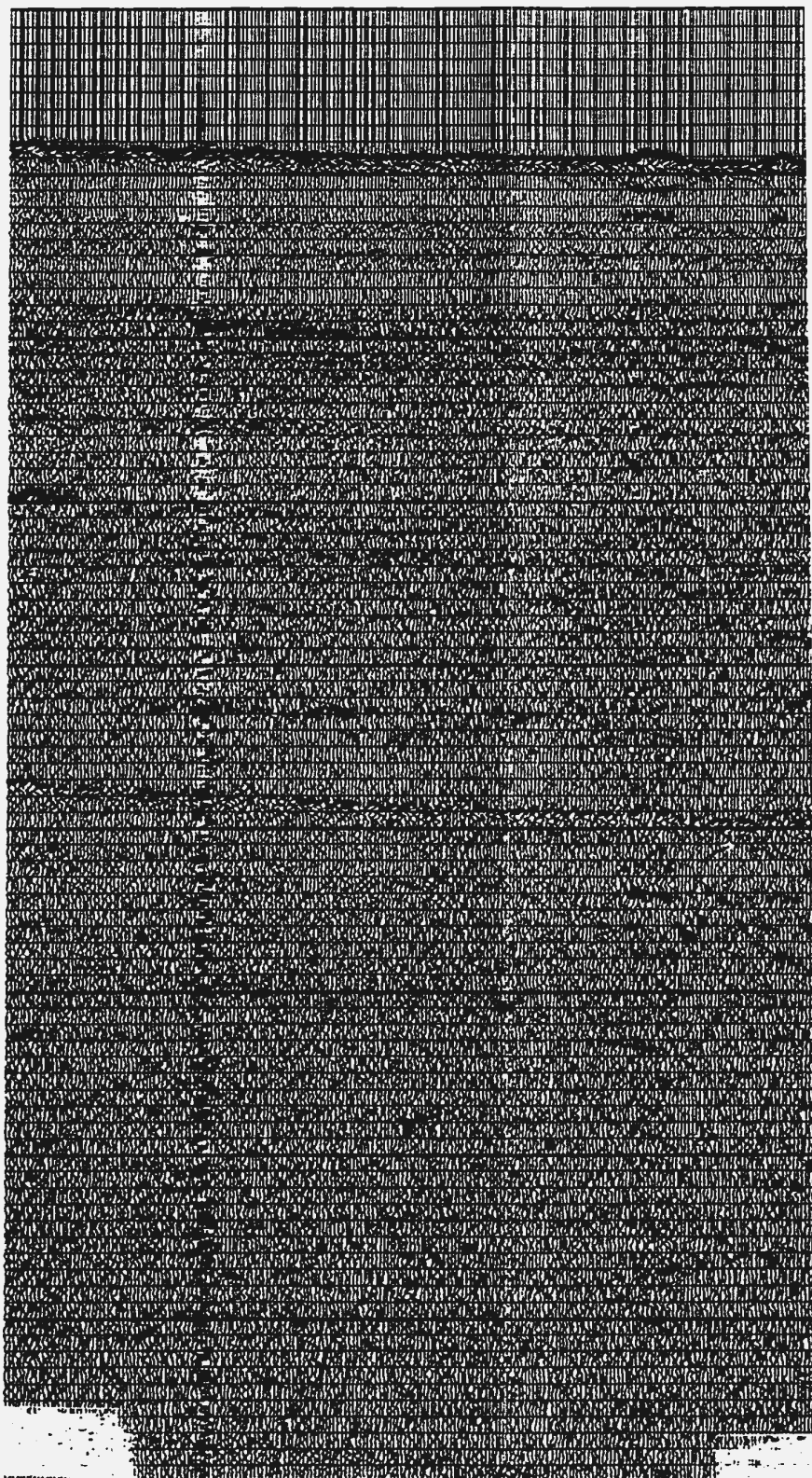
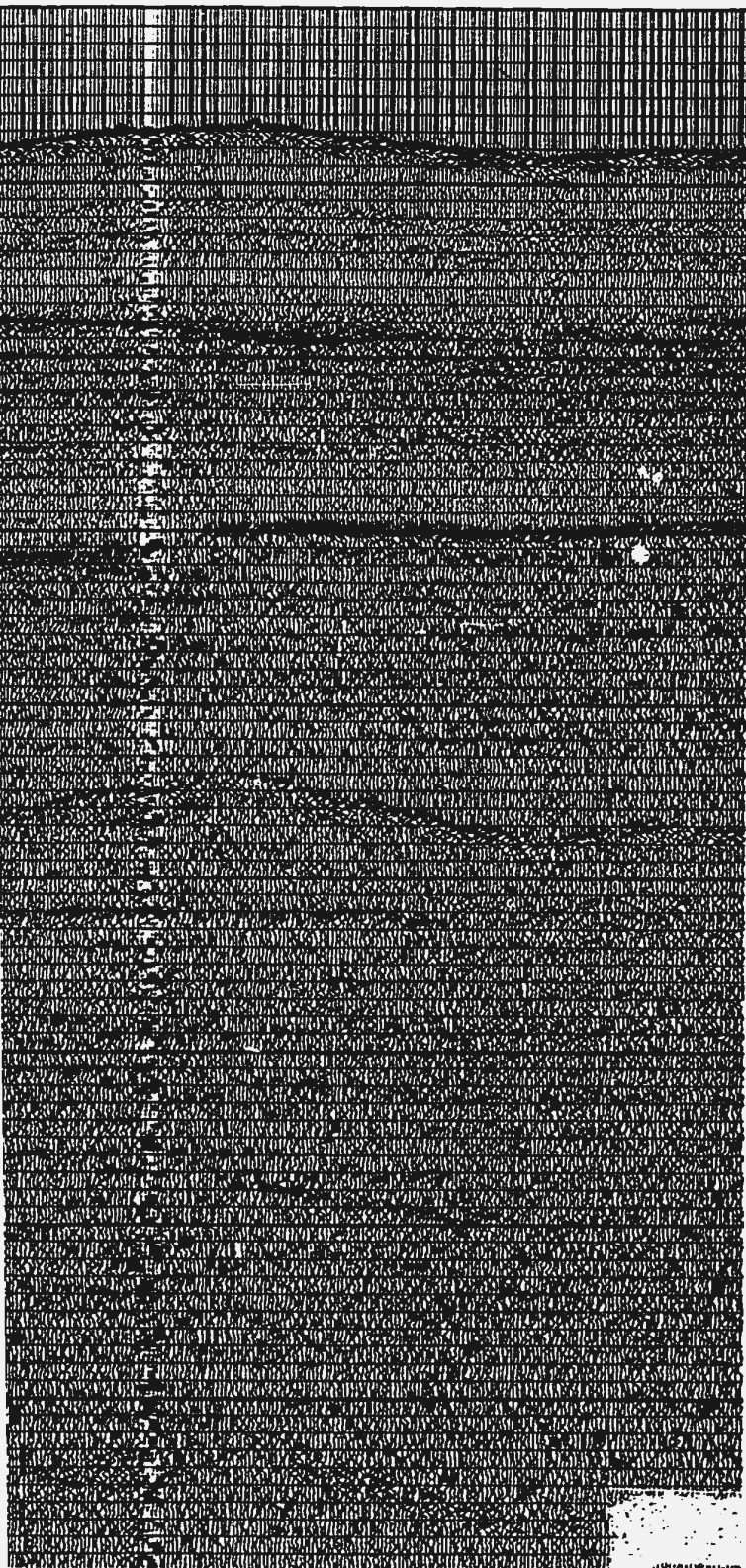


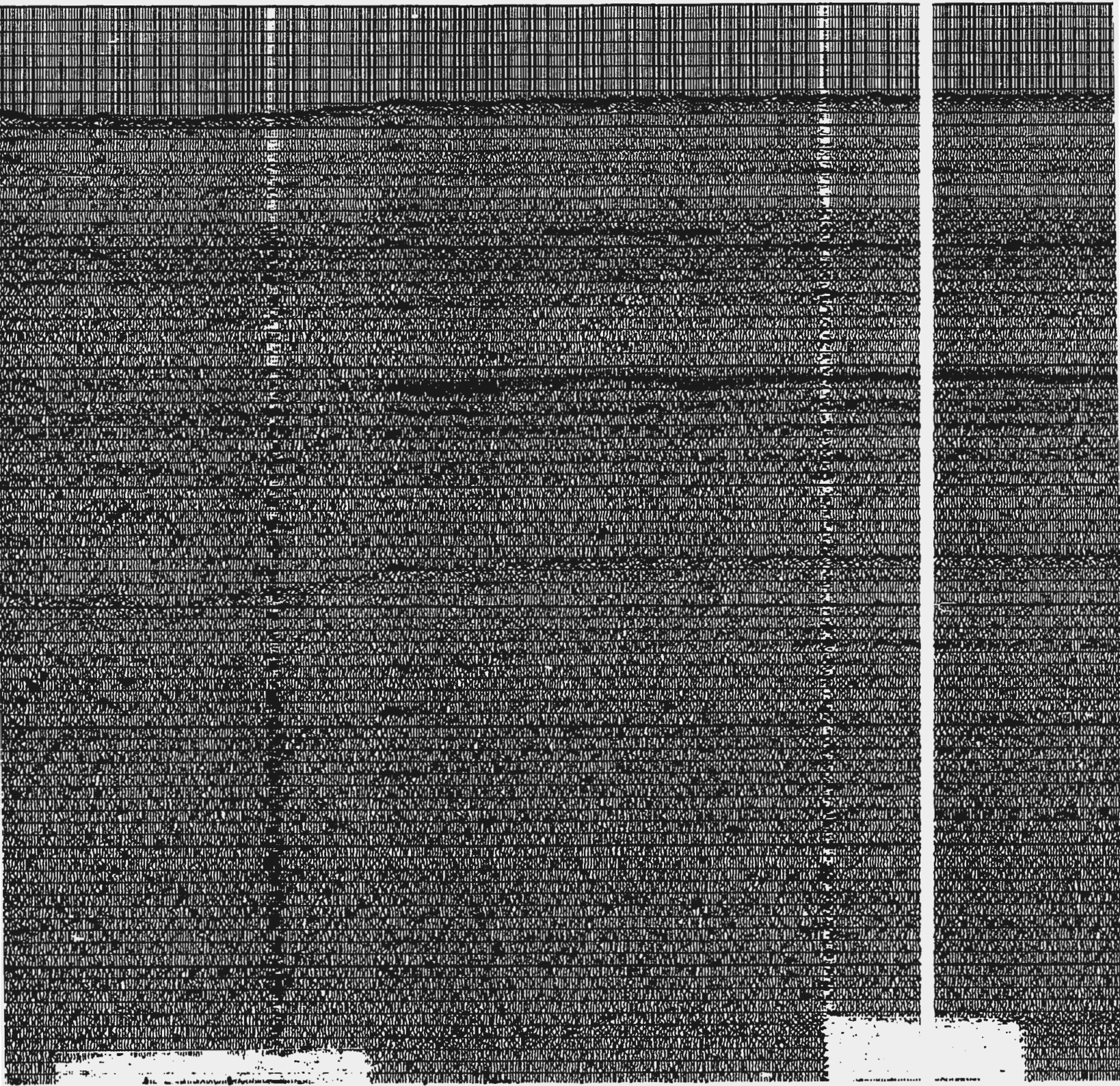
sp. 125

wp. 3

Figure 4.15 Processed Seismic Profile 4-3

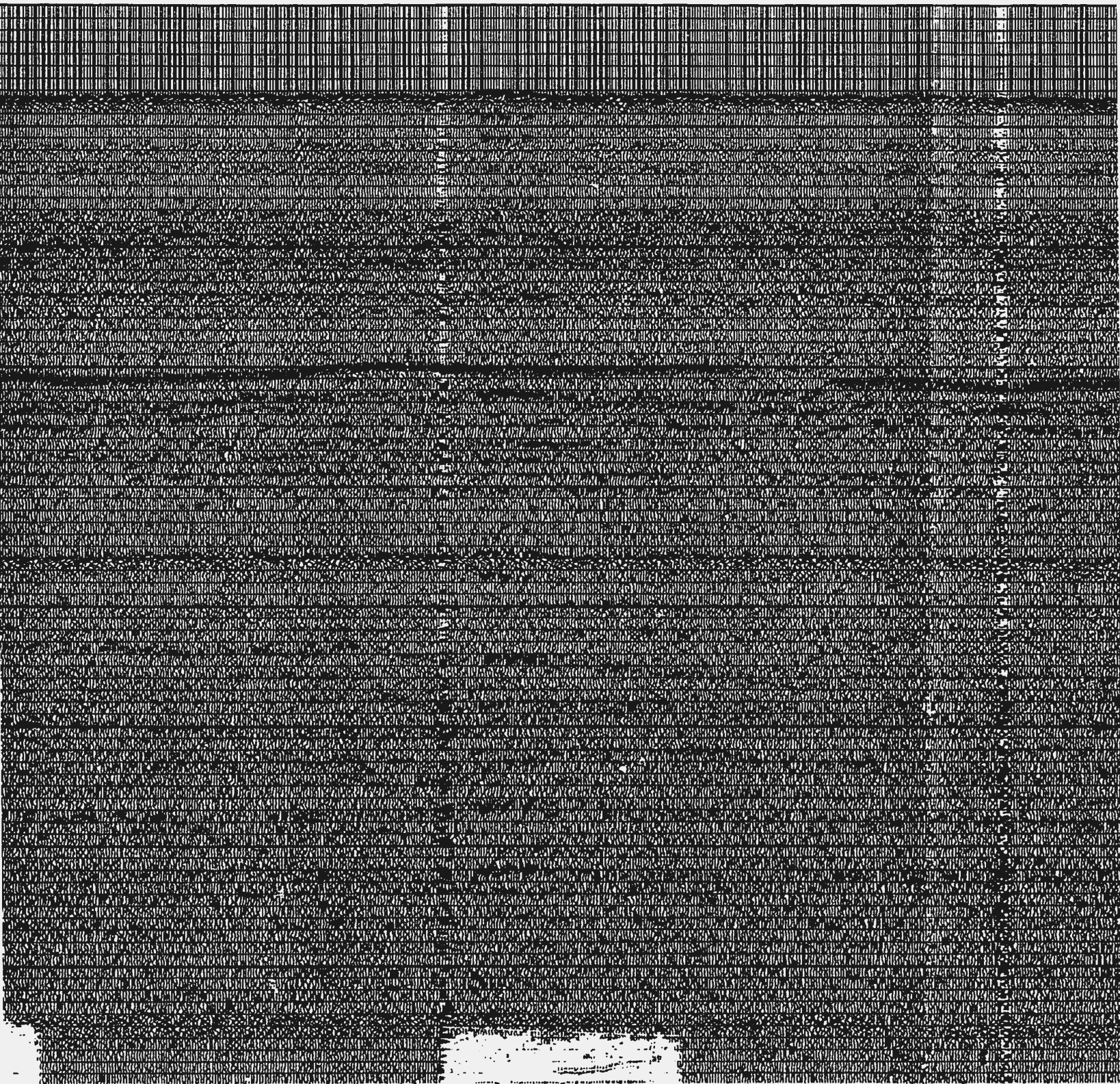


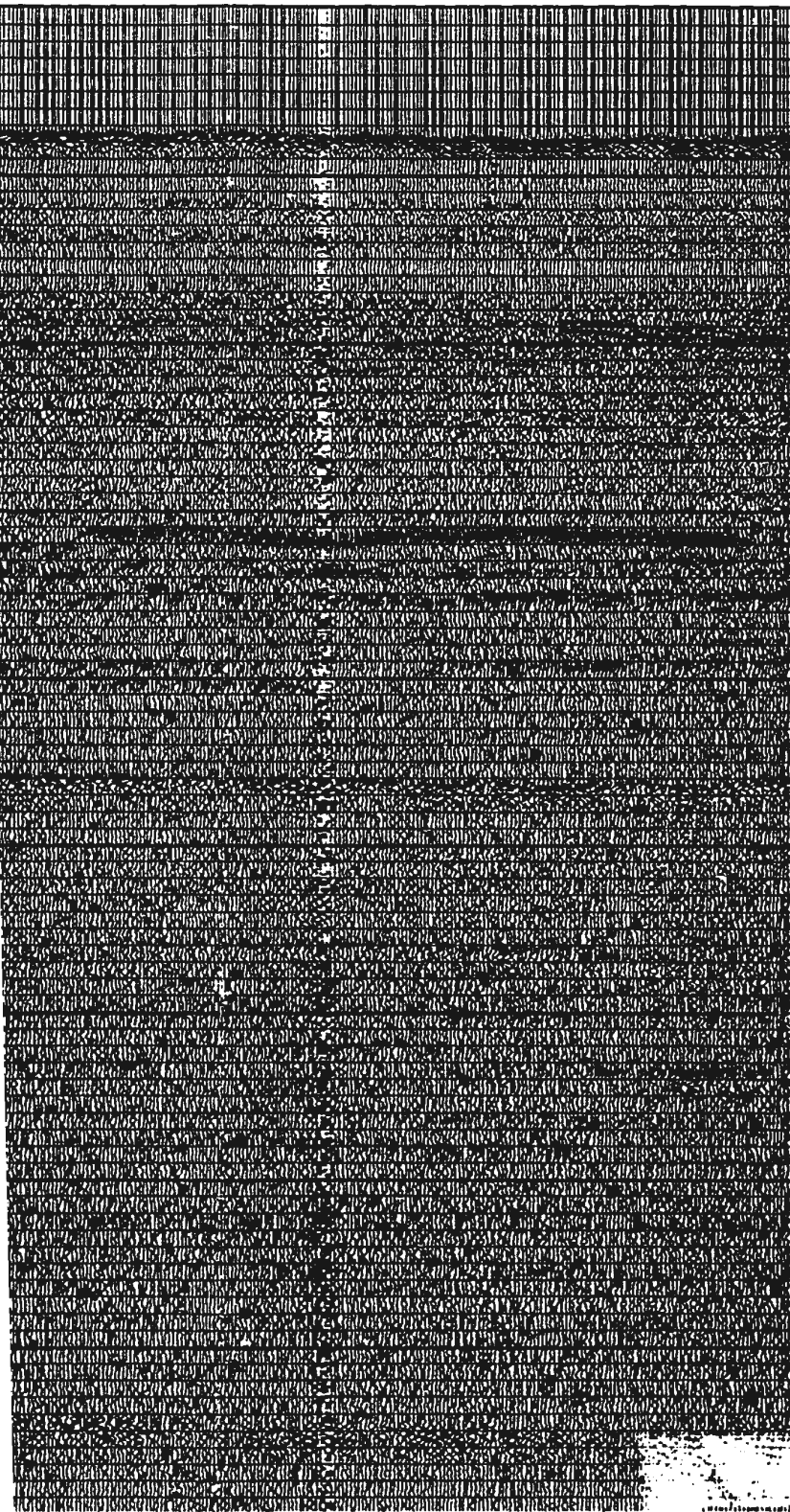




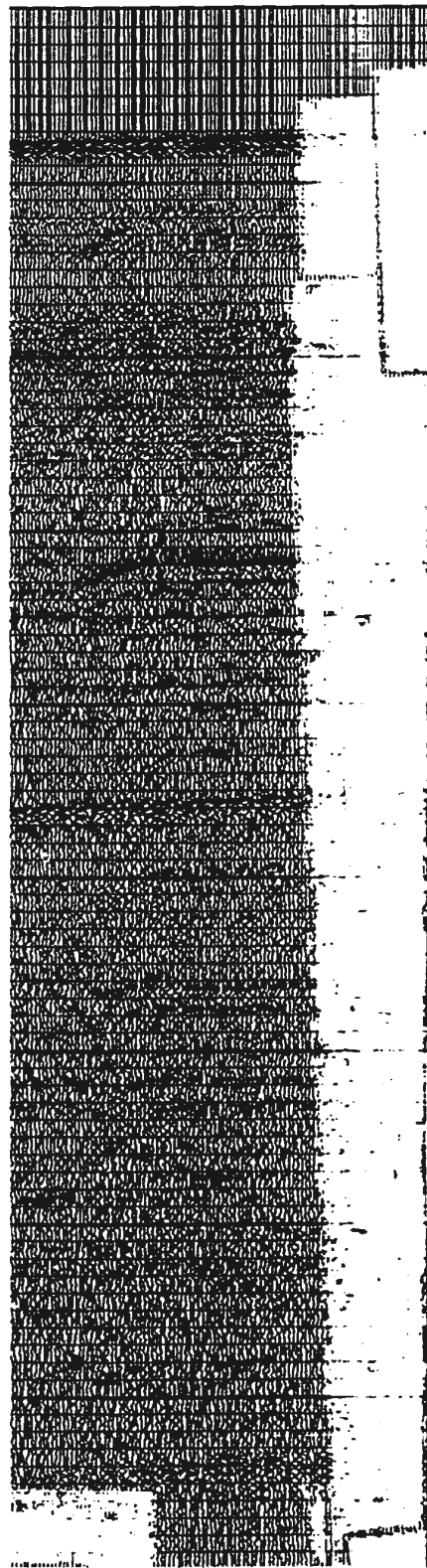
sp. 750

sp. 1000





sp. 1500



sp. 1600

40

50

60

70

80

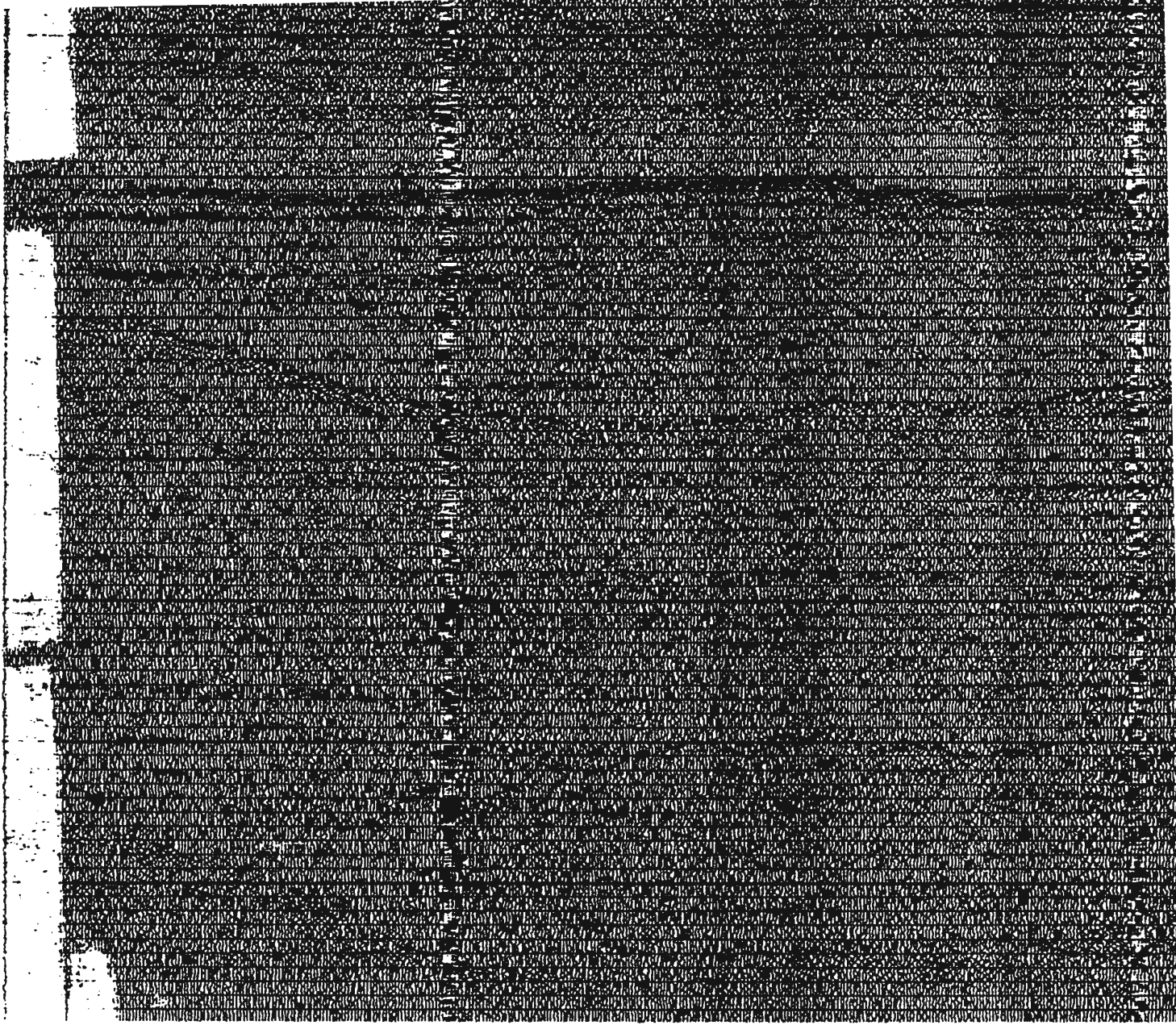
90

100

110

120

Two Way Travel Time (ms)



sp. 1

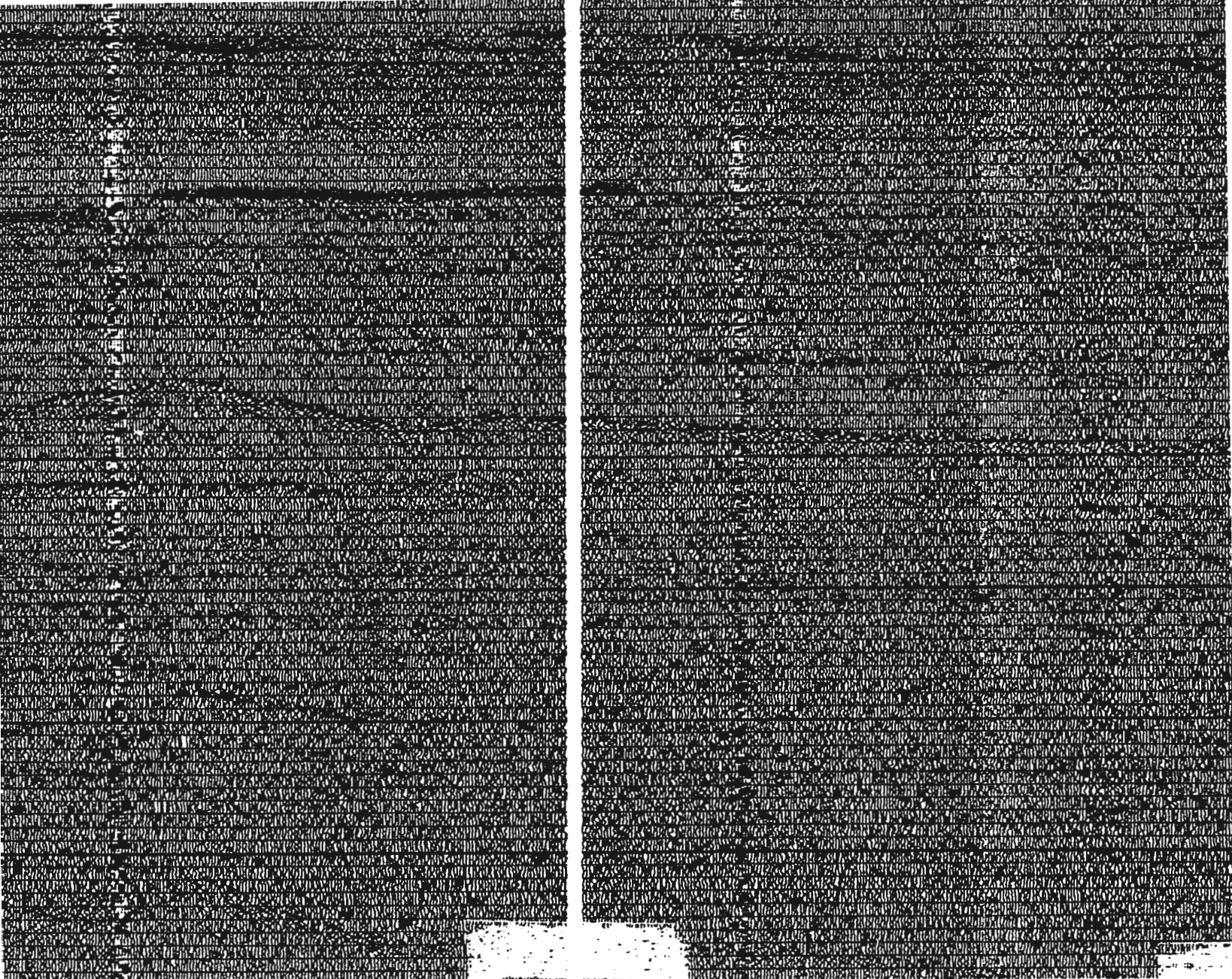
wp. 16

13

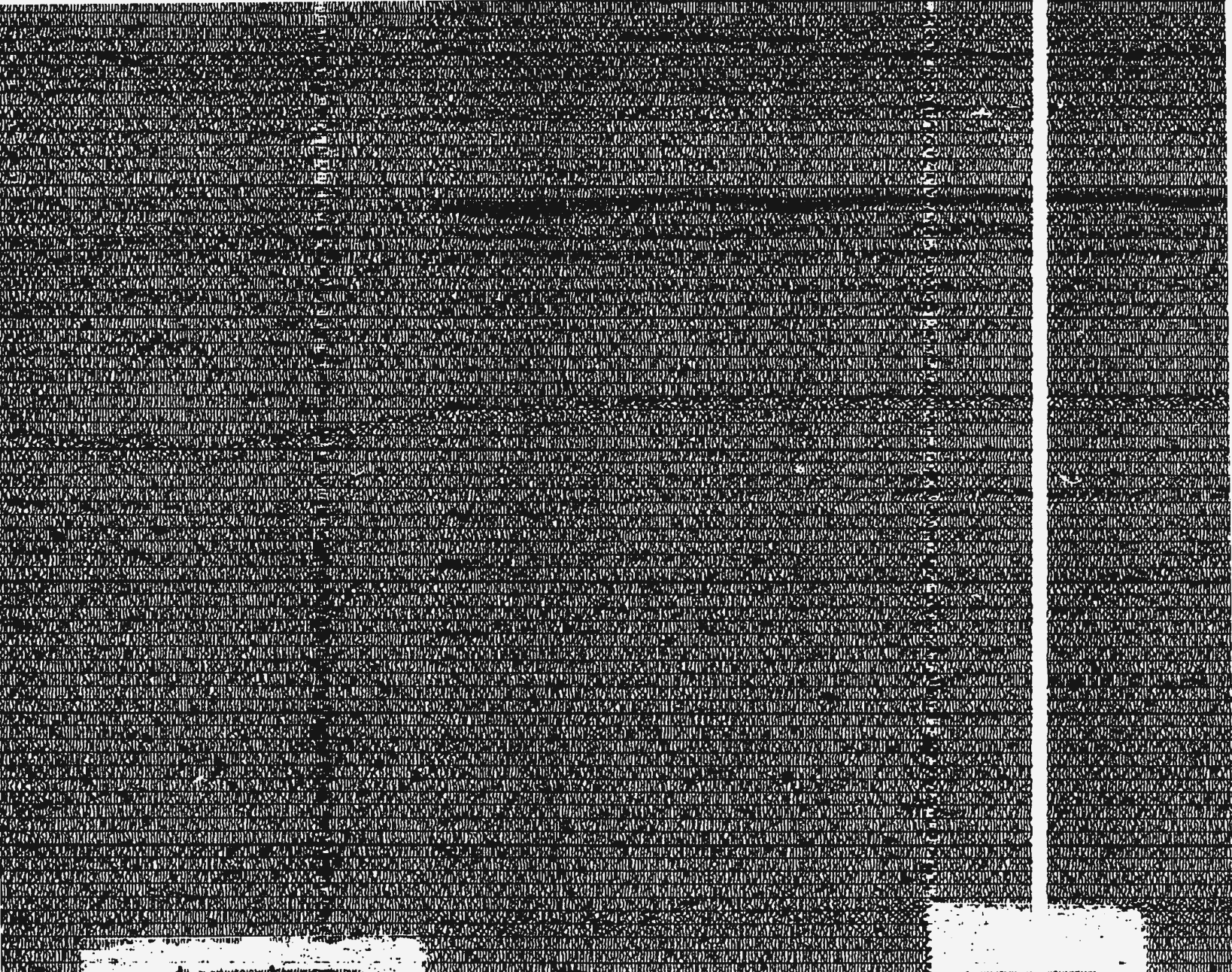
|

|

|



sp. 500



sp. 750

sp. 1000

Cross Tie
Profile 20-21
@ sp. 2590



1000 metres

sp. 1220

Cross Tie
Profile 20-21
@ sp. 330



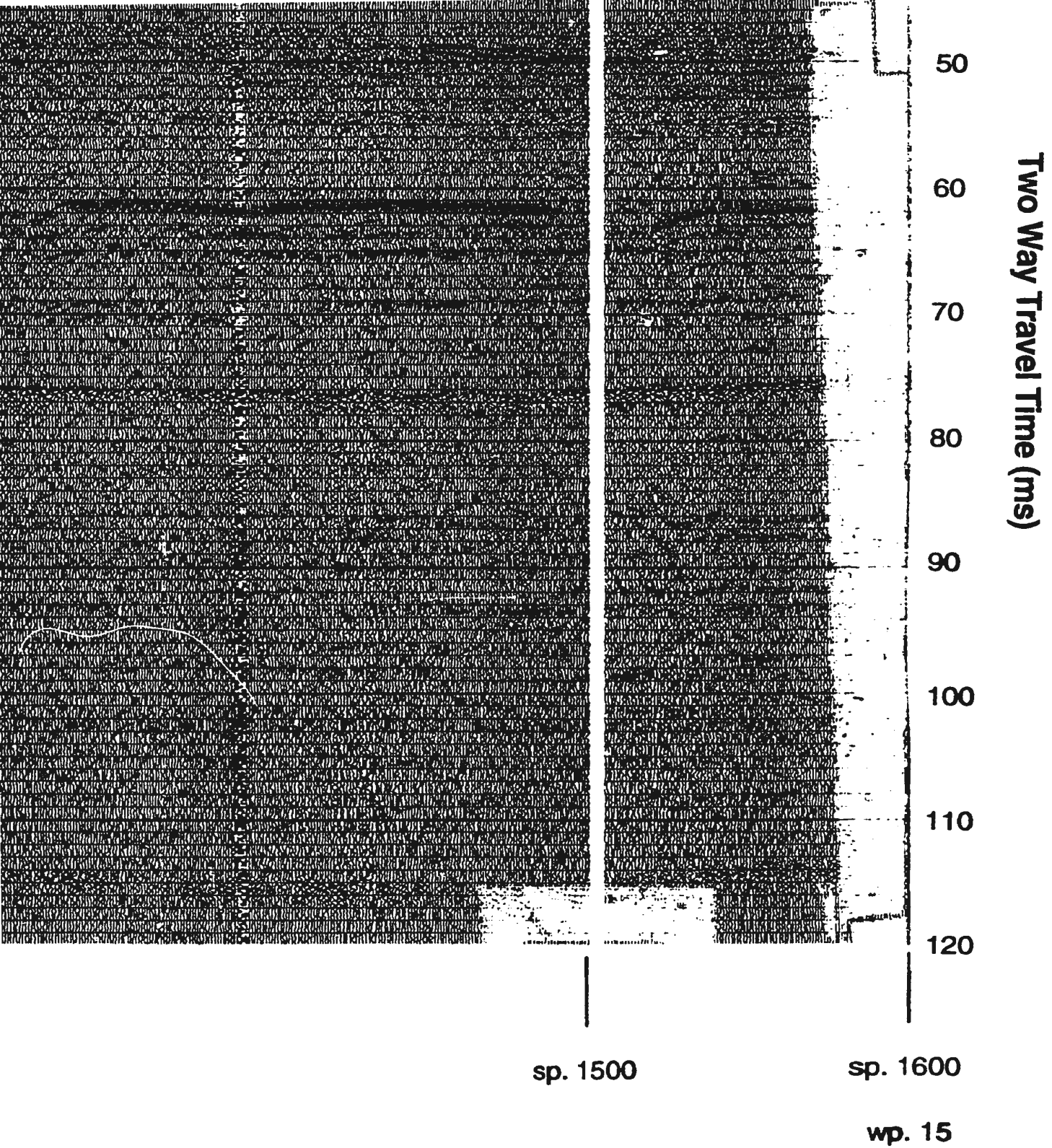
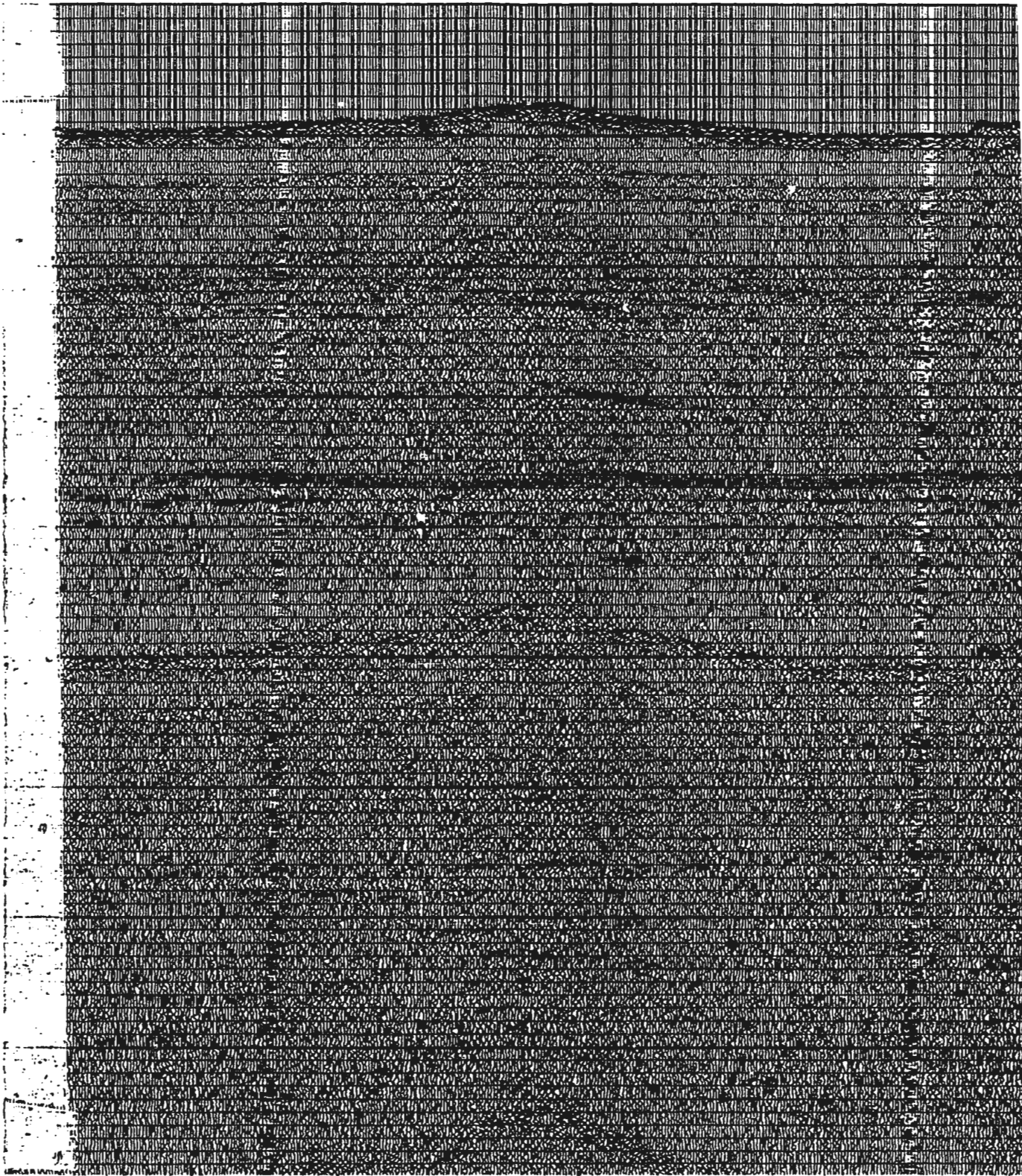
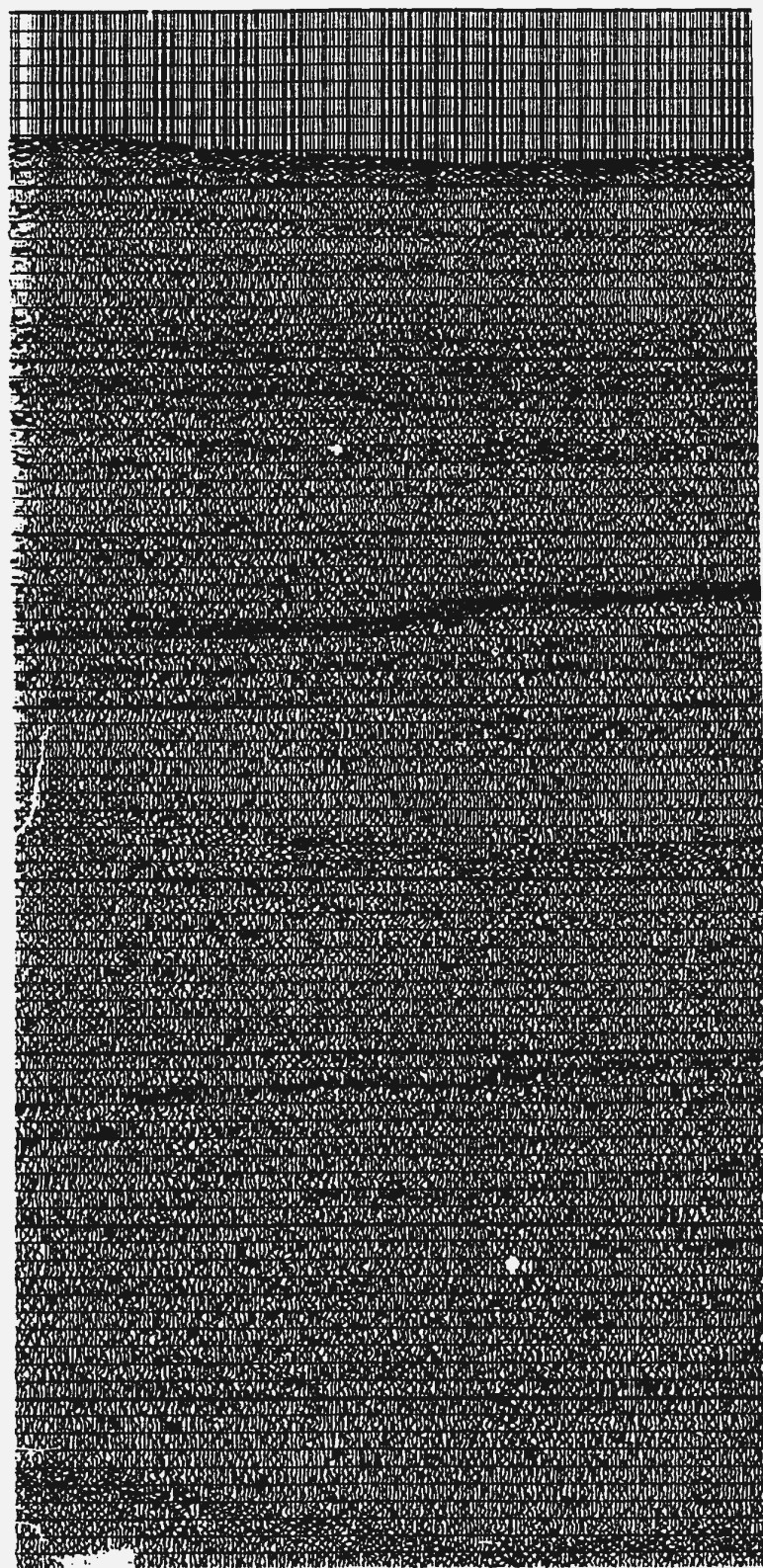
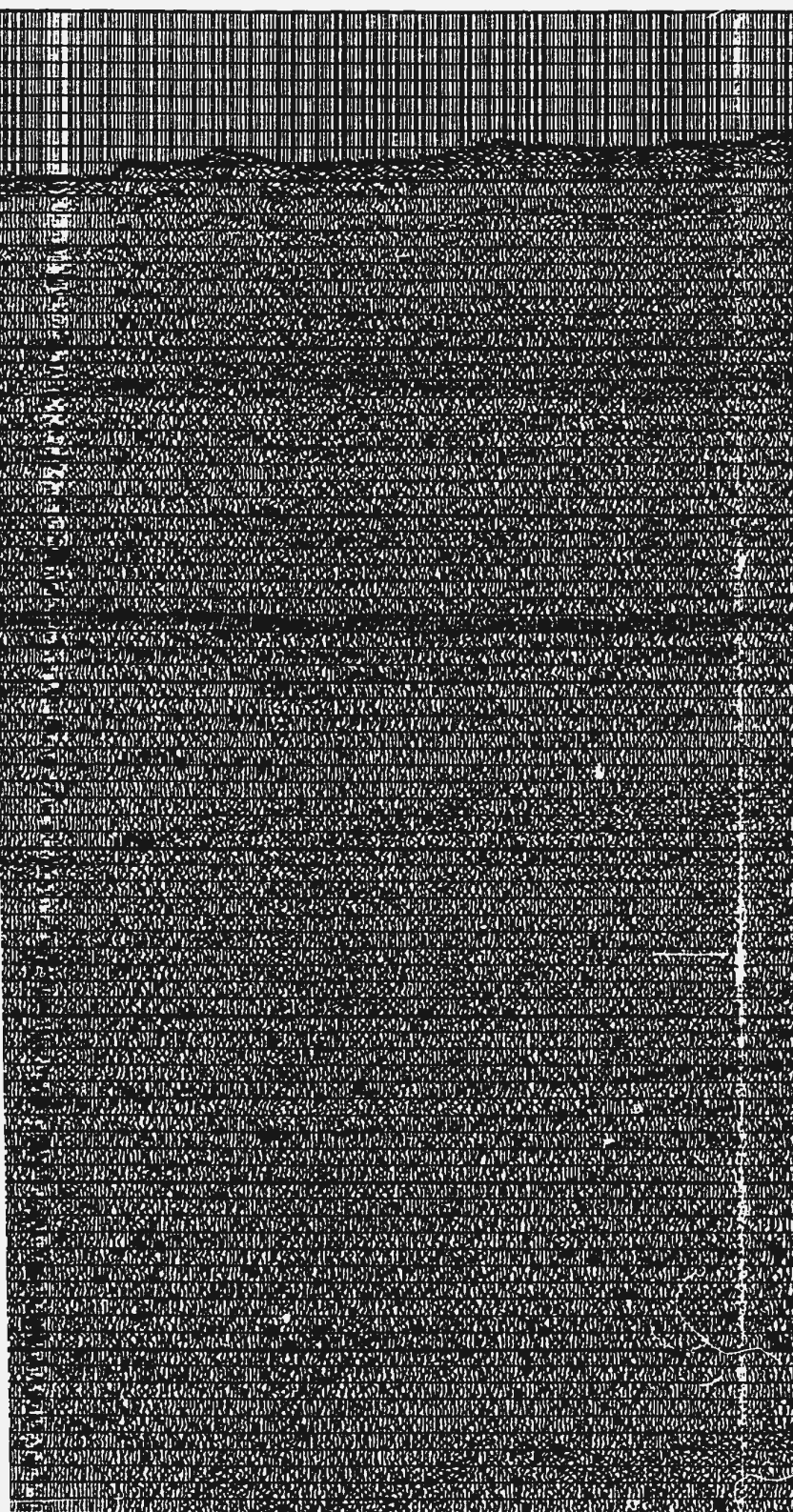
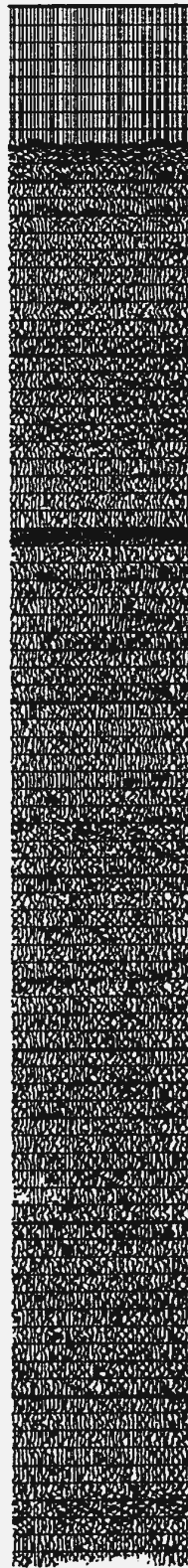
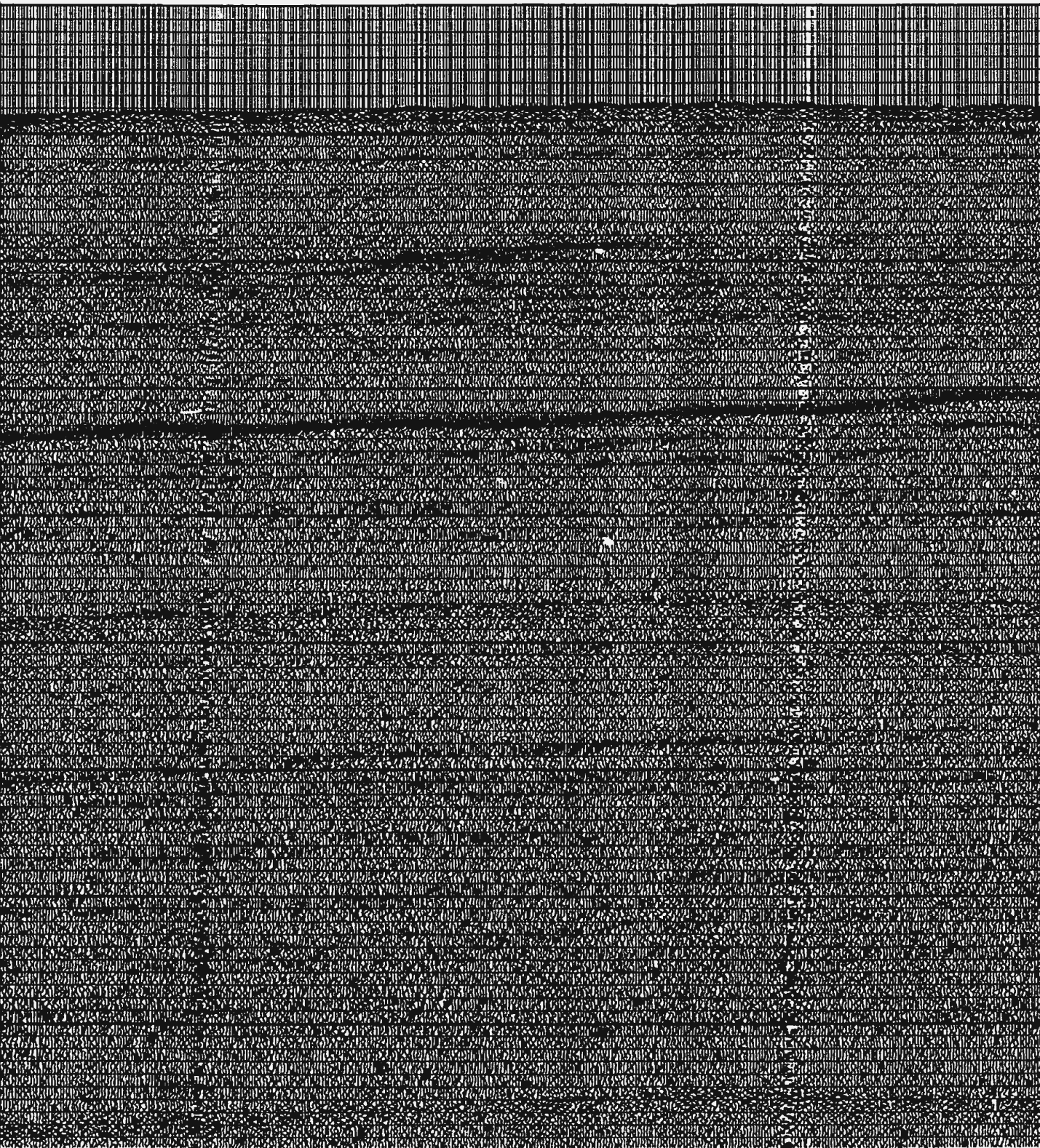


Figure 4.16 Processed Seismic Profile 16-15





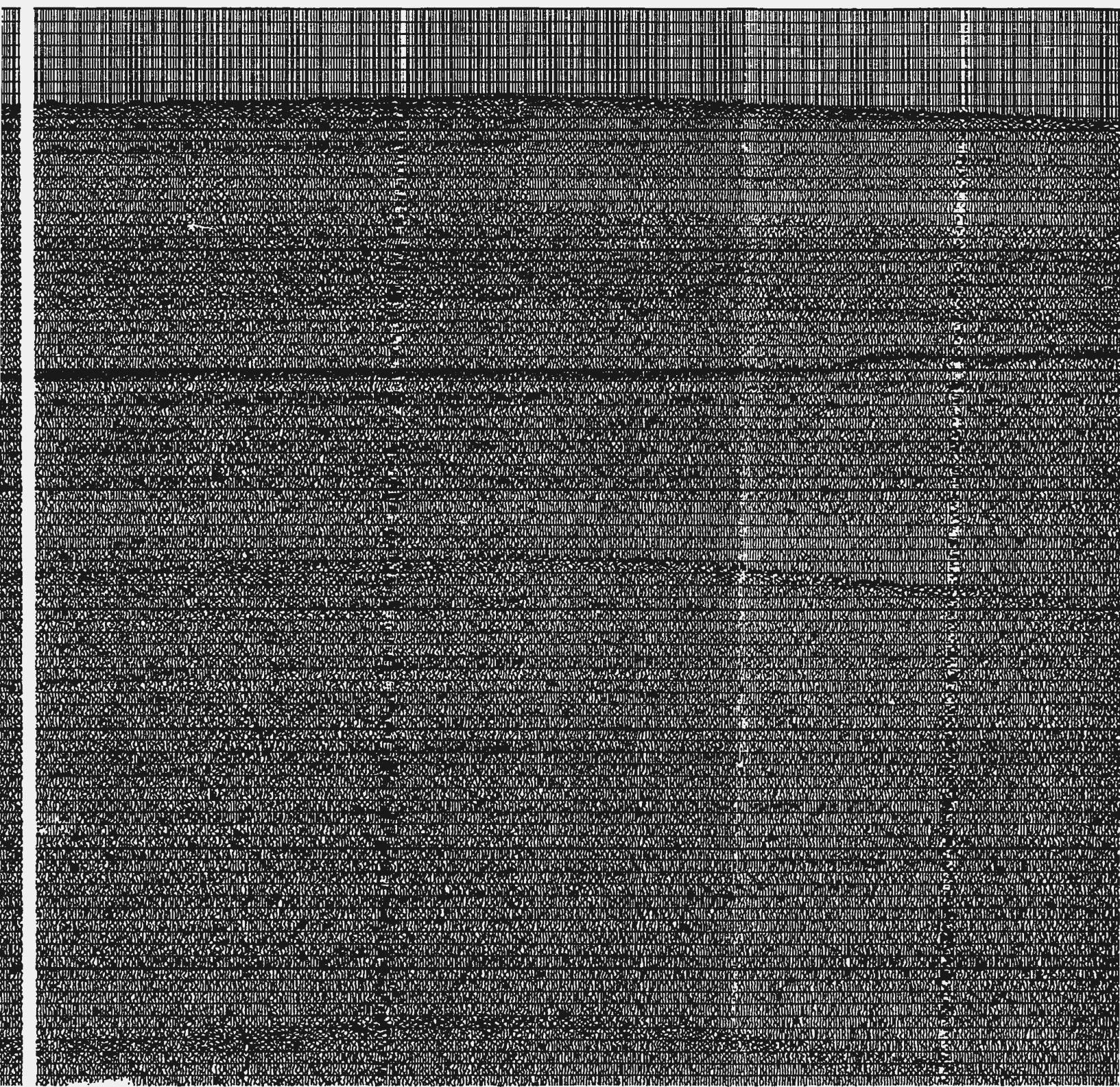
sp. 1000

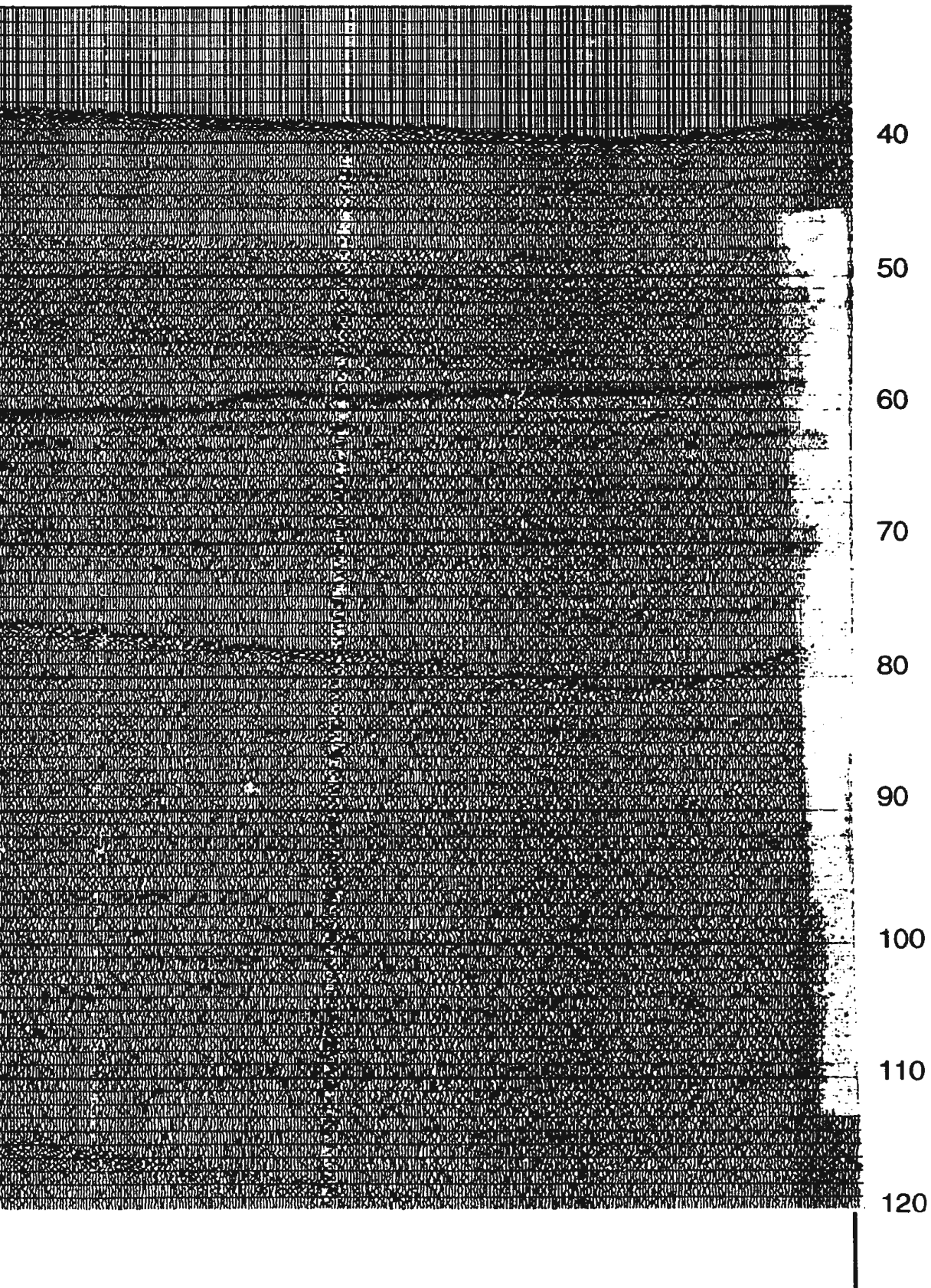


sp. 700

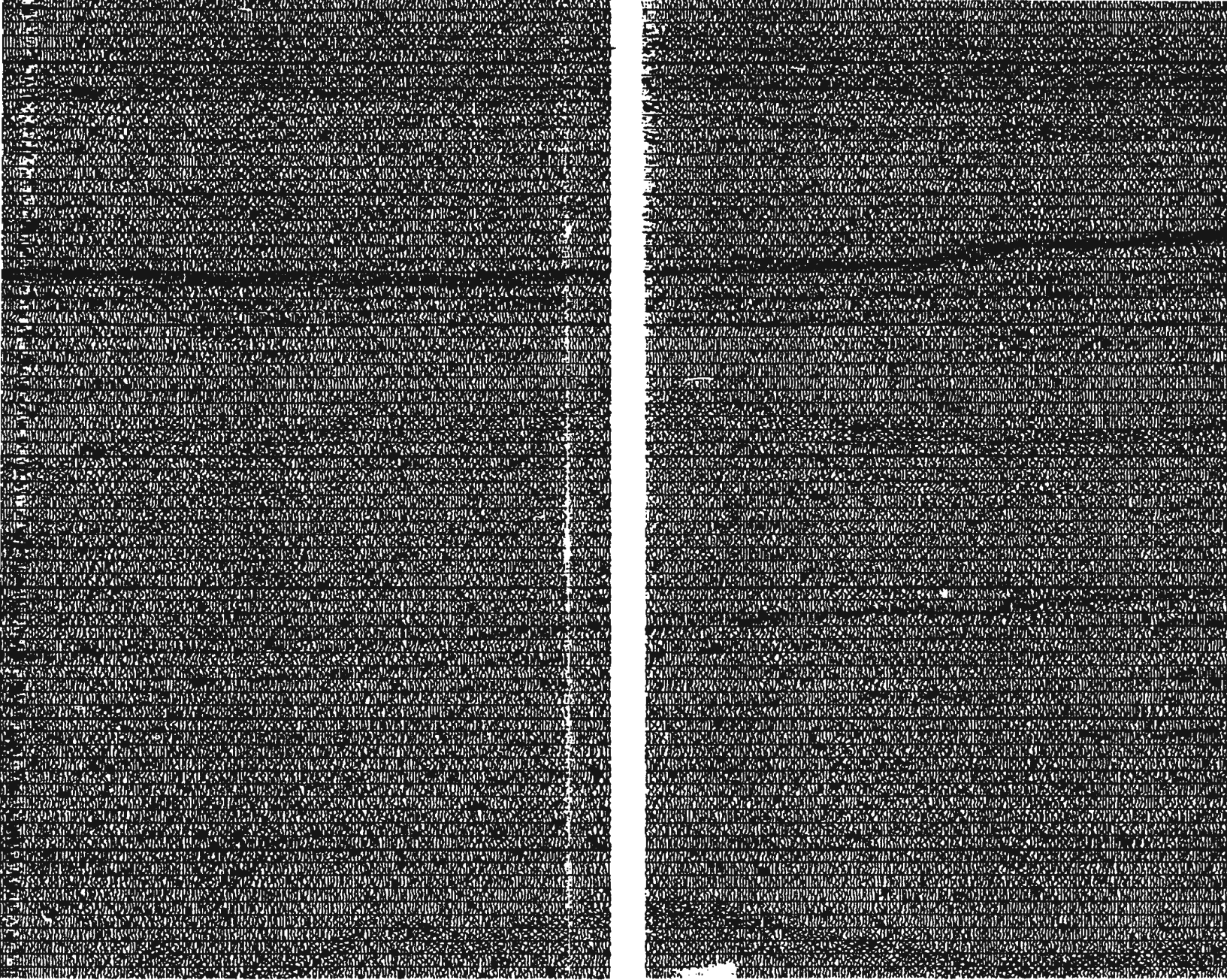
sp. 550

sp. 500





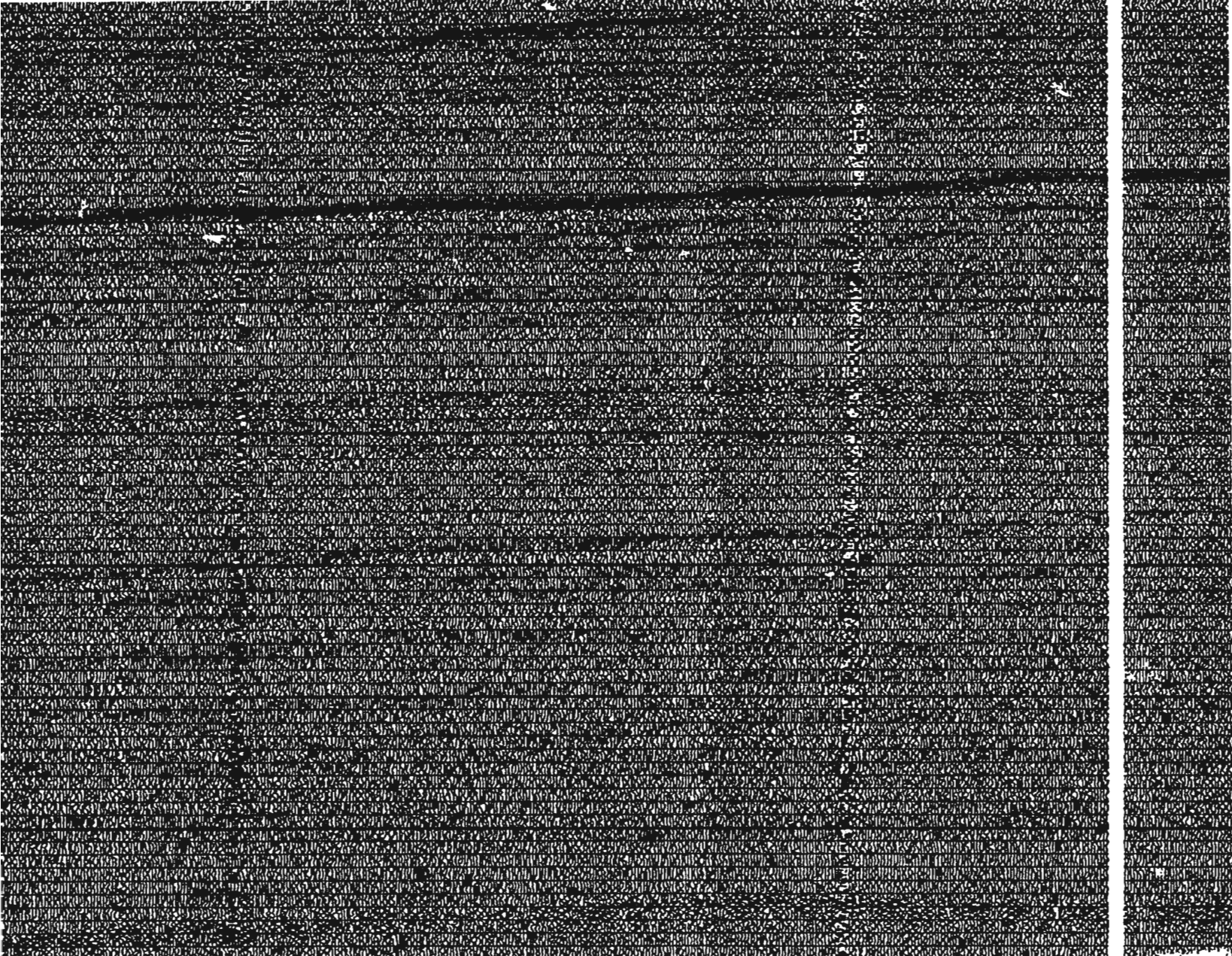
sp. 1500



sp. 1000



1000



sp. 700

sp. 550

sp. 500

Cross Tie
Profile 13-14
@ sp. 1270

Cross Tie
Profile 4-3
@ sp. 1510



1000 metres

500



p. 500

sp. 330

Cross Tie
Profile 16-15
@ sp. 1220

Figure 4.17 Processed S
Shot Points(

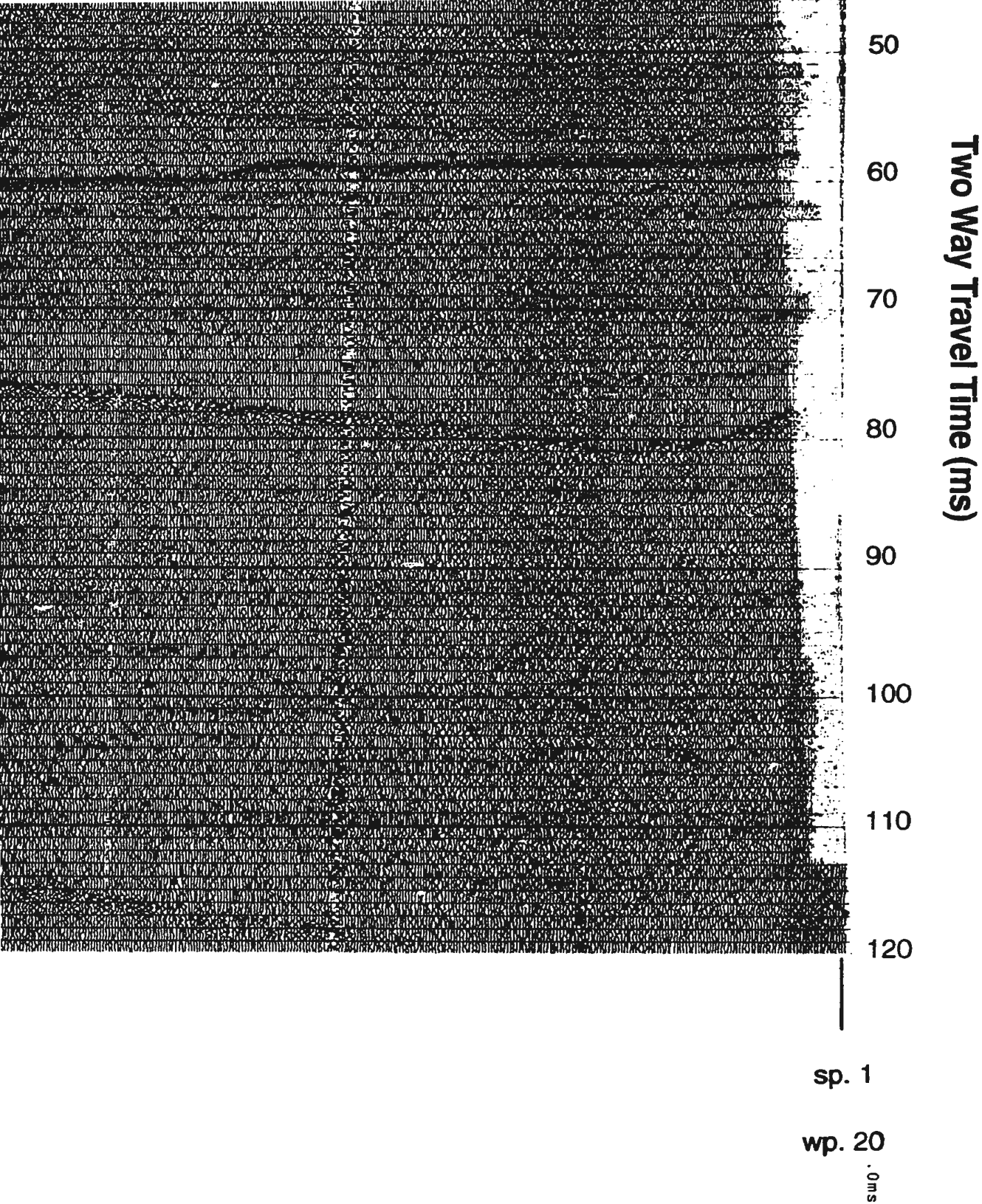
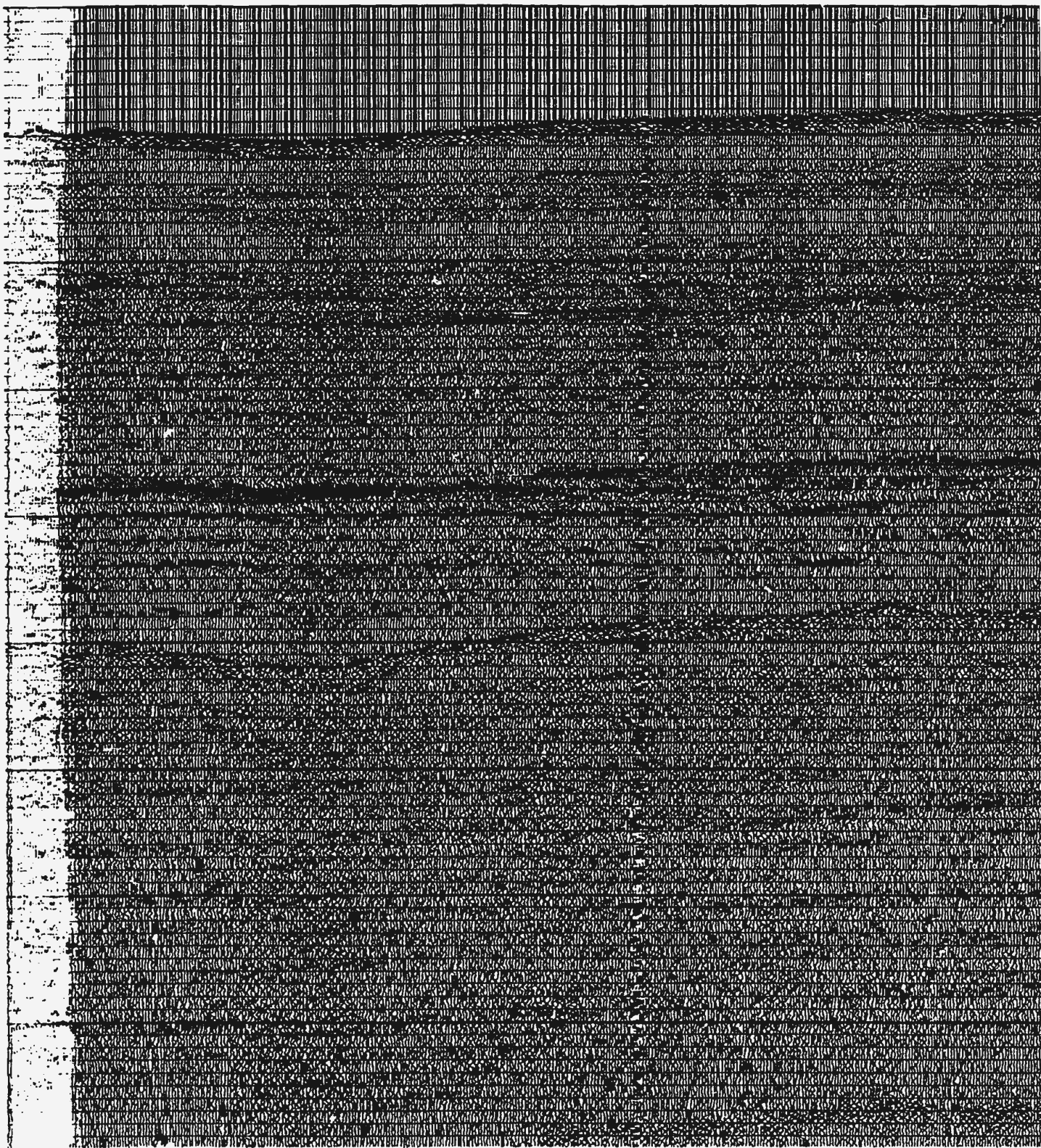
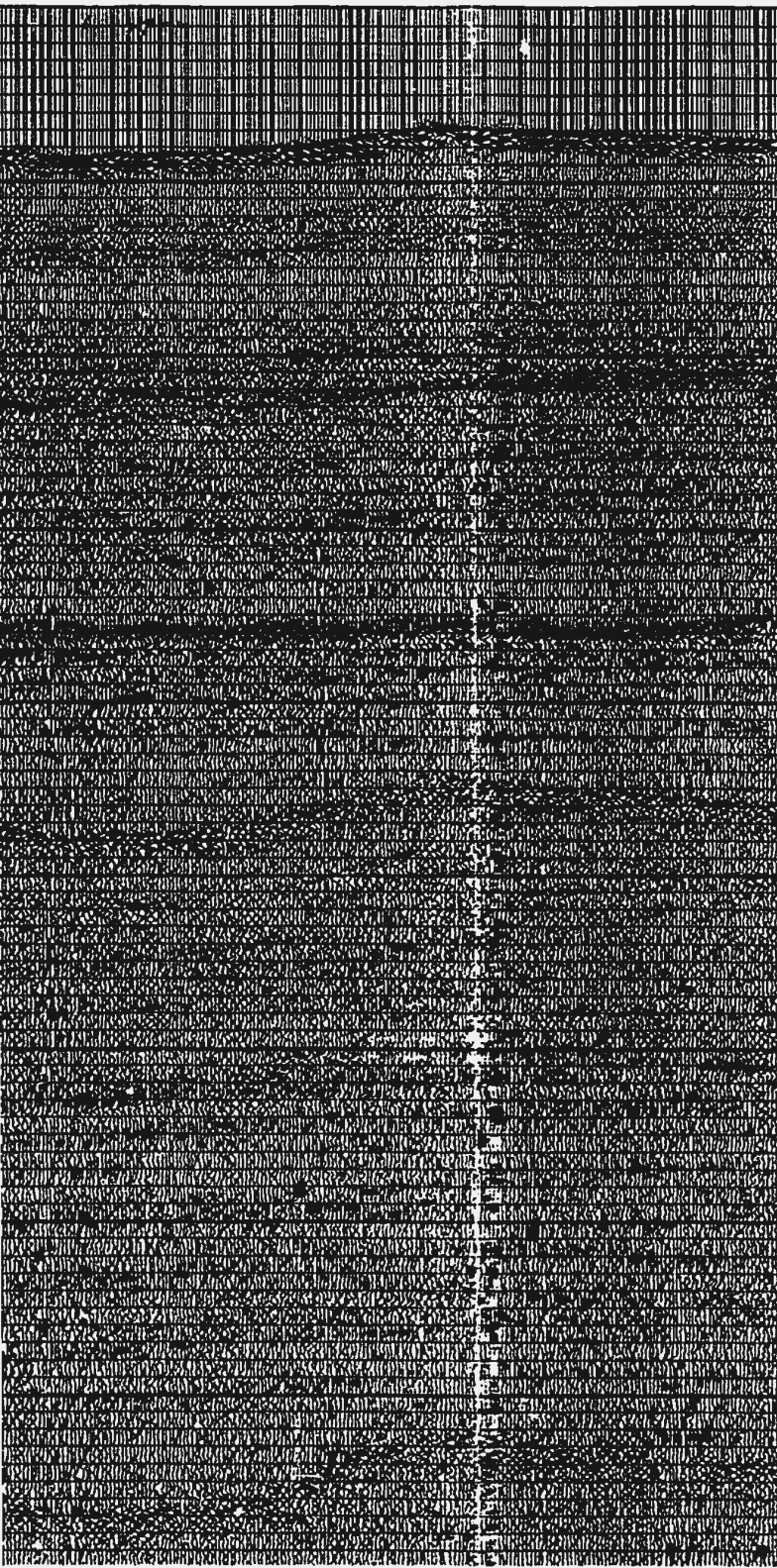


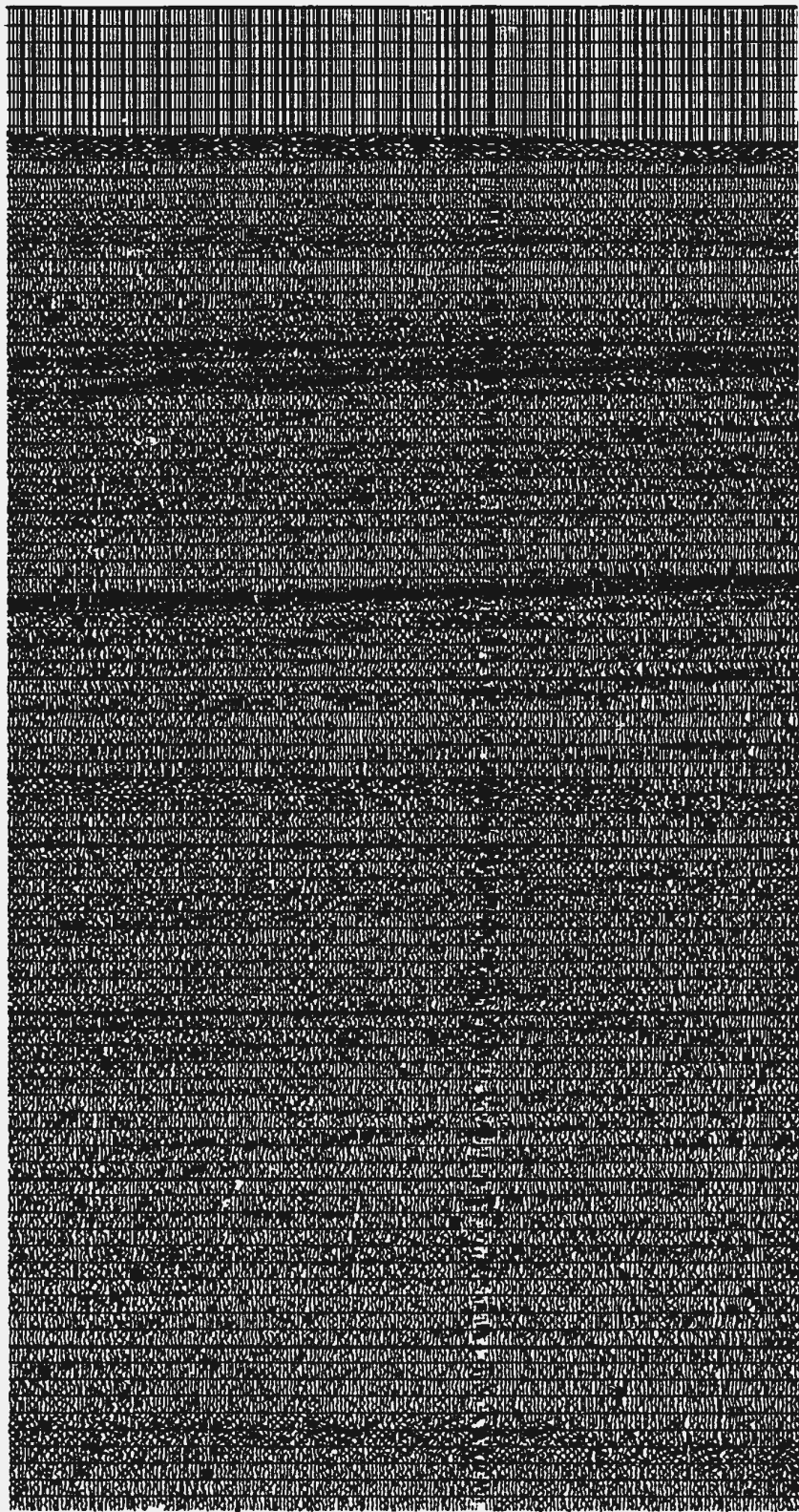
Figure 4.17 **Processed Seismic Profile (20-21)**
Shot Points(1500-1)



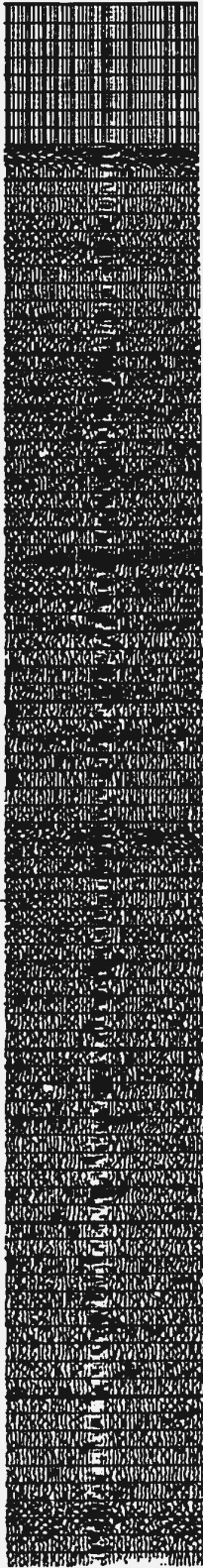
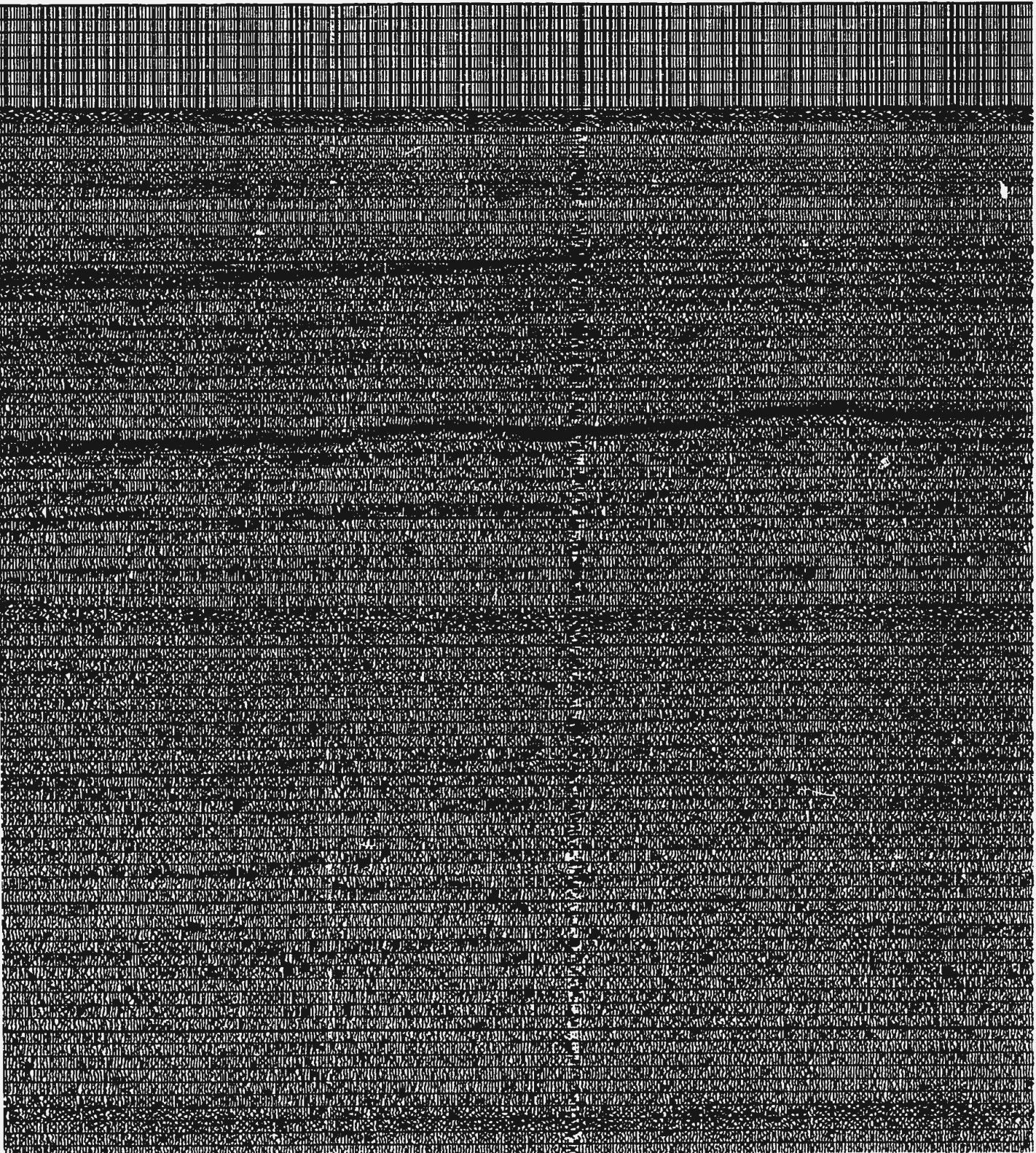
sp. 1500



sp. 2000

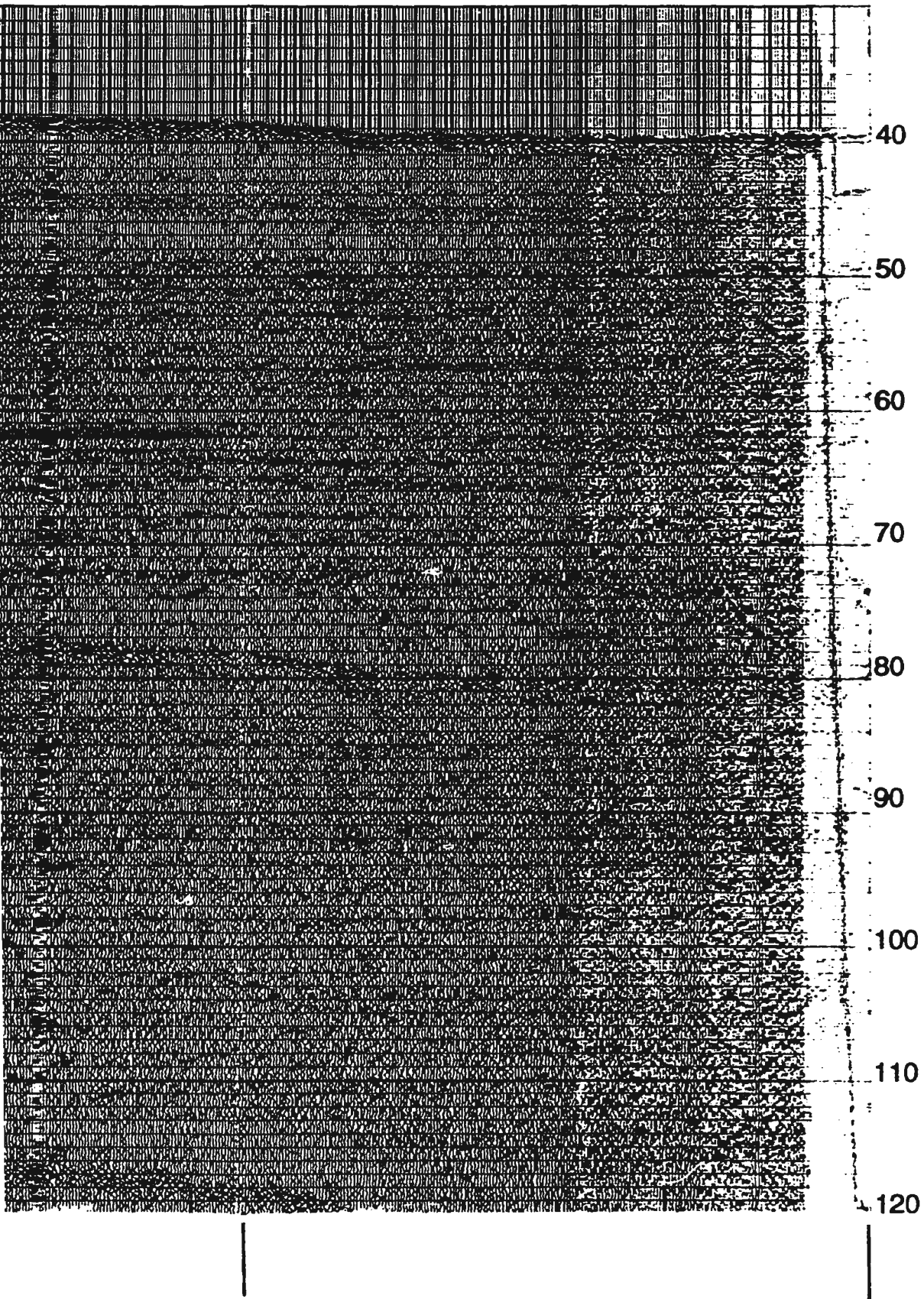


sp. 2060



sp. 2300

sp. 2500

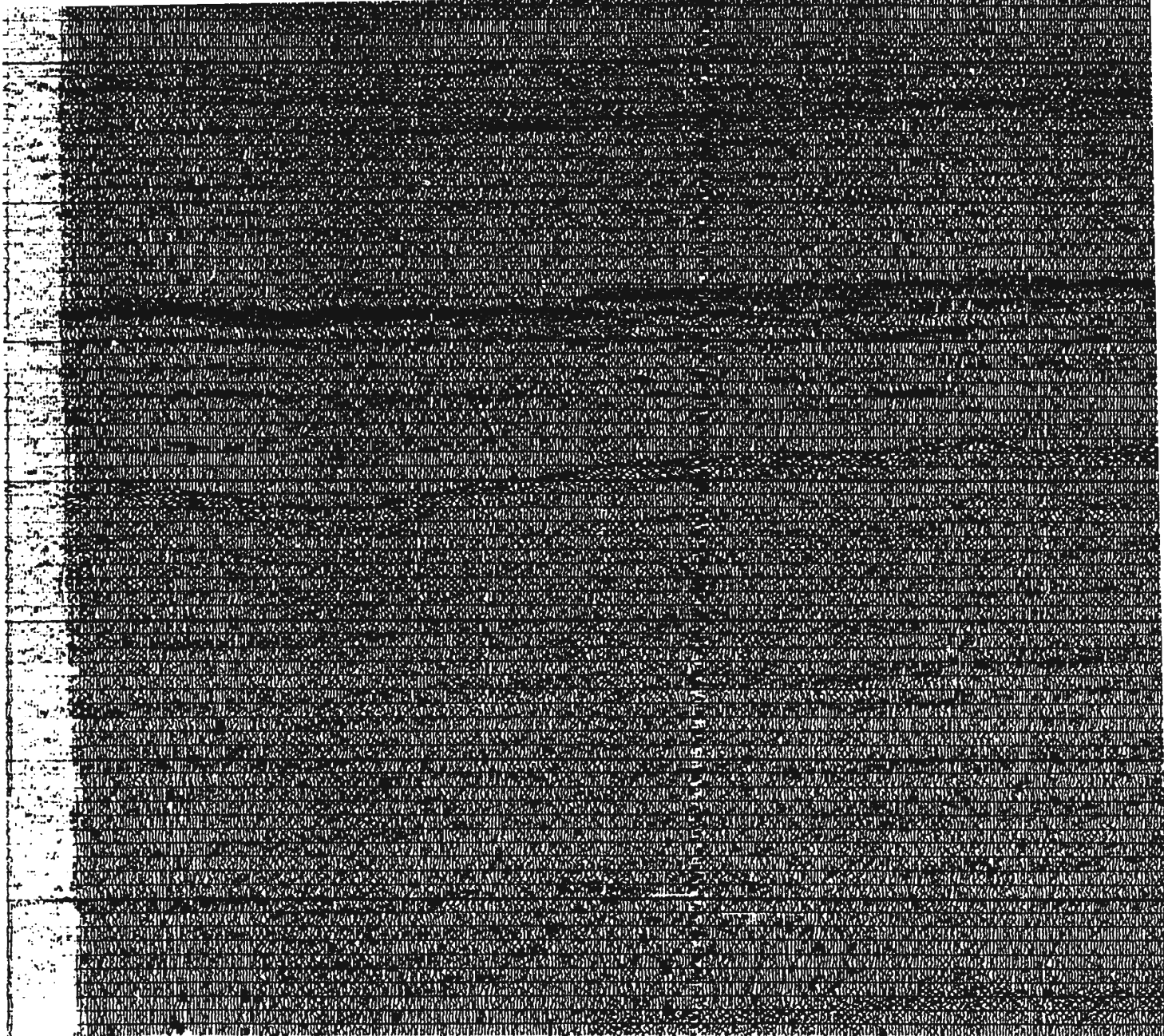


Two Way Travel Time (ms)

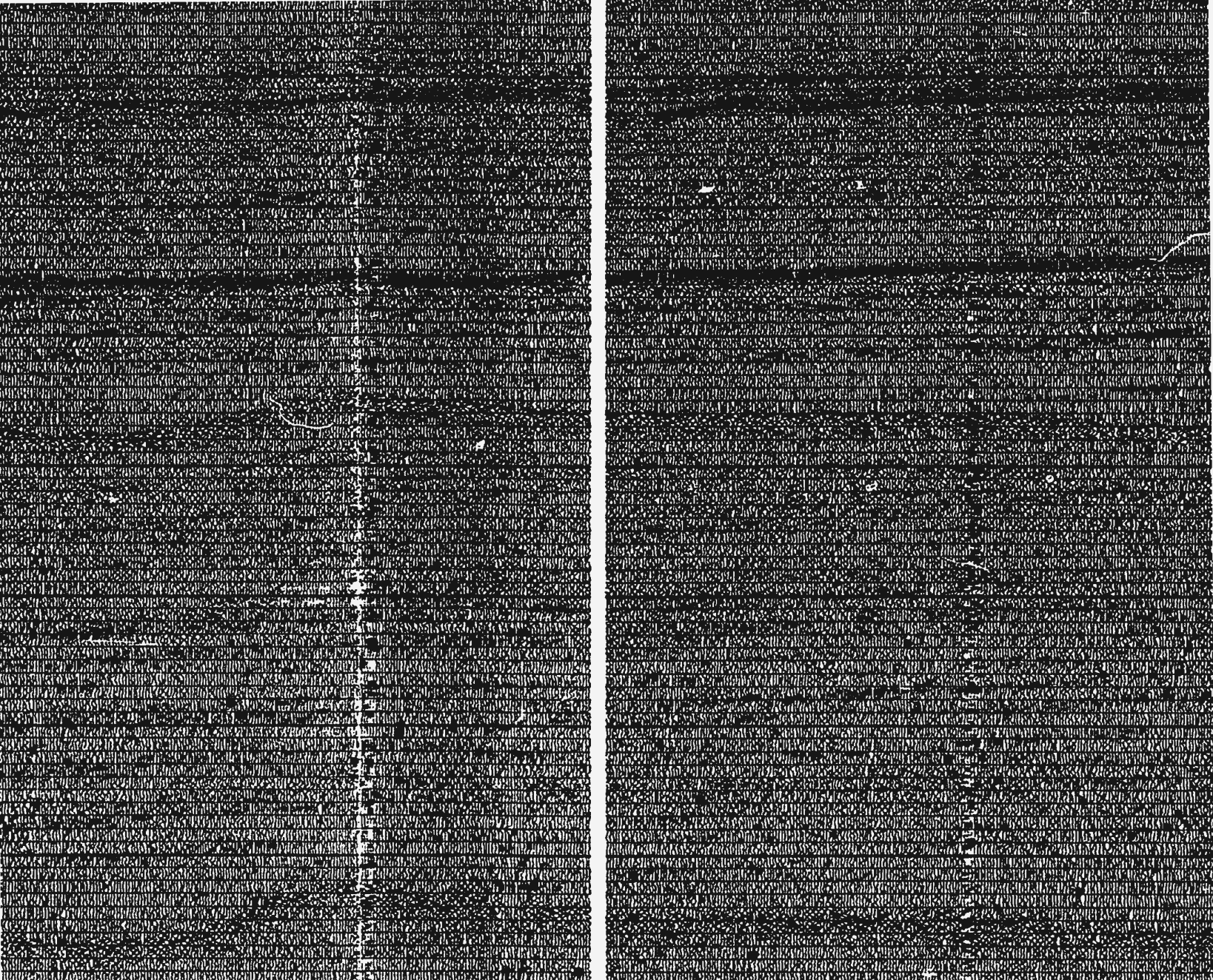
10

sp. 2590

sp. 2790



sp. 1500



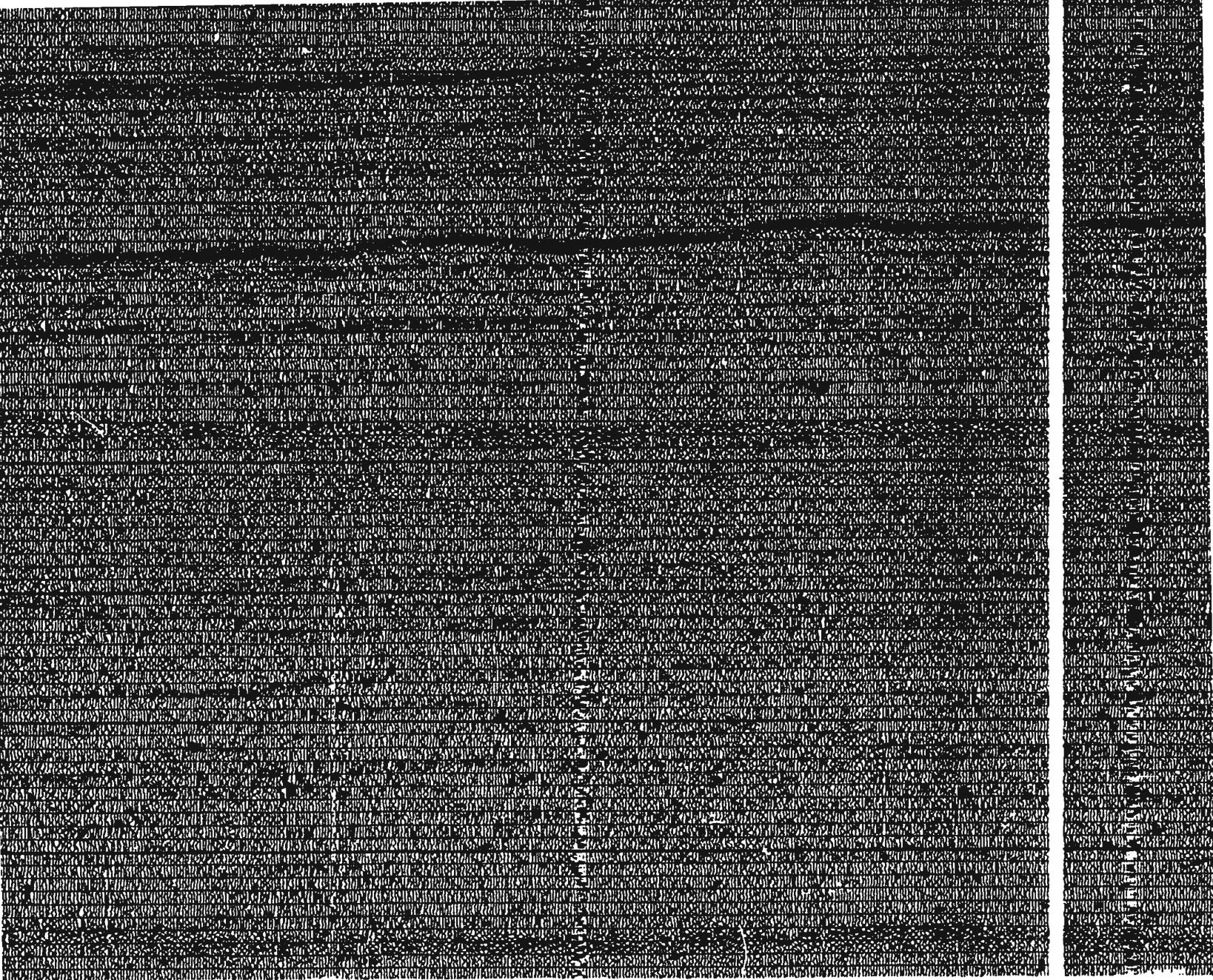
sp. 2000

sp. 2060

Cross Tie
Profile 13-14
@ sp. 800



1000 metres



sp. 2300

sp. 2500

Cross Tie
Profile 4-3
@ sp. 900



1000

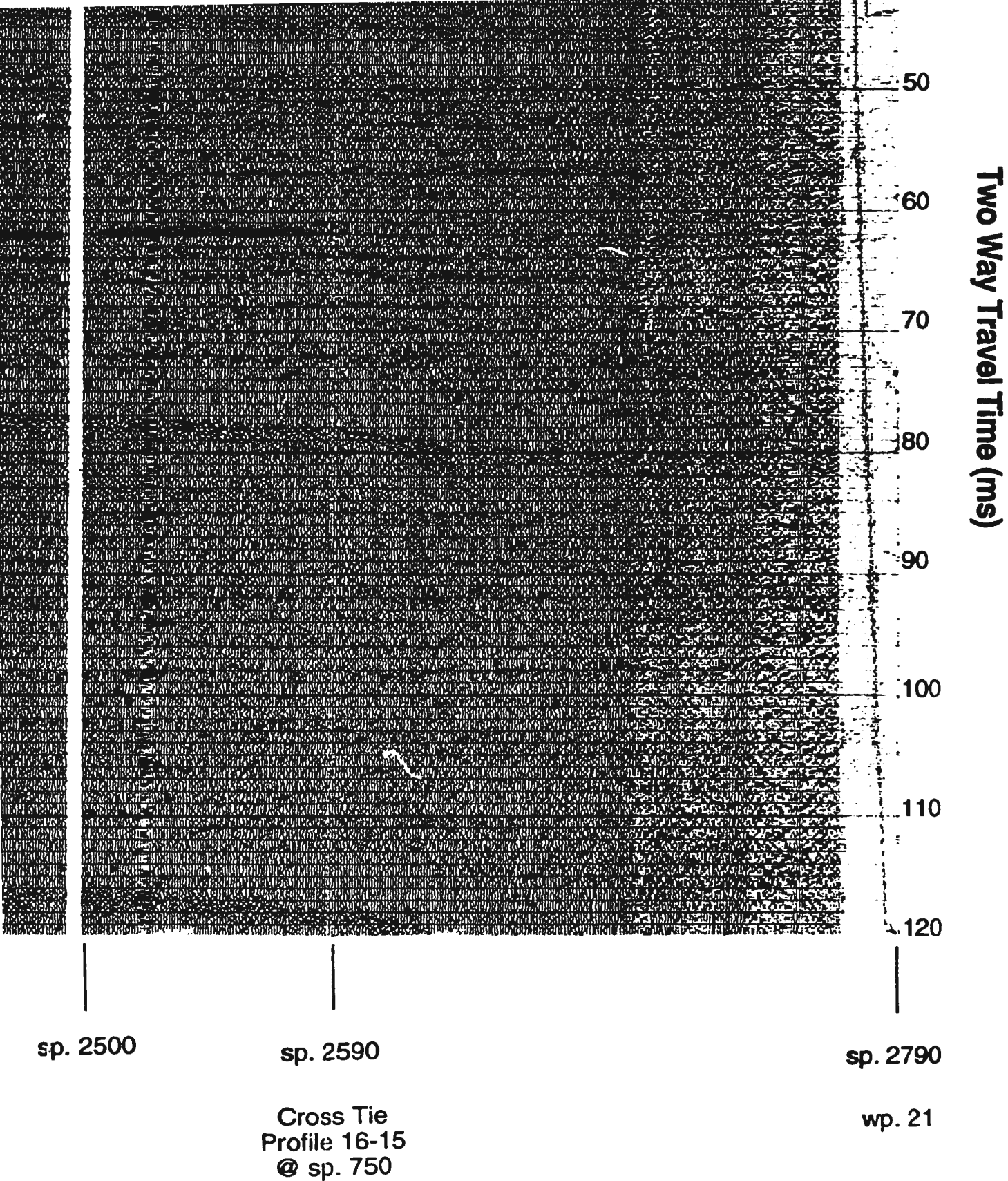


Figure 4.18 Processed Seismic Profile (20-21)
Shot Points(1500-2790)

